HOLOCENE PALEOCLIMATE RECONSTRUCTION FROM $\delta^{18}O$ CELLULOSE AND RESPONSE TO SOLAR FORCING IN EASTERN CANADA: EVIDENCE FROM MER BLEUE BOG, OTTAWA, ONTARIO.

BY

HAFIDA EL BILALI

M.Sc, University Cadi Ayyad, Marrakech, Morocco

B.Sc. (Hon.), University Chouaib Eddoukkali, El Jadida, Morocco

A thesis submitted to the Faculty of Graduate Studies and Research

in partial fulfillment of the requirements for the degree of Doctor of Philosophy

The Faculty of Graduate Studies and Research

Department of Earth Sciences

Ottawa, Ontario

Carleton University

Ottawa-Carleton Geoscience Centre

February 18, 2011

© Hafida El Bilali, 2011

Library and Archives Canada
Published Heritage Branch
395 Wellington Street
Ottawa ON K1A 0N4
Canada

Bibliothèque et Archives Canada
Direction du Patrimoine de l'édition
395, rue Wellington
Ottawa ON K1A 0N4
Canada

Your file Votre référence
ISBN: 978-0-494-81535-9
Our file Notre référence
ISBN: 978-0-494-81535-9

NOTICE:

The author has granted a non-exclusive license allowing Library and Archives Canada to reproduce, publish, archive, preserve, conserve, communicate to the public by telecommunication or on the Internet, loan, distribute and sell theses worldwide, for commercial or non-commercial purposes, in microform, paper, electronic and/or any other formats.

The author retains copyright ownership and moral rights in this thesis. Neither the thesis nor substantial extracts from it may be printed or otherwise reproduced without the author's permission.

AVIS:

L'auteur a accordé une licence non exclusive permettant à la Bibliothèque et Archives Canada de reproduire, publier, archiver, sauvegarder, conserver, transmettre au public par télécommunication ou par l'Internet, prêter, distribuer et vendre des thèses partout dans le monde, à des fins commerciales ou autres, sur support microforme, papier, électronique et/ou autres formats.

L'auteur conserve la propriété du droit d'auteur et des droits moraux qui protège cette thèse. Ni la thèse ni des extraits substantiels de celle-ci ne doivent être imprimés ou autrement reproduits sans son autorisation.

In compliance with the Canadian Privacy Act some supporting forms may have been removed from this thesis.

While these forms may be included in the document page count, their removal does not represent any loss of content from the thesis.

Conformément à la loi canadienne sur la protection de la vie privée, quelques formulaires secondaires ont été enlevés de cette thèse.

Bien que ces formulaires aient inclus dans la pagination, il n'y aura aucun contenu manquant.

Canada

ABSTRACT

This study is aimed to reconstruct the Holocene temperature history in eastern Canada derived from a 6m peat section at Mer Bleue Bog, near Ottawa, Ontario.

Geochemical, image and time-series analysis methods such as oxygen isotope analysis of plant cellulose ($\delta^{18}O_{cel}$), digital peat sediment photographs and X-ray scans, have been used to extract high-resolution paleotemperature proxy records and to detect cycles and trends, which were compared with the instrumental temperature record, solar activity proxies, and northern Hemisphere paleoclimate reconstructions. A 30 cm peat section from Glen West Bog, Northern Ireland, spanning 2880 to 2500 cal. yr. B.P., was studied to test the validity of the methods and results for maritime climate settings.

The results demonstrate that the $\delta^{18}O_{cel}$ of *Sphagnum* can provide a reliable paleotemperature proxy in continental settings (e.g., Ottawa, Ontario). $\delta^{18}O_{cel}$ based paleotemperature reconstructions must take into account significant stable oxygen isotopic differences between cellulose from *Sphagnum* and other peatland plant macrofossils, whereas the offsets between $\delta^{18}O_{cel}$ of different *Sphagnum* species are statistically insignificant.

The $\delta^{18}O_{cel}$ record obtained from the Mer Bleue Bog core correlates well with the instrumental temperature record, northern Hemisphere paleotemperature reconstructions and reconstructed solar activity records.

At the Mer Bleue Bog, solar activity fluctuations at the ~80-year to ~2500-year cycle bands recorded in peat color and X-ray density, and $\delta^{18}O_{cel}$ data appear to have a major influence on regional and global climate as are recorded in peat color and X-ray density, and isotope data throughout the Holocene. In particular the results suggest that 180-250 years "Suess" and ~1300 years "Bond" cycles controlled long-term variability in temperature and peat sedimentation in eastern Canada. The Mer Bleue Bog $\delta^{18}O_{cel}$ data correlate well with Atlantic ice-rafted debris, and European climate features such as the Little Ice Age and the Medieval Warm period, as well as pronounced northern Hemisphere cooling that is likely triggered by the Dalton solar minima from ~1810-1820 A.D. and amplified by the Mount Tambora, Indonesia eruption of 1815.

Solar activity fluctuations at the ~11-year and ~250-year cycle-band in a ~380 year record have a major influence on the North Atlantic climate as is recorded in sediment imaging and $\delta^{18}O_{cel}$ data from Northern Ireland.

ACKNOWLEDGEMENTS

Firstly, I would like to thank my supervisor, Dr. Timothy Patterson, who has generously supported my research, both financially and intellectually. I am grateful to my supervisor for giving me the opportunity to conduct this interesting research project which has allowed me to reconstruct the paleoclimate of the Ottawa area and understand our past climate here in Ottawa.

This research project is supported by The Natural Sciences and Engineering Research Council of Canada (NSERC) Discovery Grant to Dr. T.R. Patterson. Additional financial support included scholarships from Carleton University, the Ottawa-Carleton Geoscience Centre.

I would like to thank the following for their extensive help in the field and laboratory: Dr. H.M. Roe, Queens University Belfast; Dr. A. Prokoph, Department of Earth Sciences, Carleton University; Dr. L. Babalola, King Fahd University; Dr. E. Humphrey and M. Treberg from the Department of Geography at Carleton University. I also thank the National Capital Commission for permitting access to Mer Bleue Bog.

I would like to acknowledge several researchers who have offered their insightful advice, guidance, and assistance while discussing this project. Dr. Graeme Swindles, Leeds University for providing access to the Glen West monolith and Dr. H. Roe, Queens University Belfast. They both shared their expertise and knowledge in the field of peat and helped with their constructive advice and criticisms. Dr. A. Prokoph has contributed enormously with his guidance in particular in the field of time series analysis (wavelet and spectral).

My graduate student colleagues have provided advice, support, and lively discussions on all that is related to climate change reconstructions and predictions. I would especially like to thank Cherrylee Black, Andrew Macumber, Sulaiman Olangoke, Suzanne Elliott, and the remaining members of the Patterson Group for keeping a friendly, exciting, and motivating research environment.

I also thank the academic and administrative staff of the Department of Earth Sciences at Carleton University, in particular Dr. Brian Cousens, Dr. Claire Samson, Dr. John Blenkinsop, Dr. Ildi Munro, Dr. Georges Dix, Sheila Thayer, and Beth Halfkenny, Chris Rogers for their continuous support during my PhD residency.

Finally, I would like to thank my parents for their faith in me, for their help and support all these years. I would like to extend my thanks to my brothers and sisters for always believing in me. I thank Andreas and my two daughters Sophia and Jihane for their patience and understanding. Without their love and encouragement this may never have been completed.

TABLE OF CONTENTS

Abstract..ii

Acknowledgements.. ..iv

Table of ontents...vi

List of Tables... xiv

List of Figures..xv

List of Appendices...xix

CHAPTER ONE

1. GENERAL INTRODUCTION...1

1.1 Background..1

1.2 Thesis Presentation...2

1.3 Study Areas..4

1.4 Objectives..7

1.5 Methodology 8

1.6 References...10

CHAPTER TWO

2. INFLUENCE OF CELLULOSE OXYGEN ISOTOPE VARIABILITY IN SUB-FOSSIL *SPHAGNUM* AND PLANT MACROFOSSIL COMPONENTS ON THE RELIABILITY OF PALEOCLIMATE RECORDS AT THE MER BLEUE BOG, OTTAWA, ONTARIO, CANADA.

2.1 Abstract..15

2.2 Introduction..16

2.3 Geographic and Geological Setting..19

2.4 Field Sampling & Material Collection..23

2.5 Methods..25

2.5.1 Plant macrofossils separation 25

2.5.2 Cellulose oxygen isotope analytical technique...................................25

2.5.3 Analysis of variance (ANOVA)-method...26

2.6 Results..28

2.6.1 Core sedimentology...28

2.6.2 Cellulose oxygen isotope composition...30

2.6.3 Results of analysis of variance (ANOVA)...32

2.7 Discussion..39

2.8 Conclusions..42

2.9 References..43

CHAPTER THREE

3. EASTERN ONTARIO HOLOCENE PALEOCLIMATE RECONSTRUCTION: EVIDENCE FROM $\delta^{18}O$ CELLULOSE OF PLANT MACROFOSSILS FROM THE MER BLEUE BOG

3.1 Abstract……50

3.2 Introduction……51

3.3 Previous Work……53

3.3.1 *Ombrotrophic bogs as paleoclimate archives*……53

3.3.2 *Advantages of using Sphagnum for paleoclimate reconstruction*……53

3.3.3 Cellulose oxygen isotope composition and paleotemperature……54

3.3.4 Cellulose and source water oxygen signatures……55

3.4 Geographic and Geological Setting……57

3.5 Field Sampling & Material Collection……59

3.6 Methods……60

3.6.1 Plant macrofossils separation……60

3.6.2 Cellulose oxygen isotope analytical technique……62

3.6.3 Mer Bleue Bog age-depth model……63

3.7 Results……64

3.7.1 Cellulose oxygen isotope composition in depth……64

3.7.2 Mer Bleue Bog age-depth model……68

3.7.3 Cellulose oxygen isotope composition in time……73

3.8 Discussion……78

3.8.1 Influences on $\delta^{18}O_{cel}$ signature in ombrotrophic Bogs 78

3.8.2 $\delta^{18}O_{cel}$ as a paleotemperature proxy...81

3.9 Conclusions..86

3.10 References..87

CHAPTER FOUR

4. CENTENNIAL AND MILLENNIAL-SCALE CLIMATE RESPONSE TO SOLAR FORCING: EVIDENCE FROM THE MER BLEUE BOG, OTTAWA, ONTARIO.

4.1 Abstract..100

4.2 Introduction..101

4.3 Background..103

4.3.1 Climate forcing and dynamics..103

4.3.2 Cellulose in Sphagnum in ombrotrophic bogs and paleoclimate...........105

4.4 Geographic and Geological Setting..106

4.5 Field Sampling & Material Collection..109

4.6 Data and Methods..111

4.6.1 Plant macrofossils separation 111

4.6.2 Cellulose oxygen isotope analytical technique..........................112

4.6.3 The Mer Bleue Bog age-depth model..113

4.6.4 Image analyses..113

4.6.4.1 Digital core photography..113

4.6.4.2 Digital X-ray imaging..115

4.6.5. Time series analyses..115

4.6.5.1 Spectral analysis..117

4.6.5.2 Wavelet analysis..118

4.7 Results..120

4.7.1 The Mer Bleue Bog age-depth model..120

4.7.2 Cycles and trends in depth and time scales..................................123

4.7.2.1 Cellulose oxygen isotope composition in depth-scale.............123

4.7.2.2 Cellulose oxygen isotope composition and oxygen concentration in time-scale..127

4.7.2.3 Digital photo and X-ray gray-values in depth-scale..............130

4.7.2.4 Gray-values of X-ray images in time-scale.........................133

4.7.2.5 Gray-values of digital photographs in time-scale..................133

4.7.2.6 Solar activity proxies..136

4.7.2.7 Spectral analysis..138

4.8 Discussion...140

4.8.1 Image analysis...140

4.8.2 $\delta^{18}O$ variation in Sphagnum cellulose..................................142

4.8.3. Solar, volcanic and atmospheric-oceanic forcing of Holocene paleoclimate in eastern Canada..143

4.9 Conclusions...146

4.10 References..147

CHAPTER FIVE

5. MID-HOLOCENE CLIMATE RESPONSE TO SOLAR FORCING: EVIDENCE FROM THE GLEN WEST BOG, NORTHERN IRELAND, UK.

5.1 **Abstract**……………………………………………………………………161

5.2 **Introduction**…………………………………………………………………162

5.3 Background…………………………………………………………………164

5.3.1 Climate forcing and dynamics……………………………………………164

5.3.1.1. Ocean and atmospheric circulation…………………………………164

5.3.1.2 Celestial forcing……………………………………………………165

5.3.2 Sphagnum cellulose, ombrotrophic bogs and paleoclimate………………167

5.4 Study Area and Material Collection……………………………………169

5.4.1 Study area…………………………………………………………………169

5.4.2 Material collection…………………………………………………………171

5.5 Methodology…………………………………………………………………171

5.5.1 Glen West age-depth model………………………………………………172

5.5.2 Plant macrofossil separation and identification…………………………172

5.5.3 Cellulose oxygen isotope analytical technique……………………………172

5.5.4 Image analyses……………………………………………………………176

5.5.4.1 Digital core photography……………………………………………176

5.5.4.2 Digital X-ray scanning………………………………………………177

5.5.5 Time series analyses………………………………………………………178

5.5.5.1 Spectral analysis……………………………………………………178

5.5.5.2. Wavelet analysis:....180

5.6 Results....182

5.6.1 Cycles and trends in depth and time domains....182

5.6.1.1 $\delta^{18}O_{cel}$ signature and oxygen content in plant cellulose....182

5.6.1.2 Wavelet analysis....183

i) Wavelet analysis of $\delta^{18}O_{cel}$ and O%....183

ii) Gray-scale values of digital photographs....183

iii) Gray-scale values of X-ray images....184

5.6.1.3 Spectral analysis....187

5.7 **Discussion**....190

5.7.1 Image analysis....190

5.7.2 $\delta^{18}O$ variation in Sphagnum cellulose....192

5.7.3 Solar, volcanic and atmospheric-oceanic forcing on Mid-Holocene paleoclimate in Northern Ireland....195

5.8 Conclusions....196

5.9 References....197

CHAPTER SIX

6. GENERAL CONCLUSIONS

6.1 Bulk peat versus separated peat plant components 211

6.2 Sphagnum cellulose-based paleotemperature and drivers for paleoclimate fluctuations....212

6.3 Image and time series analyses..214

6.4 References..215

LIST OF TABLES

Table 2.1: Oxygen isotope ratio and oxygen concentration of plant cellulose from Mer Bleue Bog, Ottawa, Ontario........34

Table 2.2: ANOVA -Single Factor of $\delta^{18}O_{cel}$ data........37

Table 3.1: Mer Bleue ^{14}C age-dates........65

Table 3.2: Oxygen isotope ratio and oxygen concentration of plant cellulose from Mer Bleue Bog, Ottawa, Ontario........66

Table 4.1: Mer Bleue ^{14}C age-dates........120

Table 4.2: Oxygen isotope ratio and oxygen concentration of plant cellulose from Mer Bleue Bog, Ottawa, Ontario........124

Table 5.1: Results of ^{14}C determination at the Glen West core, Northern Ireland (Plunkett et al., 2004; Swindles et al., 2007a, 2007b)........173

Table 5.2: Oxygen isotopic composition and concentration of *Sphagnum* cellulose from the Glen West Bog monolith........185

LIST OF FIGURES

Figure 1.1: Mer Bleue Bog. A) The star shows the sampling site from which cores were retrieved (Touzi, 2007; Touzi et al., 2007). B) Mer Bleue bog in the spring season..........5

Figure 1.2: Peatland distribution in Canada (Tarnocai et al., 2002)..................................6

Figure 2.1: Location map of Mer Bleue Bog, Ottawa, Ontario in eastern Canada..........21

Figure 2.2: Coring strategy: (2 sets of triplicate cores of 50cm length and ~5.5cm diameter, sets with 20 cm (upper 350cm) and 10cm (lower 250cm) overlap..................24

Figure 2.3: Mer Bleue core sedimentology: A: Peat color, B: Lithology, C: Depositional environments..31

Figure 2.4: Oxygen concentration and oxygen isotope data of cellulose from different plant matter of the Mer Bleue Bog core..33

Figure 2.5: Correlation of cellulose oxygen isotope data of different plant taxa. A: *Sphagnum magellanicum* vs *Sphagnum fuscum* and B: all lumped *Sphagnum* species vs. rhizome. Black lines in graph area show linear regression lines......................................38

Figure 3.1: Location map of Mer Bleue Bog, Ottawa, Ontario in eastern Canada...........58

Figure 3.2: Mer Bleue core lithology. A: Rock color code following Munsell Chart (Munsell, 1975), B: Lithology, C: Depositional environments.......................................61

Figure 3.3: Mer Bleue core lithology, oxygen concentration and isotope data of cellulose from different plant material of the Mer Bleue Bog core. 69

Figure 3.4: Mer Bleue core age-depth model and main depositional stages, based on 10 AMS radiocarbon ages, first occurrence of *Ambrosia* pollen, and an intercept with 0m depth at October 2007 A.D. 74

Figure 3.5: Oxygen isotope record of cellulose from Mer Bleue Bog through the last 9,200 years A: Depositional environment, B: Oxygen isotope record of cellulose with mean and 210-year moving average, C: Reconstructed sunspot record (Solanki et al., 2004) at 210-year moving average, D: Global glacier advances (black bars) and high drift ice indices (0 1, 2) after Bond et al. (2001). X: ~4200 yr BP cooling in North Atlantic (Bond et al., 1997)....76

Figure 3.6: Comparison of isotope record of cellulose from Mer Bleue Bog with northern Hemisphere temperature difference to present (in °C) by Moberg et al. (2005) through last 2,000 years....77

Figure 3.7: Comparison of isotope record of cellulose of Mer Bleue Bog through the last 600 years with A: solar activity events, B: Beryllium isotope anomaly (Bard et al., 2000) and measured sunspot numbers from the last 250 years....79

Figure 3.8: Comparison of instrumental air temperature and $\delta^{18}O_{preciptiation}$ records from Ottawa Airport Weather station from ~1938-2007 (GNIP, 2001; Environment Canada, 2010) with the $\delta^{18}O_{cel}$ values from the Mer Bleue Bog. 83

Figure 4.1: Location map of the Mer Bleue Bog, Ottawa, Ontario in eastern Canada....108

Figure 4.2: Mer Bleue core Lithology. A: Rock color code following Munsell Chart (Munsell, 1975), B: Lithology, C: Depositional environments....110

Figure 4.3: Digital photo image calibration and line-scan extraction....114

Figure 4.4: Digital X-ray image calibration and line-scan extraction....116

Figure 4.5: Mer Bleue core age-depth model and main depositional stages, based on 10 AMS radiocarbon ages and an intercept with 0m depth at October 2007 A.D....122

Figure 4.6: Mer Bleue core Lithology, oxygen concentration and isotope data of cellulose in depth domain from different plant material of the Mer Bleue Bog core....126

Figure 4.7: Wavelet scalogram of $\delta\ ^{18}O_{ccl}$ of *Sphagnum* with cone of influence (stripped line) and marked important wavelengths....128

Figure 4.8: Wavelet scalogram of oxygen concentration (in %) of *Sphagnum* cellulose with cone of influence (stripped line) and marked important wavelengths....129

Figure 4.9: Wavelet analysis of Digital photo image line-scan from the Mer Bleue Bog core in depth domain....131

Figure 4.10: Wavelet analysis of X-ray image line-scan from the Mer Bleue Bog core in depth domain....132

Figure 4.11: Wavelet analysis of X-ray image line-scan from the Mer Bleue Bog core in time scale....134

Figure 4.12: Wavelet analysis of Digital photo image line-scan from the Mer Bleue Bog core in time scale....135

Figure 4.13: Wavelet analysis of reconstructed solar activity proxies: A) reconstructed sunspot number B) solar irradiance and C) ^{14}C production rate records with cone of influence (stripped line) and marked important wavelengths....137

Figure 4.14: Periodograms of spectral analysis of photo (C) and X-ray (D) line-scans, cellulose oxygen isotope composition (F) and oxygen concentration (G), and reconstructed solar activity proxies (A, D, E)....139

Figure 5.1: Map of Ireland, showing the location of Glen West Bog, County Fermanagh....170

Figure 5.2: Age model of entire Glen West core (after Swindles et al., 2007a, 2007b)....174

Figure 5.3: Digital photograph and X-ray images line-scan extraction from the monolith section of the Glen West core....179

Figure 5.4: Oxygen isotope and concentration of *Sphagnum* cellulose in depth and time-scale of the Glen West core....186

Figure 5.5: Wavelet analysis of image line-scan from digital core surface photography from the monolith segment of the Glen West core....188

Figure 5.6: Wavelet analysis of X-ray image line-scan from the monolith segment of the Glen West core....189

Figure 5.7: Periodograms of spectral analysis of photograph and X-ray line-scans and cellulose oxygen isotope data from the monolith segment with confidence intervals....191

Figure 5.8: Comparison of 5-yr average image grey-value line-scans, oxygen isotope data, water table depth and volcanic eruptions (Swindles at al., 2007a, 2007b) and ^{14}C production rate (atoms/cm2/sec) record (Reimer et al., 2009) in time and depth scale....194

Figure 6.1: Cross-plots of $\delta^{18}O$ of precipitation with annual averages of air temperature from 1970-2007 at (A) Valentia Weather Station in Ireland and (B) at the Ottawa Airport Weather Station in Ottawa (GNIP: Global Network of Isotopes in Precipitation, 2001; Environment Canada, 2010)....213

LIST OF APPENDICES

Appendix A: X-ray images - Mer Bleue Bog core....................................217

Appendix B: Digital core surface photographs - Mer Bleue Bog core....................227

Appendix C: Radiocarbon ages for Mer Bleue Bog core -Chronos Laboratories, Belfast, Ireland..262

Appendix D: Radiocarbon ages for Mer Bleue Bog core -Univ. of Georgia, USA........263

Appendix E: Calibrated radiocarbon ages for Mer Bleue Bog core using CALIB5.0.2 (Reimer et al., 2004)..264

Appendix F: Coring strategy - Mer Bleue Bog Core..268

Appendix G: Sampling - Mer Bleue Bog Core...271

Appendix H: Cellulose $\delta^{18}O$ and oxygen concentration measurements from Mer Bleue Bog Core..277

Appendix I: X-ray image – Glen West Bog Monolith...279

Appendix J: Digital core surface photographs - Glen West Bog Monolith...............280

Appendix K: Cellulose $\delta^{18}O$ and concentration measurements - Glen West Bog Monolith 282

CHAPTER ONE

1. GENERAL INTRODUCTION

1.1 Background

Global climate change is considered to have a significant impact on our future civilization (IPCC, 1996). A warming of 0.5-1.5°C is projected for Canada during the next century (Bonsal et al., 2001; Zhang et al, 2000). However, the degree to which warming is due to anthropogenic or to natural causes is disputed (e.g., Jansen, 2007; Veizer, 2005). Consequently, the world climate research community is increasingly interested in understanding the history of regional climate variations to establish improved climate projections.

The instrumental record is inadequate for differentiating often centennial- to millennial-scale natural climate cycles from short-term anthropogenic trends. In particular little is known about the climate variability in eastern Canada before the 19th century. Therefore, a more complete understanding of intermediate and long-term climate oscillations and their relationship with short-term variations can only be achieved by turning to the geological record.

My thesis project has been designed to reconstruct the Holocene temperature record for eastern Canada throughout the last ~9200 years utilizing several research methods on a peat section at Mer Bleue Bog, near Ottawa, Ontario. Peat deposits may provide robust paleoclimate archives as they are potentially capable of preserving plants that are highly sensitive to the meteorological conditions in which they lived (e.g., Brenninkmeijer et al., 1982; Booth and Jackson, 2003). In this project, oxygen isotope analysis of peat cellulose, image analysis of peat sediment photographs and X-ray images, and time-series analysis of the data have been used to extract high-resolution paleotemperature proxy records, which were then compared with solar activity proxies and northern Hemisphere paleoclimate reconstructions. To test the validity of research methods and proxy records on a more global scale, a comparative study on a peat section in Glen West Bog, Northern Ireland has been carried out in a more maritime climate setting.

1.2 Thesis Presentation

This thesis is formatted for publication of its major findings as a set of four manuscripts to be published in peer-reviewed international journals. However, this format introduces some unavoidable repetition.

Each manuscript highlights different themes of the research.

Manuscript I (chapter II) provides a new understanding of cellulose oxygen isotopic variability ($\delta^{18}O_{cel}$) in various plant macrofossils, particularly *Sphagnum*, derived from a 6m succession of Holocene peat in Mer Bleue Bog, Ottawa, Ontario, Canada. Moreover, this manuscript demonstrates the potential of stable isotope analyses of selected peat constituents such as cellulose in paleoclimate research and test the statistical significance of differences in species-specific isotope signatures.

Manuscript II (chapter III) presents the first use of an oxygen isotope paleorecord from plant cellulose as a proxy for the paleotemperature history of the last ~9200 years in eastern Canada. In addition, this manuscript provides a radiocarbon dating-based age model of peat sedimentation in Mer Bleue Bog, which results in oxygen isotope and oxygen concentration records through time. The oxygen isotope record is discussed in terms of Holocene temperature fluctuation in eastern Canada, and compared with solar irradiance proxies, northern Hemisphere paleotemperature reconstructions and major climate stages in the North Atlantic region.

Manuscript III (chapter IV) applies a novel combination of time-series analysis, image analysis of digital core surface photography and X-ray scans, and cellulose oxygen isotope of the Mer Bleue Bog core to determine the driving forces for paleoclimate fluctuations over the last 9200 years in eastern Canada. Time-series (wavelet, spectral) analysis methods are explained in detail and applied to proxy records of the Mer Bleue section. Cyclic variations of ~80-2500 year wavelength, as well as other abrupt and gradual changes in the Mer Bleue records are evaluated for their significance and compared with the published solar irradiance reconstructions.

Manuscript IV (chapter V) applies the methods outlined in manuscript III (isotope, image and time-series analysis) to a 30 cm (~400 year) Mid-Holocene peat bog section from the Glen West Bog in Northern Ireland, which has an preexisting high-resolution age model. Cycles of 11-250 years and a climate-transition at ~2800 cal BP are recognized and discussed in the context of published palynological, water table and macrofossil records from this section, as well as North Atlantic climate reconstructions and solar irradiance proxy records.

1.3 Study Areas

The Mer Bleue Bog is located in the Eastern portion of the National Capital Region of eastern Canada at about 10 km from Ottawa, (Figure 1.1), which is characterized by a moderate continental climate with cold winters and hot summers (Environment Canada, 1990). Peatlands are wetlands that began developing during the early Holocene and are now widespread across North America and Eurasia (Gajewski et al., 2001). Canada has the largest area of peatlands in the world, covering 12 percent of the nation's land area (Tarnocai et al., 2002) (Figure 1.2), but only a few peatlands such as the Mer Bleue Bog are ombrotrophic.

Ombrotrophic bogs can become excellent paleoclimate archives, because all nutrients and the water supply come strictly from precipitation rather than from ground water or river runoff, thus their surface plant growth solely depends on the climate conditions. Ombrotrophic bog sections of Eastern Ontario and Southern Quebec have been investigated by several research teams in the last decade (Fraser et al., 2001; Frolking et al., 2002; Moore et al., 2002; Lafleur et al., 2003; Muller et al., 2003; Roulet et al., 2007; Frolking et al., 2010; Talbot et al., 2010), but none of these studies reconstructed the Holocene paleoclimate in eastern Canada.

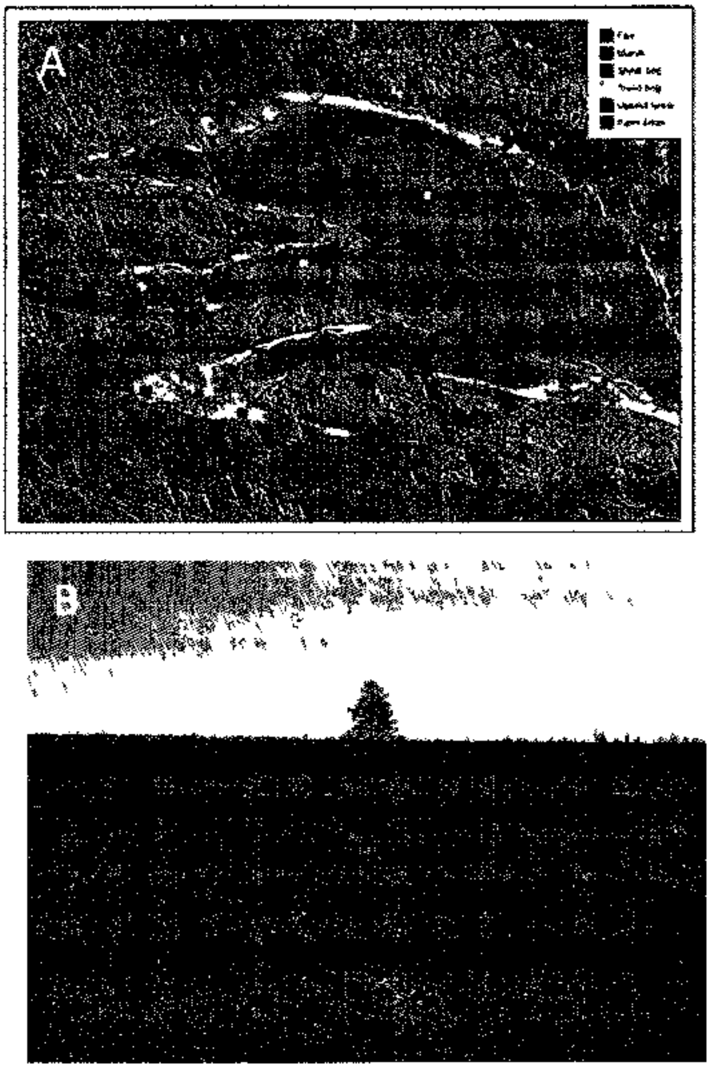

Figure 1.1: Mer Bleue Bog. A) The star shows the sampling site from which cores were retrieved (Touzi, 2007; Touzi et al., 2007). B) Mer Bleue Bog in spring season.

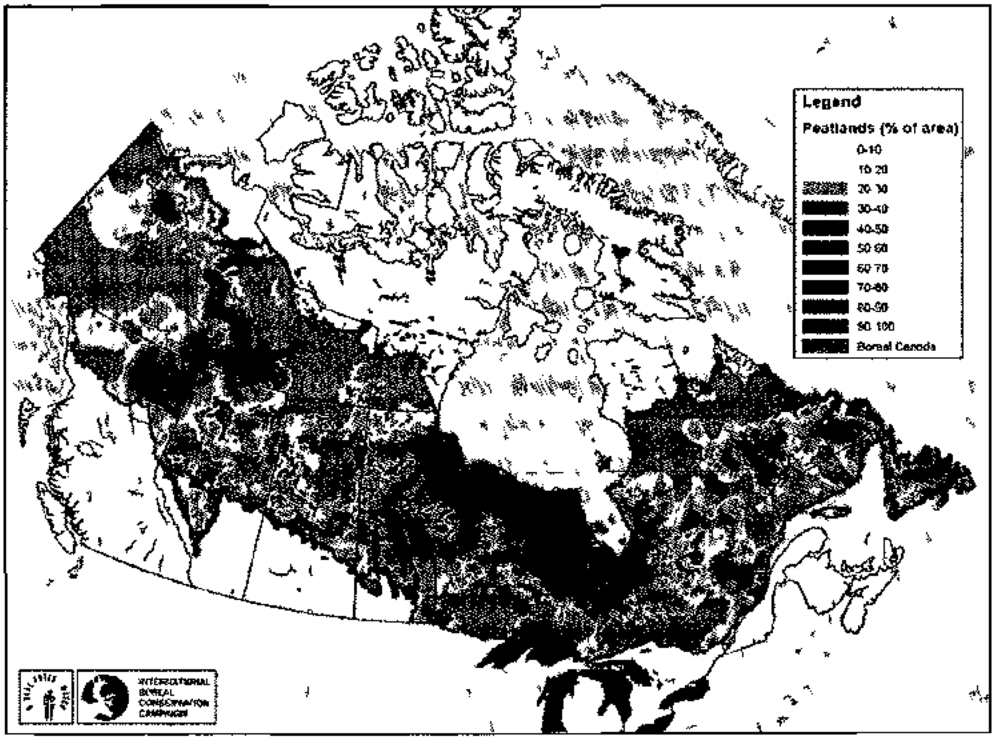

Figure 1.2: Peatland distribution in Canada (Tarnocai et al., 2002)

The Mid-Holocene peat section at Glen West Bog, Northern Ireland is located in a maritime climate setting with mild winters and warm summers. The peatlands in Northern Ireland have been studied intensively in order to reconstruct their water table and vegetation histories, but this is the first time that cellulose stable isotope and image analysis has been carried out in this region (Swindles et al., 2007a, 2007b; Plunckett and Swindles, 2008; Charman et al., 2009).

1.4 Objectives

The main objective of the present study is the reconstruction of the paleotemperature variability of the last ~9200 years in eastern Ontario based on cellulose oxygen isotopic data of peat core samples from Mer Bleue Bog, Ottawa. Moreover this study aims to determine the drivers of paleoclimate fluctuations in the region and detect cycles and trends of climate changes in eastern Ontario. Specifically, the project aims to:

1) Develop a comprehensive Holocene depositional and climatic history for eastern Ontario based on isotope geochemistry, sedimentology, cyclostratigraphy at Mer Bleue Bog;

2) Test the statistical significance of differences in species-specific cellulose isotope signatures by applying statistical techniques such as ANOVA (Davis, 2002) and therefore determine the most suitable plant macrofossils for cellulose oxygen isotope analyses and paleoclimate reconstruction.

3) Test and establish the validity of oxygen isotope measurements of different plant macrofossil species as paleotemperature proxies in different climate settings (continental: Mer Bleue Bog in Canada; and maritime: Glen West Bog in Northern Ireland).

4) Investigate the potential of image analysis techniques to identify paleoclimate-driven features in peat sedimentation in both the Glen West (Northern Ireland) and Mer Bleue (Canada) cores.

5) Recognize decadal- millennial-scale climate cycles and trends in the Holocene peat records archived in Mer Bleue Bog and Glen West Bog and compare them with patterns in solar- and cosmic-related records such as sunspot numbers (Solanki et al., 2004), solar irradiance (Bard et al., 2003); ^{14}C production rate (Reimer et al., 2009), and northern Hemisphere paleotemperature reconstructions (e.g., Moberg et al., 2005).

6) Combine isotopic, geochemical and sedimentological results in order to determine the climatic significance of observed depositional changes.

1.5 Methodology

In order to meet the objectives listed above, the following methods were used:

1) *Sample acquisition*: in March 2008 cores were retrieved at the Mer Bleue Bog with a Russian corer of ~5.5 cm core diameter to a depth where marine clay was reached (~6m depth = ~9,200 years ago). An additional ~30 cm core from the Glen West core

("Monolith"), previously investigated by Swindles et al., (2007a and 2007b) and Plunckett and Swindles (2008), has been studied using isotope geochemistry and image analysis. For details see chapters II and V.

2) *Lithological description*: the cores were examined visually in order to detect unconformities, changes in peat texture, sediment color using Munsell Rock Color Chart (Munsell Color Company, 1975), plant macrofossils, and other sedimentary features (chapter II).

3) *The chronology of the sequence*: the chronology of Mer Bleue core was based on ^{14}C age-dating of 10 peat samples collected from the Mer Bleue core and the first occurrence of *Ambrosia* pollen in the region. The ^{14}C ages were calibrated using the computer program CALIB5.0.2 (Reimer et al., 2004). For details see chapter III.

4) *Cellulose oxygen isotope analysis* of 257 plant macrofossil samples from Mer Bleue core was performed to provide a paleotemperature proxy record. Oxygen isotope analysis of 43 peat samples from the Glen West core "monolith" was conducted for comparison (chapters III, IV and V).

5) *Digital Core photography* was performed with a 6 Megapixel Sony camera with high-quality Zeiss lens (chapters IV and V).

6) *Digital X-ray image scanning* was performed with a medical image scanner for both the Mer Bleue and the Glen West cores. (chapters IV and V).

7) *Time-series analysis* such as spectral, and wavelet analysis (Appenzeller et al., 1998; Bolton et. al., 1995; Morlet et al., 1982) were applied to line-scans and isotope data in both time-scale and depth-scale to reconstruct paleotemperature records.

(a) *Wavelet analysis (WA)* was applied to detect trends, cycles and abrupt changes in the peat sedimentation pattern.

(b) Spectral analysis (SA) was used to detect stationary cycles and to determine confidence levels for these cycles using software package RedFit (Schulz and Mudelsee, 2002). SA was applied on geochemical and image linescan data after transferring the data into time-scale.

1.6 References

Appenzeller C., Stocker T.F., and Anklin, M., 1998. North Atlantic oscillation dynamics recorded in Greenland ice cores. *Science*, 282: 446-449.

Bard, E., Raisbeck, G., Yiou, F., and Jouzel, J., 2003. Reconstructed Solar Irradiance Data. IGBP PAGES/World Data Center for Paleoclimatology Data Contribution Series #2003-006. NOAA/NGDC Paleoclimatology Program, Boulder CO, USA.

Bolton, E.W., Maasch, K.A., and Lilly, J.M., 1995. A wavelet analysis of Plio-Pleistocene climate indicators: A new view of periodicity evolution. *Geophysical Research Letters*, 22: 2753-2756.

Bonsal, B.R., Zhang, X., Vincent, L.A., and Hogg, W.D., 2001. Characteristics of daily and extreme temperatures over Canada. *Journal of Climate*, 14: 1959-1976.

Booth, R.K., and Jackson, S.T., 2003. A high-resolution record of late-Holocene moisture variability from a Michigan raised bog, USA. *The Holocene*, 13: 863-876.

Brenninkmeijer, C.A.M., van Geel, B., and Mook, W.G., 1982. Variations in the D/H and 18O/16O ratios in cellulose extracted from a peat bog core. *Earth and Planetary Science Letters*, 61: 283-290.

Charman, D.J., Barber, K.E., Blaauw, M., Langdon, P.G., Mauquoy, D., Daley, T.J., Hughes, P.D.M., and Karofeld, E., 2009. Climate drivers for peatland palaeoclimate records. *Quaternary Science Reviews*, 28: 1811–1819.

Davis, J.C., 2002. Statistics and data analysis in Geology, 3rd edition, Wiley, New York, 637 pp.

Environment Canada, 1990. The Climates of Canada. Canadian Government Publishing Centre, Ottawa, 176 pp.

Fraser, C.J.D., Roulet, N.T., Moore, T.R., 2001. Hydrology and dissolved organic carbon biogeochemistry in an ombrotrophic bog. Hydrological Processes 15, 3151 – 3166.

Frolking, S., Roulet, N.T., Moore, T.R., Lafleur, P.M., Bubier, J.L., and Crill, P.M., 2002. Modeling the seasonal to annual carbon balance of Mer Bleue Bog, Ontario, Canada. *Global Biogeochemical Cycles,* 16(3): doi 10.1029/2001GB0011457.

Frolking, S., Roulet, N.T., Tuittila, E., Bubier, J.L., Quillet, A., Talbot, J., and Richard, P.J.H., 2010. A new model of Holocene peatland net primary production, decomposition, water balance, and peat accumulation. *Earth Systems Dynamics Discussions*, 1: 115–167.

Gajewski, K., Viau, A., Sawada, M., Atkinson, D., and Wilson, S., 2001. *Sphagnum* peatland distribution in North America and Eurasia during the past 21,000 years. *Global Biogeochemical Cycles*, 15(2): 297-310.

IPCC. 1996. Climate change 1995: The Science of climate change. In: Intergovernmental Panel on Climate Change. J.T. Houghton, L.G. Miro Filho, B.A. Callander, N. Harris, A. Kattenberg and K. Maskell (Eds), Cambridge University Press, Cambridge, 572 pp.

Jansen, E., Overpeck, J., Briffa, K.R., Duplessy, J.-C., Joos, F., Masson-Delmotte, V., Olago, D., Otto-Bliesner, B., Peltier, W.R., Rahmstorf, S., Ramesh, R., Raynaud, D., Rind, D., Solomina, O., Villalba, R., and Zhang, D., 2007. Palaeoclimate. In: Climate Change 2007: The Physical Science Basis. In: Contribution of Working Group I to the Fourth Assessment Report of the Intergovernmental Panel on Climate Change, In: Solomon, S., Qin, D, Manning, M, Chen, Z, Marquis, M, Averyt, K.B, Tignor M. Miller, H.L. (Eds). Cambridge University Press, Cambridge, United Kingdom and New York, NY, USA.

Lafleur, P.M., Roulet, N.T., Bubier, J.L., Frolking, S., and Moore, T.R., 2003. Interannual variability in the peatland-atmosphere carbon dioxide exchange at an ombrotrophic bog. *Global Biogeochemical Cycles*, 17(2): 1036: 5.1-5.13.

Mann, M.S., and Lees, J.M., 1996. Robust estimation of background noise and signal detection in climatic time series. *Climatic Change*, 33: 409-445.

Moberg, A., Sonechkin, D.M., Holmgren, K., Datsenko, N.M., and Karle´n, W., 2005. Highly variable northern Hemisphere temperatures reconstructed from low- and high-resolution proxy data. *Nature*, 433: 613– 617.

Moore, T.R., Bubier, J.L., Frolking, S.E., Lafleur, P.M., and Roulet, N.T., 2002. Plant biomass and production and CO2 exchange in an ombrotrophic bog. *Journal of Ecology,* 90: 25–36.

Morlet, J., Arehs, G., Fourgeau, I., and Giard, D., 1982. Wave propagation and sampling theory. *Geophysics*, 47: 203-236.

Muller, S.D., Richard, P.J.H., and Larouche, A.C., 2003. Holocene development of a peatland (southern Québec): a spatio-temporal reconstruction based on pachymetry, sedimentology, microfossils and macrofossils. *The Holocene*, 13: 649-664.

Munsell Color Company, 1975. Munsell Soil Color Charts. Munsell Color Company, MD, USA.

Plunkett, G.M., and Swindles, G.T., 2008. Determining the Sun's influence on Late Glacial and Holocene climates: a focus on climate response to centennial-scale solar forcing at 2800 cal. BP. *Quaternary Science Reviews*, 27: 175–84.

Reimer, P.J., Baillie, M.G.L., Bard, E., Bayliss, A., Beck, J.W., Bertrand, C.J.H., Blackwell, P.G., Buck, C.E., Burr, G.S., Cutler, K.B., Damon, P.E., Edwards, R.L., Fairbanks, R.G., Friedrich, M., Guilderson, T.P., Hogg, A.G., Hughen, K.A., Kromer, B., McCormac, F.G., Manning, S.W., Ramsey, C.B., Reimer, R.W., Remmele, S., Southon, J.R., Stuiver, M., Talamo, S., Taylor, F.W., van der Plicht, J., and Weyhenmeyer, C.E., 2004. IntCal04 Terrestrial radiocarbon age calibration, 26 - 0 ka BP. *Radiocarbon*, 46: 1029-1058.

Reimer P.J., Baillie M.G.L., Bard E., Bayliss A., Beck J.W., Blackwell P.G., Bronk Ramsey C., Buck C.E., Burr G.S., Edwards R.L., Friedrich M., Grootes P.M., Guilderson T.P., Hajdas I., Heaton T.J., Hogg A.G., Hughen K.A., Kaiser K.F., Kromer B., McCormac F.G., Manning S.W., Reimer R.W., Richards D.A., Southon J.R., Talamo S., Turney C.S.M, van der Plicht J., and Weyhenmeyer C.E., 2009. IntCal09 and Marine09 radiocarbon age calibration curves, 0–50,000 years cal BP. *Radiocarbon*, 51(4): 1111–50.

Roulet, N.T., Lafleur, P.M., Richard, P.J.H., Moore, T.R., Humphreys, E., and Bubier, J.L., 2007. Contemporary carbon balance and late Holocene carbon accumulation in a northern peatland. *Global Change Biology*, 13: 397–411.

Schulz, M., and Mudelsee, M., 2002. REDFIT: estimating red-noise spectra directly from unevenly spaced paleoclimatic time series. *Computers & Geosciences*, 28: 421–426.

Solanki, S.K., Usoskin, I.G., Kromer, B., Schüssler, M., and Beer. J., 2004. An unusually active Sun during recent decades compared to the previous 11,000 years. *Nature*, 431: 1084-1087.

Swindles, G.T., Plunkett, G., and Roe, H.M., 2007a. A multi-proxy climate record from a raised bog in County Fermanagh, Northern Ireland: a critical examination of the link between bog surface wetness and solar variability. *Journal of Quaternary Science*, 22: 667–679.

Swindles, G.T., Plunkett, G., and Roe, H.M., 2007b. A delayed climatic response to solar forcing at 2800 cal. BP: multi-proxy evidence from three Irish peatlands. *The Holocene*, 17: 177–82.

Talbot,J., Richard, P.J.H., Roulet, N.T., and Booth, R.K., 2010. Assessing long-term hydrological and ecological responses to drainage in a raised bog using paleoecology and a hydrosequence. *Journal of Vegetation Science*, 21: 143-156.

Tarnocai, C., Kettles, I.M., and Lacelle, B., 2002. Peatlands of Canada Database. Geological Survey of Canada, Open File 4002.

Touzi, R., 2007. Target scattering decomposition in terms of roll invariant target parameters. *IEEE TGRS*, 45: 73-84.

Touzi, R., Deschamps, A., and Rother, G., 2007. Wetland characterization using polarimetric Radarsat-2 capability. *Canadian Journal of Remote Sensing*, 33: S56–S67.

Veizer, J., 2005. Celestial Climate Driver: A Perspective From Four Billion Years Of The Carbon Cycle. *Geoscience Canada*, 32: 13-30.

Zhang, X, Vincent, L.A., Hogg, W.D., and Niitsoo, A., 2000. Temperature and precipitation trends in Canada during the 20th century. *Atmosphere-Ocean*, 38: 395-429.

CHAPTER TWO

2. INFLUENCE OF CELLULOSE OXYGEN ISOTOPE VARIABILITY IN SUB-FOSSIL *SPHAGNUM* AND PLANT MACROFOSSIL COMPONENTS ON THE RELIABILITY OF PALEOCLIMATE RECORDS AT THE MER BLEUE BOG, OTTAWA, ONTARIO, CANADA.

2.1 Abstract

This study provides a new understanding of oxygen cellulose ($\delta^{18}O_{cel}$) isotopic variability in various plant macrofossils, particularly *Sphagnum*, derived from an ~ 9200 years succession of Holocene peat in Mer Bleue Bog, Ottawa, Ontario, Canada. The significance of $\delta^{18}O_{cel}$ isotopic variation, commonly used as a proxy of paleotemperature and paleoprecipitation, was investigated between; 1) *Sphagnum* and the other plant macrofossils down core, and 2) *Sphagnum* species within and between samples.

The most common *Sphagnum* species encountered was *S. magellanicum* von Bridel, 1798 with lesser amounts of *S. capillifolium* (Breutel) Steudel, 1824, *S. fuscum* Klinggräff, 1872 and *S. angustifolium* Jensen, 1896. Results of this study show that there is a statistically significant offset in $\delta^{18}O_{cel}$ isotopic values obtained from *Sphagnum* in comparison with values obtained from other plant macrofossils, particularly rhizomes.

The $\delta^{18}O_{cel}$ isotopic offset between *Sphagnum* specimens from the same core horizons, irrespective of the species analyzed, was statistically insignificant with a <0.3 ‰ average difference. These results indicate that $\delta^{18}O_{cel}$ isotopic analysis of bulk peat material without taking into account the potentially significant $\delta^{18}O_{cel}$ signatures variation between the *Sphagnum* and other plant macrofossils could result in erroneous paleoclimate reconstructions.

Keywords: isotopes, oxygen, ombrotrophic bog, Sphagnum, cellulose, paleoclimatology.

2.2 Introduction

Proxy-derived reconstructions of past climates result in a greater understanding of the range of natural variability within present-day climatic zones and permits the development of better-informed predictions of potential future climatic trends. Analyses of peat deposits are particularly useful in this context as peat deposits have long been known to be an ideal archive of paleoclimatic variation (e.g., Brenninkmeijer et al., 1982; Francey and Farquhar, 1982; O'Leary et al., 1986; Aucour et al., 1996; Anderson et al., 1998).

Plant cellulose from these bog environments is commonly used as a paleoclimate proxy because it is amongst the most isotopically stable chemical compounds known, even under conditions of partial decomposition (Epstein et al., 1976, 1977; Feng et al., 1993; Schleser et al., 1999; Jędrysek and Skrzypek, 2005). For example, plant organic matter (i.e. bulk peat or bulk *Sphagnum*) is comprised primarily of cellulose (15%-50%), hemicellulose (10%-40%), lignin (5%-30%), proteins (2%-15%), and various lipids (Haider, 1996).

Several studies carried out on peat bog deposits have shown a strong relationship between plant cellulose isotopic signatures, and temperature and/or humidity (e.g., DeNiro and Epstein, 1979, 1981; Edwards et al., 1985; Sternberg et al., 1986; Sukumar et al., 1993; White et al., 1994). Interpretation of $\delta^{18}O_{cel}$ isotope signatures derived from the uppermost living part of the peat-bog (acrotelm) in ombrotrophic bog settings suggest that the source water utilized by plants during cellulose synthesis records the isotopic signature of meteoric water (Dansgaard, 1964; Rozanski et al., 1993; Daley et al., 2009).

As the $\delta^{18}O$ of precipitation at mid- to high latitudes covaries with local air temperature (Dansgaard, 1964; Rozanski et al., 1993; Fricke and O'Neil, 1999) several studies have concluded that analysis of $\delta^{18}O_{Cel}$ from *Sphagnum* in particular provides one of the most sensitive and reliable proxies for paleo-temperature reconstruction in ombrotrophic bog sections (Libby et al., 1976; Barbour et al., 2001; Taylor, 2008; Daley et al., 2009, 2010). This is because *Sphagnum* with its lack of roots, functioning guard cells, vascular tissues, and the simplicity by which it incorporates meteoric water into cellulose, is characterized by growth that can be directly linked to the isotopic composition of growing-season precipitation. As result, only an insignificant change in isotopic signature occurs between source water $\delta^{18}O$ and it's accumulation in *Sphagnum* $\delta^{18}O_{Cel}$ (Ménot-Combes et al., 2002; Zannazzi and Mora, 2005; Daley et al., 2009).

Paleotemperature reconstructions based on the bulk peat have also been carried out (Hong et al., 2001, 2002). However, concerns have been raised that $\delta^{18}O$ signatures obtained from bulk peat, which contains a mixture of cellulose from both vascular and non-vascular plant and other organic material derived from partly decayed plant species, might be significantly different from the $\delta^{18}O_{Cel}$ signatures obtained from *Sphagnum* cellulose alone due to diagenetic effects. This is because only the cellulose would remain largely non-altered by the effects of burial and humification over time (Ménot and Burns, 2001; Pancost et al., 2003).

A number of studies have focused on investigating the relationship between climate parameters and modern *Sphagnum* $\delta^{18}O_{Cel}$ signatures (Ménot and Burns, 2001; Ménot-Combes et al., 2002; Zanazzi and Mora, 2005; Loader et al., 2007; Skrzypek et al., 2007a, 2007b; Moschen et al., 2009). Despite this research determination, *Sphagnum* $\delta^{18}O_{Cel}$ has not yet been precisely calibrated to temperature (e.g., Epstein et al., 1976; Feng et al., 1993; Schleser et al., 1999; Jędrysek and Skrzypek, 2005). More recently Moschen et al. (2009) investigated the potential use of S*phagnum* $\delta^{18}O_{Cel}$ as a paleoclimate proxy. An analysis of cellulose extracted from both *Sphagnum* branches and stem sections was carried out on specimens from a 4000 year old peat, obtained from the Westeifel volcanic field in Germany. The results of this study revealed that there was a significant isotopic offset between *Sphagnum* branches and stem sections (1.5‰ for carbon and 0.9‰ for oxygen). An additional interesting outcome of the Moschen et al (2009) study was that the stable carbon isotopic offset between branches and stem sections decreased with increasing age of the plant material. However, the oxygen isotopic offset is less pronounced but the remained consistent in time. Questions raised by the outcome of the research of Moschen et al. (2009) as well as the studies outlined above include a quantitative assessment of the relationship between the variation in plant $\delta^{18}O_{Cel}$ and individual plant macrofossils with depth, and whether there is an offset between stable isotope values between the various *Sphagnum* species.

To address these issues considerable effort has been expended in this study to ensure that plant macrofossil species were isolated and properly identified, particularly as the research involves comparisons between *Sphagnum* and other plant macrofossils, as well as between different *Sphagnum* species within and between samples.

The purpose of this study is to; 1) provide a new understanding of $\delta^{18}O_{Cel}$ variability in peat plant macrofossils in general and in *Sphagnum* in particular with an aim to improve sampling strategies, and 2) further quantify the potential of stable isotope analyses of selected peat constituents such as cellulose in paleoclimate research. The inter- and intra-plant $\delta^{18}O_{Cel}$ variability is investigated to determine if there is a significant difference in $\delta^{18}O_{Cel}$ values between; 1) *Sphagnum* and the other plant macrofossils down core, and 2) *Sphagnum* species within and between samples.

2.3 Geographic and Geological Setting

Mer Bleue Bog is a designated Provincial Conservation Area located in the eastern portion of the National Capital Region of Canada within the city limits of Ottawa, Ontario (45.41°N latitude, 75.48°W longitude, 69 m above mean sea level). The east-west oriented and oval shaped bog encompasses ~28 km^2, and is comprised of three separate lobes (Figure 2.1). Deglaciation in the area of Mer Bleue Bog occurred ~13,200 years ago. This part of the lower Ottawa River lowlands was then inundated by post-glacial Lake Iroquois and subsequently by the Champlain Sea marine incursion, which resulted in the deposition of laminated silt and clay over sandy, silty gravel, and limestone (Anderson, 1988; Roulet et al., 2007). An extensive postglacial channel system was carved through the area as a result of fluvial outbursts of the Ottawa River during the establishment of the early upper Great Lakes between 12,000 and 9500 years ago.

Isostatic rebound resulted in a replacement of marine conditions by fresh water in the basin by ~ 10,600 years ago (Lampsilis Lake phase, Elson, 1969). The present-day Mer Bleue peatland lies within a now abandoned postglacial channel of the Ottawa River that was eroded into the floor of the Champlain Sea basin. The peatland formed over the past 8400 years, initially as fen and transitioning to a bog phase by ca. 7100-6800 cal. years before present (Auer, 1930; Mott & Camfield, 1969; Roulet et al., 2007). The modern Mer Bleue Bog is characterized by peat depths varying from 6m near the center, decreasing to 0.3m at the margins (Joyal, 1970; Roulet et al., 2007).

Mer Bleue Bog is a rare domed ombrotrophic bog, dominated by *Sphagnum*, where all nutrients and water supply derive strictly from precipitation rather than from ground water or river runoff. During the winter season, Mer Bleue Bog is completely frozen and often completely covered by snow, although the frost line only extends down a few cm below the surface. During the spring to fall growing season fast-growing *Sphagnum*

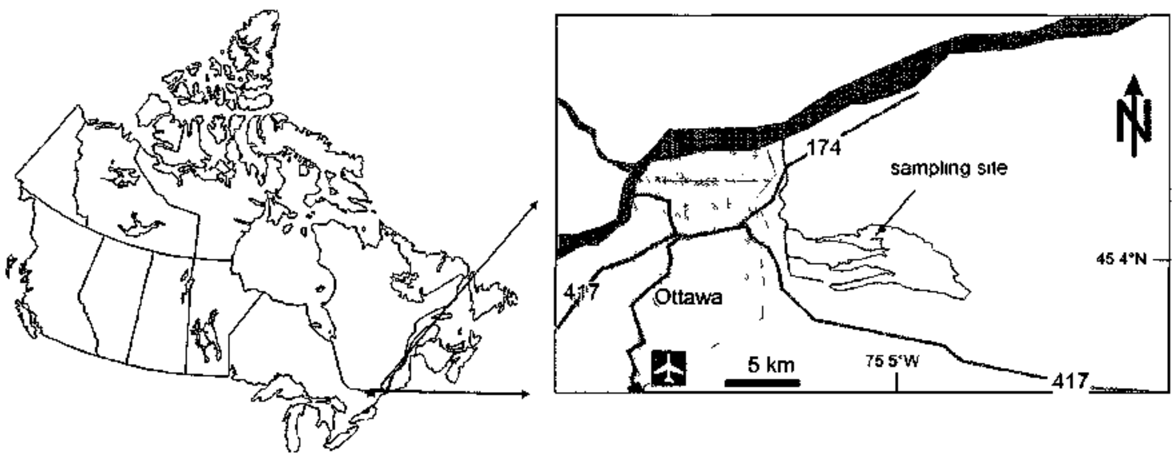

Figure 2.1: Location map of the Mer Bleue Bog, Ottawa, Ontario in eastern Canada. Asterisk marks the sampling site at the northwestern arm of Mer Bleue.

dominates the central part of the bog together with cotton grasses, and minor occurrence of cranberries and blueberries. The edge of the bog is also dominated by *Sphagnum* and other plants such as pitcher plants, wild orchids, and sundews. The overall bog surface has a hummock–hollow microtopography with both hummocks and hollows being primarily covered by *Sphagnum* mosses (Roulet et al., 2007). The margins of the Mer Bleue Bog are very wet and are characterized by the dominance of aquatic plants. These plants include *Potamogeton ssp.* (pond weed), *Nuphar ssp.* (yellow water lily), *Nymphea ssp.* (white water lily), *Typha spp.* (cattail), *Scirpus spp.* (bulrush), and *Ranunculus ssp.* (buttercup).

Hummock-forming *Sphagnum* species are mostly *Sphagnum fuscum* Klinggräff, 1872 and *Sphagnum capillifolium* (Breutel) Steudel, 1780 whereas in the hollows *Sphagnum angustifolium* Jensen, 1890 and *Sphagnum magellanicum* von Bridel, 1798 are most common.

It is often difficult to differentiate *Sphagnum* species, particularly down-core. However, there are characteristic features that make it easier to identify individual species. *Sphagnum magellanicum* is the dominant *Sphagnum* species in Mer Bleue Bog. It is characterized by a very stiff stem, many large fascicles, a prominent capitulum, and is deep red in colour. *Sphagnum capillifolium* is a smaller plant with tightly packed fascicles. It has a very large capitulum and is bright red in colour. *Sphagnum fuscum* generally occupies the driest area of the bog and occurs on the top of large hummocks. *Sphagnum fuscum* is small, with a flat capitulum, and is dark brown in colour. *Sphagnum* *angustifolium*, which can grow submerged, is small, often more compact than the other species and is characterized by a greenish colour.

2.4 Field Sampling & Material Collection

Cores used in the present study were collected in March 2008 using a Russian Auger corer from close to the center of Mer Bleue Bog at N45°24.653', W75°31.064' adjacent to the coring location of Roulet et al. (2007). After clearing 70 cm of snow cover cores were collected very near each other at the top of a very low relief hummock in an overall lawn-like area to minimize complications arising from marginal variation in the water table. Coring protocol when using a Russian Auger in bog settings stipulates that each core be comprised of offsets collected from two different holes to ensure complete recovery of the section (e.g. Jowsey, 1966). To meet the sampling requirements of this research triplicate cores were collected, which required extraction of core intervals from six closely spaced holes. The Russian corer used permitted the retrieval of 50 cm long by 5.5 cm diameter cores. Core overlap was 20 cm through the uppermost 3.5 m of the core and 10 cm through the lower 2.5 m of the core for a complete recovery of ~6 m of sediment, terminating in the uppermost few cm of the underlying Champlain Sea marine clay deposits (Figure 2.2). Retrieved cores were carefully covered in plastic wrap, secured in labelled plastic half-tubes, and stored at 4°C in a core storage facility at Carleton University. The cores were subsequently logged, photographed and X-rayed to identify any sedimentary structures. High resolution subsampling (i.e., 1 cm thick slices) was then carried-out at 2 cm intervals in preparation for microscopy and geochemical analyses (Appendices F and G).

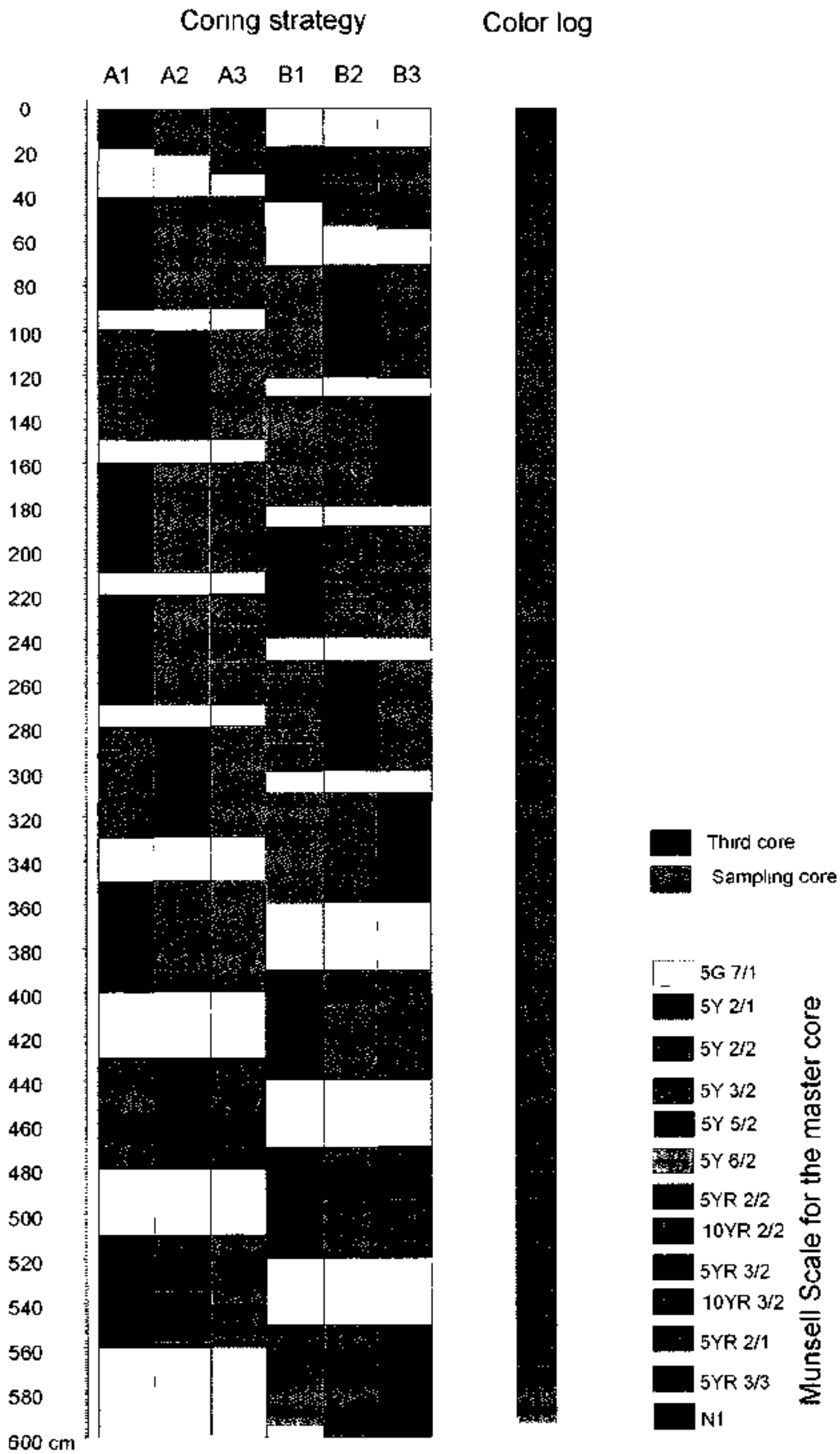

Figure 2.2: Coring strategy: (2 sets of triplicate cores of 50cm length and ~5.5cm diameter, sets with 20 cm (upper 350cm) and 10cm (lower 250cm) overlap. Best preserved core used for non-destructive lithological description and archiving ("master core"), sampling core used for geochemical analyses. Rock color code following Munsell Chart (Munsell, 1975).

2.5 Methods

2.5.1 Plant macrofossils separation

Peat samples were gently heated in a 5% KOH solution for ~30 minutes to dissolve humic and fulvic acids. The samples were then gently disaggregated on a 125 μm sieve using deionized water. Isolated plant remains on the sieve were transferred to vials and kept immersed in distilled water to avoid damage and disintegration resulting from desiccation. The suspended plant macrofossil remains were examined using an Olympus SZH-1 stereo microscope and identified using several illustrated moss identification guides (Smith, 2004; Grosse-Brauckmann 1972, 1974; Lévesque et al., 1988).

2.5.2 Cellulose oxygen isotope analytical technique

For $\delta^{18}O_{Cel}$ analyses, plant macrofossils including separated stem sections of *Sphagnum* were hand-picked from a petri-dish under a binocular microscope and placed in porcelain crucibles. Where possible pairs of samples from different *Sphagnum* species from within the same samples were selected. The plant macrofossil-bearing porcelain crucibles were then placed in an oven and dried at ~50°C for 24 hours. The samples were then powdered, weighed, labelled, placed in small plastic vials, and sent to the University of Saskatchewan for $\delta^{18}O_{Cel}$ analysis.

At the University of Saskatchewan isotope laboratories cellulose samples were baked at 60°C in a vacuum oven for 2 hours to drive off any remaining moisture, then immediately transferred and flushed in a zero blank autosampler. Samples were then analyzed using a Thermo Finnigan TC/EA coupled to a Conflo III and Delta Plus XL mass spectrometer.

Prior to analysis samples were dropped under a helium atmosphere into a carbon furnace and pyrolyzed at 1450°C to form hydrogen and/or carbon monoxide gases. These gases were then carried in a helium stream to a GC column held at 100°C to separate the gases before being diluted in the Conflo III and passed to the mass spectrometer for analysis. Isotope ratios were blank corrected and reported in per mil notation relative to the VSMOW-VSLAP scale. In-house oxygen standards were calibrated against international standards USGS-34 ($\delta^{18}O$ = -27.9‰ VSMOW) and USGS-35 ($\delta^{18}O$ = 57.5‰ VSMOW). An intermediate international standard, IAEA-NO3, gave the result $\delta^{18}O$ = 25.53 ± 0.27‰ VSMOW (n = 23) during calibration of the in-house standards compared to the accepted value of $\delta^{18}O$ = 25.6 ± 0.4‰ VSMOW. Two in-house standards were subsequently used to set up a calibration line, and a third was used to monitor the accuracy of data obtained. The accuracy of $\delta^{18}O$ data was ±0.11‰ (n = 25). The %O measurements had an accuracy of ±0.5%. The actual sampling errors may have been greater due to heterogeneity, but this factor would only have been detectable and corrected for through analytical repetition.

2.5.3 Analysis of variance (ANOVA)-method

Single factor ANOVA (e.g., Davis, 2002) was applied to test the NULL hypothesis (H_0) that $\delta^{18}O_{cel}$ variance between groups of plants is insignificant at confidence level α=0.05, which equals 95% confidence level as compared to the variability within the specific plant groups through depth. Single factor ANOVA uses only one factor in k levels i=1, 2,..k. Each level i may have different numbers of observations (= repetitions) n_i. The total number of observations N is defined by:

$$N = \sum_{i=1}^{k}\sum_{j=1}^{n_i} \tag{1}$$

The model for the independent variable to be tested is defined by: $x_{ij}=\mu+\alpha_i+\varepsilon_{ji}$ where μ is the mean of all observations, α is the effect of known factor(s) (i.e., = the variability between each level of factor), and ε is the random error. The source of variation is represented by the SUM of SQUARES (SS) where SST (total) = SSG (between levels) + SSE (within levels).

$$SST = \sum_{i=1}^{k}\sum_{j=1}^{n_i}(x_{ij}-\bar{x})^2 = \sum_{i=1}^{k}\sum_{j=1}^{n_i}(x_{ij})^2 - N\bar{x}^2 \tag{2}$$

$$SSG = SS_{\alpha} = \sum_{i=1}^{k}\sum_{j=1}^{n_i}(\bar{x}_i-\bar{x})^2 = \sum_{i=1}^{k} n_i(\bar{x}_i-\bar{x})^2 \tag{3}$$

$$SSE = \sum_{i=1}^{k}\sum_{j=1}^{n_i}(x_{ij}-\bar{x}_i)^2 \tag{4}$$

Where $\bar{x}_i$ refers to the mean values for the observations for each level *i*. Then, the means of Squares (MS) are calculated by MStotal = SStotal/DFtotal with MSG (between levels) = SSG/DFG, MSE (within levels) = SSE/DFE with DF referring to"degrees of freedom". Finally, the F-test can be used to determine the equality of variances and the F_{crit} (F critical) is provided by probability distribution called the F-distribution (e.g. Davis, 2002). The test value F is calculated by F_{calc} = MSG/MSE. If $F_{calc} >= F_{crit}$ than H_0 is rejected at the confidence level= 100 % (1-*p*). The NULL hypotheses (H_0) were tested to determine that all means of $\delta^{18}O_{cel}$ values being compared between different plant macrofossils were statistically the same.

2.6 Results

2.6.1 Core sedimentology

The Mer Bleue Bog sequence consists predominantly of well humified herbaceous peat, with abundant remains of *Sphagnum* mosses as well as the remains of monocotyledon rhizomes. The degree of decomposition within the Mer Bleue core sequence was estimated in the laboratory by evaluating the change in peat color and compaction degree with the naked eye in conjunction with the Munsell soil color chart (Munsell, 1975). As would be expected the degree of decomposition of the peat sediments increased with depth (Figure 2.2).

Recovered core material was primarily comprised of relatively fresh and uncompacted *Sphagnum* material within the top 25 cm of the core, which consist of poorly decayed and weakly compacted *Sphagnum*-dominated plant material in the oxic zone (acrotelm). Below 25 cm depth the peat becomes anaerobic (catotelm) until a depth of 73.5 cm, where the peat is fully compacted.

The interval from 73.5 to 320 cm depth consisted of compacted and decomposed peat sediments, primarily *Sphagnum* mosses. Throughout the upper 320 cm, *Sphagnum* was the dominant plant macrofossil making up ~ 80% of the core. *Sphagnum* species observed through this interval consist of S. *fuscum*, S. *magellanicum*, S. *capillifolium*, S. *angustifolium* and minor occurrence of S. *papillosum* Lindberg, 1872. Fen-deposition changes gradually to bog-deposition over a short depth interval (~330-320cm depth). The ~330-320 cm interval was made up of transitional bog and fen deposits and peat formed under fully fen conditions characterized the core from ~330-500 cm depth interval. Peat sediments deposited below 330 cm were decomposed and less compacted than the peat higher in the section, and was comprised of *Sphagnum*, rhizomes, wood fragments, roots, networks of pteridophytae, seeds, charcoal, unknown reddish-brown leaves and other minor plant macrofossil components. The lowermost meter of the core (~500-600 cm) was characterized by several alternating bands of fine peat and marine clay, with a fen-marine clay transitional zone being found between ~500-590 cm and fully marine clays being found from ~590-600 cm.

The plant macrofossil assemblages observed in the Mer Bleue Bog cores were characterized by considerable variation with depth and permitted recognition of twelve distinct macrofossil biofacies (Figure 2.3):

1. Coarse-grained *Sphagnum*-dominated facies (up to 90%);

2. *Sphagnum*-dominant facies (up to 80%) with less than 20% wood fragments, charcoal, rootlets, and rhizome;

3. Charcoal-rich facies (up to 4%);

4. Rhizome-dominant facies (up to 90%);

5. Rhizome-dominant facies with dark rootlets and root networks of pteridophytae;

6. Alternating bands of *Sphagnum*-rich layers and rhizome-rich layers;

7. *Sphagnum*-dominant facies with root networks of pteridophytae;

8. Rhizome-dominant facies (<70%) with up to 20% root networks of pteridophytae and unidentified reddish-brown leaves, minor to rare *Sphagnum* (5%), and roots + wood fragments (all about 15%);

9. *Sphagnum*-dominant facies (up to 70%) with up to 20% root network of pteridophytae and unidentified reddish-brown leaves, and minor to rare rhizome + roots + wood fragments (all about 15%);

10. > 30% root networks of pteridophytae and unknown reddish-brown leaves;

11. Marine clay-dominant facies (more than 60%) with minor tissue remains of herbacae and no *Sphagnum*;

12. Tissue remains of herbacea-dominant facies (more than 60%) with marine clay (less than 40%), minor rootlets, and no *Sphagnum*.

2.6.2 Cellulose oxygen isotope composition

Cellulose $\delta^{18}O$ signature determination was based mainly on an analysis of *Sphagnum* macrofossils. Other plant macrofossil $\delta^{18}O_{cel}$ were analysed for comparison with the *Sphagnum* $\delta^{18}O_{cel}$ results from the same horizons and on their own in some sections of the core where *Sphagnum* was absent (Figure 2.4; Table 2.1).

The results show that $\delta^{18}O_{cel}$ values for *Sphagnum* vary from ~ 25‰ at 338 cm depth to ~14‰ at 242 cm depth with a standard deviation of 1.47 (n=203). The $\delta^{18}O_{cel}$ values are characterized by a generally decreasing trend from ~19±1.2‰ (1σ, 11 samples) at 0-20 cm depth to ~16‰±0.97 (1σ, 4 samples) at 480-520 cm depth (Figure 2.4). The values

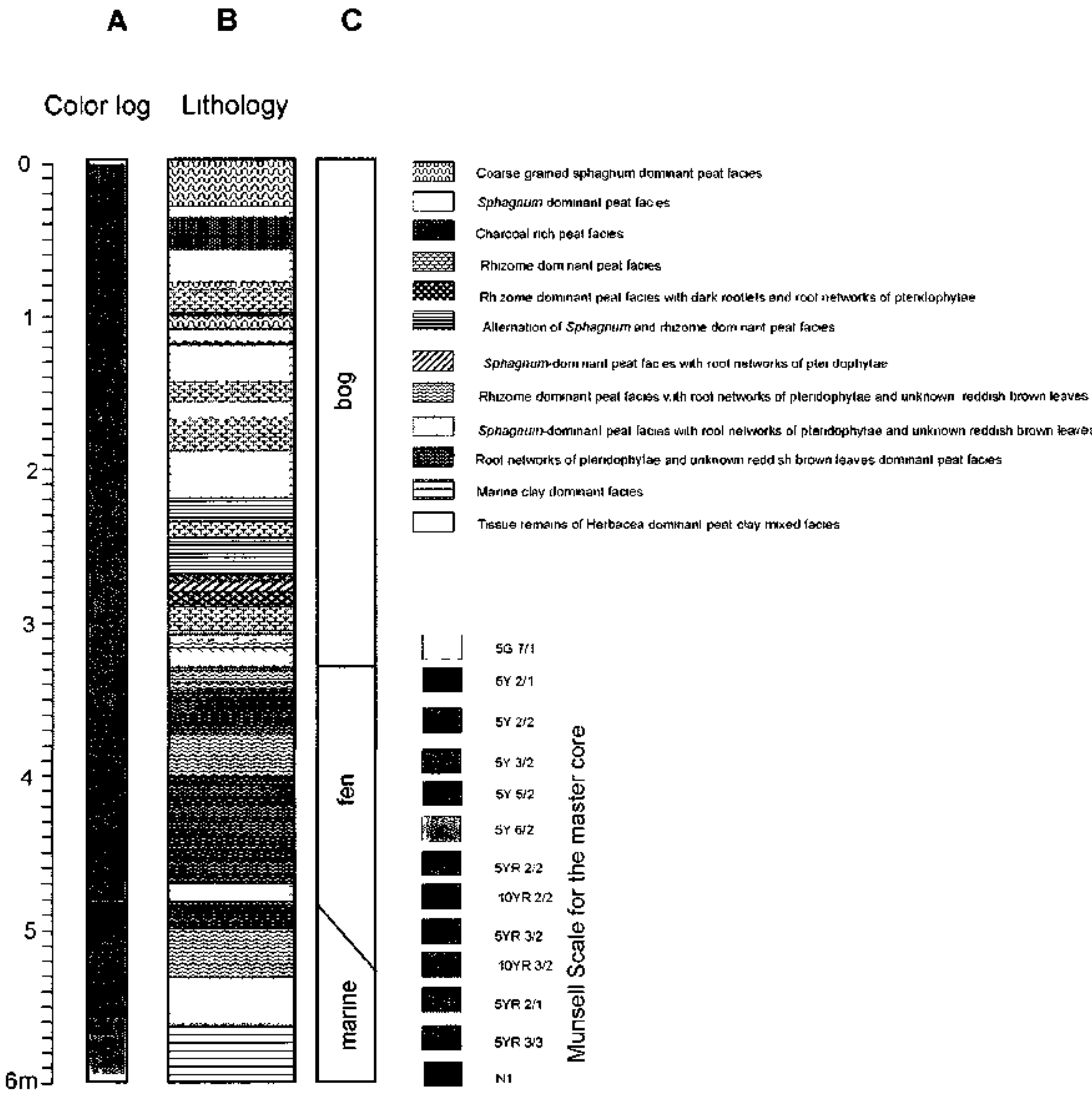

Figure 2.3: Mer Bleue core sedimentology: A: Peat color, B: Lithology, C: Depositional environments

obtained from the plant macrofossil species analyzed had $\delta^{18}O_{cel}$ values ranging from ~7 to 26‰, but were generally characterized by lower $\delta^{18}O_{cel}$ values than obtained for *Sphagnum* at the same core intervals. The plant oxygen percentage (O%) ranged from ~20% to 50% with a standard deviation of 4.24 (n=254) through the 6 m section and showed similar trends and differences between *Sphagnum* and other plant macrofossils (Figure 2.4).

2.6.3 Results of analysis of variance (ANOVA)

Eleven $\delta^{18}O_{cel}$ analyses obtained from rhizomes were compared with a single *Sphagnum* species (*S. fuscum*) within the same sample and from different depths. Nineteen $\delta^{18}O_{cel}$ analyses from rhizomes were compared to all other *Sphagnum* species. Similarly $\delta^{18}O_{cel}$ analyses obtained for five co-occurrences of *S. capillifolium* and *S. fuscum* and six co-occurrences of *S. magillanicum* with *S. fuscum* were statistically tested.

Results of ANOVA (Table 2.2) indicate that the different *Sphagnum* species have statistically similar $\delta^{18}O_{cel}$ values where they co-occur. The average difference was 0.18‰ between *S. capillifolium* and *S. fuscum* (18.14-17.96‰) and 0.06‰ (17.64-17.58‰) between *S. magellanicum* and *S. fuscum*. In contrast the $\delta^{18}O_{cel}$ values obtained for rhizomes were characterized by average values of ~16.7‰, more than 1.5‰ below the average *Sphagnum* sp. values obtained (~18.3‰; Table 2.2). To put these results in context the variability between rhizome and *Sphagnum* $\delta^{18}O_{cel}$ results within samples was

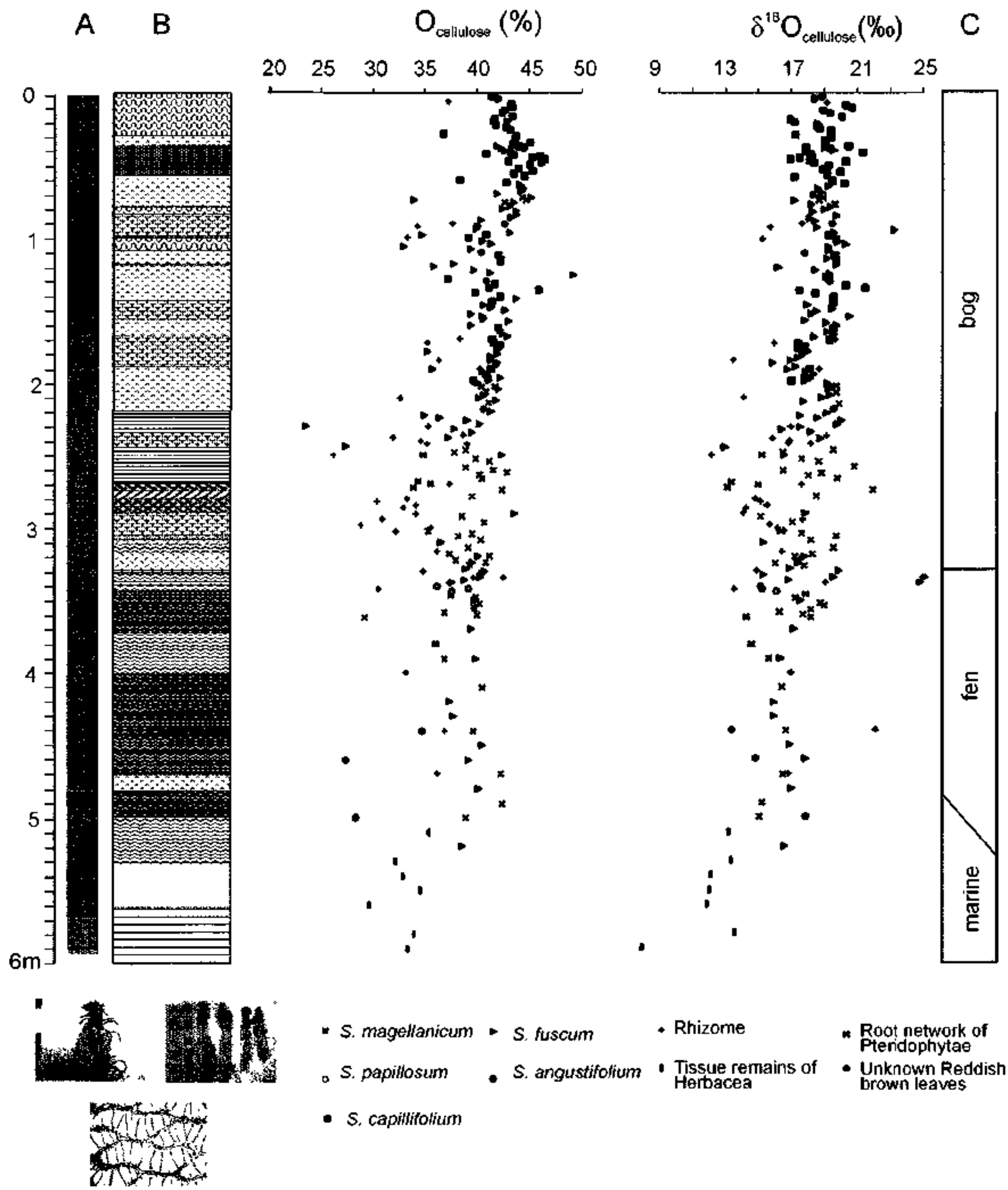

Figure 2.4: Oxygen concentration and oxygen isotope data of cellulose from different plant matter of the Mer Bleue Bog core. For details on lithology and peat color see Figure 2.3.

Table 2.1: Oxygen isotope ratio and oxygen concentration of plant cellulose from Mer Bleue Bog, Ottawa, Ontario

Sample ID	Depth (cm)	%O	$\delta^{18}O$ (‰, VSMOW)	Macrofossils Taxa	Sample ID	Depth (cm)	%O	$\delta^{18}O$ (‰, VSMOW)	Macrofossils Taxa
1yss	2	41 4	18 81	S *capillifolium*	98yss	196	41 0	17 74	S *capillifolium*
2yss	4	42 0	18 32	S *capillifolium*	99bss	198	41 2	17 80	S *fuscum*
3r	6	37 3	19 14	Rhizome	99yss	198	39 7	16 94	S *capillifolium*
4yss	8	43 3	20 22	S *capillifolium*	100	200	40 0	19 11	S *fuscum*
5yss	10	43 4	20 64	S *capillifolium*	101dbss	202	41 8	19 36	S *magellanicum*
6yss	12	42 7	18 88	S *capillifolium*	101 dbss repeat	202	40 5	19 72	S *magellanicum*
7yss	14	42 4	19 28	S *capillifolium*	102bss	204	42 1	19 18	S *fuscum*
8yss	16	43 4	20 05	S *capillifolium*	103dbss	206	40 9	19 68	S *magellanicum*
9yss	18	41 7	16 91	S *capillifolium*	104bss	208	40 6	19 26	S *fuscum*
10yss	20	41 7	17 13	S *capillifolium*	105bss	210	40 1	18 79	S *fuscum*
10bss	20	42 9	18 58	S *fuscum*	105r	210	32 7	14 05	Rhizome
11yss	22	41 9	18 48	S *capillifolium*	106bss	212	41 9	17 72	S *fuscum*
12yss	24	42 8	18 64	S *capillifolium*	107dbss	214	41 1	19 81	S *magellanicum*
13yss	26	43 2	19 34	S *capillifolium*	109bss	218	40 7	19 53	S *angustifolium*
14yss	28	38 8	17 17	S *capillifolium*	110bss	220	41 4	19 11	S *fuscum*
15yss	30	43 6	19 36	S *capillifolium*	111bss	222	35 0	17 49	S *fuscum*
16yss	32	43 7	18 95	S *capillifolium*	112bss	224	38 4	18 58	S *fuscum*
17yss	34	45 1	19 08	S *capillifolium*	113Lbss	226	39 1	20 00	S *angustifolium*
Sb1yss	35	43 6	18 99	S *capillifolium*	114bss	228	40 3	19 74	S *fuscum*
18yss	36	43 4	20 43	S *capillifolium*	115bss	230	23 7	17 55	S *fuscum*
Sb7yss	37	44 0	17 82	S *capillifolium*	115r	230	35 4	16 95	Rhizome
Sb2bss	37	41 9	18 94	S *fuscum*	116bss	232	37 9	16 43	S *fuscum*
19yss	38	44 5	19 32	S *capillifolium*	117bss	234	39 6	18 16	S *fuscum*
Sb3bss	39	42 3	19 49	S *fuscum*	118r	236	38 7	19 14	Rhizome
20bss	40	42 8	17 88	S *fuscum*	119r	238	32 0	15 86	Rhizome
Sb4yss	41	43 1	21 32	S *capillifolium*	119bss	238	37 3	18 70	S *fuscum*
21yss	42	40 8	19 13	S *capillifolium*	120r	240	34 7	18 88	Rhizome
Sb5yss	43	43 6	18 15	S *capillifolium*	121r	242	35 3	16 77	Rhizome
22yss	44	46 0	17 41	S *capillifolium*	121r repeat	242	39 1	18 18	Rhizome
Sb6yss	45	45 4	18 89	S *capillifolium*	121dbss	242	32 5	13 89	S *magellanicum*
23yss	46	46 6	18 13	S *capillifolium*	122DS	244	27 5	12 92	Root networks of Pteridophytae
Sb7yss	47	43 0	20 28	S *capillifolium*	122dbss	244	37 3	14 92	S *magellanicum*
24yss	48	46 2	18 36	S *capillifolium*	123dbss	246	39 0	19 54	S *magellanicum*
25yss	50	45 1	19 18	S *capillifolium*	124dbss	248	37 9	16 46	S *magellanicum*
26yss	52	44 0	18 92	S *capillifolium*	125r	250	34 9	15 19	Rhizome
27yss	54	45 4	19 97	S *capillifolium*	125DS	250	26 3	12 11	Root networks of Pteridophytae
27 5yss	55	44 9	19 40	S *capillifolium*	125bss	250	42 5	16 56	S *fuscum*
28yss	56	43 6	19 15	S *capillifolium*	126dbss	252	40 0	17 58	S *magellanicum*
28 5yss	57	46 6	17 21	S *capillifolium*	127dbss	254	41 3	18 67	S *magellanicum*
29yssRE	58	46 2	17 71	S *capillifolium*	129dbss	258	38 0	20 63	S *magellanicum*
29yss	58	44 7	17 09	S *capillifolium*	130dbss	260	41 6	16 47	S *magellanicum*
29 5yss	59	46 3	18 68	S *capillifolium*	131dbss	262	42 9	18 62	S *magellanicum*
30yss	60	38 3	19 47	S *capillifolium*	132dbss	264	40 2	17 98	S *magellanicum*
30 5yss	61	47 3	19 43	S *capillifolium*	133dbss	266	40 5	19 78	S *magellanicum*
31yss	62	42 8	20 15	S *capillifolium*	134DS	268	34 5	13 33	Root networks of Pteridophytae
31 5yss	63	45 4	19 06	S *capillifolium*	135DS	270	35 6	14 95	Root networks of Pteridophytae
32bss	64	44 1	19 23	S *fuscum*	135r	270	37 4	17 63	Rhizome
32 5yss	65	44 8	17 17	S *capillifolium*	136DS	272	33 9	13 11	Root networks of Pteridophytae
33bss	66	44 5	18 57	S *fuscum*	137dbss	274	42 5	21 92	S *magellanicum*
33 5yss	67	45 9	20 75	S *capillifolium*	139dbss	278	39 6	18 46	S *magellanicum*
34bss	68	44 3	18 78	S *fuscum*	139r	278	lost	lost	Rhizome
34ayss	69	45 6	18 24	S *capillifolium*	140r	280	33 3	14 80	Rhizome
35bss	70	42 0	18 34	S *fuscum*	141r	282	30 5	15 08	Rhizome
35ayss	71	45 0	20 17	S *capillifolium*	142r	284	34 1	15 54	Rhizome
36bss	72	45 3	18 74	S *fuscum*	143r	286	33 0	14 26	Rhizome
36dbss	72	44 3	18 86	S *magellanicum*	145r	290	34 2	14 06	Rhizome
36ayss	73	45 9	19 52	S *capillifolium*	145bss	290	43 7	17 82	S *fuscum*
37dbss	74	44 7	18 61	S *magellanicum*	146dbss	292	38 6	15 11	S *magellanicum*
37bss	74	34 0	17 11	S *fuscum*	147r	294	30 9	17 71	Rhizome
38dbss	76	42 7	19 57	S *magellanicum*	148dbss	296	40 8	17 03	S *magellanicum*
38bss	76	43 5	18 16	S *fuscum*	149r	298	28 9	15 67	Rhizome
39bss	78	43 1	19 36	S *fuscum*	150r	300	35 6	16 20	Rhizome

Table 2.1: con't

40bss	80	42 5	18 97	S fuscum	151r	302	32 3	16 56	Rhizome
41bss	82	43 8	18 21	S fuscum	151dbss	302	35 3	16 34	S magellanicum
42bss	84	43 7	19 68	S fuscum	152dbss	304	39 5	17 63	S magellanicum
43bss	86	43 3	18 09	S fuscum	153dbss	306	38 3	19 71	S magellanicum
44bss	88	40 4	18 45	S fuscum	154dbss	308	40 5	18 18	S magellanicum
45r	90	37 7	17 60	Rhizome	155dbss	310	36 6	15 27	S magellanicum
45Lbss	90	42 7	19 43	S angustifolium	157dbss	314	39 2	19 54	S magellanicum
46bss	92	40 1	18 49	S fuscum	158r	316	36 2	18 40	Rhizome
46r	92	34 3	15 65	Rhizome	159dbss	318	37 4	18 25	S magellanicum
47bss	94	39 9	23 21	S fuscum	160bss	320	40 2	17 75	S fuscum
48yss	96	43 1	19 56	S capillifolium	160dbss	320	41 3	17 21	S magellanicum
49bss	98	34 8	19 18	S fuscum	161dbss	322	38 1	17 34	S magellanicum
49yss	98	41 0	19 23	S capillifolium	162dbss	324	40 9	15 97	S magellanicum
50r	100	33 3	15 22	Rhizome	162bss	324	39 6	17 38	S fuscum
50yss	100	39 3	19 73	S capillifolium	163dbss	326	39 4	17 76	S magellanicum
51bss	102	40 5	19 80	S fuscum	164bss	328	39 0	16 89	S fuscum
52bss	104	41 4	20 27	S fuscum	165r	330	35 0	14 89	Rhizome
53dbss	106	33 0	19 21	S magellanicum	165bss	330	40 8	19 89	S fuscum
54dbss	108	39 6	19 22	S magellanicum	166bss	332	40 6	15 26	S fuscum
55Lbss	110	40 5	17 76	S angustifolium	167r	334	42 6	24 96	Rhizome
56yss	112	42 1	19 65	S capillifolium	167 r repeat	334	39 8	25 18	Rhizome
57bss	114	42 3	19 12	S fuscum	167bss	334	40 4	19 51	S fuscum
58yss	116	42 2	19 68	S capillifolium	168bss	336	38 9	16 79	S fuscum
59bss	118	37 8	19 70	S fuscum	169r	338	37 4	19 06	Rhizome
60bss	120	35 9	16 20	S fuscum	169bss	338	37 7	24 82	S fuscum
61bss	122	39 8	18 44	S fuscum	170syss	340	36 3	15 13	S papillosum
62bss	124	41 2	19 32	S fuscum	171r	342	30 6	13 53	Rhizome
63bss	126	49 3	19 06	S fuscum	171syss	342	39 3	15 17	S papillosum
64yss	128	37 2	19 23	S capillifolium	172syss	344	37 7	16 08	S papillosum
65Lbss	130	40 9	19 31	S angustifolium	173DS	346	37 5	17 88	Root networks of Pteridophytae
66yss	132	41 7	20 29	S capillifolium	174dbss	348	39 9	17 23	S magellanicum
67yss	134	41 1	21 42	S capillifolium	175bss	350	39 8	17 51	S fuscum
68yss	136	45 9	17 47	S capillifolium	176dbss	352	40 3	18 71	S magellanicum
69yss	138	39 8	18 37	S capillifolium	177dbss	354	39 7	18 99	S magellanicum
70yss	140	42 3	19 49	S capillifolium	178dbss	356	39 8	18 14	S magellanicum
71bss	142	43 7	19 50	S fuscum	179dbss	358	37 0	16 21	S magellanicum
72yss	144	41 5	19 50	S capillifolium	180dbss	360	40 0	17 69	S magellanicum
73bss	146	40 7	17 95	S fuscum	181DS	362	22 1	14 24	Root networks of Pteridophytae
74bss	148	41 4	19 42	S fuscum	181dbss	362	29 3	18 18	S magellanicum
75bss	150	42 6	18 50	S fuscum	185bss	370	39 5	17 08	S fuscum
76bss	152	39 5	18 16	S fuscum	190DS	380	36 1	14 59	Root networks of Pteridophytae
77bss	154	40 5	20 52	S fuscum	195bss	390	39 9	16 33	S fuscum
78bss	156	40 6	17 80	S fuscum	195dbss	390	37 0	15 63	S magellanicum
79bss	158	43 1	19 02	S fuscum	200r	400	33 3	16 97	Rhizome
80bss	160	39 4	19 60	S fuscum	205dbss	410	40 5	16 39	S magellanicum
81yss	162	42 1	19 50	S capillifolium	210bss	420	37 4	15 88	S fuscum
82bss	164	42 2	19 15	S fuscum	215bss	430	37 8	15 91	S fuscum
83bss	166	42 5	19 56	S fuscum	220 r	440	36 9	22 08	Rhizome
84bss	168	43 0	18 30	S fuscum	220rbl	440	34 8	13 38	Unknown Reddish brown leaves
85yss	170	41 5	19 28	S capillifolium	220dbss	440	39 7	16 65	S magellanicum
85r	170	38 4	19 61	Rhizome	225bss	450	40 6	16 85	S fuscum
86r	172	35 3	15 93	Rhizome	230bss	460	39 2	17 85	S fuscum
86yss	172	41 6	17 34	S capillifolium	230rbl	460	27 4	14 77	Unknown Reddish brown leaves
87yss	174	42 3	17 78	S capillifolium	235dbss	470	42 3	16 49	S magellanicum
88yss	176	42 0	17 37	S capillifolium	235r	470	36 3	16 83	Rhizome
89bss	178	35 3	17 94	S fuscum	240bss	480	40 2	16 99	S fuscum
90bss	180	41 9	17 61	S fuscum	245bss	490	42 5	15 17	S fuscum
91bss	182	41 4	17 36	S fuscum	250rbl	500	28 4	17 88	Unknown Reddish brown leaves
92bss	184	41 4	16 90	S fuscum	250dbss	500	39 0	15 08	S magellanicum
92r	184	36 4	13 47	Rhizome	255trh	510	35 5	13 19	Tissue remains of Herbacea
93bss	186	42 0	15 86	S fuscum	260bss	520	38 6	16 56	S fuscum
94bss	188	41 9	17 18	S fuscum	265trh	530	32 2	13 37	Tissue remains of Herbacea
95yss	190	41 3	18 09	S capillifolium	270trh	540	33 0	12 15	Tissue remains of Herbacea
95bss	190	35 8	16 74	S fuscum	275trh	550	34 7	12 10	Tissue remains of Herbacea
95r	190	40 2	18 66	Rhizome	280trh	560	29 8	11 94	Tissue remains of Herbacea
96bss	192	40 6	17 82	S fuscum	290trh	580	34 0	13 55	Tissue remains of Herbacea
97bss	194	41 0	18 29	S fuscum	295trh	590	33 5	7 99	Tissue remains of Herbacea
98bss	196	42 2	18 06	S fuscum					

more than 3 times higher than the observed variability between samples (see F_{calc}, Table 2.2). This difference was below the 95% confidence level but retained a very high level of 92% confidence based on 1-P=1-0.08=0.92 (Table 2.2).

For the *Sphagnum* pairs $F_{calc} \ll F_{crit}$ and the NULL hypothesis could be rejected. A linear correlation test was also applied to determine whether the $\delta^{18}O_{cel}$ signature obtained from the rhizomes displayed the same variability as *Sphagnum* samples with depth to determine whether rhizomes could be used if a static offset was applied. Unfortunately the correlation between pairs of rhizomes and *Sphagnum* was insignificant (r=0.07; Figure 2.5), indicating that rhizome $\delta^{18}O_{cel}$ data cannot be used interchangeably for temperature reconstruction even after applying static offset. In contrast, the correlation between *S. magellanicum* with *S. fuscum* data was high (r=0.71).

Thus, cellulose $\delta^{18}O$ values obtained from both *Sphagnum* species could be used interchangeably for temperature reconstruction. As an additional test $\delta^{18}O_{cel}$ analyses were carried out on sub-samples of *S. magellanicum* and rhizomes from samples at 202 cm and 242 cm core depths, respectively (Table 2.2).

Table 2.2: ANOVA -Single Factor of $\delta^{18}O$ data

Group 1	Group 2	Average Group 1	Average Group 2	No of pairs	Mean of Squares between Groups	within Groups	F_{calc}	P-value	F_{crit} 95%
S capillifolium	*S fuscum*	17 96	18 14	5	0 08	0 82	0 10	0 76	5 32
S magellanicum	*S fuscum*	17 64	17 58	6	0 01	1 67	0 01	0 93	4 96
S fuscum	Rhizome	18 71	16 36	11	30 27	9 20	3 29	0 08	4 35
Sphagnum sp	Rhizome	18 26	16 70	19	22 98	7 26	3 17	0 08	4 11

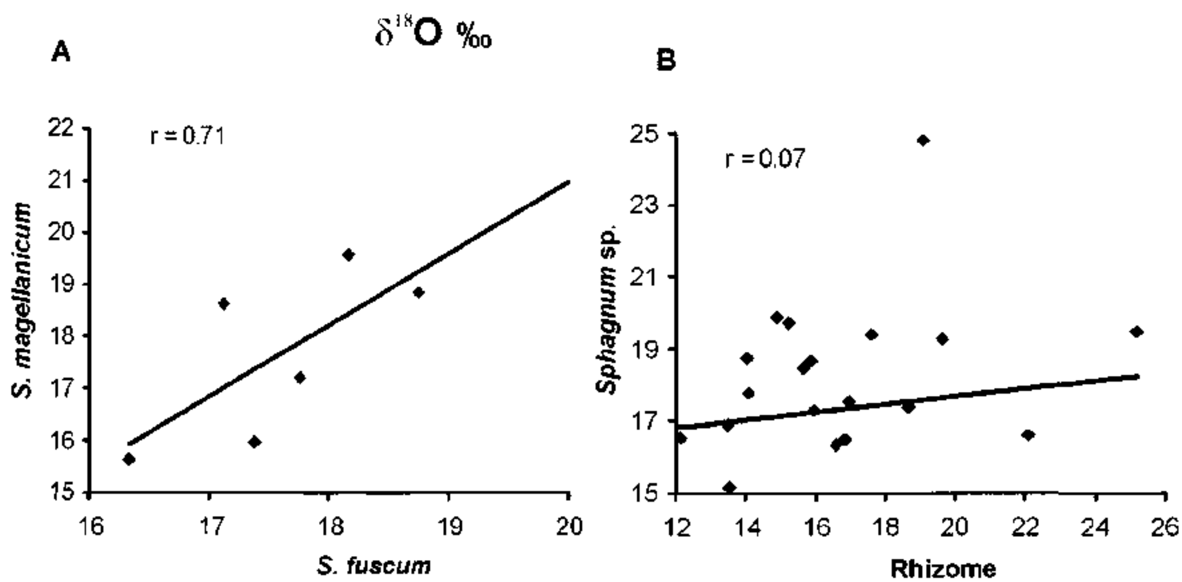

Figure 2.5: Correlation of cellulose oxygen isotope data of different plant taxa. A: *Sphagnum magellanicum* vs *Sphagnum fuscum* and B: all lumped *Sphagnum* species vs. rhizome. Black lines in graph area show linear regression lines.

Analysis results show only a small offset (19.72-19.36=0.36‰) between the *S. magellanicum* duplicates, whereas the difference between the two rhizome subsamples was four times larger (18.18-16.77‰=1.41‰). Analytical results from the two samples pairs also indicated that root networks of pteridophytae are characterized by significantly lower $\delta^{18}O_{cel}$ values than the *Sphagnum* samples (sample #125, #181, see Table 2.1).

Similarly, three sample pairs of *Sphagnum* and unknown reddish-brown leaves (samples #220, #230, and #250) also showed large and highly varying cellulose oxygen isotope value differences ranging from +3‰ to -2‰ (see Table 2.1). *Sphagnum* and tissue remains of herbacea were never found together in the same samples. Thus offsets and variability between these two groups could not be evaluated.

2.7 Discussion

The comparative approach taken in this study, where the $\delta^{18}O_{cel}$ values for a variety of individual *Sphagnum* species and other plant macrofossils from the same core horizons were compared against each other, indicates that the use of bulk peat cellulose could lead to erroneous paleotemperature reconstructions. Our $\delta^{18}O_{cel}$ results have shown that there is a significant offset between results obtained for non-vascular *Sphagnum* species, and vascular plants such as rhizomes and other plant macrofossils. This finding indicates that the mixing of vascular and non-vascular plants during $\delta^{18}O_{cel}$ isotopic analysis in a stratigraphic section could also result in an erroneous paleotemperature reconstruction. Consequently, given the significant differences and inconsistencies characterizing $\delta^{18}O_{cel}$ signatures obtained for rhizome and other non-*Sphagnum* plants, the use of such $\delta^{18}O_{cel}$

signatures in paleotemperature reconstructions misrepresents the true $\delta^{18}O$ signature of source waters. This conclusion is also applicable to the use of $\delta^{18}O_{cel}$ signatures obtained from bulk peat samples as these results would also be comprised of mixed sources of $\delta^{18}O_{cel}$ and were thus not the equivalent $\delta^{18}O$ in source water. In the case of *Sphagnum*, $\delta^{18}O_{cel}$ in a single *Sphagnum* species or in a mixture of different *Sphagnum* species will provide much more accurate paleotemperature reconstructions.

Although not dealt with in this reseach, previous research on $\delta^{13}C_{cel}$ isotopic signatures in various bog plant macrofossils, came to similar conclusions (Ménot and Burns, 2001). In that study the reproducibility and the shift between $\delta^{13}C$-values in the cellulose fraction and whole plant (bulk) in both vascular and non-vascular plants from ombrotrophic peat bogs, along an altitude transect in the Swiss Alps was examined. Ménot and Burns (2001) correlated the difference between bulk and cellulose $\delta^{13}C$ values to the presence in bulk plant material of lipid and lignin fractions, depleted in $\delta^{13}C$ (Park and Epstein, 1960). They suggested that for paleoclimate work it is important to not neglect the effect of burial and humification of peat material on $\delta^{13}C$ values. In their view, these factors (i.e., burial and humification) will remove the more labile organic fractions, which could change the $\delta^{13}C$ values of bulk organic matter even within individual species.

The observations of Ménot and Burns (2001) regarding the applicability of $\delta^{13}C_{cel}$ are in accordance with our conclusions regarding the applicability of $\delta^{18}O_{cel}$ analysis in bog settings. We conclude that the $\delta^{18}O_{cel}$ analysis of individual non-vascular species (i.e. *Sphagnum*) is crucial if reliable isotope-proxy temperature records are to be obtained from peat. Our conclusions thus contrast considerably with those of Skrzypek et al., (2007a) who reported that because plant cellulose is considered the most isotopically stable chemical compound, even under conditions of partial decomposition (Epstein et al., 1976; Feng et al., 1993; Schleser et al., 1999; Jędrysek and Skrzypek, 2005), the primary $\delta^{18}O_{cel}$ plant composition can be well preserved in bulk organic matter, especially in acid bog or fen conditions (Jędrysek and Skrzypek, 2005). The results reported in the present study indicate that while bulk samples obtained from a bog surface may be internally consistent the $\delta^{18}O_{cel}$ obtained for non-*Sphagnum* components rapidly diverges down core.

The observed statistically insignificant $\delta^{18}O_{cel}$ isotopic offset between *Sphagnum* pairs within samples and between species at the same core horizons suggests that down core identification of the exact *Sphagnum* species is not critical. This finding is fortunate as identification of exact *Sphagnum* species can be particularly difficult in old peat material where leaves are mostly detached from their branches and or their stems. As the $\delta^{18}O_{cel}$ isotopic ratio remains uniform the mixing of *Sphagnum* species is unlikely to contribute to any erroneous estimates of paleoclimate variation.

Our findings are also consistent with the results of a recent study that focused on carbon and oxygen isotope ratios in cellulose extracted from *Sphagnum* branches and stem sections sampled from a 4000 year old peat located in the Westeifel volcanic field in Germany (Moschen et al., 2009). Although the Moschen et al. (2009) study did not quantify the offset in $\delta^{18}O_{cel}$ values between different *Sphagnum* species, it did demonstrate that the $\delta^{18}O_{cel}$ offset observed between branches and stem sections obtained from the same *Sphagnum* specimens at various core depths was statistically insignificant. This insignificance is confirmed herein through the $\delta^{18}O_{cel}$ isotopic analysis of *Sphagnum* pairs from different species and indicates that paleotemperature proxy reconstructions utilizing *Sphagnum* will provide reliable results.

Based on our observation that *Sphagnum* plants provide a much more reliable $\delta^{18}O_{cel}$ isotopic results than obtained from either rhizomes or vascular plants we make two specific recommendations regarding $\delta^{18}O_{cel}$ isotopic analysis of peat bog material as follows:

1) Either individual *Sphagnum* stems or branches may be analyzed; and 2) although it is preferable to restrict analysis to a single *Sphagnum* species the statistically insignificant offsets observed between species will result in reliable results even if hard to identify stems from different species are analyzed.

2.8 Conclusions

The results of this study suggest that:

1. There is a statistically significant difference in the $\delta^{18}O_{cel}$ isotopic ratios obtained from non-vascular *Sphagnum* and the vascular plant macrofossils typically found in cores. This offset is recorded within and between samples. This result suggests that the use of bulk peat material without consideration of the observed differences between the isotopic composition of *Sphagnum* and the other plant macrofossils could lead to erroneous conclusions concerning the magnitude of paleoclimate variation.

2. There is a consistent and significant correlation between the $\delta^{18}O_{cel}$ isotopic ratios obtained from different *Sphagnum* species analyzed from the same samples. The observed statistically insignificant offsets between the cellulose oxygen isotopic composition of the different *Sphagnum* species analyzed implies that segregation of these species prior to isotope analyses is not necessary. Since the $\delta^{18}O_{cel}$ ratios observed are statistically insignificant, the use of bulk *Sphagnum* in analyses will unlikely result in any misrepresentation of the $\delta^{18}O_{cel}$ signature.

3. Our results demonstrate that paleoclimate reconstructions based on $\delta^{18}O_{cel}$ derived from peat archives must take into account that there exist significant stable oxygen isotopic offset between cellulose from *Sphagnum* and rhizomes. As a result, we recommend that only *Sphagnum* remains be used for $\delta^{18}O_{cel}$ based temperature reconstructions.

2.9 References

Anderson, T.W., 1988. Late Quaternary pollen stratigraphy of the Ottawa valley – Lake Ontario region and its application in dating the Champlain Sea. In: Gadd, N.R., (Ed.), The Late Quaternary Development of the Champlain Sea Basin. *Geological Association of Canada, Canada. Special Paper*, 35: 207–224.

Anderson, W. T., Bernasconi, S. M., and McKenzie, J. A., 1998. Oxygen and Carbon Isotopic Record of Climatic Variability in Tree Ring Cellulose (Picea abies): An example from Central Switzerland. *J. Geophys. Res.*, 103: 31625–31636.

Aucour, A.-M., Hillaire-Marcel, C., and Bonnefille, R., 1996. Oxygen isotopes in cellulose from modern and Quaternary intertropical peatbogs: implications for palaeohydrology. *Chemical Geology*, 129: 341–359.

Auer, V., 1930. Peat bogs in southeastern Canada. Canada Department of Mines, Ottawa. *Memoir,* 162: 32 pp.

Barbour, M. M., Andrews, T. J., and Farquhar, G. D., 2001. Correlations between oxygen isotope ratios of wood constituents of Quercus and Pinus samples from around the world. *Australian Journal of Plant Physiology*, 28: 335–348.

Brenninkmeijer, C. A. M., van Geel, and Mook, B. W. G., 1982. Variations in the D/H and $^{18}O/^{16}O$ ratios in cellulose extracted from a peat bog core. *Earth and Planetary Science Letters*, 61: 283-290.

Daley, T.J., Barber, K.E., Street-Perrott, F.A., Loader, N.J., Marshall, J.D., Crowley, S.F., and Fisher, E.H., 2010. Holocene climate variability revealed by oxygen isotope analysis of *Sphagnum* cellulose from Walton Moss, northern England. *Quaternary Science Reviews*, 29: 1590-1601.

Daley, T.J., Street-Perrott, F.A., Loader, N.J., Barber, K.E., Hughes, P.D.M., Fisher, E.H., and Marshall, J.D., 2009. Terrestrial climate signal of the '8200 yr B.P. cold event' in the Labrador Sea region. *Geology*, 37: 831–834.

Dansgaard, W., 1964. Stable isotopes in precipitation. *Tellus*, 16: 436-468.

Davis, J.C., 2002. Statistics and data analysis in Geology, 3rd edition. Wiley, New York: 637 pp.

DeNiro, M.J., and Epstein, S., 1979. Relationship between the oxygen isotope ratios of terrestrial plant cellulose, carbon dioxide, and water. *Science*, 204: 51–53.

DeNiro, M.J., and Epstein, S., 1981. Isotopic composition of cellulose from aquatic organisms. *Geochimica et Cosmochimica Acta*, 45: 1885–1894.

Edwards, T.W.D., Aravena, R.O., Fritz, P., and Morgan, A.V., 1985. Interpreting paleoclimate from 18O and 2H in plant cellulose: comparison with evidence from fossil insects and relict permafrost in southwestern Ontario. *Canadian Journal of Earth Sciences*, 22: 1720–1726.

Elson, J.A., 1969. Radiocarbon dates, Mya arenaria phase of the Champlain Sea. *Canadian Journal of Earth Sciences*, 6: 367–372.

Epstein, S., Thompson, P., and Yapp, C.J., 1977. Oxygen and Hydrogen Isotopic Ratios in Plant Cellulose. *Science*, 198: 1209 – 1215.

Epstein, S., Yapp, C.J., and Hall, J.H., 1976. Determination of the D/H Ratios of Nonexchangeable Hydrogen in Cellulose Extracted from Aquatic and Land Plants. *Earth and Planetary Science Letters*, 30: 241–251.

Feng, X., Krishnamurthy, R.V., and Epstein, S., 1993. Determination of D/H Ratios of Nonexchangeable Hydrogen in Cellulose: A Method Based on the Cellulose-Water Exchange Reaction. *Geochimica et Cosmochimica Acta*, 57: 4249-4256.

Francey, R.J., and Farquhar, G.D., 1982. An explanation for the $^{13}C/^{12}C$ variations in tree rings. *Nature*, 297: 28–31.

Fricke, H.C., and O'Neil, J.R., 1999. The correlation between $^{18}O/^{16}O$ ratios of meteoric water and surface temperature: its use in investigating terrestrial climate change over geologic time. *Earth and Planetary Science Letters*, 170: 181–196.

Grosse-Brauckmann, G., 1972. Über pflanzliche Makrofossilien mitteleuropäischer Torfe. I. Gewebereste krautiger Pflanzen und ihre Merkmale. *Telma*, 2: 19-55.

Grosse-Brauckmann, G., 1974. Über pflanzliche Makrofossilien mitteleuropäischer Torfe. II. Weitere Reste (Früchte und Samen, Moose u. a.) und ihre Bestimmungsmöglichkeiten. *Telma*, 4: 51-117.

Haider, K., 1996. Biochemie des Bodens (1st ed.), Enke Verlag, Stuttgart: 174 pp.

Hong Y.T., Jiang, H.B., Liu, T.S., Zhou, L.P., Beer, J., Li, H.D., Leng, X.T., and Hong, B., 2000. Response of climate to solar forcing recorded in a 6000-year 18O time-series of Chinese peat cellulose. *The Holocene*, 10: 1-7.

Hong, Y.T., Wang, Z.G., Jiang, H.B., Lin, Q.H., Hong, B., Zhu, Y.X., Wang, Y., Xu, L.S., Leng, X.T., and Li, H.D., 2001. A 6000-year record of changes in drought and precipitation in northeastern China based on a δ13C time series from peat cellulose. *Earth and Planetary Science Letters*, 185: 111-119.

Jędrysek, M. O., and Skrzypek, G., 2005. Hydrogen, Carbon, and Sulphur Isotope Ratios in Peat: The Role of Diagenessis and Water Regimes in Reconstruction of Past Climates. *Environmental Chemistry Letters*, 2Q: 179–183.

Jowsey P.C., 1966. An improved peat sampler. *The New Phytologist*, 65: 245–248.

Joyal, R., 1970. Description de la tourbière à Sphaignes Mer Bleue près d'Ottawa. 1. Végétation. *Canadian Journal of Botany*, 48: 1405–1418.

Lévesque, P.E.M., Dinel, H., and Larouche, A., 1988. Guide to The identification of Plant Macrofossils in Canadian Peatlands. Research Branch, Agriculture Canada, Publication 1817: 65pp.

Libby, L.M., and Pandolfi, L.J., 1974. Temperature Dependence of Isotope Ratios in Tree Rings. *Proceedings of the National Academy of Sciences*, 71: 2482–2486.

Loader, N.L., McCarroll, D., van der Knaap, W.O., Robertson, I., and Gagen, M., 2007. Characterizing carbon isotopic variability in *Sphagnum*. *Holocene*, 17: 403–410.

Ménot, G., Burns, S.J., 2001. Carbon Isotopes in Ombrogenic Peat Bog Plants as Climatic Indicators: Calibration from an Altitudinal Transect in Switzerland. *Organic Geochemistry*, 32: 233–245.

Ménot-Combes, G., Burns, S.J., and Leuenberger, M., 2002. Variations of $^{18}O/^{16}O$ in plants from temperate peat bogs (Switzerland): implications for paleoclimatic studies. *Earth and Planetary Science Letters*, 202: 419–434.

Moschen, R., Kühl, N., Rehberger, I., and Lücke, A., 2009. Stable carbon and oxygen isotopes in sub-fossil *Sphagnum*: Assessment of their applicability for palaeoclimatology. *Chemical Geology*, 259: 262–272.

Mott, R.J., and Camfield, M., 1969. Palynological Studies in the Ottawa Area. Geological Survey of Canada, Ottawa: 1–16.

Munsell Color Company, 1975. Munsell Soil Color Charts. Munsell Color Company, MD, USA.

O'Leary, M.H., Treichel, I., and Rooney, M., 1986. Short-term measurement of carbon isotope fractionation in plants. *Plant Physiology*, 80: 578–582.

Pancost, R.D., Baas, M., van Geel, B., and Sinninghe Damasté, J.S., 2003. Response of an ombrotrophic bog to a regional climate event revealed by macrofossil, molecular and carbon isotopic data. *Holocene*, 13: 921–932.

Park, R., and Epstein, S., 1960. Carbon Isotope Fractionation During Photosynthesis. *Geochimica Cosmochimica Acta*, 21: 110-126.

Roulet, N.T., Lafleur, P.M., Richard, P.J.H., Moore, T.R., Humphreys, E., and Bubier, J.L., 2007. Contemporary carbon balance and late Holocene carbon accumulation in a northern peatland. *Global Change Biology*, 13: 397–411.

Rozanski, K., Araguas-Araguas, L., and Gonfiantini, R., 1993. Isotopic patterns in modern global precipitation. *Climate Change in Continental Isotopic Records*, 78: 1–36.

Rydin, H., 1986. Competition and Niche Separation in *Sphagnum*. *Canadian Journal of Botany*, 64: 1817–1824.

Schleser, G.H., Frielingsdorf, J., and Blair, A., 1999. Carbon Isotope Behavior in Wood and Cellulose During Artificial aging. *Chemical Geology*, 158: 121–130.

Skrzypek, G., Kałużny, A., and Jędrysek, M.O., 2007a. Carbon stable isotope analyses of mosses—comparisons of bulk organic matter and extracted nitrocellulose. *Journal of the American Society for Mass Spectrometry*, 18: 1453–1458.

Skrzypek, G., Kałużny, A., Wojtuń, B., and Jędrysek, M.O., 2007b. The carbon stable isotopic composition of mosses—the record of temperature variations. *Organic Geochemistry*, 38: 1770–1781.

Skrzypek, G., and Jędrysek, M.O., 2005. 13C/12C Ratio in Peat Cores: Record of Past Climates. In Lichtfouse, E., Schwarzbauer, J., and Robert, D., (Eds.). Environmental Chemistry—Green Chemistry and Pollutants in Ecosystems; Springer-Verlag, Berlin, Heidelberg, Germany: pp. 65–73.

Smith, A.J.E., 2004. The moss flora of Britain and Ireland, Second edition. Cambridge University Press, Cambridge: 986 pp.

Sternberg, L., DeNiro, M.J., and Savidge, R.A., 1986. Oxygen isotope exchange between metabolites and water during biochemical reactions leading to cellulose synthesis. *Plant Physiology*, 82: 423–427.

Stevenson, F.J., 1994. Humus Chemistry—Genesis, Composition, Reactions, 2nd ed. John Wiley and Sons, New York: 512 pp.

Sukumar, R., Ramesh, R., Pant, R.K., and Rajagopalan, G., 1993. A $\delta^{13}C$ record of late Quaternary climate change from tropical peat in southern India. *Nature*, 364: 703-706.

Taylor, M.A., 2008. Continental-scale validation of the temperature signal in oxygen isotopes of *Sphagnum* cellulose and its application as paleoclimate proxy. M.Sc. thesis, University of Wyoming, USA, 86 p.

White, J.W.C., Ciais, P., Figge, R.A., Kenny, R., and Margraft, V. 1994a. A high-resolution record of atmospheric CO2 content from carbon isotopes in peat. *Nature*, 367: 153-56.

White, J.W.C., Figge, R.A., Markraft, V., Ciais, P., and Kenny, R. 1994b. Climate in the Pleistocene. *Nature*, 371: 111-12.

Zanazzi, A., and Mora, G., 2005. Paleoclimatic Implications of the Relationship Between Oxygen Isotope Ratios of Moss Cellulose and Source Water in Wetlands of Lake Superior. *Chemical Geology*, 222: 281–291.

CHAPTER THREE

3. EASTERN ONTARIO HOLOCENE PALEOCLIMATE RECONSTRUCTION: EVIDENCE FROM $\delta^{18}O$ CELLULOSE OF PLANT MACROFOSSILS FROM THE MER BLEUE BOG

3.1 Abstract

We present a ~9200-year high-resolution oxygen isotope record of plant cellulose ($\delta^{18}O_{cel}$) from an ombrotrophic bog in Eastern Ontario to demonstrate its potential as a proxy for paleotemperature reconstruction in peat deposits. We measured the $\delta^{18}O_{cel}$ extracted from selected plant macrofossils collected from Mer Bleue Bog. The results show that $\delta^{18}O_{cel}$ of *Sphagnum* follows the general pattern of Holocene sunspot number reconstruction through the last ~5500 years, following development of the ombrotrophic phase of Mer Bleue Bog, and the northern Hemisphere reconstructed paleotemperature record for the last 2000 years. Three distinct time intervals have low $\delta^{18}O_{cel}$ values: 200 to 800 cal. yr. B.P. (Little Ice Age); 2800 to 3400 cal. yr. B.P. synchronous to a cooling period reported elsewhere in North America, and; 4200 to 4600 cal. yr. B.P corresponding to a cooling interval in the North Atlantic region. These cooling periods also correlate well with negative excursions in the Holocene sunspot and cosmogenic ^{10}Be records. A fourth period of low $\delta^{18}O_{cel}$ values between A.D. 1810 and 1820 may be related to the extremely cold summer of 1816 and cooler subsequent years, which occurred in the aftermath of the Tambora volcanic eruption, or possibly cooling

associated with the early 19^{th} century Dalton solar Minimum. The results also indicate the presence of millennial scale cycles (1300 yr) possibly comparable to the globally recognized Dansgaard-Oeschger/Bond (~1500 yr) events that have been correlated to fluctuations in solar irradiance.

Keywords: oxygen isotopes, cellulose, ombrotrophic bog, Holocene, northern Hemisphere, paleotemperatures, solar activity.

3.2 Introduction

The Earth's climate is controlled by many factors such as water vapor, CO_2, methane, volcanic degassing, solar activity, biological activity, and land use change (Jansen et al., 2007; Veizer, 2005). Since the 1980's there has been a realization that rapid climate change on the scale of the human life span was possible (IPCC, 1996). Climate change projections for southern Canada through the 21^{st} century predict a 0.5-1.5°C temperature increase, at least partially driven by anthropogenic causes (Bonsal et al., 2001; Zhang et al, 2000).

The instrumental record is barely adequate for analyzing the characteristics of decadal-millennial scale climate variability. This is particularly true in eastern Canada where systematic measurement and collection of temperature data only began in the late 19^{th} century. These records generally follow the worldwide temperature record, which suggest that there has been a global increase of 0.3-0.6°C through the last century (Jansen et al., 2007). Long-term trends in regional and global temperatures are influenced by low-frequency events that are difficult to resolve with the short historical records. Therefore, a more complete understanding of intermediate and long-term climate oscillations and their relationship with short-term variations can only be achieved by turning to the geological record. Paleolimnological, dendrochronological, and paleoceanographic studies have revealed cyclic changes in moisture levels in climate records from the NE Pacific (Patterson, et al., 2004) and interior of North America at decadal to millennial scales (Yu and Ito, 1999; Dean et al., 2002). Complicating the understanding of natural climate variability are climate change projections for southern Canada through the 21st century, which predict a 0.5-1.5°C temperature increase, at least partially driven by anthropogenic causes (Bonsal et al., 2001; Zhang et al, 2000).

Here we present the first detailed paleoclimate reconstruction using the oxygen isotope composition of plant cellulose ($\delta^{18}O_{cel}$) as a proxy for paleotemperature reconstruction in eastern Canada. We utilize cellulose ($\delta^{18}O_{cel}$) from *Sphagnum* stems from ombrotrophic Mer Bleue Bog near Ottawa to reconstruct the paleotemperature variability of the last ~9200 years in eastern Ontario. The present study applies oxygen isotope analysis to plant cellulose solely derived from *Sphagnum* stems and permits us to resolve paleoclimate fluctuations with wavelengths from ~100 to 2000 years, thus allowing comparisons with major northern Hemisphere climate and solar insolation fluctuations of >100 years duration (e.g., Moberg et al., 2005; Bond et al., 2001; Suess, 1980). For the last 600 years the paleoclimate record from Mer Bleue Bog can be resolved with a precision of <20 years, which allows comparison with solar activity proxies and short-term climate events.

3.3 Previous Work

3.3.1 Ombrotrophic bogs as paleoclimate archives

Northern Hemisphere peatlands began developing during the early Holocene, ~9000 cal yr. B.P., and are now widespread across North America and Eurasia (Gajewski et al., 2001). Peatlands are common in cool and moist regions where precipitation exceeds evaporation, but only a few of these systems are ombrotrophic. Ombrotrophic bogs are a sensitive indicator of climate variations because they lack groundwater influence and receive water and nutrients solely from precipitation. Anoxic and acidic conditions in ombrotrophic bogs reduce microbial decomposers and prevent the decomposition process (Clymo and Hayward, 1982). As a result, ombrotrophic bogs are considered excellent archives of paleoclimatic variation as shown through isotope-geochemical studies and paleoecological analysis (Brenninkmeijer et al., 1982; Booth and Jackson, 2003; Booth et al., 2006).

3.3.2 Advantages of using Sphagnum for paleoclimate reconstruction

Many peatlands in the mid to high latitudes are *Sphagnum*-dominated (Brenninkmeijer et al., 1982; Booth and Jackson, 2003; Booth et al., 2006). *Sphagnum* mosses decay very slowly and their structure may be preserved for thousands of years in bog environments (van Breeman, 1995; Taylor, 2008). *Sphagnum* mosses, comprising over 30 species in North America, are non-vascular plants. *Sphagnum* is restricted to areas of high relative humidity and to short growth forms relative to other bryophytes and photosynthesis is limited to the top ~1-3 cm of *Sphagnum* tissue. (Taylor, 2008). They are ectohydric bryophytes and thus the water is conducted to the plants by external capillaries (Taylor, 2008). The combination of this constant water supply and generally short height of *Sphagnum* support the assumption that stem water and leaf water are very well mixed (Clymo and Hayward, 1982; Proctor, 1982; Admiral and Lafleur, 2007; Taylor, 2008).

Previous paleoclimate studies have utilized stable isotope variability obtained from bulk peat (Ménot and Burns, 2001; Skrzypek et al., 2007) or stable isotope variability of the cellulose fraction of bulk peat (Hong et. al., 2000, 2001). However, some of these studies have shown that $\delta^{18}O$ of bulk peat is quite variable, likely due to the mixture of non-vascular (*Sphagnum* mosses) and vascular plant remains (Brenninkmeijer et al., 1982; Ménot and Burns, 2001; Ménot-Combes et al., 2002). Due to the absence of stomata and vascular tissues, *Sphagnum* mosses possess limited ability to control water loss, which forces them to follow a simple physiological water-used strategy. Given its lack of roots and functioning guard cells, all fractionation of the plant water is environmentally controlled prior to its assimilation and cellulose synthesis (Ménot-Combes et al., 2002). Therefore, *Sphagnum* cellulose stable isotope records from ombrotrophic bogs are now considered the most reliable proxies for paleoclimate reconstructions from peat deposits (Taylor, 2008; Daley et al., 2009, 2010).

3.3.3 Cellulose oxygen isotope composition and paleotemperature

The stable isotope composition of plant macrofossils and other organic matter from peat profiles has been considered to be an important potential source of paleoclimate information (e.g., O'Leary et al., 1986; Francey and Farquhar, 1982; Aucour et al., 1996). Several studies have demonstrated a direct correlation between the isotopic carbon, oxygen, and hydrogen composition of cellulose and mean annual temperature (e.g. Libby and Pandolfi, 1974; Epstein et al., 1976; Epstein et al., 1977; DeNiro and Epstein, 1981; Edwards et al., 1985; Sternberg et al., 1986; Sukumar et al., 1993; White et al., 1994). Other studies have shown that the stable isotope composition of meteoric water at mid to high latitudes is strongly correlated with temperature and relative humidity, and meteoric water is often the source water for plant cellulose (Dansgaard, 1964; Fricke and O'Neil, 1999; Rozanski et al., 1993).

The isotopic composition of *Sphagnum* cellulose is potentially a widely applicable proxy that may be used to reconstruct the isotopic composition of meteoric water (Aucour et al., 1996; Pendall et al., 2001; Ménot -Combes et al., 2002; Zanazzi and Mora, 2005). Studies from European bogs showed significant oxygen isotope ratio differences between different bog plant genera in raised bogs (e.g., Loader et al., 2007; Moschen et al., 2009), but no significant differences between different *Sphagnum* species (e.g., Daley et al., 2010; See Chapter II).

3.3.4 *Cellulose and source water oxygen signatures*

The relationship between cellulose oxygen isotope composition and that of the source water (Yapp and Epstein, 1982; Roden et al., 2000; Pendall et al., 2001; Anderson et al., 2002; Zanazzi and Mora, 2005) can be expressed as follows:

$$\delta_{cell} = \delta_{sw} + \varepsilon_b + (\varepsilon_e + \varepsilon_k)(1 - h) \qquad (1)$$

where

δ_{cell} : isotopic composition of cellulose,

δ_{sw} : isotopic composition of the source water,

ε_b : biochemical enrichment factor,

ε_e : liquid-vapour equilibrium enrichment factor,

ε_k : liquid-vapour kinetic enrichment factor due to evaporation,

h : relative humidity (value from 0 to 1).

Sphagnum inhabits moist environments where the relative humidity is close to 100% where h is close to 1 (Vitt et al., 1975; Clymo and Hayward, 1982; Zanazzi and Mora, 2005). Consequently equation (1) can be simplified to:

$$\delta_{cell} = \delta_{sw} + \varepsilon_b \qquad (2)$$

Experimental measurements suggest that the biochemical enrichment factor (ε_b) value is equal to 27 ± 3‰ for oxygen (Epstein et al., 1977; DeNiro and Epstein, 1981; Sternberg, 1989; Farquhar et al, 1998; Wolfe et al., 2001).

Previous studies have reported the preservation of this evaporative-enrichment signal in the cellulose of surface *Sphagnum* relative to peat pore waters (Brenninkmeijer et al., 1982; Aravena and Warner, 1992). Whereas other studies have revealed that such evaporative effects are not maintained (Daley, 2007; Taylor, 2008; Daley et al., 2009). Daley (2007) reported that the data yielded a constant cellulose-precipitation fractionation factor (1.0274 ± 0.0010), statistically identical to the biochemical enrichment of oxygen isotopes during photosynthesis as determined by laboratory experiments (Sternberg et al., 1986). Daley (2007) suggests that although leaf water in

Sphagnum is subject to some evaporative enrichment prior to cellulose synthesis, the data suggests that this enrichment is minimal. Daley et al. (2009) observed that $\delta^{18}O$ and δD of summer bog-surface water from Newfoundland are within the scatter of regional precipitation values, and confirmed that the isotopic impact of evaporation was negligible. Taylor (2008) also demonstrated that at mid to high latitudes, the isotopic composition of precipitation in ombrotrophic bogs is highly correlated with growing season temperature, and this relationship is maintained in *Sphagnum* cellulose oxygen isotopic data, providing additional evidence that evaporative fractionation is negligible.

3.4 Geographic and Geological Setting

Mer Bleue Bog is a Provincial Conservation Area located 10 km east of Ottawa, Ontario (45.41°N latitude, 75.48°W longitude, 69 m above mean sea level) (Figure 3.1). Mer Bleue Bog covers approximately 28 km^2 and is roughly an east-west oriented oval broken into three separate lobes (Figure 3.1). The bog is slightly domed, with peat depths varying from 6 m near the center, decreasing to 0.3 m at the margins (Joyal, 1970; Roulet et al., 2007). Deglaciation in the area of Mer Bleue Bog occurred ~13,200 years ago. This part of the lower Ottawa River lowlands was subsequently inundated by post-glacial Lake Iroquois and the marine Champlain Sea, which resulted in the accumulation of laminated silt and clay deposited over sand, silt, gravel, and limestone between 12,000 and 9500 years ago (Anderson, 1988; Roulet et al., 2007). Fresh water dominated in the basin by ~ 10,600 years ago (the Lampsilis Lake phase; Elson & Elson, 1969). The present-day Mer Bleue peatland deposits lies within a now abandoned postglacial channel of the Ottawa River that was eroded into the floor of the Champlain Sea basin.

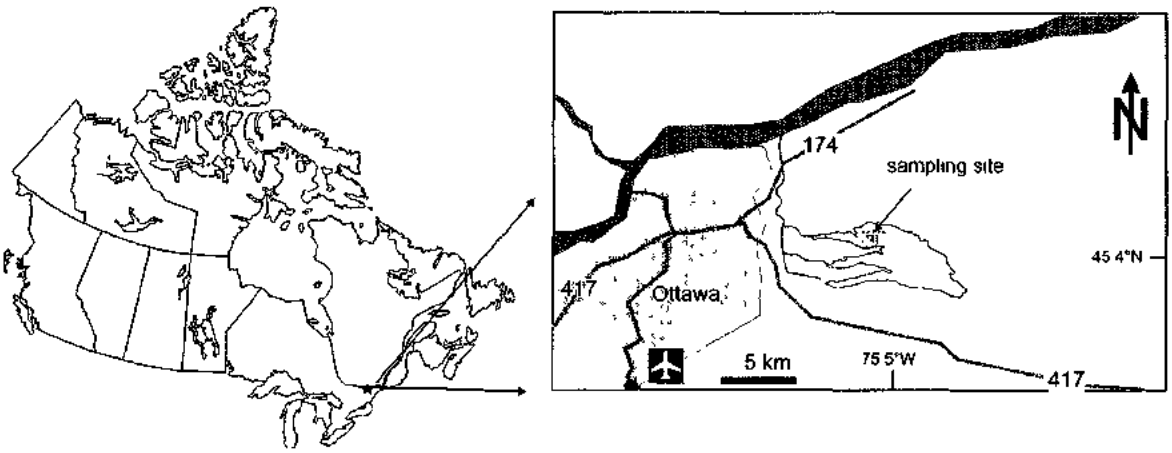

Figure 3.1: Location map of the Mer Bleue Bog, Ottawa, Ontario in eastern Canada. Asterisk marks the sampling site at the northwestern arm of Mer Bleue.

The peatland formed over the past 8400 years, initially as fen and transitioning to a bog phase by ~7100-6800 years ago (Auer, 1930; Mott & Camfield, 1969; Roulet et al., 2007). The present-day Mer Bleue Bog is an ombrotrophic bog where all nutrients and the water supply come strictly from precipitation rather than from ground water or river runoff. Sedimentation is entirely composed of autigenic plant growth, which is dominated by *Sphagnum* moss, cotton grasses and minor occurrence of cranberries and blueberries. Plant growth occurs from the end of April to early October. During the winter season, Mer Bleue Bog is totally frozen and covered by snow. During spring and summer, the bog surface is covered by a blanket of reddish to greenish vegetation.

The bog surface is generally characterized by a hummock–hollow microtopography that is mostly comprised of *Sphagnum* mosses. The most common hummock-forming *Sphagnum* species are *Sphagnum fuscum* and *Sphagnum capillifolium. Sphagnum fuscum* occupies the driest portion of the bog and occurs on the top of large hummocks. *Sphagnum fuscum* is small and dark brown, with a flat capitulum. *Sphagnum capillifolium* is a smaller bright red plant with tightly packed fascicles and has a very large capitulum. *Sphagnum magellanicum* is a very common dark-red plant characterized by a very stiff stem, many large fascicles and a prominent capitulum. *Sphagnum angustifolium*, which can grow submerged, is a green compact small plant.

3.5 Field Sampling & Material Collection

A series of closely spaced Russian cores were collected in March 2008 (N45°24.653', W75°31.064') from the centre of the Mer Bleue Bog near the previous coring location of

Roulet et al. (2007). Coring protocol when using a Russian Auger requires that each core be comprised of offsets collected from two closely spaced adjacent holes (e.g., Jowsey, 1966). The 5.5 cm diameter Russian corer used permitted retrieval of 50 cm long cores. For this research triplicates of the two overlapping cores were collected from a total six closely spaced holes. Core overlap was 20 cm through the uppermost 3.5 m of the core and 10 cm through the lower 2.5 m of the core to a total depth of ~6 m, terminating at the top of Champlain Sea marine clay deposits (Figure 3.2).

Recovered cores were carefully covered in plastic wrap, secured in labelled plastic half-tubes, and stored at 4°C in a core storage facility at Carleton University. The core material consists of relatively fresh *Sphagnum* material through the uppermost 73.5 cm and decomposed *Sphagnum*-dominated peat from 73.5 to 500 cm depth (Figure 3.2). The sets of triplicate cores were separated into two sets of cores for sampling and one core for archiving and non-invasive core for surface analysis. Subsampling was carried out using a stainless steel knife and stainless steel spatula. One centimetre thick slices were subsampled in preparation for stereo-microscopic and geochemical analysis.

3.6 Methods

3.6.1 Plant macrofossils separation

Subsamples were gently heated in a 5% KOH solution for ~ 30min to dissolve humic and fulvic acids. Plant macrofossil samples were then disaggregated using a 125 μm sieves using deionized water. Isolated plant remains were kept immersed to minimize damage and disintegration and subsequently transferred to a plastic container. Distilled water was

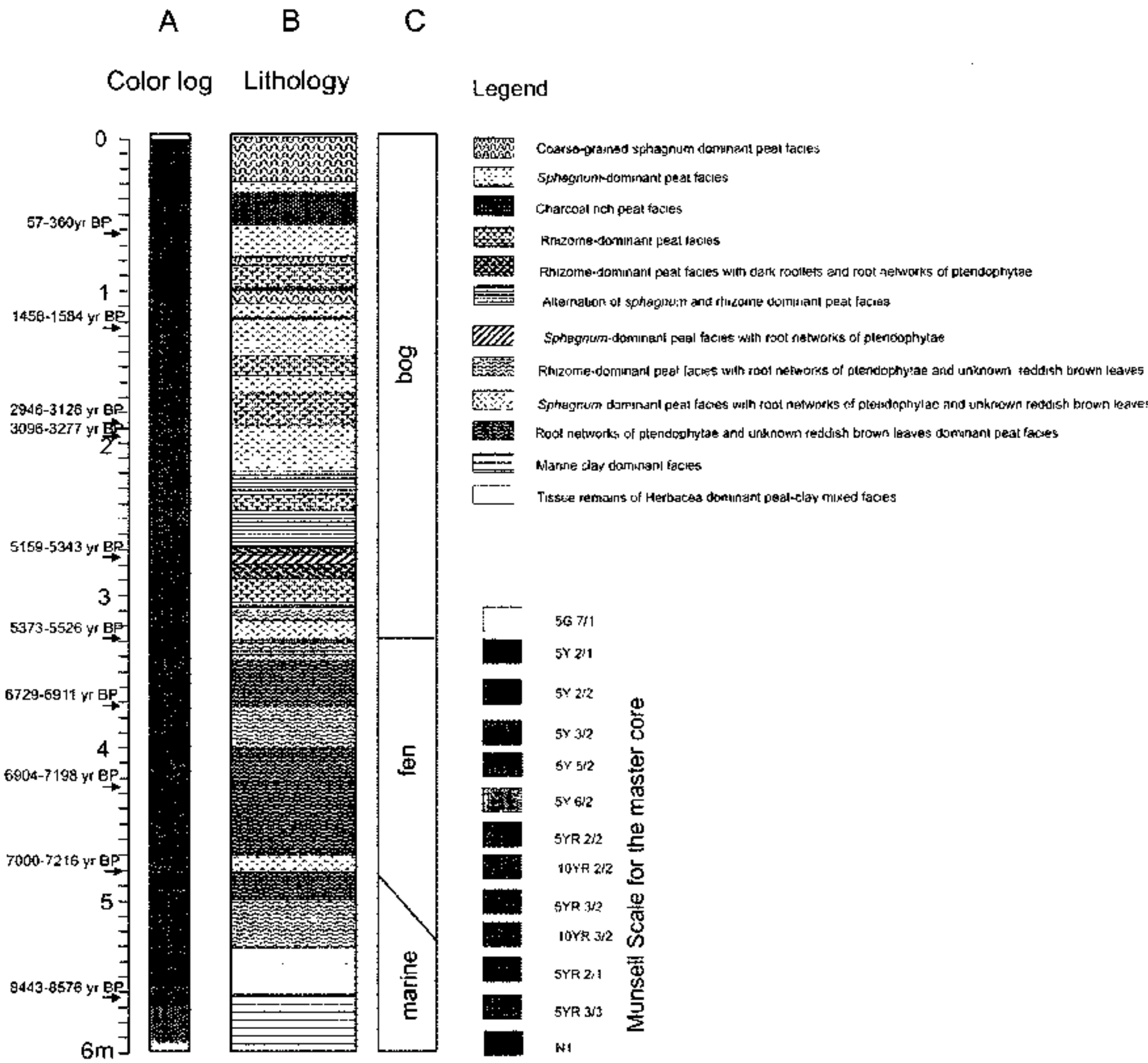

Figure 3.2: Mer Bleue core sedimentology: A: Rock color code following Munsell Chart (Munsell, 1975), B: Lithology, C: Depositional environments

added to suspend the plant macrofossil remains prior to examination using an Olympus SZH-1 stereo microscope. Macrofossils were identified using several illustrated moss identification guides (Smith, 2004; Lévesque et al., 1988; Mauquoy and van Geel, 2007). Once the optical macrofossil analysis was completed, each sample was stored in a sealed plastic container with deionized water in the dark at 4°C.

3.6.2 Cellulose oxygen isotope analytical technique

For cellulose isotopic analyses, plant macrofossils were hand-picked from petri dishes and placed in porcelain crucibles. *Sphagnum* stem sections were preferentially handpicked under an Olympus SZH-1 stereo microscope. Other plant macrofossils were selected for isotopic analysis from selected samples as well. Hand-picked plant macrofossils were placed in porcelain crucibles and dried in an oven at about 50°C for 24 hours. The samples were then powdered, weighed, labeled, and placed in small plastic vials.

Cellulose isotopic analyses were performed at the University of Saskatchewan isotope laboratories. Cellulose samples were baked at 60°C in a vacuum oven for 2 hours to drive off moisture, then immediately transferred and flushed in the zero blank autosampler. Samples were analyzed using a Thermo Finnigan TC/EA coupled to a Conflo III and a Delta Plus XL mass spectrometer. Samples were dropped under helium into a glassy carbon furnace and pyrolyzed at 1450°C to form hydrogen and/or carbon monoxide gases. The gases were carried in a helium stream to a GC column held at 100°C to separate the gases before being diluted in the Conflo III and passed to the mass spectrometer for analysis. Isotope ratios were blank corrected and reported in per mil notation relative to the VSMOW-VSLAP scale.

In-house oxygen standards were calibrated against international standards USGS-34 ($\delta^{18}O$ = -27.9‰ VSMOW) and USGS-35 ($\delta^{18}O$ = 57.5‰ VSMOW). An intermediate international standard, IAEA-NO3, gave the result $\delta^{18}O = 25.53 \pm 0.27$‰ VSMOW (n = 23) during calibration of in-house standards and compared to the accepted value of $\delta^{18}O = 25.6 \pm 0.4$‰ VSMOW. Two in-house standards were used to set up a calibration line, and a third was used to monitor the accuracy of the data. For the $\delta^{18}O$ data the accuracy was ±0.11‰ (n = 25) and for %O measurements the accuracy was ±0.5%. Actual sample errors may have been greater than these due to heterogeneity, and more accurate data may have been obtained through analytical repetition.

3.6.3 Mer Bleue Bog age-depth model

Thirteen samples were chosen for radiocarbon AMS dating. Nine samples were analysed at the CHRONOS laboratories at Queens University of Belfast and four samples were analysed at the AMS laboratory at the University of Georgia. Roots and twigs were removed from the samples. A palynostratigraphic date was obtained based on the first occurrence of *Ambrosia* pollen in the section (S. Elliott, pers. Comm., 2010). The ^{14}C dates were calibrated using the computer program CALIB5.0.2 using the Intcal04 ^{14}C calibration data set (Reimer et al., 2004) as shown in Table 3.1.

3.7 Results

3.7.1 Cellulose oxygen isotope composition in depth

Sampling of plant macrofossils focused primariy on *Sphagnum*. Other plant fossils were analysed for comparison and to substitute for *Sphagnum* in core intervals where *Sphagnum* was missing (Table 3.2, Figure 3.3). Cellulose $\delta^{18}O$ values obtained for plant macrofossils indicate a clear difference in the isotopic signatures between *Sphagnum* species and other plant macrofossils analysed such as rhizomes, red leaves, and root networks of pteridophytae (see Chapter II). In particular there is a clear offset in $\delta^{18}O_{cel}$ values between rhizome and *Sphagnum* in most samples (Figure 3.3). On the other hand, the differences in the isotopic composition between different *Sphagnum* species in the same samples are mostly <0.5‰ (See Chapter II).

The plant macrofossil assemblage through the upper 5 m of the Mer Bleue cores consists of several *Sphagnum* species, rhizomes, root networks of pteridophytae, tissue remains of herbacae and unknown reddish-brown leaves. *Sphagnum* dominates in the ombrotrophic bog section through the upper 3.2 m, whereas root networks of pteridophytae and unknown-reddish brown leaves dominate in the fen part between 3.2 m and 5 m. The lowermost part of the core from 5 to 6 m depth is characterized by a step-wise transition from peat in a fen environment towards marine clay where herbacea tissue remains are dominant (Figure 3.2 and Figure 3.3).

Table 3.1: Mer Bleue ^{14}C samples

Sample	Sample ID	Depth (cm)	UBA No. *UGAMS No	Material Dated	^{14}C Age (BP)	Cal. Ages (95 4%)			Cal. Ages (95.4%)			Cal Ages (95.4%)			mean Cal Ages (BP)
						min	max	prob	min	max	prob	min	max	prob	
1	MB16	32 - 33	11976	peat	postbomb (< 1964 A D)										
2	MB22	44 - 45	11977	peat	postbomb (< 1964 A D)										
3	MB31	62 - 63	11978	peat	204 ± 28	1648	1684	0 291	**1734**	**1806**	**0.554**	1930	1951	0 155	238
4	MB61	122 - 123	11979	peat	1566 ± 26	**424**	**552**	**1.000**							1520
5	MB93	186 - 187	11980	peat	2860 ± 22	**1118**	**973**	**0.939**	958	938	0 061				3053 5
6	MB99	198 - 199	11981	peat	2959 ± 22	**1269**	**1112**	**0.982**	1100	1085	0 013	1064	1058	0 005	3198 5
7	MB137	274 - 275	11982	peat	4449 ± 32	3335	3210	0 418	3192	3151	0 080	**3138**	**3010**	**0.470**	5082
8	MB163	326 - 327	11983	peat	4659 ± 31	**3518**	**3365**	**1.000**							5449 5
9	MB185	370 - 371	11984	peat	5934 ± 33	4903	4864	0 107	**4856**	**4721**	**0.893**				6806 665
10	MB23	46-47	*5026	peat	postbomb (< 1964 A D)										
11	MB210	420-421	*5027	peat	6070± 30	5190	5185	0 004	**5057**	**4896**	**0 97**	4867	4851	0 025	6984 5
12	MB240	480-481	*5028	peat	6130± 30	**5208**	**4992**	**1.000**							7108
13	MB280	560-561	*5029	peat	7640± 30	6568	6544	0 065	**6531**	**6435**	**0.935**				8491

bold calibrated Ages used from mean calibrated age calculation

Table 3.2: Oxygen isotope ratio and oxygen concentration of plant cellulose from Mer Bleue Bog, Ottawa, Ontario

Sample ID	Depth (cm)	%O	δ18O (‰, VSMOW)	Macrofossils Taxa	Sample ID	Depth (cm)	%O	δ18O (‰, VSMOW)	Macrofossils Taxa
1yss	2	41.4	18.81	*S. capillifolium*	98yss	198	41.0	17.74	*S. capillifolium*
2yss	4	42.0	18.32	*S. capillifolium*	99bss	198	41.2	17.80	*S. fuscum*
3r	6	37.3	19.14	Rhizome	99yss	198	39.7	16.94	*S. capillifolium*
4yss	8	43.3	20.22	*S. capillifolium*	100	200	40.0	19.11	*S. fuscum*
5yss	10	43.4	20.64	*S. capillifolium*	101dbss	202	41.8	19.36	*S. magellanicum*
6yss	12	42.7	18.88	*S. capillifolium*	101dbss repeat	202	40.5	19.72	*S. magellanicum*
7yss	14	42.4	19.28	*S. capillifolium*	102bss	204	42.1	19.18	*S. fuscum*
8yss	16	43.4	20.05	*S. capillifolium*	103dbss	206	40.9	19.68	*S. magellanicum*
9yss	18	41.7	16.91	*S. capillifolium*	104bss	208	40.6	19.26	*S. fuscum*
10yss	20	41.7	17.13	*S. capillifolium*	105bss	210	40.1	18.79	*S. fuscum*
10bss	20	42.9	18.58	*S. fuscum*	105r	210	32.7	14.05	Rhizome
11yss	22	41.9	18.48	*S. capillifolium*	106bss	212	41.9	17.72	*S. fuscum*
12yss	24	42.8	18.64	*S. capillifolium*	107dbss	214	41.1	19.81	*S. magellanicum*
13yss	26	43.2	19.34	*S. capillifolium*	109bss	218	40.7	19.53	*S. angustifolium*
14yss	28	36.8	17.17	*S. capillifolium*	110bss	220	41.4	19.11	*S. fuscum*
15yss	30	43.8	19.36	*S. capillifolium*	111bss	222	35.0	17.49	*S. fuscum*
16yss	32	43.7	18.95	*S. capillifolium*	112bss	224	38.4	18.58	*S. fuscum*
17yss	34	45.1	19.08	*S. capillifolium*	113Lbss	226	39.1	20.00	*S. angustifolium*
Sb1yss	35	43.6	18.99	*S. capillifolium*	114bss	228	40.3	19.74	*S. fuscum*
18yss	36	43.4	20.43	*S. capillifolium*	115bss	230	23.7	17.55	*S. fuscum*
Sb2yss	37	44.0	17.82	*S. capillifolium*	115r	230	35.4	16.95	Rhizome
Sb2bss	37	41.9	18.94	*S. fuscum*	116bss	232	37.9	18.43	*S. fuscum*
19yss	38	44.5	19.32	*S. capillifolium*	117bss	234	39.8	18.16	*S. fuscum*
Sb3bss	39	42.3	19.49	*S. fuscum*	118r	236	38.7	19.14	Rhizome
20bss	40	42.6	17.88	*S. fuscum*	119r	238	32.0	15.88	Rhizome
Sb4yss	41	43.1	21.32	*S. capillifolium*	119bss	238	37.3	18.70	*S. fuscum*
21yss	42	40.8	18.13	*S. capillifolium*	120r	240	34.7	16.86	Rhizome
Sb5yss	43	43.6	19.15	*S. capillifolium*	121r	242	35.3	16.77	Rhizome
22yss	44	46.0	17.41	*S. capillifolium*	121r repeat	242	39.1	18.18	Rhizome
Sb6yss	45	45.4	16.89	*S. capillifolium*	121dbss	242	32.5	13.89	*S. magellanicum*
23yss	46	46.6	18.13	*S. capillifolium*	122DS	244	27.5	12.92	Root networks of Pteridophytae
Sb7yss	47	43.0	20.28	*S. capillifolium*	122dbss	244	37.3	14.92	*S. magellanicum*
24yss	48	46.2	18.36	*S. capillifolium*	123dbss	246	30.0	18.54	*S. magellanicum*
25yss	50	45.1	18.18	*S. capillifolium*	124dbss	248	37.9	16.46	*S. magellanicum*
26yss	52	44.0	18.92	*S. capillifolium*	125r	250	34.9	15.19	Rhizome
27yss	54	45.4	19.97	*S. capillifolium*	125DS	250	26.3	12.11	Root networks of Pteridophytae
27.5yss	55	44.9	19.40	*S. capillifolium*	125bss	250	42.5	16.56	*S. fuscum*
28yss	56	43.6	19.15	*S. capillifolium*	126dbss	252	40.0	17.58	*S. magellanicum*
28.5yss	57	46.6	17.21	*S. capillifolium*	127dbss	254	41.3	18.67	*S. magellanicum*
29yssRE	58	46.2	17.71	*S. capillifolium*	129dbss	258	39.0	20.83	*S. magellanicum*
29yss	58	44.7	17.09	*S. capillifolium*	130dbss	260	41.6	16.47	*S. magellanicum*
29.5yss	59	46.3	18.68	*S. capillifolium*	131dbss	262	42.9	18.82	*S. magellanicum*
30yss	60	38.3	19.47	*S. capillifolium*	132dbss	264	40.2	17.98	*S. magellanicum*
30.5yss	61	47.3	19.43	*S. capillifolium*	133dbss	266	40.5	19.78	*S. magellanicum*
31yss	62	42.8	20.15	*S. capillifolium*	134DS	268	34.5	13.33	Root networks of Pteridophytae
31.5yss	63	45.4	19.06	*S. capillifolium*	135DS	270	35.6	14.95	Root networks of Pteridophytae
32bss	64	44.1	19.23	*S. fuscum*	135r	270	37.4	17.63	Rhizome
32.5yss	65	44.8	17.17	*S. capillifolium*	136DS	272	33.9	13.11	Root networks of Pteridophytae
33bss	66	44.5	18.57	*S. fuscum*	137dbss	274	42.5	21.92	*S. magellanicum*
33.5yss	67	45.9	20.75	*S. capillifolium*	139dbss	278	39.6	18.48	*S. magellanicum*
34bss	68	44.3	18.78	*S. fuscum*	139r	278	lost	lost	Rhizome
34ayss	69	45.5	18.24	*S. capillifolium*	140r	280	33.3	14.80	Rhizome
35bss	70	42.0	18.34	*S. fuscum*	141r	282	30.5	15.08	Rhizome
35ayss	71	45.0	20.17	*S. capillifolium*	142r	284	34.1	15.54	Rhizome
36bss	72	45.3	19.74	*S. fuscum*	143r	286	33.0	14.26	Rhizome
36dbss	72	44.3	18.86	*S. magellanicum*	145r	290	34.2	14.06	Rhizome
36ayss	73	45.9	19.52	*S. capillifolium*	145bss	290	43.7	17.82	*S. fuscum*
37dbss	74	44.7	18.61	*S. magellanicum*	146dbss	292	38.6	15.11	*S. magellanicum*
37bss	74	34.0	17.11	*S. fuscum*	147r	294	30.9	17.71	Rhizome
38dbss	76	42.7	19.57	*S. magellanicum*	148dbss	296	40.8	17.03	*S. magellanicum*
38bss	76	43.5	18.16	*S. fuscum*	149r	298	28.9	15.67	Rhizome
39bss	78	43.1	18.36	*S. fuscum*	150r	300	35.6	16.20	Rhizome

Table 3.2: con't

40bss	80	42.5	18.97	S. fuscum	151r	302	32.3	16.56	Rhizome
41bss	82	43.8	18.21	S. fuscum	151dbss	302	35.3	16.34	S. magellanicum
42bss	84	43.7	19.68	S. fuscum	152dbss	304	39.5	17.63	S. magellanicum
43bss	86	43.3	18.09	S. fuscum	153dbss	306	38.3	19.71	S. magellanicum
44bss	88	40.4	18.45	S. fuscum	154dbss	308	40.5	18.16	S. magellanicum
45r	90	37.7	17.00	Rhizome	155dbss	310	36.6	15.27	S. magellanicum
45Lbss	90	42.7	19.43	S. angustifolium	157dbss	314	39.2	19.54	S. magellanicum
46bss	92	40.1	18.49	S. fuscum	158r	316	36.2	18.40	Rhizome
46r	92	34.3	15.65	Rhizome	159dbss	318	37.4	18.25	S. magellanicum
47bss	94	39.9	23.21	S. fuscum	160bss	320	40.2	17.75	S. fuscum
48yss	96	43.1	19.56	S. capillifolium	160dbss	320	41.3	17.21	S. magellanicum
49bss	98	34.8	19.18	S. fuscum	161dbss	322	38.1	17.34	S. magellanicum
49yss	98	41.0	19.23	S. capillifolium	162dbss	324	40.9	15.97	S. magellanicum
50r	100	33.3	15.22	Rhizome	162bss	324	39.6	17.38	S. fuscum
50yss	100	39.3	19.73	S. capillifolium	163dbss	326	39.4	17.76	S. magellanicum
51bss	102	40.5	19.80	S. fuscum	164bss	328	39.0	16.89	S. fuscum
52bss	104	41.4	20.27	S. fuscum	165r	330	35.0	14.89	Rhizome
53dbss	106	33.0	19.21	S. magellanicum	165bss	330	40.8	19.89	S. fuscum
54dbss	108	39.5	19.22	S. magellanicum	166bss	332	40.6	15.26	S. fuscum
55Lbss	110	40.5	17.76	S. angustifolium	167r	334	42.6	24.96	Rhizome
56yss	112	42.1	19.65	S. capillifolium	167 r repeat	334	39.8	25.18	Rhizome
57bss	114	42.3	19.12	S. fuscum	167bss	334	40.4	19.51	S. fuscum
58yss	116	42.2	19.68	S. capillifolium	168bss	336	38.9	16.79	S. fuscum
59bss	118	37.8	19.70	S. fuscum	169r	338	37.4	19.06	Rhizome
60bss	120	35.9	16.20	S. fuscum	169bss	338	37.7	24.82	S. fuscum
61bss	122	39.8	18.44	S. fuscum	170syss	340	36.3	15.13	S. papillosum
62bss	124	41.2	19.32	S. fuscum	171r	342	30.6	13.53	Rhizome
63bss	126	49.3	19.06	S. fuscum	171syss	342	39.3	15.17	S. papillosum
64yss	128	37.2	19.23	S. capillifolium	172syss	344	37.7	16.08	S. papillosum
65Lbss	130	40.9	19.31	S. angustifolium	173DS	346	37.5	17.88	Root networks of Pteridophytae
66yss	132	41.7	20.29	S. capillifolium	174dbss	348	39.9	17.23	S. magellanicum
67yss	134	41.1	21.42	S. capillifolium	175bss	350	39.8	17.51	S. fuscum
68yss	136	45.9	17.47	S. capillifolium	176dbss	352	40.3	16.71	S. magellanicum
69yss	138	39.8	18.37	S. capillifolium	177dbss	354	39.7	18.99	S. magellanicum
70yss	140	42.3	19.49	S. capillifolium	178dbss	356	39.8	18.14	S. magellanicum
71bss	142	43.7	19.50	S. fuscum	179dbss	358	37.0	16.21	S. magellanicum
72yss	144	41.5	19.50	S. capillifolium	180dbss	360	40.0	17.69	S. magellanicum
73bss	146	40.7	17.95	S. fuscum	181DS	362	22.1	14.24	Root networks of Pteridophytae
74bss	148	41.4	19.42	S. fuscum	181dbss	362	29.3	18.18	S. magellanicum
75bss	150	42.6	18.50	S. fuscum	185bss	370	39.5	17.08	S. fuscum
76bss	152	39.5	18.16	S. fuscum	190DS	380	36.1	14.59	Root networks of Pteridophytae
77bss	154	40.5	20.52	S. fuscum	195bss	390	39.9	16.33	S. fuscum
78bss	156	40.6	17.80	S. fuscum	195dbss	390	37.0	15.63	S. magellanicum
79bss	158	43.1	19.02	S. fuscum	200r	400	33.3	16.97	Rhizome
80bss	160	39.4	19.69	S. fuscum	205dbss	410	40.5	16.39	S. magellanicum
81yss	162	42.1	19.50	S. capillifolium	210bss	420	37.4	15.88	S. fuscum
82bss	164	42.2	19.15	S. fuscum	215bss	430	37.8	15.91	S. fuscum
83bss	166	42.5	19.56	S. fuscum	220 r	440	36.9	22.08	Rhizome
84bss	168	43.0	18.30	S. fuscum	220rbl	440	34.8	13.38	Unknown Reddish brown leaves
85yss	170	41.5	19.28	S. capillifolium	220dbss	440	39.7	16.65	S. magellanicum
85r	170	38.4	19.61	Rhizome	225bss	450	40.6	16.85	S. fuscum
86r	172	35.3	15.93	Rhizome	230bss	460	39.2	17.85	S. fuscum
86yss	172	41.6	17.34	S. capillifolium	230rbl	460	27.4	14.77	Unknown Reddish brown leaves
87yss	174	42.3	17.78	S. capillifolium	235dbss	470	42.3	16.49	S. magellanicum
88yss	176	42.0	17.37	S. capillifolium	235r	470	36.3	16.83	Rhizome
89bss	178	35.3	17.94	S. fuscum	240bss	480	40.2	16.99	S. fuscum
90bss	180	41.9	17.61	S. fuscum	245bss	490	42.5	15.17	S. fuscum
91bss	192	41.4	17.36	S. fuscum	250rbl	500	28.4	17.88	Unknown Reddish brown leaves
92bss	184	41.4	16.90	S. fuscum	250dbss	500	39.0	15.08	S. magellanicum
92r	184	38.4	13.47	Rhizome	255trh	510	35.5	13.19	Tissue remains of Herbacea
93bss	186	42.0	15.86	S. fuscum	260bss	520	38.6	16.58	S. fuscum
94bss	188	41.9	17.18	S. fuscum	265trh	530	32.2	13.37	Tissue remains of Herbacea
95yss	190	41.3	18.09	S. capillifolium	270trh	540	33.0	12.15	Tissue remains of Herbacea
95bss	190	35.8	16.74	S. fuscum	275trh	550	34.7	12.10	Tissue remains of Herbacea
95r	190	40.2	18.66	Rhizome	280trh	560	29.8	11.94	Tissue remains of Herbacea
96bss	192	40.6	17.82	S. fuscum	290trh	580	34.0	13.56	Tissue remains of Herbacea
97bss	194	41.0	18.29	S. fuscum	295trh	590	33.5	7.99	Tissue remains of Herbacea
98bss	196	42.2	18.06	S. fuscum					

The cellulose $\delta^{18}O$ values of plant macrofossils analysed ranged from ~8‰ (tissue remains of herbacae at 590 cm depth) to ~26‰ (rhizomes at 334 cm depth). Non-*Sphagnum* plant cellulose yielded generally lower cellulose $\delta^{18}O$ values with the lowest values recorded in tissue remains of herbacae from the lowermost 60cm of the Mer Bleue Bog core. *Sphagnum* $\delta^{18}O_{cel}$ values vary from ~ 25‰ at 338 cm depth to ~14‰ at 242 cm depth with a standard deviation of 1.47 (n=203). There is a generally decreasing trend from ~19±1.2‰ (1σ, 11 samples) at 0-20 cm depth to ~16‰±0.97 (1σ, 4 samples) at 480-520 cm depth (Figure 3.3). Plant cellulose oxygen concentrations range from ~20% to 50% with a standard deviation of 4.24 (n=254) through the 6 m section. As observed with the isotopic values, the oxygen concentrations decreased with core depth and were generally higher in *Sphagnum* compared to other plant macrofossils (Figure 3.3).

3.7.2 Mer Bleue Bog age-depth model

The top of the section = 0 cm depth corresponded to the end of the 2007-growing season, because the samples were taken from frozen ground in March 2008. The obtained ^{14}C dates for three samples from near the top of the core (MB16 (32-33cm), MB22 (44-45cm) and MB22 (46-47cm)) provided very young ages, which may have been related to post-bomb (~1964) influence.

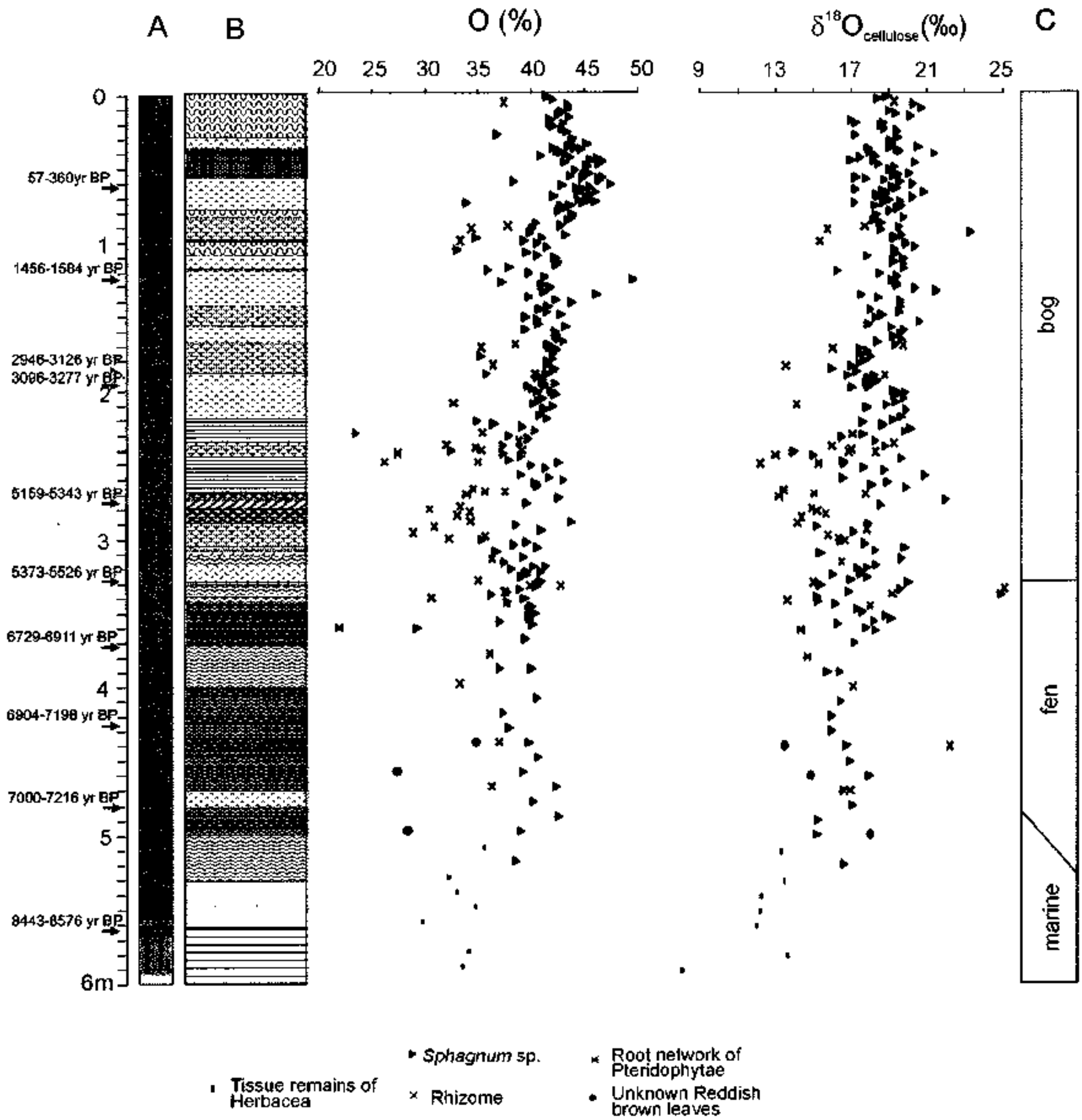

Figure 3.3: Mer Bleue core sedimentology, oxygen concentration and isotope data of cellulose from different plant material of the Mer Bleue Bog core.

A: Rock color code following Munsell Chart (Munsell, 1975) and calibrated age (Table 3.1), B: Sedimentology, C: Depositional environments.

Kilian (1995) found that ^{14}C dates obtained from bulk peat samples are sometimes affected by the reservoir effect and time-averaging due to sample heterogeneity and contamination from younger plant material. Samples that are not completely cleaned of rootlets or fungal remains may also provide suspect results (e.g., Kilian et al., 2000; Goslar et al., 2005). Great care was thus taken when subsampling for ^{14}C dating. Thus, the age of the three post-bomb samples that had a ^{14}C date with post-bomb signature (maximum age of 1964 A.D.) could be as much as a few decades older. Fortunately, the age of the upper part of the core was constrained by the first appearance of *Ambrosia* in the section at the 52-53 cm sampling interval, which in this area corresponds to an age of ~ 1860 A.D. (Talbot et al., 2010). Further evidence supporting an age estimate of ~1860 A.D. for the first *Ambrosia* appearance are as follows:

1) Kennett and Heritage Quest Inc. (1999) indicated in their archaeological assessment report of the existing Hydro Corridor between the Hawthorne Transformer Station in Ottawa and the Cumberland Junction that only two farms existed in the Mer Bleue area around 1870 A.D., and
2) The Ramsar Convention on Wetlands (1975) reported that farming and logging in the area began in the 1870s.

The statistical errors (standard deviations) associated with the 10 radiocarbon-dates were characterized by prominent probability peaks that ranged from 22-33 years (see Table 3.1). The 2σ confidence interval of the age model below 62 cm was determined based on the average of the confidence intervals of the individual samples. From 62 cm toward the top of the core the 2σ confidence interval gradually decreased to 0.5 years by 2007 A.D.

The age-depth model of the Mer Bleue Bog core was constructed using exponential, linear and polynomial regression functions that reflect different stages of peat decomposition, and gradual to abrupt changes in the depositional environment through the last ~ 9200 years (Figure 3.4). The age model utilized the 10 calibrated mean ages, an estimated palynological age of ~1860 A.D. for first *Ambrosia* appearance detected in sample interval of 52-53 cm, and the 0 yr. B.P. intercept at the top. The following aspects were also considered prior to age model reconstruction:

(1) Fen-deposition changes gradually to bog-deposition over a short depth interval (~330-320 cm depth), which is reflected by a discontinuity in the age model.

(2) The top 25 cm of the core consisted of poorly decayed and weakly compacted *Sphagnum*-dominated plant material in the oxic zone (acrotelm). Based on current surface measurements, an uncompacted plant thickness of 5.5 cm was set for the 2007 growth season (E. Humphreys, pers. comm. 2010). The sedimentation rate of the acrotelm decreases to 0.55 cm/year from 2006 to 1972 A.D. due to increased compaction.

(3) Below 25 cm depth the peat becomes anaerobic (catotelm) and the age model follows an exponential decay model according to Clymo (1992) until a depth of 73.5 cm, where the peat is fully compacted (see appendix B). The model is adjusted to the carbon-decay model for the catotelm mass specifically designed for Mer Bleue Bog by Frolking et al. (2001, 2010). Frolking et al. (2001) proposed a peat layer mass decomposition for Mer Bleue Bog of

$$m(t)=m(0)/(1+k_o t) \qquad (3)$$

with $m(0)$ as the initial peat mass litter input (in $kg/(m^2y)$ at time t=0 (in years) with m(t) being the remaining peat mass at time t. Parameter k_o represents the moss initial mass loss rate, which is ~0.05cm/year for this bog. Following this model, the age model for the 25-73.5 cm is calculated by

$$d(t)=d(0)/(1+k_o t) \qquad (4)$$

with $d(0)$ =0.55 cm annual peat mass litter thickness at the onset of the catotelm at 25 cm depth. The model uses k_o =0.0275/year, because the integration of this equation to total thickness results in good accordance to the tie ages of 52.5 cm depth older than 1860 A.D., and 62.5 cm = ~238±36 cal. yr. B.P. This results in sedimentation rates decreasing from ~0.55 cm/year at 25 cm depth to 0.048 cm/year at ~73.5 cm depth.

(4) From 73.5 cm to 262 cm depth, the calibrated ages fit a straight line best represented by the linear regression model from five calibrated ^{14}C ages: t=23(years/cm)s-1266years where s=depth in cm, and t= time in years before present, yielding a sedimentation rate of ~ 0.04348 cm/year.

(5) From 262 cm to the fen-bog transition at 327 cm depth, the age model is calculated from a 3[rd] order polynomial function $t=-0.0003224(year/cm^3)\ s^3+0.167(year/cm^2)\ s^2-3(year/cm)s-119years$. This provides a continuous transition from the linear model above

and results in sedimentation rates from 0.05-0.33cm/year.

6) At 327 cm depth, an age model discontinuity is assigned corresponding with peat sedimentological changes at the fen-bog boundary (see appendix B). From 327 cm to the bottom of the core at 600 cm the age is modelled with a 4th order polynomial function t=0.000004925(year/cm^4)s^4+0.009666(year/cm^3)s^3-6.98(year/cm^2) s^2 +2207(year/cm)s - 251494years to the bottom of the core at 600 cm depth. This part of the age model would provide time-reversals between ~400 cm and 450 cm depth. For this reason, the 4th order polynomial was replaced by t(years)=2.74year/cm(s-375cm)+6852.65year for the intervals from 375 cm to 482cm depth (Figure 3.4), resulting in sedimentation rates varying from 0.04 to 1cm/year, yielding an average sedimentation for the fen deposits of ~0.07cm/year. The model age of 9112 ± 80 cal. yr. B.P. of the lowermost occurrence of terrestrial plant material at ~590 cm supports a previous age model by Frolking et al. (2010).

3.7.3 Cellulose oxygen isotope composition in time

The transformation of the isotope record from a depth to time-scale results in an average sampling interval of ~50 years from ~80 years BP to 7300 cal. yr. B.P., a much higher sampling resolution through the most recent 80 years, and a less frequent ~200 years sampling interval through the interval of the core deposited from ~7300 to 9200 cal. yr. B.P. (Figure 3.5B). The oxygen isotope record reveals a general trend toward heavier isotopic compositions from ~7300 cal. yr. B.P. to present as well as several multicentennial to millennial fluctuations with >1 ‰ amplitude(Figure3.5B).

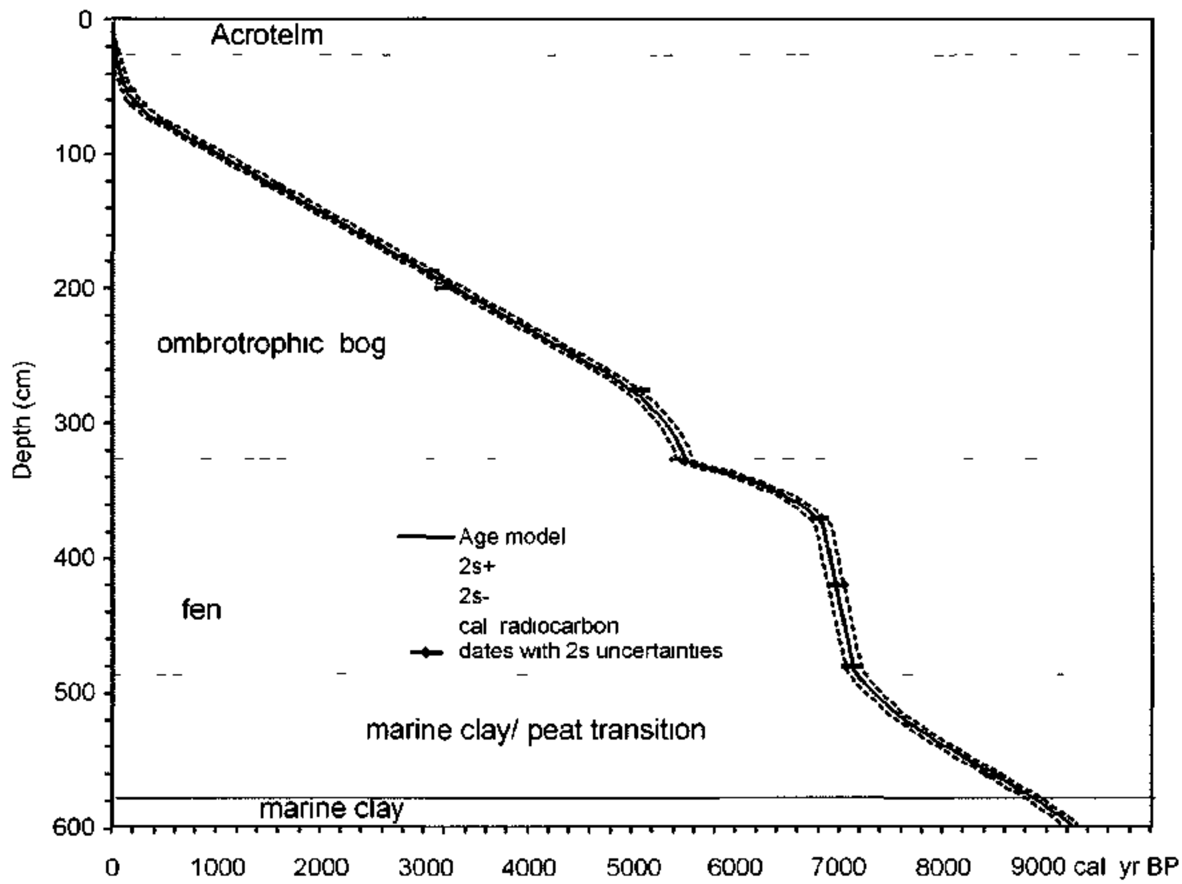

Figure 3.4: Mer Bleue core age-depth model and main depositional stages, based on 10 AMS radiocarbon ages, first occurrence of *Ambrosia* pollen (1860 A.D. at 52-53cm sample depth), and an intercept with 0m depth at October 2007 A.D. The top 25 cm consisted of poorly decayed and weakly compacted *Sphagnum*-dominated plant material in the oxic zone (Acrotelm).

The record appears relatively constant with only a few > 1 ‰ deviations from the average through the last 2800 years. The cellulose $\delta^{18}O$ record contains low-value excursions with minima at ~4200, ~3000, and ~1500 cal. yr. B.P. Relatively low cellulose $\delta^{18}O$ values at Mer Bleue through these intervals were found to coincide with global and North Atlantic climate cooling intervals (Bond et al., 1997), glacier advances and high ice-rafted sediment indices (Bond et al., 2001) (Figure 3.5C, D).

The Mer Bleue Bog $\delta^{18}O_{cel}$ record deposited through the last 2000 years shows a good correlation with the northern Hemisphere temperature reconstruction of Moberg et al. (2005). There is a particularly good correlation between the record at Mer Bleue Bog and the timing of most major warming and cooling events (Figure 3.6). In contrast the $\delta^{18}O_{cel}$ values obtained from the Mer Bleue Bog record that correspond to the Medieval warm period are higher than recorded through most of the Modern Maximum, suggesting that the climate in eastern Ontario was on average warmer during the Medieval warm period (~1000 cal. yr. B.P.) than at present.

The Mer Bleue Bog temporal $\delta^{18}O_{cel}$ record generally correlates with the Beryllium (^{10}Be) isotope anomaly, sunspot number, and solar variation events records. The Maunder minima and maximum cooling is less pronounced in the $\delta^{18}O_{cel}$ data than in the northern Hemisphere reconstructed paleotemperature record (Moberg et al., 2005), which may be due to less pronounced cooling in eastern Ontario.

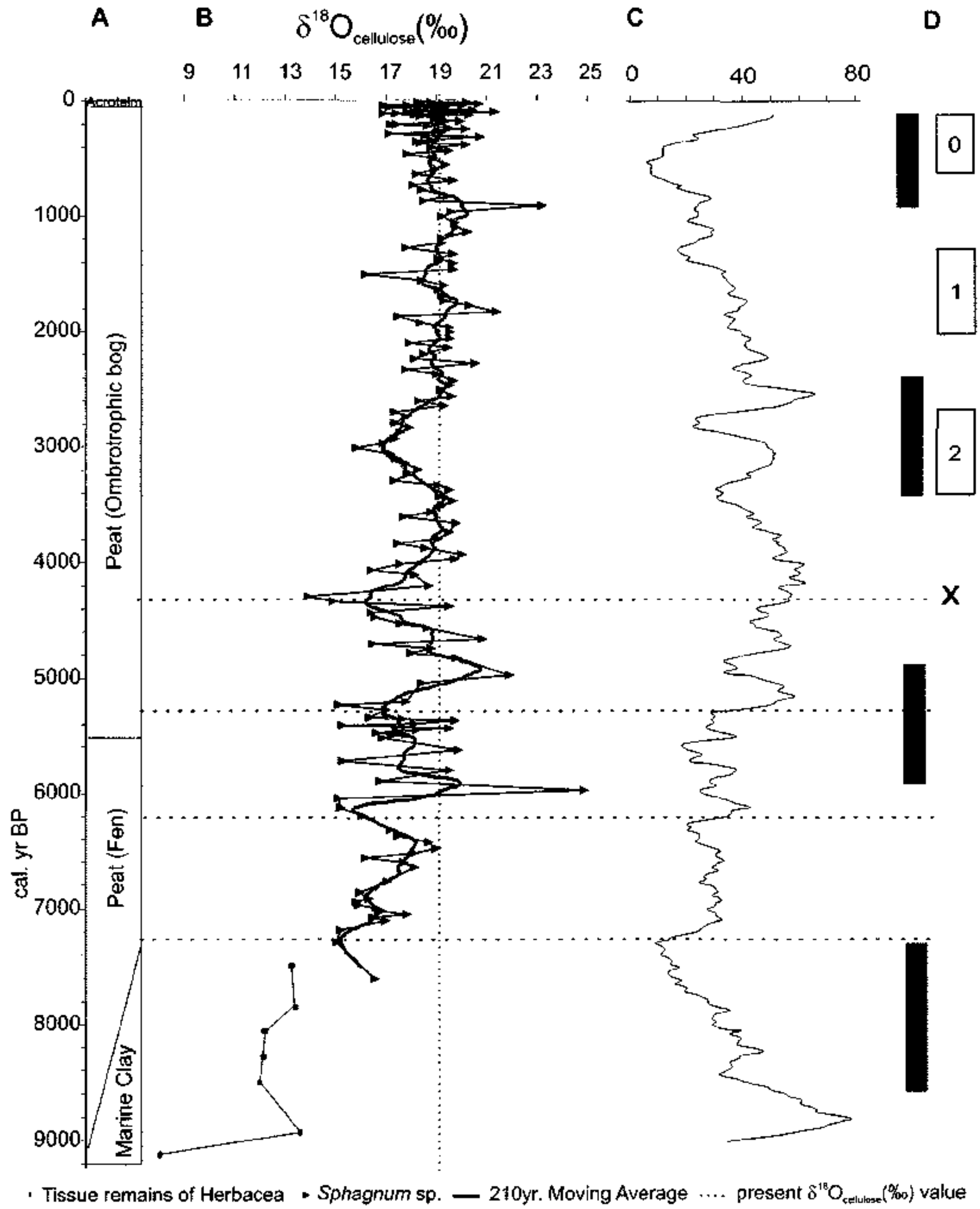

Figure 3.5: Oxygen isotope record of cellulose from Mer Bleue Bog through the last 9,200 years lined up at the same ages at 10-year steps. A: Depositional environment, B: Oxygen isotope record of cellulose with mean and 210-year moving average, C: Reconstructed sunspot record (Solanki et al., 2004) at 210-year moving average, D: Global glacier advances (black bars) and high drift ice indices (0, 1, 2) after Bond et al. (2001). X: ~4200 cal. yr. B.P. cooling in North Atlantic (Bond et al., 1997).

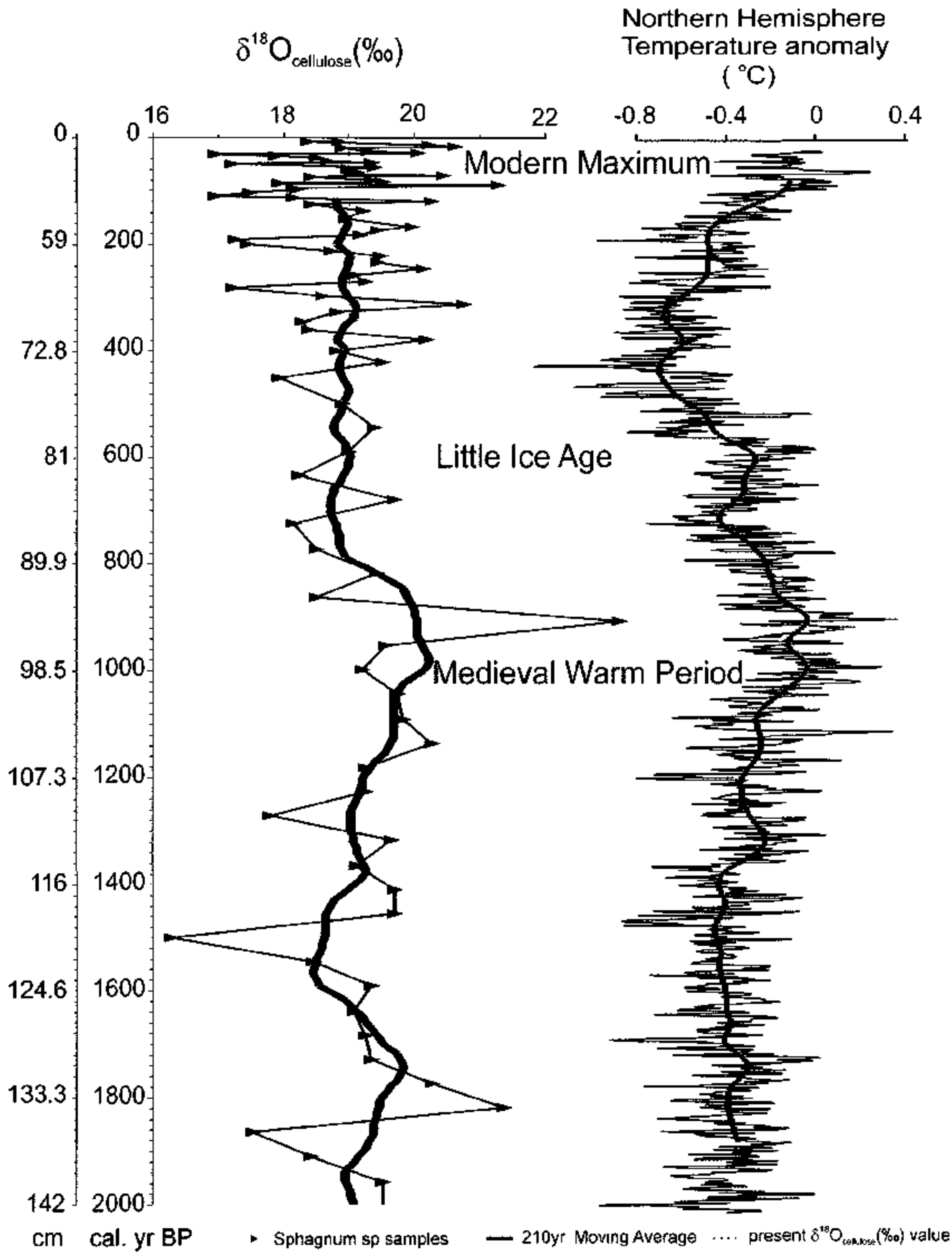

Figure 3.6: Comparison of isotope record of cellulose from Mer Bleue Bog with the northern Hemisphere temperature difference to present (in °C) by Moberg et al. (2005) through last 2,000 years. Gray-shaded area marks the Medieval Warm Interval.

The $\delta^{18}O_{cel}$ record from Mer Bleue Bog shows a good correlation with the smoothed ^{10}Be-record (Figure 3.7A, B). The low $\delta^{18}O_{cel}$ values at ~1810-1820 A.D. may be related to the lower solar activity during the Dalton Minimum (Figure 3.7), to the cooling influence of the Tambora volcanic eruption for the summer of 1816 A.D. and subsequent years, or both.

3.8 Discussion

3.8.1 Influences on $\delta^{18}O_{cel}$ signature in ombrotrophic bogs

The present-day global mean $\delta^{18}O_{cel}$ value for *Sphagnum* is ~19‰ (Daley et al., 2010), which is comparable to our results from the current study. In addition, there is a good correlation between our paleotemperature reconstruction for eastern Ontario through the last 2000 years and the northern Hemisphere reconstructed paleotemperature record (Moberg et al., 2005). Such correlations have been more difficult to establish in other areas due to a lack of long records or as a result of different climate settings (e.g., northwest Europe).

In the maritime realm of northwest Europe, comparison of instrument data with reconstructed water table changes indicates that precipitation plays a much more important role than temperature on bog surface wetness (BSW) (Charman et al., 2004; Daley et al., 2010). For example, the summer season in the northwestern U.K. is characterized by stronger and more frequent westerly airflow, which brings in cool moist air from the Atlantic, significant cloud cover, low air temperatures and persistent precipitation (Charman and Hendon, 2000; Magny, 2004; De Jong et al., 2006; Charman et. al., 2009). In northwest Europe, shifts in air mass trajectories during the growing

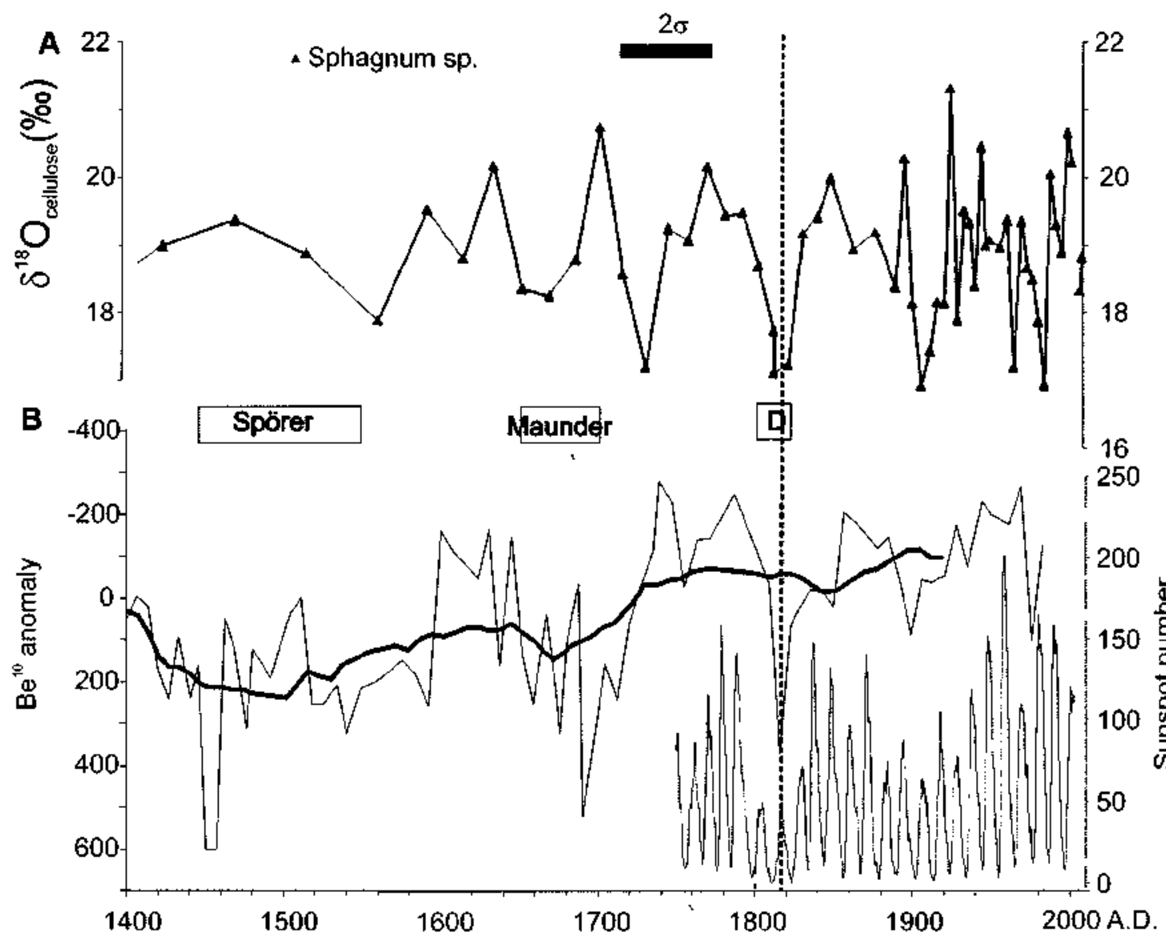

Figure 3.7: Comparison of isotope record of cellulose of Mer Bleue Bog through the last 600 years with A: solar activity events Spörer, Maunder and Dalton minima and B: Beryllium isotope anomaly (Bard et al., 2000) and measured sunspot numbers from the last 250 years. The vertical dashed line marks 1816 A.D., "the year without a summer" in eastern North America, which immediately followed the Tambora eruption.

season strongly influence BSW, which drives stable isotope variations in *Sphagnum* peat in these areas (Daley et al., 2010).

In more continental climate areas, such as prevails in eastern Canada, the sensitivity of *Sphagnum* growth in ombrotrophic bogs to temperature and precipitation variability is much different from that observed in northwest Europe counterparts. As such the relationship between temperature and precipitation has to be evaluated differently. Most European raised bogs are characterized by a longer growing season than experienced in eastern Canadian bogs, and European bogs are generally not significantly influenced by snow meltwater. Mer Bleue Bog, for example, is covered by about 70cm of snow during the winter months. At the end of April when *Sphagnum* growth begins, snow cover has disappeared but the bog water is still very cold and is sometimes still frozen a few cm below the surface.

The effects of warm summer temperature, variable precipitation (including periodic droughts) and related water table height are preserved in eastern Canadian ombrotrophic bogs by a lateral variation in the peat vegetation across bog surfaces. In Mer Bleue Bog the fen section is dominated by root and herbaceaous-rich flora, and the wetter ombrotrophic bog parts by rhizomes. Whereas the dryer ombrotrophic areas, that were established during the last ~5000-6000 years in the section studied, are primarily dominated by *Sphagnum* (>90%). The observed $\delta^{18}O_{cel}$ has remained relatively independent of change in peat lithology and sediment wetness throughout this depositional interval (Figure 3.3).

Mer Bleue Bog shows a much higher variability in both *Sphagnum* accumulation and decomposition rates due to significant year-over-year variability in summer conditions, characteristic for continental climatic zones (see Figure 3.4, and Frolking et al., 2001; Roulet et al., 2007) than in the raised bogs in northwest Europe (e.g., Charman et al., 2004; Swindles et al., 2007a, 2007b; Daley et al., 2010). However, observed stratigraphic variation in *Sphagnum* cellulose $\delta^{18}O$ are not significantly influenced by accumulation rate changes (Figures 3.5, 3.6) supporting the hypothesis that the $\delta^{18}O_{cel}$ record at Mer Bleue Bog predominantly represents temporal paleotemperature variation as opposed to geographic, plant physiological or hydrological variations related to precipitation.

3.8.2 $\delta^{18}O_{cel}$ as a paleotemperature proxy

Based on recent paleotemperature reconstructions it has been estimated that there was an ~1°C difference in the mean decadal temperature between the temperature minimum during the coldest part of the Little Ice Age, which occurred in the early 17th century and the Medieval Warm Period temperature maximum at ~1000 A.D. (e.g. Moberg et al., 2005; Frank et al., 2007; Mann et al., 2008). When compared with the range of $\delta^{18}O_{cel}$ values in this study through the same intervals (Figure 3.7) there is a calibration ratio of ~2‰/°C for temperature reconstructions using *Sphagnum* cellulose. Furthermore comparison of instrumental temperature and $\delta^{18}O_{preciptiation}$ records from Ottawa Airport weather station from ~1938-2007 with the $\delta^{18}O_{cel}$ values from Mer Bleue Bog suggest that there is a strong relationship between air temperature and $\delta^{18}O_{cel}$ values (GNIP: Global Network of Isotopes in Precipitation, 2001; Environment Canada, 2010) (Figure

3.8). The $\delta^{18}O_{cel}$ values through this interval best correlate with growing season temperatures in contrast to mean annual air temperature, demonstrating that there is a strong empirical foundation for application of the $\delta^{18}O_{cel}$ proxy (Figure 3.8).

An ~4‰ variation in *Sphagnum* derived $\delta^{18}O_{cel}$ values through the last 4000 years and ~2‰ variation in *Sphagnum* derived $\delta^{18}O_{cel}$ through the last 2000 years (Figures 3.5, 3.6) has also been confirmed by analysis of European ombrotrophic bog sections (Daley et al., 2010). A higher amplitude $\delta^{18}O_{cel}$ flux was also reported in paleotemperature reconstructions based on Chinese peat bogs, but these studies employed cellulose derived from a variety of plant types (Hong et al., 2000; 2001).

The $\delta^{18}O_{cel}$ fluctuations within the Mer Bleue Bog core are much higher through the top portion (< ~60 cm) than below. This can be attributed to the higher accumulation rate in the acrotelm above ~25 cm depth. Obtaining a reliable $\delta^{18}O_{cel}$ record through the top of the core was difficult as the uncompressed samples from the upper part of the core often correspond to monthly growth records, or short-lived weather fluctuations, which get averaged out in the more homogenized sections of the core lower down. The youngest relatively consistent low $\delta^{18}O_{cel}$ interval is recognizable through the 1970's (Figure 3.7), which corresponds to an interval of lower temperatures in eastern Ontario (e.g., Prokoph and Patterson, 2004).

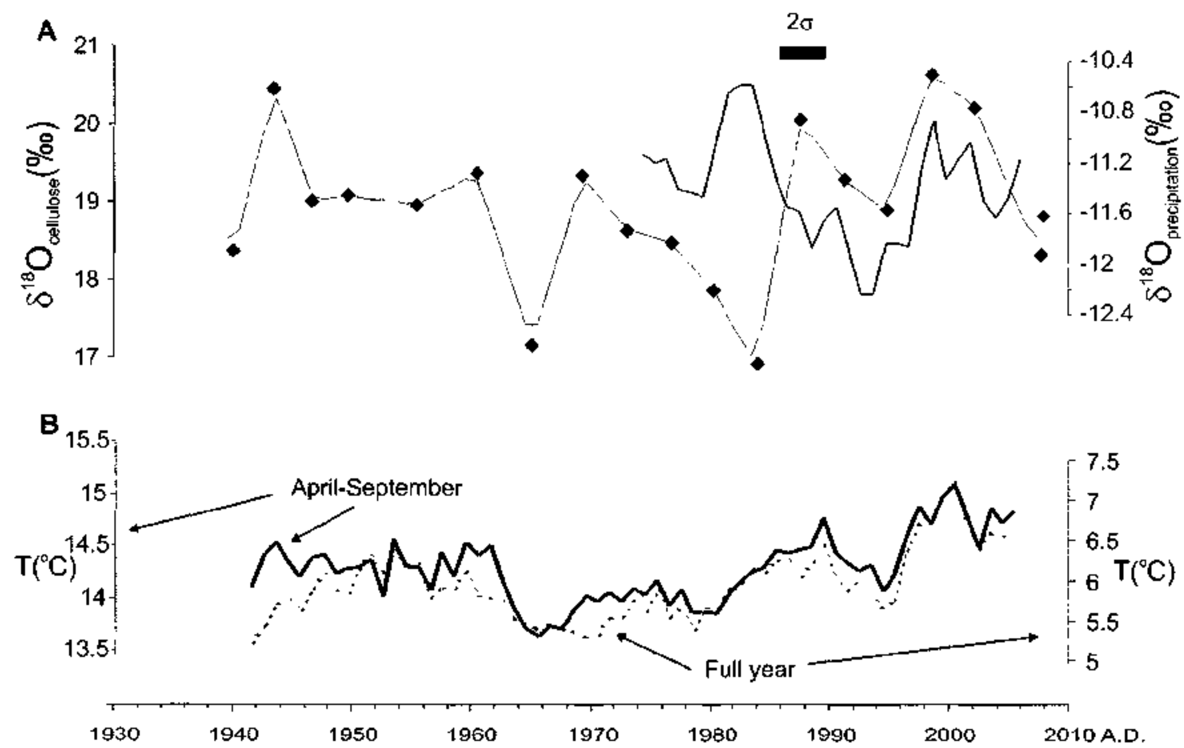

Figure 3.8: Comparison of instrumental air temperature and $\delta^{18}O_{preciptiation}$ records from Ottawa Airport Weather station from ~1938-2007 with the $\delta^{18}O_{cel}$ values from the Mer Bleue Bog (GNIP, 2001; Environment Canada, 2010).

The paleotemperature reconstruction based on *Sphagnum* $\delta^{18}O_{cel}$ from the ombrotrophic section of the Mer Bleue Bog (0-320 cm depth) is most reliable. Great care should be taken when interpreting *Sphagnum* $\delta^{18}O_{cel}$ data in the fen part of the bog below 320 cm. In the fen, plants receive their water not only from precipitation but also from groundwater and surface runoff. However, *Sphagnum* does not have roots and therefore its growth is upward from the apex only (Goslar et al., 2005). This means that there is less opportunity for the *Sphagnum* in the center of the bog to derive water from groundwater or surface runoff. Indeed, most paleoclimate reconstructions seem to interpret their *Sphagnum* $\delta^{18}O_{cel}$ record irrespective of the depositional environment (fen or ombrotrophic section) (Daley et al., 2009, 2010; Taylor, 2008) and shows good correlation with the sunspot number reconstruction by Solanki et al., (2004) from present to ~7400 years ago (Figure 3.5). Nonetheless there is more uncertainity involved in the paleotemperature interpretation in these data. In addition to the careful microscopic examination of the sampled material, the $\delta^{18}O_{cel}$ signatures do not exhibit a fan-shape pattern with depth but fall within a tight band (e.g., Veizer et al., 1999). In addition, the O% also generally decreases down-core. The *Sphagnum* $\delta^{18}O_{cel}$ varies in accordance with solar records through time, while the $\delta^{18}O_{cel}$ record shows increased variability through depth/time (e.g., Veizer et al. 1999). This results provides supporting evidence of the primary nature of geochemical signatures.

Most of the observed $\delta^{18}O_{cel}$ record obtained from Mer Bleue Bog core correlates well with other northern Hemisphere paleotemperature reconstructions (e.g., Moberg, 2005; Frank et al., 2007) as well as the reconstructions of solar activity for the interval (e.g., Bard et al., 2000; 2003; Solanki et al., 2004). The record for the modern warm period and Little Ice Age present an exception though as the amplitude of the Modern warming maximum and the signature of Little Ice Age are weaker in the Mer Bleue Bog record when compared against the entire northern Hemisphere record. This suggests, as has been observed elsewhere, that 20th century warming was not as great as some other areas (e.g. Prokoph and Patterson, 2004). In addition, a good correlation between the Mer Bleue Bog core $\delta^{18}O_{cel}$ record and the ice-rafted sediment record from the Atlantic Ocean (Bond et al., 2001) and European records (e.g., Bond et al., 1997) indicate that eastern Canada experienced a similar ~1300 year climate cycle as recognized in those areas. The low $\delta^{18}O_{cel}$ values through the 4200-4600 year BP interval coincide with the North Atlantic Cooling event (e.g., Bond et al., 1997) and provide further evidence of a strong paleoclimate link to the North Atlantic region during the Mid-Holocene.

Low $\delta^{18}O_{cel}$ values characterizing the ~3000-3300 cal. yr. B.P. interval in the Mer Bleue Bog record document a cool interval that has been recognized in other parts of North America and NE Asia (e.g., Patterson et al., 2004; Raspopov et al., 2004; Taylor, 2008; Daley et al., 2009, 2010). Also notable in the $\delta^{18}O_{cel}$ record at Mer Bleue Bog is an excursion that correlates well with pronounced cooling during the ~1810-1820 A.D. interval in eastern Canada. This cooling was brought on by climatic change triggered by the Dalton solar minima and amplified by the Mount Tambora, Indonesia eruption of 1815 (e.g., Rampino et al., 1988; Usoskin and Kovaltsov, 2004). The Mount Tambora eruption, the world's largest eruption in over 1600 years, spewed enormous quantities of volcanic dust into the atmosphere. The ensuing global cooling beginning in 1816 A.D., which became known as the "Year Without a Summer", was particularly devastating in Eastern North America. Frosts and snowfall throughout the region in June 1816 A.D., culminated in a 30 cm snowfall on Quebec City, destroying crops in the fields. Attempts at replanting failed due to further frosts in July and August when lake and river ice was observed as far south as Pennsylvania (Oppenheimer, 2003).

3.9 Conclusions

The results of this study demonstrate that:

1. $\delta^{18}O$ of *Sphagnum* cellulose can provide a reliable proxy for paleotemperature through at least the ombrotrophic bog section of Mer Bleue Bog (the last ~5400 years) for eastern Canada.

2. The $\delta^{18}O_{cel}$ record obtained from the Mer Bleue Bog core correlates well with other northern Hemisphere paleotemperature reconstructions (e.g., Moberg, 2005; Frank et al., 2007) as well as the reconstructions of solar activity for the interval (e.g., Solanki et al., 2004; Bard et al., 2000; 2003). There is however no evidence for a significant warming trend since 1850 as indicated in paleoclimate reconstructions (e.g., Jansen, 2007) and analysis of historical temperature records from the region (Prokoph and Patterson, 2004).

3. A good correlation between the Mer Bleue Bog $\delta^{18}O_{cel}$ record, and records based on ice-rafted debris from the Atlantic Ocean (Bond et al., 2001) and Europe (e.g., Bond et

al., 1997) suggest that eastern Canada experienced a similar ~1300 year climate cycle as recognized in those areas.

4. The low $\delta^{18}O_{ccl}$ values through the 4200-4600 years BP interval coincide with a North Atlantic cooling event (e.g., Bond et al., 1997; Bond et al.; 2001).

5. Low $\delta^{18}O_{cel}$ values characterizing the ~3000-3300 years BP interval in the Mer Bleue Bog record document a cool interval that has been recognized in other parts of North America and NE Asia (e.g., Patterson et al., 2004; Raspopov et al., 2004; Daley et al., 2009; 2010).

6. The $\delta^{18}O_{cel}$ record at Mer Bleue Bog shows an excursion that correlates well with pronounced cooling during the ~1810-1820 A.D. interval in eastern Canada that may have been triggered by the Dalton solar minima and amplified by global cooling associated with the Mount Tambora, Indonesia eruption of 1815 A.D. (e.g., Rampino et al., 1988; Usoskin and Kovaltsov, 2004).

3.10 References

Admiral, S.W., and Lafleur, P.M., 2007. Modeling of a latent heat partitioning at a bog peatland. *Agricultural and Forest Meteorology*, 144: 213-229.

Anderson, T.W., 1988. Late Quaternary pollen stratigraphy of the Ottawa valley – Lake Ontario region and its application in dating the Champlain Sea. In: Gadd, N.R., (Ed.), The Late Quaternary Development of the Champlain Sea Basin. *Geological Association of Canada Special Paper*, 35: 207–224.

Anderson, W.T., Bernasconi, S.M., McKenzie, J.A., Saurer, M., and Schweingruber, F., 2002. Model evaluation for reconstructing the oxygen isotopic composition in precipitation from tree ring cellulose over the last century. *Chemical Geology*, 182: 121–137.

Aravena, R., and Warner, B.G., 1992. Oxygen-18 composition of Sphagnum, and microenvironmental water relations: *The Bryologist*, 95: 445–448.

Aucour, A.-M., Hillaire-Marcel, C., and Bonnefille, R., 1996. Oxygen isotopes in cellulose from modern and Quaternary intertropical peat bogs: implications for palaeohydrology. *Chemical Geology*, 129: 341-359.

Auer, V., 1930. Peat bogs in southeastern Canada. *Canada Department of Mines, Ottawa. Memoir*, 162: 32 p.

Bard, E., Raisbeck, G., Yiou, F., and Jouzel, J., 2000. Solar Irradiance during the last 1200 years based on cosmogenic nuclides. *Tellus*, 52B: 985-992.

Bard, E., Raisbeck, G., Yiou, F., and Jouzel, J., 2003. Reconstructed Solar Irradiance Data. IGBP PAGES/World Data Center for Paleoclimatology Data Contribution Series #2003-006. NOAA/NGDC Paleoclimatology Program, Boulder CO, USA.

Bond, G., Showers, W., Cheseby, M., Lotti, R., Almasi, P., deMenocal, P., Priore, P., Cullen, H., Hajdas, I., and Bonani, G., 1997. A Pervasive Millennial-Scale Cycle in North Atlantic Holocene and Glacial Climates. *Science*, 278: 1257–1266.

Bond, G., Kromer, B., Beer, J., Muscheler, R., Evans, M.N., Showers, W., Hoffmann, S., Lotti-Bond, R., Hajdas, I., and Bonani, G., 2001. Persistent Solar Influence on North Atlantic Climate During the Holocene. *Science*, 294: 2130-2136.

Bonsal, B.R., Zhang, X., Vincent, L.A., and Hogg, W.D., 2001. Characteristics of daily and extreme temperatures over Canada. *J. Climate*, 14: 1959-1976.

Booth, R.K., and Jackson, S.T., 2003. A high-resolution record of late-Holocene moisture variability from a Michigan raised bog, USA. *The Holocene*, 13: 863-876.

Booth, R.K., Notaro, M., Jackson, S.T., and Kutzbach, J.E., 2006. Widespread drought episodes in the western Great Lakes during the past 2000 years: geographic extent and potential mechanisms. *Earth and Planetary Science Letters*, 242: 415-427.

Brenninkmeijer, C.A.M., van Geel, B., and Mook, W.G., 1982. Variations in the D/H and 18O/16O ratios in cellulose extracted from a peat bog core. *Earth and Planetary Science Letters*, 61: 283-290.

Charman, D.J., Barber, K.E., Blaauw, M., Langdon, P.G., Mauquoy, D., Daley, T.J., Hughes, P.D.M., and Karofeld, E., 2009. Climate drivers for peatland palaeoclimate records. *Quaternary Science Reviews*, 28: 1811–1819.

Charman, D.J., Brown, A.D., Hendon, D., and Karofeld, E., 2004. Testing the relationship between Holocene peatland palaeoclimate reconstructions and instrumental data at two European sites. *Quaternary Science Reviews*, 23: 137–143.

Charman, D.J., and Hendon, D., 2000. Long-term changes in soil water tables over the past 4500 years: relationships with climate and North Atlantic atmospheric circulation and sea surface temperature. *Climatic Change*, 47: 45–59.

Clymo, R.S., and Hayward, P.M., 1982. The Ecology of *Sphagnum*. In: Smith, A.J.E. (Ed.), Bryophyte Ecology. Chapman and Hall, London, New York, 511 p.

Daley, T.J., 2007. Tracking Holocene climate change using peat bog stable isotopes. Ph.D. thesis, University of Southampton, UK, 358 p.

Daley, T.J., Street-Perrott, F.A., Loader, N.J., Barber, K.E., Hughes, P.D.M., Fisher, E.H., and Marshall, J.D., 2009. Terrestrial climate signal of the '8200 yr B.P. cold event' in the LabradorSea region. *Geology,* 37: 831–834.

Daley, T.J., Barber, K.E., Street-Perrott, F.A., Loader, N.J., Marshall, J.D., Crowley, S.F., and Fisher, E.H., 2010. Holocene climate variability revealed by oxygen isotope analysis of *Sphagnum* cellulose from Walton Moss, northern England. *Quaternary Science Reviews*, 29: 1590-1601.

Dansgaard, W., 1964. Stable isotopes in precipitation. *Tellus*, 16: 436–468.

De Jong, R., Bjorck, S., Bjorkman, L., and Clemmensen, L.B., 2006. Storminess variation during the last 6500 years as reconstructed from an ombrotrophic peat bog in Halland, southwest Sweden. *Journal of Quaternary Science*, 21: 905–919.

Dean, W., Anderson, R., Bradbury, J.P., and Anderson, D., 2002. A 1500-year record of climatic and environmental change in Elk Lake, Minnesota I: Varve thickness and grey-scale density. *Journal of Paleolimnology*, 27: 287-299.

DeNiro, M.J., and Epstein, S., 1981. Isotopic composition of cellulose from aquatic organisms. *Geochimica et Cosmochimica Acta,* 45: 1885–1894.

Edwards, T.W.D., Aravena, R.O., Fritz, P., and Morgan, A.V., 1985. Interpreting paleoclimate from 18O and 2H in plant cellulose: comparison with evidence from fossil insects and relict permafrost in southwestern Ontario. *Canadian Journal of Earth Sciences*, 22: 1720–1726.

Elson, J.A., Elson, J.B., 1969. Phases of the Champlain sea indicated by littoral mollusks. *Geological Society of America Bulletin*, 70: 1596.

Environment Canada, 2010. National Climate Data and Information Archive. www.climate.weatheroffice.gc.ca

Epstein, S., Yapp, C.J., and Hall, J.H., 1976. Determination of the D/H Ratios of Nonexchangeable Hydrogen in Cellulose Extracted from Aquatic and Land Plants. *Earth Planet Science Letters,* 30: 241–251.

Epstein, S., Thompson, P. and Yapp, C.J., 1977. Oxygen and Hydrogen Isotopic Ratios in Plant Cellulose. *Science*, 198: 1209 – 1215.

Farquhar, G.D., Barbour, M.M., and Henry, B.K., 1998. Interpretation of oxygen isotope composition of leaf material. In: Griffiths, H. (Ed.), Stable Isotopes: integration of biological, ecological, and geochemical processes. Environmental Plant Biology. BIOS Scientific Publishers Ltd, Oxford, UK, pp. 27-60.

Francey, R.J., and Farquhar, G.D., 1982. An explanation for the $^{13}C/^{12}C$ variations in tree rings. *Nature*, 297: 28–31.

Frank, D., Esper, J.D., and Cook, E.R., 2007. Adjustment for proxy number and coherence in a large-scale temperature reconstruction. *Geophysical Research Letters*, 34: L16709, doi:10.1029/2007GL030571.

Fricke, H.C., and O'Neil, J.R., 1999. The correlation between 18O/16O ratios of meteoric water and surface temperature: its use in investigating terrestrial climate change over geologic time. *Earth and Planetary Science Letters*, 170: 181–196.

Frolking, S., Roulet, N.T., Tuittila, E., Bubier, J.L., Quillet, A., Talbot, J., and Richard, P.J.H., 2010. A new model of Holocene peatland net primary production, decomposition, water balance, and peat accumulation. *Earth Syst. Dynam. Discuss.*, 1: 115–167.

Frolking, S., Roulet, N.T., Moore, T.R., Lafleur, P.M., Bubier, J.L., and Crill, P.M., 2001. Modeling the seasonal to annual carbon balance of Mer Bleue Bog, Ontario, Canada. *Global Biogeochemical Cycles*, 16: doi 10.1029/2001GB0011457.

Gajewski, K., Viau, A., Sawada, M., Atkinson, D., and Wilson, S., 2001. *Sphagnum* peatland distribution in North America and Eurasia during the past 21,000 years. *Global Biogeochemical Cycles*, 15: 297-310.

Global Network of Isotopes in Precipitation (GNIP/ISOHIS) 2001. http://isohis.iaea.org/. International Atomic Energy Agency.

Goslar T., van der Knaap W.O., Hicks S., Andric M., Czernik J., Goslar E., Räsänen S., and Hyötylä H.H. 2005. Radiocarbon dating of modern peat profiles: pre- and post-bomb 14C variations in the construction of agedepth models. *Radiocarbon*, 47: 115–134.

Hong, Y.T., Jiang, H.B., Liu, T.S., Zhou, L.P., Beer, J., Li, H.D., Leng, X.T., and Hong, B., 2000. Response of climate to solar forcing recorded in a 6000-year ^{18}O time-series of Chinese peat cellulose. *The Holocene*, 10: 1-7.

Hong, Y.T., Wang, Z.G., Jiang, H.B., Lin, Q.H., Hong, B., Zhu, Y.X., Wang, Y., Xu, L.S., Leng, X.T., and Li, H.D., 2001. A 6000-year record of changes in drought and precipitation in northeastern China based on a δ^{13}C time series from peat cellulose. *Earth and Planetary Science Letters*, 185: 111-119.

IPCC, 1996. Climate change 1995: The science of climate change. In: Intergovernmental Panel on Climate Change. Houghton, J.T., Miro Filho, L.G., Callander, B.A., Harris, N., Kattenberg, A., and Maskell, K. (Eds.), Cambridge University Press, Cambridge: 572 pp.

Jansen, E., Overpeck, J., Briffa, K.R., Duplessy, J.-C., Joos, F., Masson-Delmotte, V., Olago, D., Otto-Bliesner, B., Peltier, W.R., Rahmstorf, S., Ramesh, R., Raynaud, D., Rind, D., Solomina, O., Villalba, R., and Zhang, D. 2007. Palaeoclimate. In: Climate Change 2007: The Physical Science Basis. In: Contribution of Working Group I to the Fourth Assessment Report of the Intergovernmental Panel on Climate Change, In: Solomon, S., Qin, D, Manning, M, Chen, Z, Marquis, M, Averyt, K.B, Tignor M., and Miller, H.L. (Eds.). Cambridge University Press, Cambridge, United Kingdom and New York, NY, USA.

Jowsey, P.C., 1966. An improved peat sampler. *The New Phytologist*, 65: 245–248.

Joyal, R., 1970. Description de la tourbière à Sphaignes Mer Bleue près d'Ottawa. 1. Végétation. *Canadian Journal of Botany*, 48: 1405–1418.

Kennett, B., and Heritage Quest Inc., 1999. Stage 1 Archaeological Assessment of the Hydro Transmission Corridor from the Hawthorne Transformer Station (Ottawa) to the Cumberland Junction. Regional Municipality of Ottawa Carleton, Ottawa, Canada.

Kilian M.R., van der Plicht J., and van Geel B., 1995. Dating raised bogs: new aspects of AMS 14C wiggle matching, a reservoir effect and climatic change. *Quaternary Science Reviews*, 14: 959–966.

Kilian M.R., van Geel B., and van der Plicht J. 2000. 14C AMS wiggle matching of raised bog deposits and models of peat accumulation. *Quaternary Science Reviews*, 19: 1011–1033.

Lévesque, P.E.M., Dinel, H., and Larouche, A., 1988. Guide to The identification of Plant Macrofossils in Canadian Peatlands. Research Branch, Agriculture Canada, Publication No. 1817: 65pp.

Libby, L.M., and Pandolfi, L.J., 1974. Temperature Dependence of Isotope Ratios in Tree Rings. *Proceedings of the National Academy of Sciences*, 71: 2482–2486.

Loader, N.L., McCarroll, D., van der Knaap, W.O., Robertson, I., and Gagen, M., 2007. Characterizing carbon isotopic variability in *Sphagnum*. *Holocene*, 17: 403–410.

Magny, M., 2004. Holocene climate variability as reflected by mid-European lake level fluctuations and its probable impact on prehistoric human settlements. *Quaternary International*, 113: 65–79.

Mann, M.E., Zhang, Z., Hughes, M.K., Bradley, R.S., Miller, S.K., Rutherford, S., and Ni, F., 2008. Proxy-based reconstructions of hemispheric and global surface temperature variations over the past two millennia. *PNAS*, 105:13252-13257.

Mauquoy, D., and van Geel, B., 2007. Plant Macrofossil Methods and Studies/Mire and Peat Macros. Elsevier, Amsterdam: pp. 2315-2336.

Ménot, G., and Burns, S.J., 2001. Carbon isotopes in ombrogenic peat bog plants as climatic indicators: calibration from an altitudinal transect in Switzerland. *Organic Geochemistry*, 32: 233–245.

Ménot-Combes, G., Burns, S.J., and Leuenberger, M., 2002. Variations of 18O/16O in plants from temperate peat bogs (Switzerland): implications for paleoclimatic studies. *Earth and Planetary Science Letters*, 202: 419–434.

Moberg, A., Sonechkin, D.M., Holmgren, K., Datsenko, N.M., and Karle´n, W., 2005. Highly variable northern Hemisphere temperatures reconstructed from low- and high-resolution proxy data, *Nature*, 433: 613– 617.

Moschen, R., Kühl, N., Rehberger, I., and Lücke, A., 2009. Stable carbon and oxygen isotopes in sub-fossil *Sphagnum*: Assessment of their applicability for palaeoclimatology. *Chemical Geology*, 259: 262-272.

Mott, R.J., and Camfield, M., 1969. Palynological Studies in the Ottawa Area. Geological Survey of Canada, Ottawa: pp. 1–16.

Munsell Color Company, 1975. Munsell Soil Color Charts. Munsell Color Company, MD, USA.

O'Leary, M.H., Treichel, I., and Rooney, M., 1986. Short-term measurement of carbon isotope fractionation in plants. *Plant Physiology*, 80: 578–582.

Oppenheimer, C., 2003. Climatic, environmental and human consequences of the largest known historic eruption: Tambora volcano (Indonesia) 1815. *Progress in Physical Geography*, 27: 230–259.

Patterson, R.T., Prokoph, A., and Chang, A.S., 2004. Late Holocene sedimentary response to solar and cosmic ray activity influenced climate variability in the NE Pacific. *Sedimentary Geology*, 172: 67-84.

Pendall, E., Markgraf, V., White, J.W.C., Dreier, M., and Kenny, R., 2001. Multiproxy record of late Pleistocene–Holocene climate and vegetation changes from a peat bog in Patagonia. *Quaternary Research*, 55: 168–178.

Proctor, M.C.F., 1982. Physiological Ecology: Water Relations, Light, and Temperature Responses, Carbon Balance. In: A.J.E. Smith (Editor), Bryophyte Ecology. Chapman and Hall, New York, pp. 333-381.

Prokoph, A., and Patterson, R.T., 2004. Application of wavelet and regression analysis in assessing temporal and geographic climate variability; Eastern Ontario, Canada as a case study. *Atmosphere-Ocean*, 42: 201-212.

Rampino, M.R., Self, S., and Stothers, R.B., 1988. Volcanic Winters. *Annual Review of Earth and Planetary Sciences*, 16: 73-99.

Raspopov, O.M., Dergachev, V.A., and Kolstroem, T., 2004. Periodicity of climate conditions and solar variability derived from dendrochronological and other palaeoclimatic data in high latitudes. *Palaeogeography, Palaeoclimatology, Palaeoecology*, 209: 127-139.

Reimer, P.J., Baillie, M.G.L., Bard, E., Bayliss, A., Beck, J.W., Bertrand, C.J.H., Blackwell, P.G., Buck, C E., Burr, G.S., Cutler, K.B., Damon, P.E., Edwards, R.L., Fairbanks, R.G., Friedrich, M., Guilderson, T.P., Hogg, A.G., Hughen, K.A., Kromer, B., McCormac, F.G., Manning, S.W., Ramsey, C.B., Reimer, R.W., Remmele, S., Southon, J.R., Stuiver, M., Talamo, S., Taylor, F.W., van der Plicht, J., and Weyhenmeyer, C.E., 2004. IntCal04 Terrestrial radiocarbon age calibration, 26 - 0 ka BP. *Radiocarbon*, 46: 1029-1058.

Roden, J.S., Lin, G.G., and Ehleringer, J.R., 2000. A mechanistic model for interpretation of hydrogen and oxygen isotope ratios in tree-ring cellulose. *Geochimica et Cosmochimica Acta*, 64: 21–35.

Roulet, N.T., Lafleur, P.M., Richard, P.J.H., Moore, T.R., Humphreys, E., and Bubier, J.L., 2007. Contemporary carbon balance and late Holocene carbon accumulation in a northern peatland. *Global Change Biology*, 13: 397–411.

Rozanski, K., Araguas-Araguas, L., and Gonfiantini, R., 1993. Isotopic patterns in modern global precipitation. *Climate Change in Continental Isotopic Records*, 78: 1–36.

Skrzypek, G., Kałużny, A., Wojtuń, B., and Jędrysek, M.O., 2007. The carbon stable isotopic composition of mosses—the record of temperature variations. *Organic Geochemistry*, 38: 1770–1781.

Smith, A.J.E., 2004. The moss flora of Britain and Ireland, Second edition. Cambridge University Press, Cambridge.

Solanki, S.K., Usoskin, I.G., Kromer, B., Schüssler , M., and Beer., J., 2004. An unusually active Sun during recent decades compared to the previous 11,000 years. *Nature*, 431: 1084-1087.

Sternberg, L., Da, S.L., DeNiro, M.J., and Savidge, R.A., 1986. Oxygen isotope exchange between metabolites and water during biochemical reactions leading to cellulose synthesis. *Plant Physiology*, 82: 423–427.

Suess, H.E., 1980. The radiocarbon record in tree rings of the last 8000 years. *Radiocarbon*, 22: 200–209.

Sukumar, R., Ramesh, R., Pant, R.K., and Rajagopalan, G., 1993. A $\delta^{13}C$ record of late Quaternary climate change from tropical peat in southern India. *Nature*, 364: 703-706.

Swindles, G.T., Plunkett, G., and Roe, H.M., 2007a. A multiproxy climate record from a raised bog in County Fermanagh, Northern Ireland: a critical examination of the link between bog surface wetness and solar variability. *J. Quaternary Science*, 22: 667-679.

Swindles, G.T., Plunkett, G., and Roe, H.M., 2007b. A delayed climatic response to solar forcing at 2800 cal. BP: multi-proxy evidence from three Irish peatlands. *The Holocene*, 17: 177–82.

Talbot, J., Richard, P.J.H., Roulet, N.T., and Booth, R.K., 2010. Assessing long-term hydrological and ecological responses to drainage in a raised bog using paleoecology and a hydrosequence. *Journal of Vegetation Science*, 21: 143-156.

Taylor, M.A., 2008. Continental-scale validation of the temperature signal in oxygen isotopes of *Sphagnum* cellulose and its application as paleoclimate proxy. M.Sc. thesis, University of Wyoming, USA, 86 p.

Usoskin, I.G., and Kovaltsov, G.A., 2004. Long-Term Solar Activity: Direct and Indirect Study. *Solar Phys.*, 224: 37–47.

Van Breeman, N., 1995. How *Sphagnum* bogs down other plants. *TREE*, 10: 270-275.

Veizer, J., 2005. Celestial Climate Driver: A Perspective From Four Billion Years Of The Carbon Cycle. *Geoscience Canada*, 32: 13-30.

Vitt, D.H., Crum, H., and Snider, A.J., 1975. The vertical zonation of *Sphagnum* species in hummock-hollow complexes in northern Michigan. *Michigan Botany*, 14: 190–200.

White, J.W.C., Ciais, P., Figge, R.A., Kenny, R., and Markgraf, V., 1994. A high resolution record of atmospheric CO2 content from carbon isotopes in peat. *Nature*, 367: 153–156.

Wolfe, B.B., Edwards, T.W.D., Beuning, K.R.M., and Elgood, R.J., 2001. Carbon and oxygen isotope analysis of lake sediment cellulose: methods and applications. In: Last, W.M., and Smol, J.P. (Eds.), Tracking Environmental Change Using Lake Sediments.

Physical and Geochemical Methods, Vol. 2. Kluwer Academic Publishers, Dordrecht, The Netherlands, pp. 373–400.

Yapp, C.J., and Epstein, S., 1982. A reexamination of cellulose carbon bound hydrogen dD measurements and some factors affecting plant-water D/H relationships. *Geochimica et Cosmochimica Acta*, 46: 955–965.

Yu, Z. and Ito, E., 1999. Possible solar forcing of century-scale drought frequency in the northern Great Plains. *Geology*, 27: 263-266.

Zanazzi, A., and Mora, G., 2005. Paleoclimatic Implications of the Relationship Between Oxygen Isotope Ratios of Moss Cellulose and Source Water in Wetlands of Lake Superior. *Chemical Geology*, 222: 281–291.

Zhang, X., Vincent, L.A., Hogg, W.D., and Niitsoo, A., 2000. Temperature and precipitation trends in Canada during the 20th century. *Atmosphere-Ocean*, 38: 395-429.

CHAPTER FOUR

4. CENTENNIAL AND MILLENNIAL-SCALE CLIMATE RESPONSE TO SOLAR FORCING: EVIDENCE FROM THE MER BLEUE BOG, OTTAWA, ONTARIO.

4.1 Abstract

A novel combination of time-series (trend, spectral and wavelet) analysis on digital core surface photographs, X-ray scans, and cellulose oxygen isotope data was applied to determine and understand the driving forces of paleoclimate variability in eastern Canada over the last 9200 years.

Significant sedimentary and geochemical trends, cycles and abrupt cycle pattern shifts from the Mer Bleue peat core, Ottawa, eastern Canada, were characterized and compared with global solar activity proxy records such as ^{14}C production rate, sunspot numbers, and solar irradiance. Our results correlate with previously recognized solar activity fluctuations at the 150-year, ~200-250-year, ~1300-year, and ~2200-2500year cycle-bands. These solar cycles exhibit a major influence on regional climate recorded in the peat coloration and X-ray density, and oxygen isotope data from the Mer Bleue Bog core. Other more intermittent cycles such as the 80-90 years wavelength cycle detected in photographs and %O records also correlate with solar irradiance and sunspot number

variations. A shift in the isotope and sediment color cycle pattern from a ~1300 year to a ~650 year cyclicity at ~3500 cal. yr B.P. is coincident with a similar pattern shift in the solar activity cyclicity and corresponds to an onset of cool period from ~3400-2800 cal. yr B.P. in eastern Canada and in the North Atlantic region.

Keywords: Raised bog, oxygen isotopes, plant cellulose, cyclicity, solar irradiance, climate variability.

4.2 Introduction

Peatlands contain a large range of potential paleoclimate proxies including plant macrofossils such as *Sphagnum*, testate amoebae, measurements on peat humification, and biomarkers (Patterson et al., 2004; Booth et al., 2006; Plunkett and Swindles, 2008; Charman, 2010; Daley et al., 2010). Peatlands are therefore considered important archives of Holocene palaeoclimate change and particularly well suited for climate reconstructions over decadal to millennial timescales (e.g., Brenninkmeijer et al., 1982; Francey and Farquhar, 1982; O'Leary et al., 1986; Charman et al., 1999; Chiverrell, 2001).

Several studies on peat sections have found relationships between solar cycles and climate change (e.g.. Kilian et al., 1995; van Geel et al., 1996, 1998; Speranza et al., 2002; Blaauw et al., 2004; Plunkett and Swindles, 2008; Daley et al., 2010; Charman, 2010). Paleolimnological, dendrochronological and paleoceanographic studies have documented cyclic changes in moisture levels from climate records from the interior of

North America at decadal to millennial scales (Yu and Wright, 2001; Dean et al., 2002; Cumming et al., 2002; Schubert et al., 2004). For example, Crawford Lake situated in southern Ontario records evidence of rapid, regional climate change, including a rapid cooling at 11,000 cal. yr. B.P., and an equally abrupt warming at 10,200 cal. yr. B.P., possibly related to the Younger Dryas Cold Episode (Yu andd Eicher, 1998). Wavelet analysis of multi-proxy records of late Holocene laminated sediments from Elk Lake, Minnesota revealed decadal to centennial-scale climate cycles that correlate with known droughts. These cycles may be worldwide phenomena resulting from global-scale air-sea interactions or solar forcing (Mann et al., 1995; Frankignoul et al., 1997; Patterson et al., 2004).

Several studies have investigated the sensitivity of peat paleoclimate reconstructions by comparing proxy records with instrumental records of temperature and precipitation (Epstein et al., 1976, 1977; Burk and Stuiver, 1976; Charman et al., 2004; Barber and Langdon, 2007; Charman et al., 2009; Daley et al., 2009; Booth et al., 2006; Daley et al., 2010). In addition, a strong linear relationship exists between air temperature and $\delta^{18}O$ of *Sphagnum* cellulose in the Ottawa area during the last 40 years (GNIP (Global Network of Isotopes in Precipitation, 2001; Chapter III of this study).

As part of an effort to improve our understanding of the history of rapid climate change and our ability to recognize evidence of climate trends and cycles in eastern Canada, we obtained climate information for this region from the Mer Bleue Bog. The bog is located in eastern Ontario, which is characterized by a moderate continental climate

(Environment Canada, 1990) due to the moderating effects of the Great Lakes in the region. But regional controls such as latitude, air mass, storm movement, altitude, and topography of the region as well as local controls such as urbanization, surface cover and soil characteristics also strongly influence the local climate. In addition, the region lies across one of the major storm tracks of North America, with the frequent passage of low- and high-pressure systems producing wide variations in day-to-day weather.

This study applies Wavelet analysis (WA) and spectral analysis (SA) to a novel combination of oxygen isotope data, and digital records of sediment surface photographs and X-ray scans from a 6m peat section of an ombrotrophic bog (Mer Bleue, Ottawa, Ontario). The results are used to produce the first reconstruction of long-term climate trends and multidecadal–millennial scale cycles through the entire Holocene in continental eastern Canada. We further evaluate the roles of external (orbital, solar and volcanic) and internal (ocean and atmosphere) forcing factors on Holocene climate fluctuations in eastern Canada. The detected cycles and trends are compared to solar activity fluctuations (^{14}C production rate, sunspot numbers, and solar irradiance) over the last 9200 years and discussed in the context of Holocene paleoclimate reconstructions in the North Atlantic realm and North America (e.g., Bond et al., 2001; Daley et al., 2010).

4.3 Background

4.3.1 Climate forcing and dynamics

The Earth's climate is controlled by many factors in addition to greenhouse gases, and there are different scientific opinions about the significance of these factors (e.g., Jansen et al., 2007; Veizer, 2005). Besides anthropogenic greenhouse warming due to CO_2 emissions, several natural factors, such as variability in solar irradiance, size and frequency of volcanic eruptions or variations of Earth's orbit (e.g., eccentricity, obliquity and precession) may play an important primary role on climate fluctuations.

The magnitude of variations in the output of solar energy is thought to be too small to explain observed climate variability. However, it is now understood that Cosmic Ray Flux (CRF) modulation of solar irradiance controls global low-altitude cloud cover, thus cloud albedo, and, consequently enhances the climate impact of solar irradiance fluctuations (Svensmark and Friis-Christensen, 1997, Carslaw et al., 2002). The solar irradiance cyclicity is well documented in the observational record at the frequency of the ~9-12 year "Schwabe" sunspot cycle (Friis-Christensen and Lassen, 1991), and quasi-periodic ~80-90 year "Gleissberg" cycles (Gleissberg, 1958; Garcia and Mouradian, 1998). Global sea-surface temperature (SST) fluctuations of up to 0.4°C have been attributed to solar irradiance variability during a "Schwabe" sunspot cycle (Jones et al, 2001).

Longer solar activity cycles cannot be studied using direct observations, but several such cycles have been found in cosmogenic ^{14}C and ^{10}Be isotope fluctuations (e.g., Bond et al., 2001). A solar cycle with a period of 205–210 years, which is often called the de Vries or Suess cycle, has been detected in ^{14}C production rate records (e.g., Suess, 1980; Sonett and Finney, 1990; Zhentao, 1990; Usoskin et al., 2004). Solar activity lows during a "Suess-cycle" are associated with several worldwide cool periods through the last millennium such as the Maunder Minimum of the Little Ice Age (McCracken et al., 2001). Millennial scale (1000-1500 years) cycles in paleoclimate records throughout the northern Hemisphere (e.g., Esper et al., 2002; Hu et al., 2003) are also recognized in coeval fluctuations in cosmogenic nuclides ^{14}C and ^{10}Be and ice-rafted debris distribution (e.g., Bond et al., 2001). A ~2200-2500 year cycle has also been found in the cosmogenic ^{14}C record and called the "Hallstatt" solar cycle (Vasiliev and Dergachev, 2002).

4.3.2 Cellulose in Sphagnum in ombrotrophic bogs and paleoclimate

Ombrotrophic bogs are *Sphagnum*-dominated (Brenninkmeijer et al., 1982; Booth and Jackson, 2003; Booth et al., 2006) and their surface moisture is tightly coupled to atmospheric moisture. Due to the absence of stomata and vascular tissues, *Sphagnum* mosses possess limited ability to control water loss and thus follow a simple physiological water-use strategy. Given its lack of roots and stomata cells, all isotopic fractionation of the plant water, and its oxygen, is controlled environmentally prior to its assimilation by the plant and cellulose synthesis (Ménot-Combes et al., 2002).

In recent years the stable isotope composition of plant macrofossils and other organic matter from peat profiles has been considered to be an important source of paleoclimate information (e.g., O'Leary et al., 1986; Francey and Farquhar, 1982; Aucour et al., 1996). Several studies have demonstrated a direct correlation between the isotopic carbon, oxygen, and hydrogen values of cellulose and mean annual temperature (e.g., Libby et al., 1976; Epstein et al., 1976, 1977; DeNiro and Epstein, 1981; Edwards et al., 1985; Sternberg et al., 1986; Sukumar et al., 1993; White et al., 1994). Therefore, *Sphagnum* cellulose stable isotope records from ombrotrophic bogs are now considered to be very reliable proxies in paleoclimate reconstructions (Daley, 2007; Taylor, 2008; Daley et al., 2009). In chapter III (Figures 3.5 and 3.6) of the present study, it is shown that the $\delta^{18}O_{cel}$ record from the Mer Bleue Bog follows the general trend of the reconstructed sunspot number record for the last 9200 years (Solanki et al., 2004) and the reconstructed temperature record for the last 2000 years in the northern Hemisphere (Moberg et al, 2005), suggesting that $\delta^{18}O_{cel}$ could be used as paleotemperature proxy.

In order to quantify the relationship between $\delta^{18}O_{cel}$ and air temperature, we compared $\delta^{18}O_{cel}$ with the measured monthly $\delta^{18}O$ in precipitation data since 1970 A.D. from the Ottawa Airport weather station from the GNIP (Global Network of Isotopes in Precipitation) (2001) and with the monthly average air temperature data since 1938 A.D. from the same location (Environment Canada, 2010). The result shows that the $\delta^{18}O_{cel}$ record from the Mer Bleue Bog correlates well with the measured temperature for the last 70 years, with some offset probably attributable to uncertainties in the age-model for Mer Bleue (Chapter III, Figure 3.8). However, there is no apparent mismatch between the trends of $\delta^{18}O_{cel}$ and $\delta^{18}O$ in precipitation. These results are comparable to those in previous studies of continental regions (Daley, 2007; Taylor, 2008; Daley et al., 2009) confirming that $\delta^{18}O_{cel}$ could be used as a paleotemperature proxy.

4.4 Geographic and Geological Setting

The Mer Bleue Bog is a Provincial Conservation Area located in the eastern portion of the National Capital Region of Canada, about 10 km east of Ottawa, Ontario (45.41°N latitude, 75.48°W longitude, 69 m above mean sea level) (Figure 4.1). The Mer Bleue

Bog covers an area of approximately 28 km^2 and forms a roughly oval shape oriented east-west with three separate lobes in the west end of the bog (Figure 4.1). The Mer Bleue Bog is slightly domed in shape, with peat depths varying from 6 m near the centre decreasing to 0.3 m at the margins (Joyal, 1970; Roulet et al., 2007).

Deglaciation in the area of Mer Bleue Bog occurred ~13,200 years ago (Anderson, 1988). Fresh water dominated in the basin by ~10,600 cal. yr. B.P. (Lampsilis Lake phase, Elson & Elson, 1969). The present-day Mer Bleue peatland lies within an abandoned postglacial channel of the Ottawa River that was cut into the floor of the Champlain Sea basin (Anderson, 1988; Roulet et al., 2007). The peatland formed over the last 8400 years, initially as fen and transitioning to a bog phase by ca. 7100-6800 cal. yr. B.P. (Auer, 1930; Mott & Camfield, 1969; Roulet et al., 2007).

Mer Bleue Bog is an ombrotrophic bog where all nutrients and the water supply come strictly from precipitation rather than from ground water or river runoff. Sedimentation is entirely composed of autigenic plant growth, which is dominated by *Sphagnum* moss. Plant growth occurs from the end of April to early October. During the winter season, the Mer Bleue Bog is totally frozen and covered by snow. During spring and summer, the Mer Bleue surface is covered by a blanket of reddish to greenish vegetation. *Sphagnum* remains the dominant evergreen and covers the most central part of the bog together with cotton grasses, and minor occurrence of cranberries and blueberries.

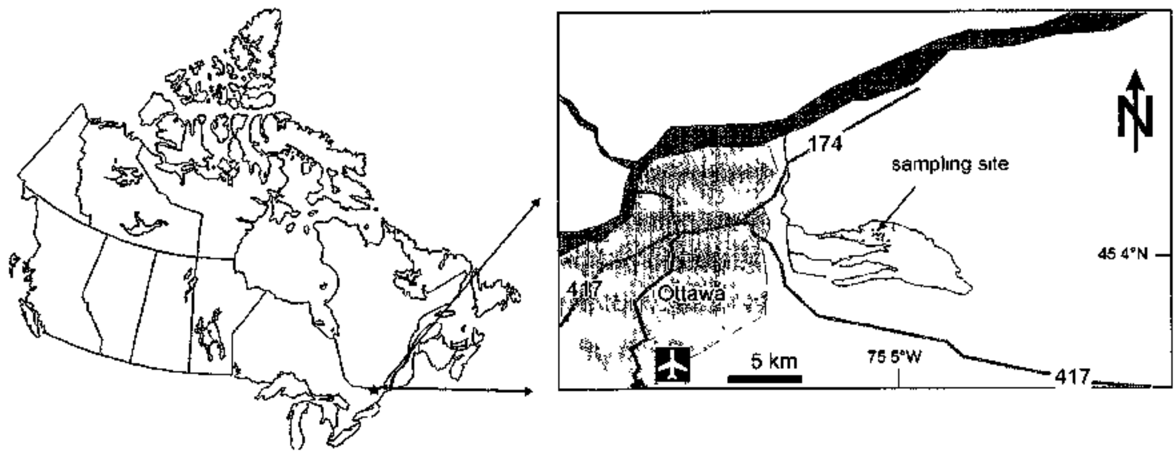

Figure 4.1: Location map of the Mer Bleue Bog, Ottawa, Ontario in eastern Canada. Asterisk marks the sampling site at the northwestern arm of Mer Bleue.

4.5 Field Sampling & Material Collection

Cores used in the present study were collected in March 2008 using a Russian Auger corer from close to the center of Mer Bleue Bog at N45°24.653', W75°31.064' adjacent to the coring location of Roulet et al. (2007). Coring protocol when using a Russian Auger in bog settings stipulates that each core be comprised of offsets collected from two different holes to ensure complete recovery of the section (e.g., Jowsey, 1966). To meet the sampling requirements of this research triplicate cores were collected, which required extraction of core intervals from six closely spaced holes. The Russian corer used permitted the retrieval of 50 cm long by 5.5 cm diameter cores. Core overlap was 20 cm through the uppermost 3.5 m of the core and 10 cm through the lower 2.5 m of the core for a complete recovery of ~ 6 m of sediment, terminating in the uppermost few cm of the underlying Champlain Sea marine clay deposits (Figure 4.2). The core material consists of relatively fresh *Sphagnum* material within the top 25 cm, and humified and decomposed peat from 25 to 500 cm depth (Figure 4.2). The peat is fully compacted below ~70 cm depth.

The macrofossil plant assemblage in the upper 5 m of the Mer Bleue cores consists of several *Sphagnum* species, rhizome, root networks of pteridophytae, tissue remains of herbacae and unknown reddish-brown leaves. *Sphagnum* dominates in the ombrotrophic bog section in the upper 3.2 m, whereas root networks of pteridophytae and unknown-reddish brown leaves dominate in the fen part between 3.2 m and 5 m. The lowermost part of the core is characterized by a step-wise transition from marine clay towards peat

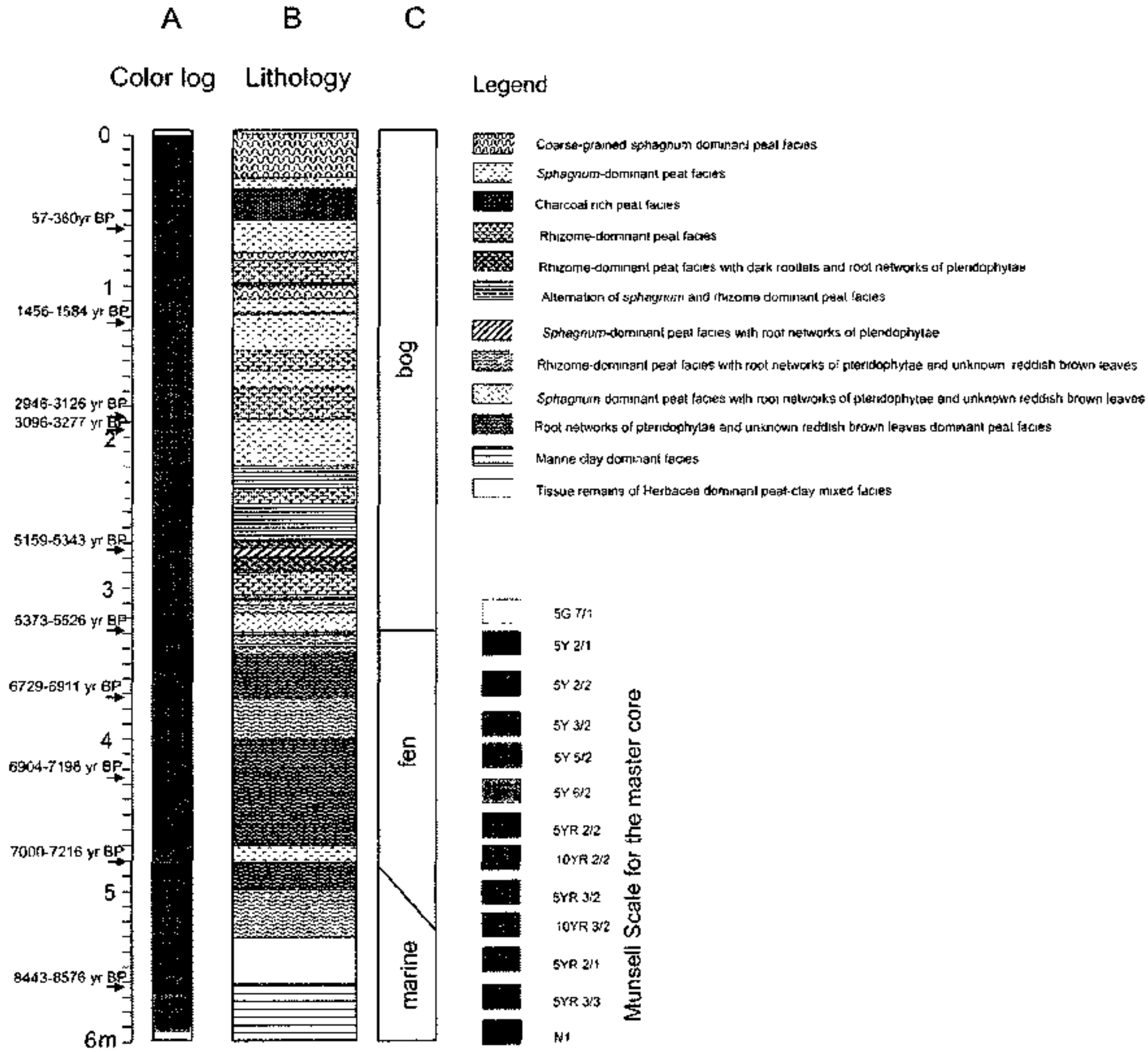

Figure 4.2: Mer Bleue core sedimentology: A: Rock color code following Munsell Chart (Munsell, 1975), B: Lithology, C: Depositional environments

in a fen environment. Tissue remains of herbacea are dominant organic macrofossils in this section (Figure 4.2).

4.6 Data and Methods

4.6.1 Plant macrofossils separation

Peat samples were gently heated in a 5% KOH solution for about 30min to dissolve humic and fulvic acids. Plant macrofossil samples were then disaggregated on a 125 μm sieves using deionized water. Isolated plant remains were kept immersed while sieving to avoid too much damage and disintegration and subsequently transferred to a plastic container. Plant macrofossil remains were suspended in distilled water for examination using an Olympus SZH-1 stereo microscope. Macrofossils were identified using several illustrated moss identification guides (Smith, 2004; Grosse-Brauckmann 1972, 1974; Lévesque et al., 1988; Mauquoy and van Geel, 2007). Once the optical analysis was completed, the remains of each sample were stored in a sealed plastic container with deionized water in the dark cooling room at 3-4°C.

Sphagnum stem sections were preferentially handpicked from petri-dishes under an Olympus SZH-1 stereo microscope. Some samples did not contain sufficient *Sphagnum* remains, in which case other plant macrofossils were selected for oxygen isotopic analysis. Hand-picked plant macrofossils were placed in porcelain crucibles and dried in an oven at about 50°C for 24 hours. The samples were then powdered, weighed, labeled, placed in small plastic vials, and sent to the University of Saskatchewan isotope laboratories for cellulose isotopic analysis.

4.6.2 Cellulose oxygen isotope analytical technique

Cellulose isotopic analyses were performed at the University of Saskatchewan isotope laboratories. Cellulose samples were baked at 60°C in a vacuum oven for 2 hours to drive off moisture, then immediately transferred and flushed in the zero blank autosampler. Samples were analyzed using a Thermo Finnigan TC/EA coupled to a Conflo III and a Delta Plus XL mass spectrometer. Samples were dropped under helium into a glassy carbon furnace and pyrolyzed at 1450°C to form hydrogen and/or carbon monoxide gases. The gases were carried in a helium stream to a GC column held at 100°C to separate the gases before being diluted in the Conflo III and passed to the mass spectrometer for analysis.

Isotope ratios were blank corrected and reported in per mil notation relative to the VSMOW-VSLAP scale. In-house oxygen standards were calibrated against international standards USGS-34 ($\delta^{18}O$ = -27.9‰ VSMOW) and USGS-35 ($\delta^{18}O$ = 57.5‰ VSMOW). An intermediate international standard, IAEA-NO3, gave the result $\delta^{18}O$ = 25.53 ± 0.27‰ VSMOW (n = 23) during calibration of in-house standards compared to the accepted value of $\delta^{18}O$ = 25.6 ± 0.4‰ VSMOW. Two in-house standards were used to set up a calibration line, and a third is used to monitor accuracy of data. Accuracy of $\delta^{18}O$ data is ±0.11‰ (n = 25). %O measurements have an accuracy of ±0.5%. Actual sample errors may be greater than these due to heterogeneity, and more accurate data may be obtained through repetition.

4.6.3 The Mer Bleue Bog age-depth model

Thirteen samples were chosen for radiocarbon AMS dating. Nine samples were analysed at the CHRONOS laboratories at Queens University of Belfast and four samples were analysed at the AMS laboratory at the University of Georgia, USA. Roots and twigs were removed from the samples. Only above-ground plant remains, preferably *Sphagnum* remains (branches or stems with leaves), were selected from the macrofossil samples.

4.6.4 Image analyses

4.6.4.1 Digital core photography

A photography unit was set up consisting of 4 lamps, a 6 Mega pixel (~3000 x ~2000 pixel) digital Sony camera with Zeiss lens fixed about 20cm high and almost directly over the peat core. Each core photograph was labelled according to core number and segment (top/bottom) (Figure 4.3A). During image processing each digital photograph image was rotated so that the top (lowest depth) is always to the left. Furthermore, a gamma-balance of 1.79 was applied to all digital photograph images to reduce the effect of reflections and to permit an easier detection of cracks and holes in the photographs.

Core photograph gray-value line-scans were obtained from the gamma-balanced photograph images (Figure 4.3B,C) using the publicly available software ImageJ (www.nih.gov) and calibrated (see appendix B) following mostly the methodology outlined by Schaaf and Thurow (1995). Data reduction was performed to remove random noise from the gray-value records. The original gray-value line-scan constitutes ~58,000 pixels over 6 m depth providing an average data interval of 0.0965 pixel/mm. The time

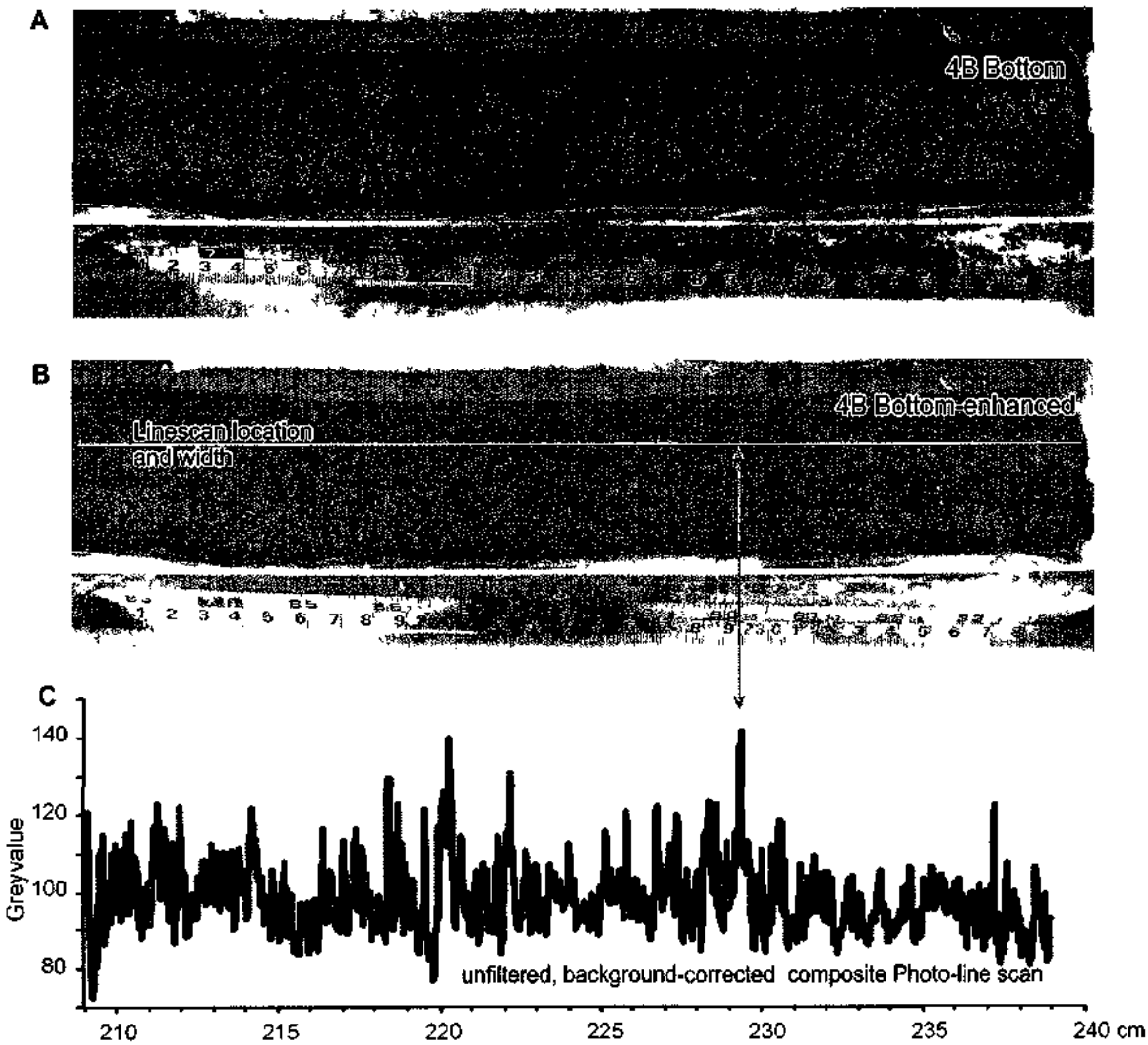

Figure 4.3: Digital photo image calibration and line-scan extraction.

A) Depth scale of the 4B section of the Mer Bleue Bog core. B) Calibration and line-scan extraction from the 4B section of the Mer Bleue Bog. Illumination problems and line-scan segments perpendicular to bedding that have been stacked to compile complete and equidistant line-scan dataset. C) Compiled gray-values line-scan from color photographs.

series dataset was reduced in two ways by averaging data (i) over 0.5 mm equidistant intervals to produce 12,000 data points, and (ii) over 5 mm equidistant intervals to produce 1,200 points. The original dataset was used to detect annual lamination, while (i) is suitable for El Nino and 11-year sunspot cycle detection, respectively and (ii) suitable for resolution of multidecadel (e.g., Pacific Decadal Oscillations (PDO), North Atlantic Oscillations (NAO), Gleissberg) cycles and longer cycles and trends.

4.6.4.2 Digital X-ray imaging

Digital *X-ray* image scanning was performed with a medical image scanner that provides a 4 Mega pixel resolution over an area of 30x30 cm. From the three duplicate cores taken, the best-preserved core ("Master-core" with least cracks, smears etc.) was selected for X-ray imaging identical to the ones used for digital core surface photography. A ruler with mm-division is included on the side of the digital images. X-ray gray-value line-scans were also obtained from the balanced digital X-ray images using ImageJ (Figure 4.4) and similarly calibrated and assembled as the digital photograph line-scan (see appendix A). The original gray-value line-scan of ~31,000 pixels over 6m depth provided an average data interval of ~0.2 pixel/mm. This dataset was reduced by averaging data over 1 mm equidistant intervals to produce 6,000 data points for time-series analysis.

4.6.5. Time series analyses

Time-series analysis such as spectral and wavelet analysis (Mann and Lees, 1996;

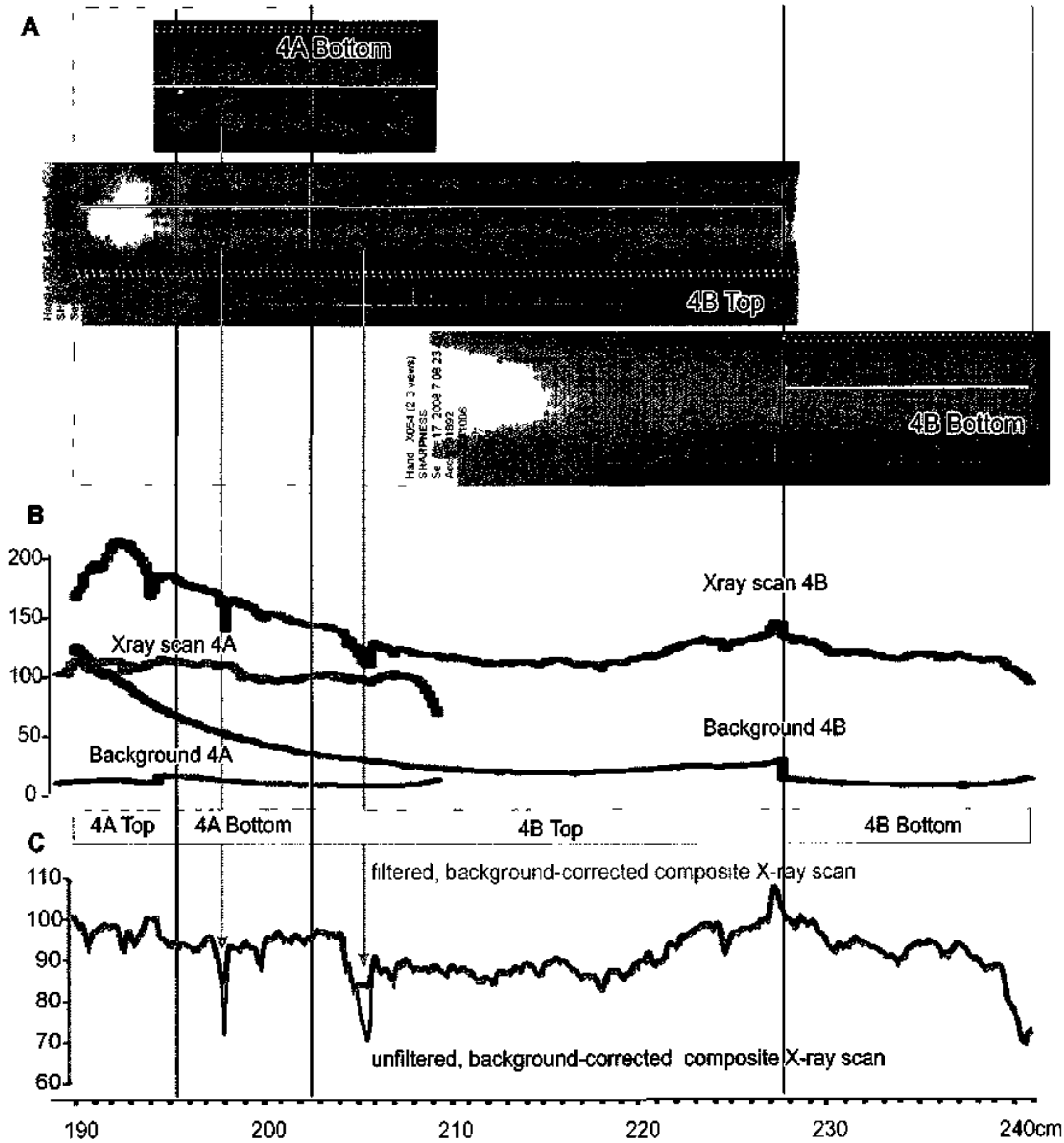

Figure 4.4: Digital X-ray image calibration and line-scan extraction of the Mer Bleue Bog core section.

A) Overlapping digital X-ray photographs,

B) calibration and line-scan extraction from the 4B section, line-scan segments perpendicular to bedding that have been stacked,

C) Compiled gray-values line-scan from X-ray photographs. Vertical lines and arrows are included for correlation.

Appenzeller, 1998; Bolton et. al., 1995; Morlet et al., 1982) were used on image gray-value line-scans, isotope data, and solar activity proxy reconstructions in both time-scale and depth-scale to detect and compare trends and cycles over the last ~9,200 years in the Mer Bleue record. Time-series analysis was also used to evaluate trends and relationships in and between the isotope and image gray-value datasets.

Spectral analysis (SA) was used to detect and determine confidence levels of sedimentary and solar intensity cycles (e.g., Davis, 1986), whereas wavelet analysis (WA) was predominantly used to detect abrupt and gradual changes in the cyclicity pattern (e.g., Torrence and Compo, 1998). SA was applied to geochemical and line-scan data in time-scale (Prokoph and Patterson, 2004a), whereas WA is applied to records in both depth- and time-scale.

4.6.5.1 Spectral analysis

Spectral analysis (Fourier transform) is defined by

$$P^2{}_f = \int x(t)e^{-i2\pi ft}dt \ , \qquad (1)$$

with $x(t)$ the discrete time series, f the frequency, and P^2 the spectral power (Davis, 1986). The spectral power is illustrated by its "power spectrum". There are different ways to calculate the spectral power. Here, we used the software REDFIT (Schulz and Mudelsee, 2002) that calculates the periodogram to express the spectral power, that is, the raw, squared Fourier coefficients, and confidence intervals for the spectral peaks.

Confidence intervals were calculated using the combined white noise and red noise assumption outlined by Mann and Lees (1996).

4.6.5.2 Wavelet analysis

Wavelet Analysis (WA) emerged as a filtering and data compression method in the 1980s (e.g., Morlet et al., 1982). WA transforms a time-series simultaneously in the 'depth' or 'time' domain and scale (or frequency) domain by using various shapes and sizes of short filtering functions called 'wavelets'. Continuous Wavelet transform (CWT) allows for the automatic localization of periodic-signals, gradual shifts and abrupt interruptions, trends and onsets of trends in time series (Rioul and Vetterli, 1991). CWT uses narrow band analysis windows at high frequencies, and wide analysis windows at low frequencies, in contrast to the Sliding-Window Fourier transform that uses shifting analysis windows of constant width (Rioul and Vetterli, 1991). The wavelet coefficients W of a time series x(s) are calculated by a simple convolution

$$W_{\psi}(a,b)=\left(\frac{1}{\sqrt{a}}\right)\int x(s)\psi\left(\frac{s-b}{a}\right)ds \tag{2}$$

where ψ is the mother wavelet; the variable a is the scale factor that determines the characteristic frequency or wavelength; and b represents the shift of the wavelet over $x(s)$ (Chao and Naito, 1995). The bandwidth resolution for a wavelet transform varies with $\Delta a=\Delta f=\frac{\sqrt{2}}{4\pi al}$, and a location resolution $\Delta b=\frac{al}{\sqrt{2}}$. Note that due to Heisenberg's uncertainty principle $\Delta f \Delta b \geq 1/4\pi$ the resolution of Δb and Δf cannot be arbitrarily small. Parameter l is used to modify wavelet transform bandwidth resolution either in favor of time or in favor of frequency. In this study, the CWT was used with the Morlet wavelet as the mother function (Morlet et al., 1982). The Morlet wavelet is simply a sinusoid with wavelength/period a modulated by a Gaussian function, and has provided robust results in analyses of climate-related records (Torrence and Compo, 1998; Prokoph and Patterson, 2004b). The influence of the edge effects is well defined for the Morlet wavelet, and increases with increasing wavelength (scale) and parameter l. The boundary of edge effects on the wavelet coefficients forms a wavelength dependent curve, called the 'cone of influence' (Torrence and Compo, 1998). The wavelet coefficient W was normalized to represent the amplitude of Fourier frequencies by replacing $\sqrt{a}$ with a, which allows for a simplified reconstruction of frequency dependent signals. The parameter $l = N^*\Delta t = 6$ was chosen for all analyses, which gives sufficiently precise results in resolution of depth and frequency (Ware and Thomson, 2000). The shifted and scaled Morlet mother wavelet is defined as

$$\psi_{a,b}^{l}(s) = \pi^{-\frac{1}{4}}(al)^{-\frac{1}{2}} e^{-i2\pi\frac{1}{a}(s-b)} e^{-\frac{1}{2}\left(\frac{s-b}{al}\right)^2} \tag{3}$$

The relative bandwidth error is constant in all scales and is, for $l = 6$: ~1/6 = 0.16 = 16%. The wavelet analysis technique used in this study is explained in detail in Prokoph and Barthelmes (1996). The matrix of the wavelet coefficients $W_l(a,b)$, the so called "scalogram", was coded with color-scale (orange: high W, blue: low W) for superior graphical interpretation. Details of the extraction methodology and its accuracy are explained in Prokoph and Patterson (2004a).

4.7 Results

4.7.1 The Mer Bleue Bog age-depth model

In the present study, the top of the section = 0 cm depth corresponds to the end of the 2007-growth season, because the samples were taken from frozen ground in March 2008. Furthermore,

the age of the upper part of the core is constrained by the first appearance of *Ambrosia* in the section at the 52-53 cm sampling interval (S. Elliott, pers. comm.), which in this area corresponds to an age of ~1860 A.D. (Talbot et al., 2010). The age model utilizes the 10 calibrated mean ages, 1860 A.D. at 52-53 cm (*Ambrosia* appearance), and the 0 cal. yr. B.P. (=2008 A.D.) intercept at the top.

The statistical errors (standard deviations) of the 10 radiocarbon-dated samples of the most prominent probability peak range from 22-33 years (see Table 4.1). ^{14}C dates are calibrated using the computer program CALIB5.02 using calibration data set intcal04.^{14}C (Reimer et al., 2004). The 2σ confidence interval of the age model below 60 cm is determined from the average of the confidence intervals of the individual samples. From 60 cm toward the top the 2σ confidence interval gradually decreases to 0.5 years at 2007 A.D. (Table 4.1).

The age-depth model (Figure 4.5.) of the Mer Bleue Bog core was constructed using combined exponential, linear and polynomial regression functions that reflect different stages of peat decomposition, and gradual to abrupt changes in the depositional

Table 4.1: Mer Bleue ^{14}C samples

Sample	Sample ID	Depth (cm)	UBA No. *UGAMS No	Material Dated	^{14}C Age (BP)	Cal. Ages (95.4%)			Cal. Ages (95.4%)			Cal Ages (95.4%)			mean Cal. Ages (BP)
						min	max	prob	min	max	prob	min	max	prob	
1	MB16	32 - 33	11976	peat	postbomb (< 1964 A D)										
2	MB22	44 - 45	11977	peat	postbomb (< 1964 A D)										
3	MB31	62 - 63	11978	peat	204 ± 28	1648	1684	0 291	**1734**	**1806**	**0.554**	1930	1951	0 155	238
4	MB61	122 - 123	11979	peat	1566 ± 26	**424**	**552**	**1.000**							1520
5	MB93	186 - 187	11980	peat	2860 ± 22	**1118**	**973**	**0.939**	958	938	0 061				3053 5
6	MB99	198 - 199	11981	peat	2959 ± 22	**1269**	**1112**	**0.982**	1100	1085	0 013	1064	1058	0 005	3198 5
7	MB137	274 - 275	11982	peat	4449 ± 32	3335	3210	0 418	3192	3151	0 080	**3138**	**3010**	**0.470**	5082
8	MB163	326 - 327	11983	peat	4659 ± 31	**3518**	**3365**	**1.000**							5449 5
9	MB185	370 - 371	11984	peat	5934 ± 33	4903	4864	0 107	**4856**	**4721**	**0.893**				6806 665
10	MB23	46-47	*5026	peat	postbomb (< 1964 A D)										
11	MB210	420-421	*5027	peat	6070± 30	5190	5185	0 004	**5057**	**4896**	**0 97**	4867	4851	0 025	6984 5
12	MB240	480-481	*5028	peat	6130± 30	**5208**	**4992**	**1.000**							7108
13	MB280	560-561	*5029	peat	7640± 30	6568	6544	0 065	**6531**	**6435**	**0 935**				8491

bold calibrated Ages used from mean calibrated age calculation

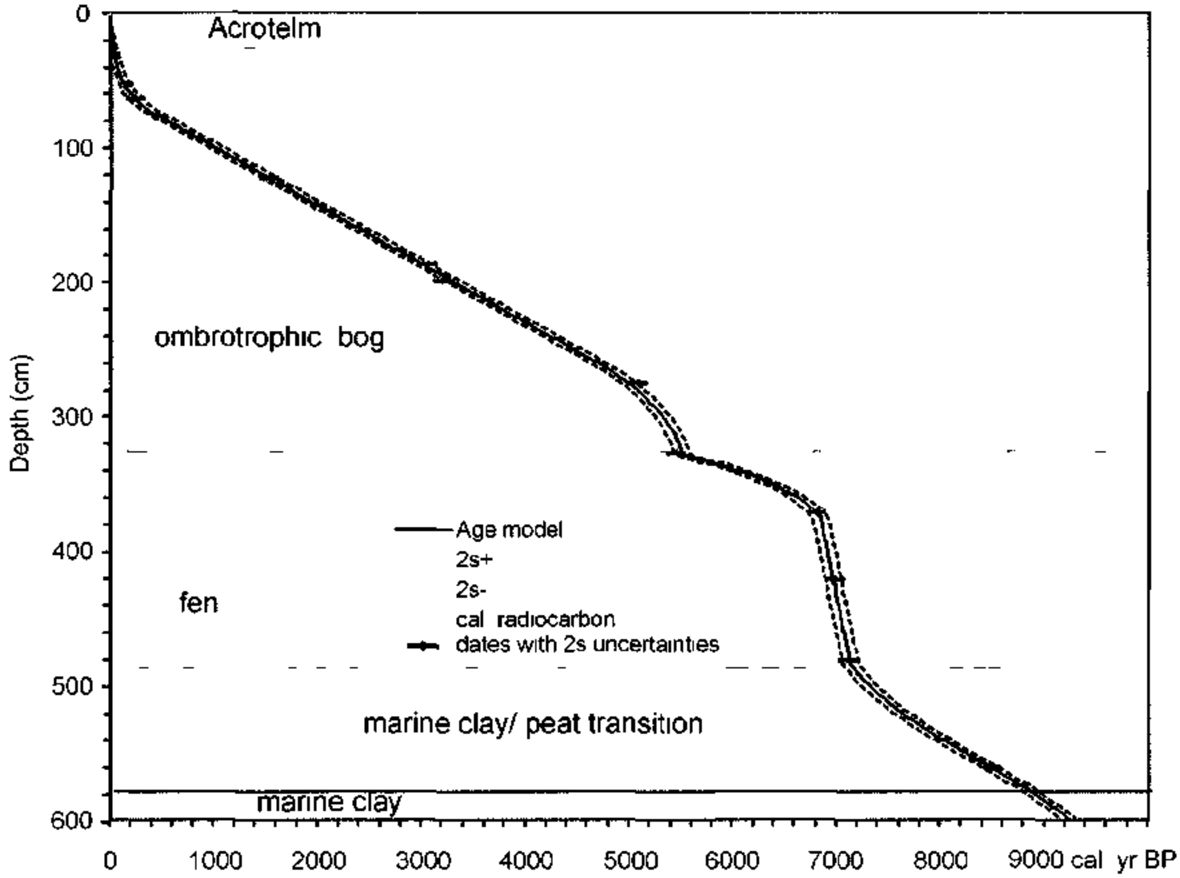

Figure 4.5: Mer Bleue core age-depth model and main depositional stages, based on 10 AMS radiocarbon ages, first occurrence of *Ambrosia* pollen (1860 A.D. at 52-53cm sample depth), and an intercept with 0m depth at October 2007 A.D. The top 25 cm consisted of poorly decayed and weakly compacted *Sphagnum*-dominated plant material in the oxic zone (Acrotelm).

environment through the last ~9200 years. From 25-73.5 cm depth the age-depth model is adjusted to the exponential carbon-decay model for the catotelm mass proposed for Mer Bleue Bog by Frolking et al. (2001, 2010), followed by a linear model from 73.5-262 cm depth and a fourth-order polynomial from 262-590 cm. The model age of 9112 ± 80 cal. yr. B.P. of the lowermost occurrence of terrestrial plant material at ~590 cm concurs with a previous age model by Frolking et al. (2010).

4.7.2 Cycles and trends in depth and time scales

<u>4.7.2.1 Cellulose oxygen isotope composition in depth-scale</u>

The cellulose $\delta^{18}O$ values of plant macrofossils range from ~8‰ (tissue remains of herbacae at 590 cm depth) to ~26‰ (rhizomes at 334 cm depth). The cellulose $\delta^{18}O$ values from rhizomes are commonly lower than cellulose $\delta^{18}O$ values of *Sphagnum*. The lowest values are recorded in tissue remains of herbacae in the last 60 cm of the Mer Bleue Bog core. The *Sphagnum* $\delta^{18}O_{cel}$ values vary from ~ 25‰ at 338 cm depth to ~14‰ at 242 cm depth with a standard deviation of 1.47 (n=203). There is a generally decreasing trend from ~19±1.2‰ (1σ, 11 samples) at 0-20 cm depth to ~16‰±0.97 (1σ, 4 samples) at 480-520 cm depth (Table 4.2, Figure 4.6). Plant cellulose oxygen concentrations range from ~20% to 50% with a standard deviation of 4.24 (n=254) through the 6 m section and show a similar decreasing trend and differences between *Sphagnum* and other plant macrofossils as the isotope values (Table 4.2, Figure 4.6).

Table 4.2: Oxygen isotope ratio and oxygen concentration of plant cellulose from Mer Bleue Bog, Ottawa, Ontario

Sample ID	Depth (cm)	%O	$\delta^{18}O$ (‰, VSMOW)	Macrofossils Taxa	Sample ID	Depth (cm)	%O	$\delta^{18}O$ (‰, VSMOW)	Macrofossils Taxa
1yss	2	41.4	18.81	*S. capillifolium*	98yss	196	41.0	17.74	*S. capillifolium*
2yss	4	42.0	18.32	*S. capillifolium*	99bss	198	41.2	17.80	*S. fuscum*
3r	6	37.3	19.14	Rhizome	99yss	198	39.7	16.94	*S. capillifolium*
4yss	8	43.3	20.22	*S. capillifolium*	100	200	40.0	19.11	*S. fuscum*
5yss	10	43.4	20.64	*S. capillifolium*	101dbss	202	41.8	19.36	*S. magellanicum*
6yss	12	42.7	18.88	*S. capillifolium*	101 dbss repeat	202	40.5	19.72	*S. magellanicum*
7yss	14	42.4	19.28	*S. capillifolium*	102bss	204	42.1	19.18	*S. fuscum*
8yss	16	43.4	20.05	*S. capillifolium*	103dbss	206	40.9	19.68	*S. magellanicum*
9yss	18	41.7	16.91	*S. capillifolium*	104bss	208	40.6	19.26	*S. fuscum*
10yss	20	41.7	17.13	*S. capillifolium*	105bss	210	40.1	18.79	*S. fuscum*
10bss	20	42.8	18.58	*S. fuscum*	105r	210	32.7	14.05	Rhizome
11yss	22	41.9	18.48	*S. capillifolium*	106bss	212	41.9	17.72	*S. fuscum*
12yss	24	42.8	18.64	*S. capillifolium*	107dbss	214	41.1	19.81	*S. magellanicum*
13yss	26	43.2	19.34	*S. capillifolium*	109bss	218	40.7	19.53	*S. angustifolium*
14yss	28	36.8	17.17	*S. capillifolium*	110bss	220	41.4	19.11	*S. fuscum*
15yss	30	43.8	19.36	*S. capillifolium*	111bss	222	35.0	17.49	*S. fuscum*
16yss	32	43.7	18.95	*S. capillifolium*	112bss	224	36.4	18.56	*S. fuscum*
17yss	34	45.1	19.08	*S. capillifolium*	113Lbss	226	39.1	20.00	*S. angustifolium*
Sb1yss	35	43.8	18.99	*S. capillifolium*	114bss	228	40.3	19.74	*S. fuscum*
18yss	36	43.4	20.43	*S. capillifolium*	115bss	230	23.7	17.55	*S. fuscum*
Sb2yss	37	44.0	17.82	*S. capillifolium*	115r	230	35.4	16.95	Rhizome
Sb2bss	37	41.9	18.94	*S. fuscum*	116bss	232	37.9	16.43	*S. fuscum*
19yss	38	44.5	19.32	*S. capillifolium*	117bss	234	39.6	18.16	*S. fuscum*
Sb3bss	39	42.3	19.49	*S. fuscum*	118r	236	38.7	19.14	Rhizome
20bss	40	42.6	17.88	*S. fuscum*	119r	738	32.0	15.86	Rhizome
Sb4yss	41	43.1	21.32	*S. capillifolium*	119bss	238	37.3	16.70	*S. fuscum*
21yss	42	40.8	18.13	*S. capillifolium*	120r	240	34.7	16.88	Rhizome
Sb5yss	43	43.6	18.15	*S. capillifolium*	121r	242	35.3	16.77	Rhizome
22yss	44	46.0	17.41	*S. capillifolium*	121r repeat	242	39.1	18.18	Rhizome
Sb6yss	45	45.4	16.89	*S. capillifolium*	121dbss	242	32.5	13.89	*S. magellanicum*
23yss	46	46.6	18.13	*S. capillifolium*	122DS	244	27.5	12.92	Root networks of Pteridophytae
Sb7yss	47	43.0	20.28	*S. capillifolium*	122dbss	244	37.3	14.92	*S. magellanicum*
24yss	48	46.2	18.36	*S. capillifolium*	123dbss	246	39.0	19.54	*S. magellanicum*
25yss	50	45.1	19.18	*S. capillifolium*	124dbss	248	37.9	16.40	*S. magellanicum*
26yss	52	44.0	18.92	*S. capillifolium*	125r	250	34.9	15.19	Rhizome
27yss	54	45.4	19.97	*S. capillifolium*	125DS	250	26.3	12.11	Root networks of Pteridophytae
27.5yss	55	44.8	19.40	*S. capillifolium*	125bss	250	42.5	16.56	*S. fuscum*
28yss	56	43.6	19.15	*S. capillifolium*	126dbss	252	40.0	17.58	*S. magellanicum*
28.5yss	57	46.6	17.21	*S. capillifolium*	127dbss	254	41.3	18.67	*S. magellanicum*
29yssRE	58	46.2	17.71	*S. capillifolium*	129dbss	258	39.0	20.83	*S. magellanicum*
29yss	58	44.7	17.09	*S. capillifolium*	130dbss	260	41.6	16.47	*S. magellanicum*
29.5yss	59	46.3	18.68	*S. capillifolium*	131dbss	262	42.8	18.82	*S. magellanicum*
30yss	60	38.3	19.47	*S. capillifolium*	132dbss	264	40.2	17.98	*S. magellanicum*
30.5yss	61	47.3	19.43	*S. capillifolium*	133dbss	266	40.5	19.78	*S. magellanicum*
31yss	62	42.8	20.16	*S. capillifolium*	134DS	268	34.5	13.33	Root networks of Pteridophytae
31.5yss	63	45.4	19.06	*S. capillifolium*	135DS	270	35.6	14.95	Root networks of Pteridophytae
32bss	64	44.1	18.23	*S. fuscum*	135r	270	37.4	17.63	Rhizome
32.5yss	65	44.8	17.17	*S. capillifolium*	136DS	272	33.9	13.11	Root networks of Pteridophytae
33bss	66	44.5	18.57	*S. fuscum*	137dbss	274	42.5	21.92	*S. magellanicum*
33.5yss	67	45.9	20.75	*S. capillifolium*	139dbss	278	39.6	18.46	*S. magellanicum*
34bss	68	44.3	18.78	*S. fuscum*	139r	278	lost	lost	Rhizome
34ayss	69	45.5	18.24	*S. capillifolium*	140r	280	33.3	14.80	Rhizome
35bss	70	42.0	18.34	*S. fuscum*	141r	282	30.5	15.08	Rhizome
35ayss	71	45.0	20.17	*S. capillifolium*	142r	284	34.1	15.54	Rhizome
36bss	72	45.3	18.74	*S. fuscum*	143r	286	33.0	14.26	Rhizome
36dbss	72	44.3	18.88	*S. magellanicum*	145r	290	34.2	14.08	Rhizome
36ayss	73	45.8	19.52	*S. capillifolium*	145bss	290	43.7	17.82	*S. fuscum*
37dbss	74	44.7	18.61	*S. magellanicum*	146dbss	292	38.6	15.11	*S. magellanicum*
37bss	74	34.0	17.11	*S. fuscum*	147r	294	30.9	17.71	Rhizome
38dbss	76	42.7	19.57	*S. magellanicum*	148dbss	296	40.8	17.03	*S. magellanicum*
38bss	76	43.5	18.16	*S. fuscum*	149r	298	28.9	15.67	Rhizome
39bss	78	43.1	19.36	*S. fuscum*	150r	300	35.6	16.20	Rhizome

Table 4.2: con't

40bss	80	42 5	18 97	*S fuscum*	151r	302	32 3	16 56	Rhizome
41bss	82	43 8	18 21	*S fuscum*	151dbss	302	35 3	16 34	*S magellanicum*
42bss	84	43 7	19 69	*S fuscum*	152dbss	304	39 5	17 63	*S magellanicum*
43bss	86	43 3	18 09	*S fuscum*	153dbss	306	38 3	19 71	*S magellanicum*
44bss	88	40 4	18 45	*S fuscum*	154dbss	308	40 5	18 16	*S magellanicum*
45r	90	37 7	17 60	Rhizome	155dbss	310	36 6	15 27	*S magellanicum*
45Lbss	90	42 7	19 43	*S angustifolium*	157dbss	314	39 2	19 54	*S magellanicum*
46bss	92	40 1	18 49	*S fuscum*	158r	316	38 2	16 40	Rhizome
46r	92	34 3	15 65	Rhizome	159dbss	318	37 4	18 25	*S magellanicum*
47bss	94	39 9	23 21	*S fuscum*	160bss	320	40 2	17 75	*S fuscum*
48yss	96	43 1	19 56	*S capillifolium*	160dbss	320	41 3	17 21	*S magellanicum*
49bss	98	34 8	19 18	*S fuscum*	161dbss	322	38 1	17 34	*S magellanicum*
49yss	98	41 0	19 23	*S capillifolium*	162dbss	324	40 9	15 97	*S magellanicum*
50r	100	33 3	15 22	Rhizome	162bss	324	39 6	17 38	*S fuscum*
50yss	100	39 3	19 73	*S capillifolium*	163dbss	326	39 4	17 76	*S magellanicum*
51bss	102	40 5	19 80	*S fuscum*	164bss	328	39 0	16 89	*S fuscum*
52bss	104	41 4	20 27	*S fuscum*	165r	330	35 0	14 89	Rhizome
53dbss	106	33 0	19 21	*S magellanicum*	165bss	330	40 8	19 89	*S fuscum*
54dbss	108	39 5	19 22	*S magellanicum*	166bss	332	40 6	15 26	*S fuscum*
55Lbss	110	40 5	17 76	*S angustifolium*	167r	334	42 6	24 96	Rhizome
56yss	112	42 1	19 65	*S capillifolium*	167 r repeat	334	39 8	25 18	Rhizome
57bss	114	42 3	19 12	*S fuscum*	167bss	334	40 4	19 51	*S fuscum*
58yss	116	42 2	19 68	*S capillifolium*	168bss	336	38 9	16 79	*S fuscum*
59bss	118	37 8	19 70	*S fuscum*	169r	338	37 4	19 06	Rhizome
60bss	120	35 9	16 20	*S fuscum*	169bss	338	37 7	24 82	*S fuscum*
61bss	122	39 8	18 44	*S fuscum*	170syss	340	36 3	15 13	*S papillosum*
62bss	124	41 2	19 32	*S fuscum*	171r	342	30 6	13 53	Rhizome
63bss	126	40 3	19 06	*S fuscum*	171syss	342	39 3	15 17	*S papillosum*
64yss	128	37 2	19 23	*S capillifolium*	172syss	344	37 7	16 09	*S papillosum*
65Lbss	130	40 9	19 31	*S angustifolium*	173DS	346	37 5	17 88	Root networks of Pteridophytae
66yss	132	41 7	20 29	*S capillifolium*	174dbss	348	39 9	17 23	*S magellanicum*
67yss	134	41 1	21 42	*S capillifolium*	175bss	350	39 8	17 51	*S fuscum*
68yss	136	45 9	17 47	*S capillifolium*	176dbss	352	40 3	19 71	*S magellanicum*
69yss	138	39 8	18 37	*S capillifolium*	177dbss	354	39 7	18 99	*S magellanicum*
70yss	140	42 3	19 49	*S capillifolium*	178dbss	356	39 9	18 14	*S magellanicum*
71bss	142	43 7	19 50	*S fuscum*	179dbss	358	37 0	16 21	*S magellanicum*
72yss	144	41 5	19 50	*S capillifolium*	180dbss	360	40 0	17 69	*S magellanicum*
73bss	146	40 7	17 95	*S fuscum*	181DS	362	22 1	14 24	Root networks of Pteridophytae
74bss	148	41 4	19 42	*S fuscum*	181dbss	362	29 3	18 16	*S magellanicum*
75bss	150	42 6	18 50	*S fuscum*	185bss	370	39 5	17 08	*S fuscum*
76bss	152	39 5	18 16	*S fuscum*	190DS	380	36 1	14 59	Root networks of Pteridophytae
77bss	154	40 5	20 52	*S fuscum*	195bss	390	39 9	16 33	*S fuscum*
78bss	156	40 6	17 80	*S fuscum*	195dbss	390	37 0	15 63	*S magellanicum*
79bss	158	43 1	19 02	*S fuscum*	200r	400	33 3	16 97	Rhizome
80bss	160	39 4	19 69	*S fuscum*	205dbss	410	40 5	16 39	*S magellanicum*
81yss	162	42 1	19 50	*S capillifolium*	210bss	420	37 4	15 88	*S fuscum*
82bss	164	42 2	19 15	*S fuscum*	215bss	430	37 8	15 91	*S fuscum*
83bss	166	42 5	19 56	*S fuscum*	220 r	440	36 9	22 08	Rhizome
84bss	168	43 0	18 30	*S fuscum*	220rbl	440	34 8	13 38	Unknown Reddish brown leaves
85yss	170	41 5	19 28	*S capillifolium*	220dbss	440	39 7	16 65	*S magellanicum*
85r	170	38 4	19 61	Rhizome	225bss	450	40 6	16 85	*S fuscum*
86r	172	35 3	15 93	Rhizome	230bss	460	39 2	17 85	*S fuscum*
86yss	172	41 0	17 34	*S capillifolium*	230rbl	460	27 4	14 77	Unknown Reddish-brown leaves
87yss	174	42 3	17 79	*S capillifolium*	235dbss	470	42 3	16 49	*S magellanicum*
88yss	176	42 0	17 37	*S capillifolium*	235r	470	36 3	16 83	Rhizome
89bss	178	35 3	17 94	*S fuscum*	240bss	480	40 2	16 99	*S fuscum*
90bss	180	41 9	17 81	*S fuscum*	245bss	490	42 5	15 17	*S fuscum*
91bss	182	41 4	17 36	*S fuscum*	250rbl	500	28 4	17 88	Unknown Reddish brown leaves
92bss	184	41 4	16 90	*S fuscum*	250dbss	500	39 0	15 08	*S magellanicum*
92r	184	38 4	13 47	Rhizome	255trh	510	35 5	13 19	Tissue remains of Herbacea
93bss	186	42 0	15 36	*S fuscum*	260bss	520	38 6	16 56	*S fuscum*
94bss	188	41 9	17 19	*S fuscum*	265trh	530	32 2	13 37	Tissue remains of Herbacea
95yss	190	41 3	18 09	*S capillifolium*	270trh	540	33 0	12 15	Tissue remains of Herbacea
95bss	190	35 8	16 74	*S fuscum*	275trh	550	34 7	12 10	Tissue remains of Herbacea
95r	190	40 2	18 66	Rhizome	280trh	560	29 8	11 94	Tissue remains of Herbacea
96bss	192	40 6	17 82	*S fuscum*	290trh	580	34 0	13 55	Tissue remains of Herbacea
97bss	194	41 0	18 29	*S fuscum*	295trh	590	33 5	7 99	Tissue remains of Herbacea
98bss	196	42 2	18 06	*S fuscum*					

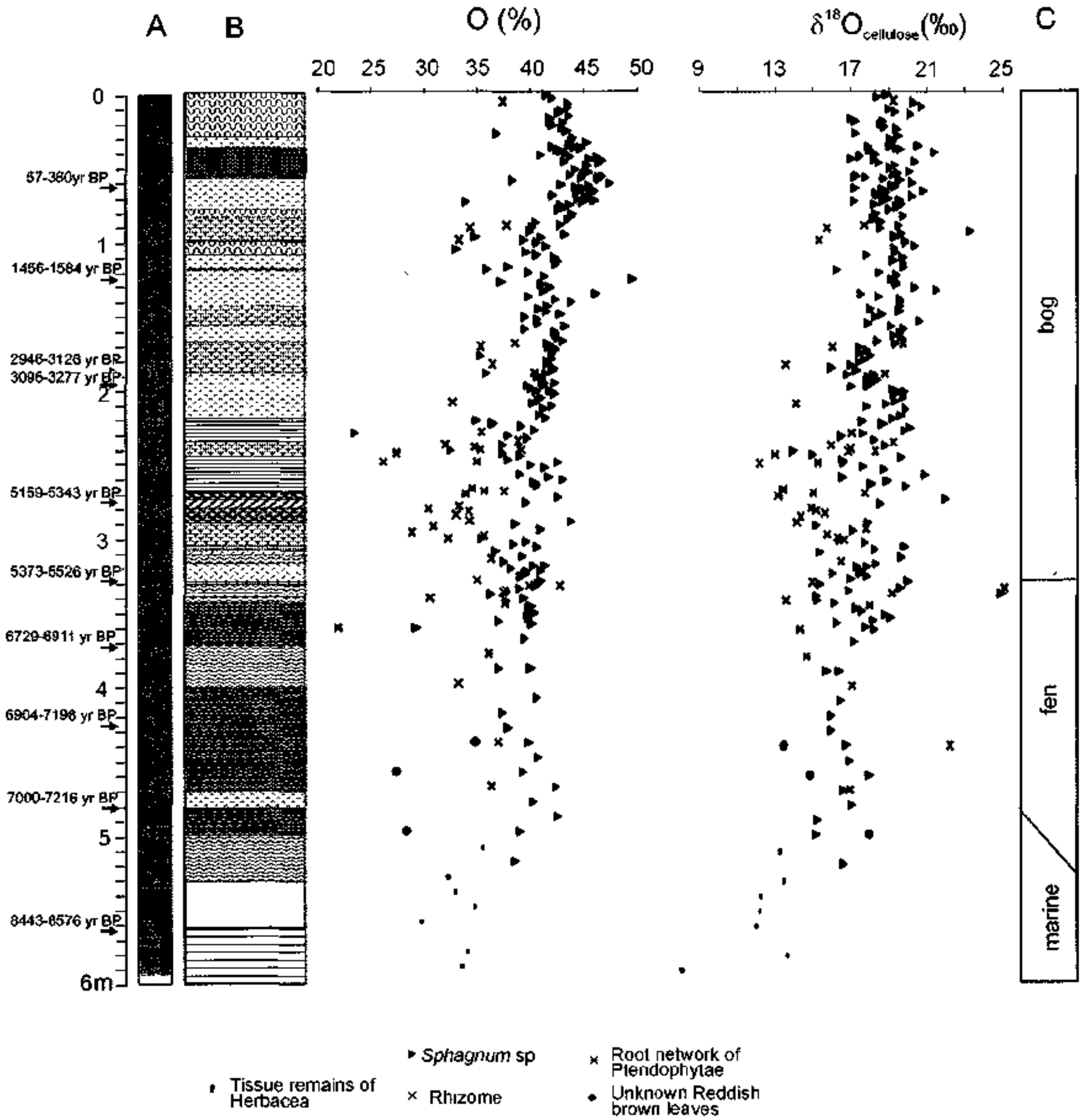

Figure 4.6: Mer Bleue core Lithology, oxygen concentration and isotope data of cellulose in depth scale from different plant material of the Mer Bleue Bog core. A: Rock color code following Munsell Chart (Munsell, 1975), B: Lithology, C: Depositional environments.

4.7.2.2 Cellulose oxygen isotope composition and oxygen concentration in time-scale

The $\delta^{18}O_{cel}$ record for the last ~7500 cal. B.P. is shown in Figure 4.7A. Red-yellow colors in the wavelet scalogram reveal cycles in the ranges ~180-250 years, ~700-800 years, and ~1300 years. The ~180-250 year cycles are strong between ~1000-2500 cal. yr. B.P. and ~3500-6500 cal. yr. B.P., and relatively weak between ~2500-3500 cal. yr. B.P. and the last ~1000 cal. yr. B.P. A strong low-frequency cyclicity in the ~700-800 year and ~1300 year bands is persistent and dominates the entire section of the core (Figure 4.7A). The ~1300 year cycles are stronger between ~1500-6500 cal. yr. B.P. and cover intervals of cooling ~3500 and ~4200 cal. yr. B.P. as shown by $\delta^{18}O_{cel}$ records (Figure 4.7A and C).

The %O record shows strong low-frequency cyclicities of ~110-120 years, ~180-250 years, ~220-350 years, ~600 years, ~1300 years, and 2500 years (Figure 4.8). The ~110-120 years cycle is discontinuous and is very strong between ~1000-2500 cal. yr. B.P., ~3500-6500 cal. yr. B.P., and 6500-7300 cal. yr. B.P. The ~180-250 years and ~220-350 years cycles show similar high wavelet coefficients (=magnitudes) to that of the ~110-120 years cycle (Figure 4.8A). The ~600 year cycles are strong between ~5500-7500 cal. yr. B.P. and weak in the last ~5500 cal. yr. B.P. (Figure 4.8A). The ~1300 and 2500 year bands are persistent over the entire section of the core (Figure 4.8A). The %O record shows strong low-frequency cycles of ~110-150 years, ~180-250 years, ~220-350 years, ~600 years, in intervals of low %O (~1200 cal. yr. B.P, ~4100 cal. yr. B.P, and ~6500 cal. yr. B.P.) whereas the ~1300 years and ~2500 years cycles occur over the entire section of the core (Figure 4.8A and C).

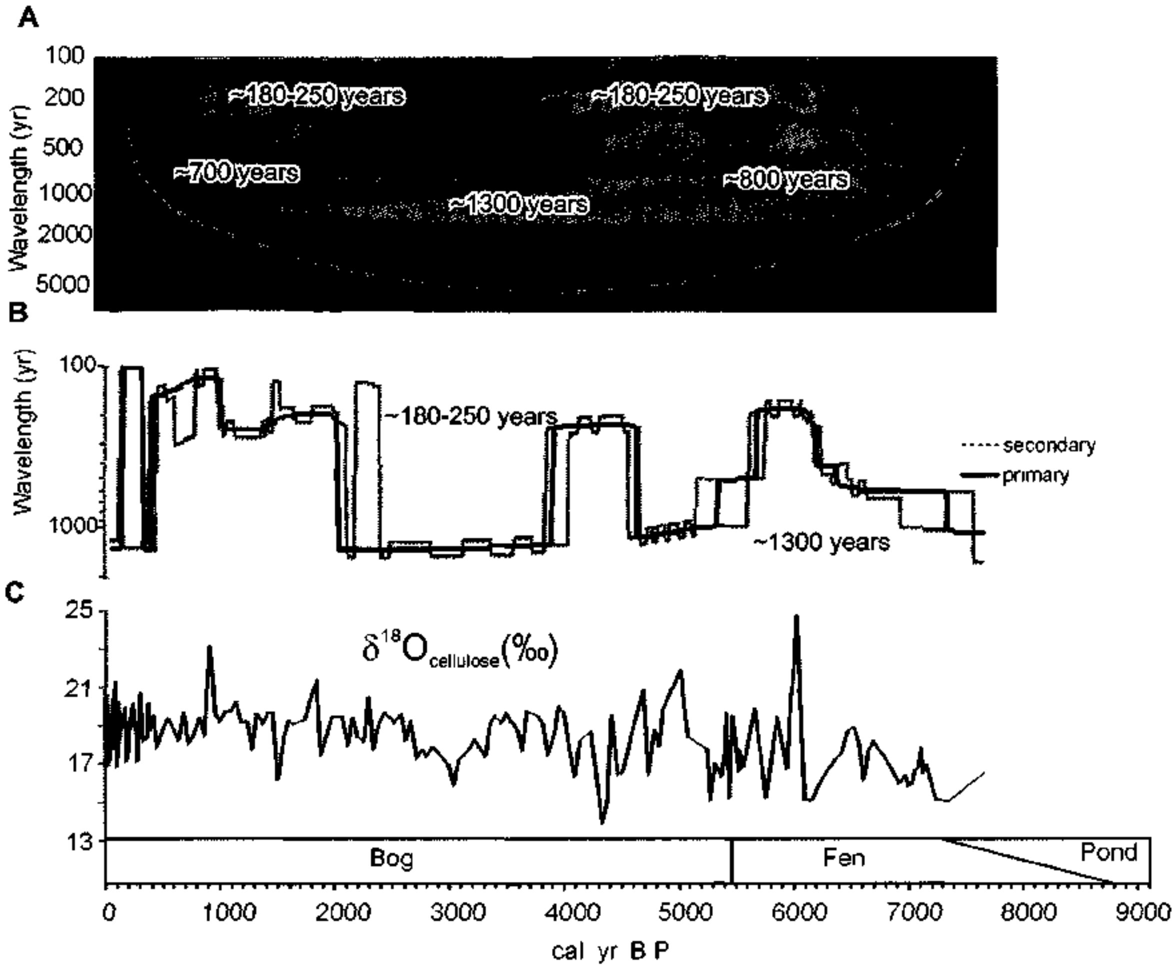

Figure 4.7: wavelet scalogram of $\delta\,^{18}O_{cel}$ of *Sphagnum* with cone of influence (stripped line) and marked important wavelengths (A and B) C) $\delta^{18}O_{cel}$ in ‰ SMOW,

for A: Yellow-red indicates high magnitude of signal and blue low or no signal in specific wavelength at a specific time.

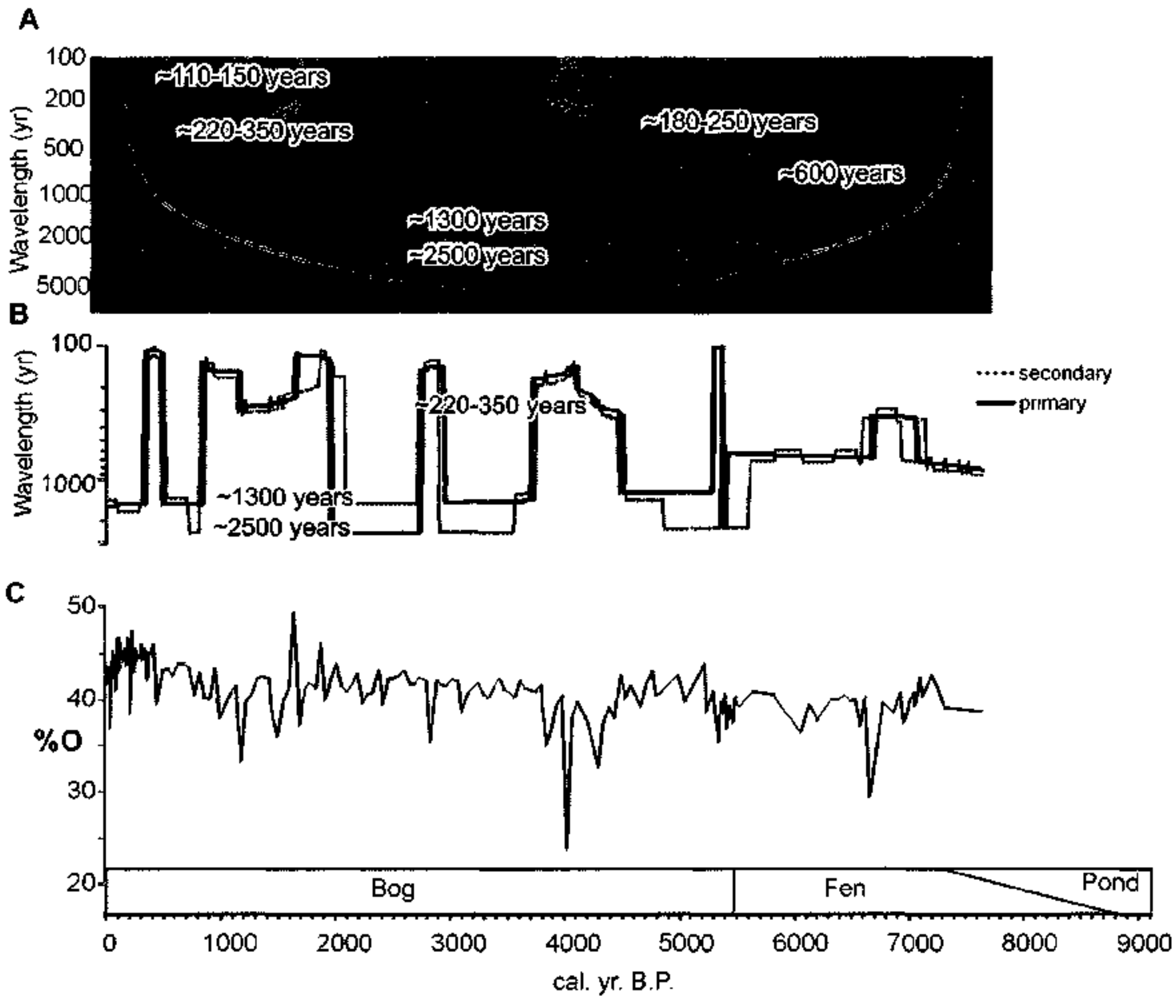

Figure 4.8: A: and B: wavelet scalogram of oxygen concentration (in %) of *Sphagnum* cellulose with cone of influence (stripped line) and marked important wavelengths.

C: oxygen concentration (in %).

for A) Yellow-red indicates high magnitude of signal and blue low or no signal in specific wavelength at a specific time.

4.7.2.3 Digital photo and X-ray gray-values in depth-scale

The digital photo line-scan has relatively stable gray-values of ~90 (50-130) throughout the top 520 cm of peat deposition, whereas the bottom 80 cm (520-600 cm) shows gradually increasing gray-values, corresponding to the transition from peat to clay sedimentation (Figure 4.9). The photo gray-values of the peat deposition are characterized by cycles of ~1.5 cm, ~2.5 cm, ~5.5 cm, ~10 cm, ~25 cm, ~80 cm, ~180 cm and ~300 cm length. The ~180 cm and 300 cm cycles are persistent throughout the core. An ~80 cm cycle disappears above ~330 cm depth, at the fen-to-bog transition, and is replaced by a ~25 cm cycle, which disappears above ~70 cm depth, when the peat becomes less compacted.

The X-ray line-scan is characterized by gradually increasing gray-values from the top to ~70 cm depth, reflecting the increasing compaction with depth. From ~70 cm to 520 cm depth, the gray-values are relative constant at ~80 (60-100). From 520 cm depth to the bottom at the core, the gray-values increase exponentially from ~80 to ~250 (Figure 4.10). In contrast to the photo line-scan, the X-ray gray-value fluctuations are characterized by longer cycles (i.e. >20 cm) and cycles from 2-18 cm length occur only sporadically (Figure 4.10). Throughout the core a ~120 cm cycle is most prominent, except for the fen-bog transition at ~350-250 cm depth, where a ~65 cm cycle dominates (Figure 4.10).

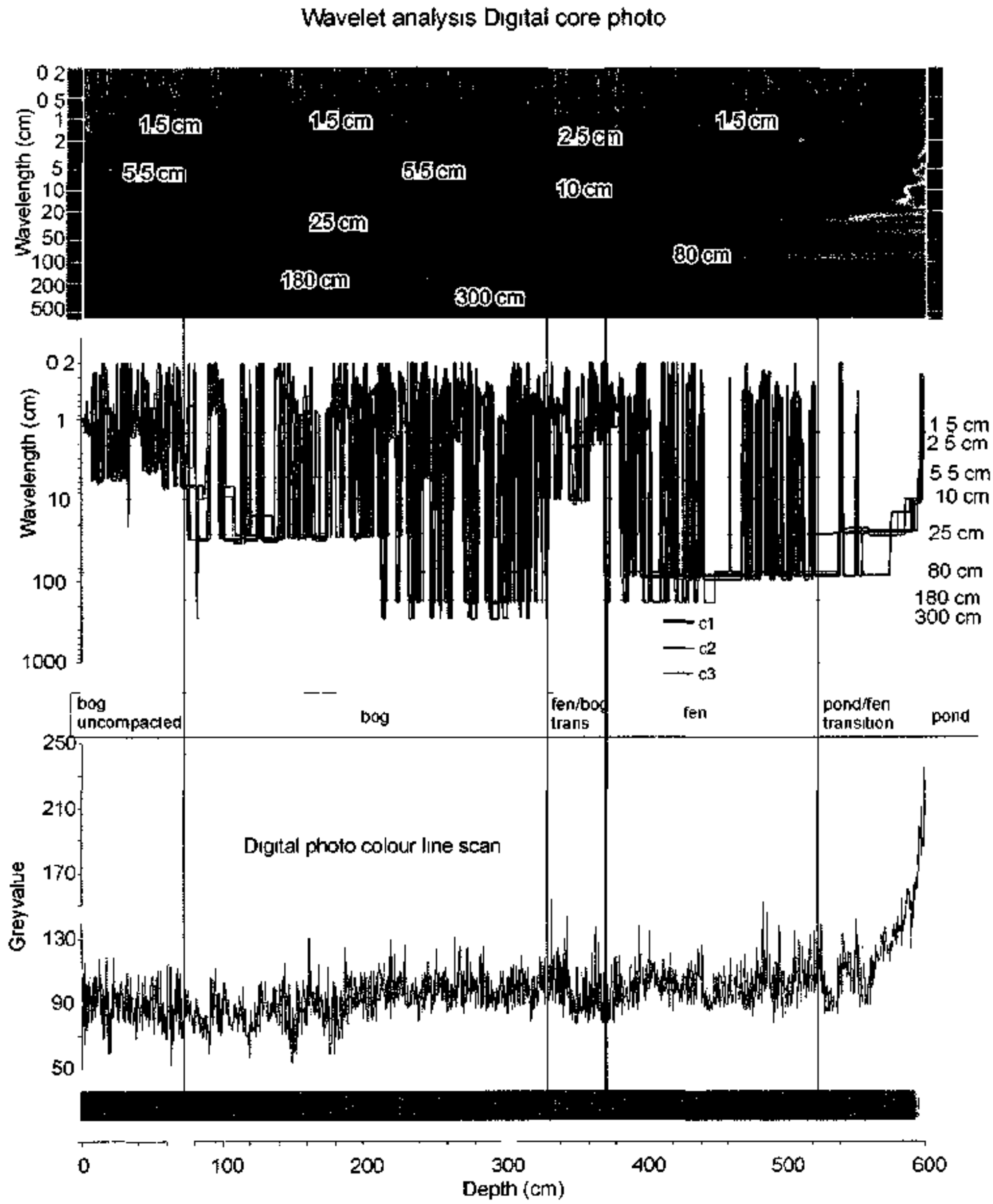

Figure 4.9: Wavelet analysis of Digital photo image line-scan from the Mer Bleue Bog core in depth scale:

Top: wavelet scalogram of line-scan of digital photo image with cone of influence (stripped line) and marked important wavelengths; for color scale Yellow-red indicates high magnitude of signal and blue low or no signal in specific wavelength as specific time, Middle: temporal changes of wavelength with strongest (primary) and second strongest (secondary) signals in line-scan of X-ray image, Bottom: line-scan of photo image with depth scale. Red-lined boxes separate intervals with different cycle patterns.

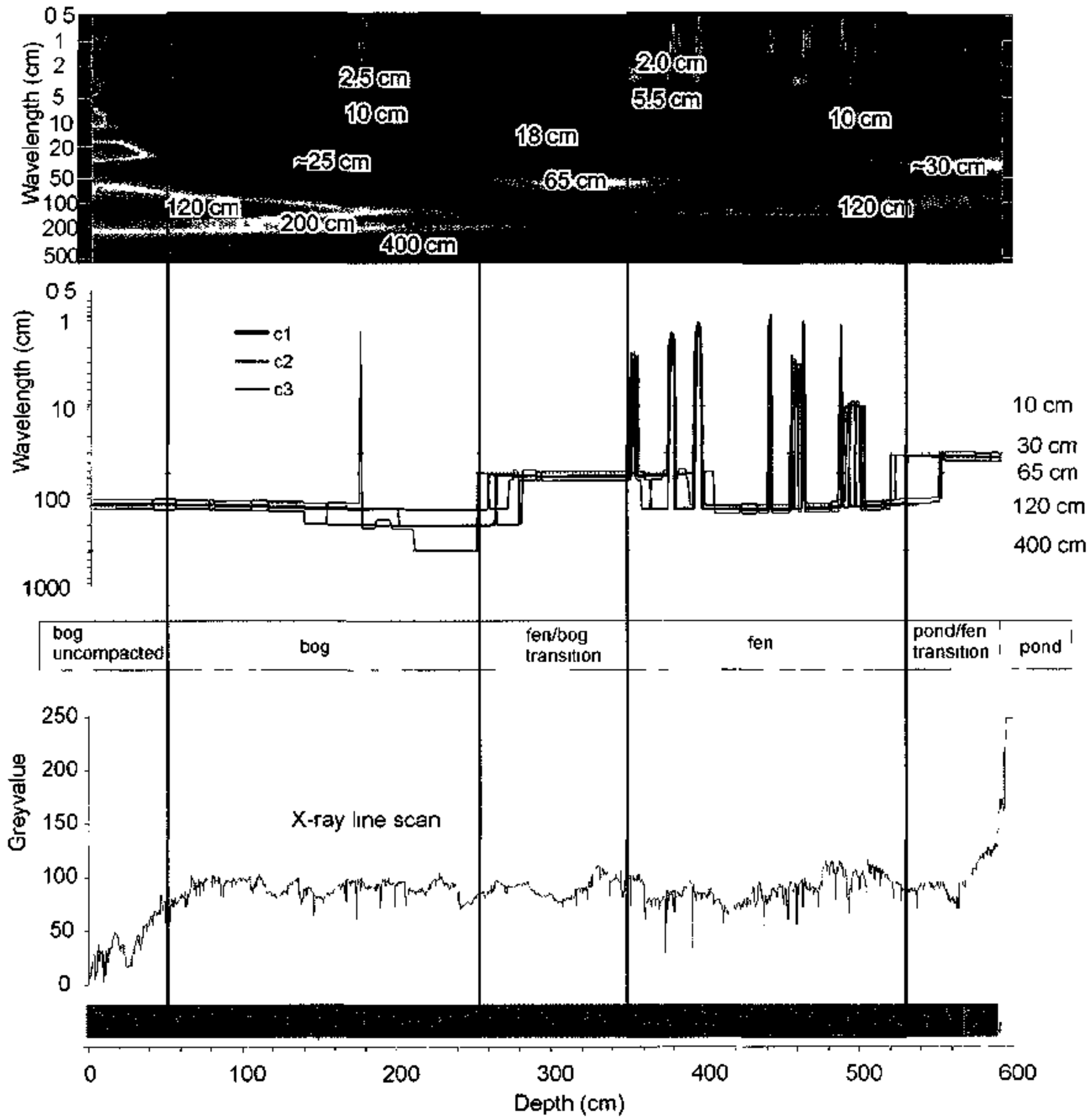

Figure 4.10: Wavelet analysis of X-ray image line-scan from the Mer Bleue Bog core in depth scale:

Top: wavelet scalogram of line-scan of X-ray image with cone of influence (stripped line) and marked important wavelengths; for color scale Yellow-red indicates high magnitude of signal and blue low or no signal in specific wavelength as specific time, Middle: temporal changes of wavelength with strongest (primary) and second strongest (secondary) signals in line-scan of X-ray image, Bottom: line-scan of X-ray image with depth scale. Red-lined boxes separate intervals with different cycle patterns.

4.7.2.4 Gray-values of X-ray images in time-scale

The wavelet analysis of the X-ray image line-scan revealed a wide spectrum of stationary and non-stationary cycles in wavebands >150 years (Figure 4.11). Strong cycles of ~700, ~900 and ~2600 years dominate the entire section of the Mer Bleue Bog core (Figure 4.11A,B). A ~180-250 year cycle in the X-ray line-scan produces a strong signal between ~1500-2500 cal. B.P. and ~5500-7300 cal. yr. B.P., and appears to be weaker in the remaining section of the core (Figure 4.10A). The ~700 year band dominates the entire section of the Mer Bleue Bog core and overprints weaker ~900 years cycle in the last ~2500 cal. yr. B.P. Furthermore, the X-ray gray-values have ~900 year cycles between ~2500 and 7300 cal. yr. B.P. (Figure 4.11A). The ~2600 year cyclicity dominates the entire section of the Mer Bleue Bog core and appears to merge with the ~900 years cycle from ~6500 cal. yr. B.P. towards the end of the Mer Bleue Bog core (Figure 4.11A).

The wavelet analysis of the X-ray image line-scan shows similar cycles of the ~180-250, ~700-800, and ~900 years compared to those on both the $\delta^{18}O_{cel}$ and %O records. In addition the X-ray image line-scan exhibits strong ~2600 year cyclicity that is otherwise only observed in the %O record.

4.7.2.5 Gray-values of digital photographs in time-scale

Wavelet time series analysis of the peat sediment color (gray-scale values) data of the upper 560 cm of the Mer Bleue core revealed a wide spectrum of stationary and non-stationary cycles (Figure 4.12).

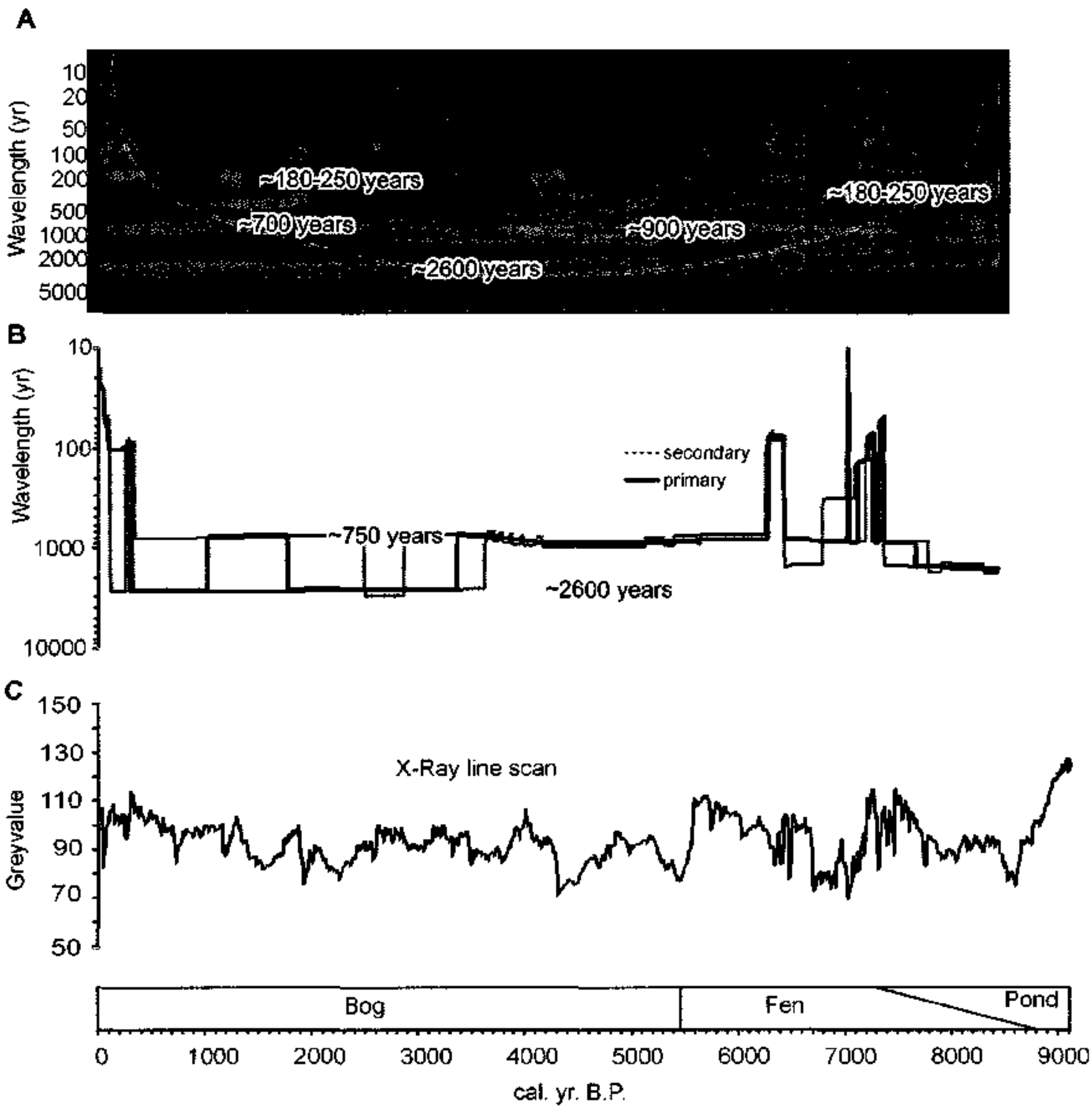

Figure 4.11: Wavelet analysis of X-ray image line-scan from the Mer Bleue Bog core in time scale:

A: wavelet scalogram of line-scan of X-ray image with cone of influence (stripped line) and marked important wavelengths; for color scale Yellow-red indicates high magnitude of signal and blue low or no signal in specific wavelength as specific time,

B: temporal changes of wavelength with strongest (primary) and second strongest (secondary) signals in line-scan of X-ray image,

C: line-scan of X-ray image in time scale.

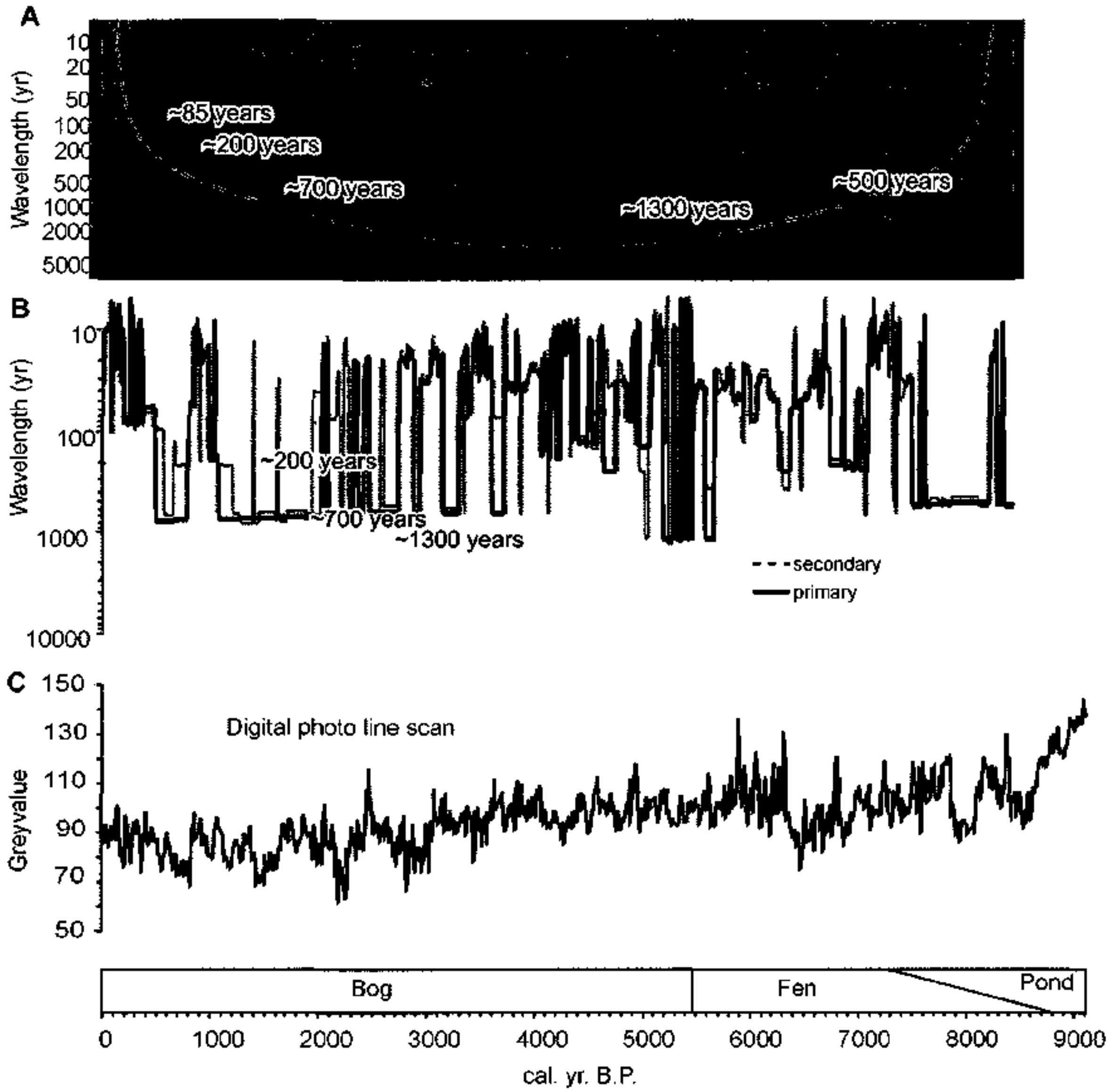

Figure 4.12: Wavelet analysis of Digital photo image line-scan from the Mer Bleue Bog core in time scale:

A: wavelet scalogram of line-scan of digital photo image with cone of influence (stripped line) and marked important wavelengths; for color scale Yellow-red indicates high magnitude of signal and blue low or no signal in specific wavelength as specific time,

B: temporal changes of wavelength with strongest (primary) and second strongest (secondary) signals in line-scan of X-ray image,

C: line-scan of photo image in time scale.

The wavelet analysis of the digital photo line-scan shows ~200 year and ~500-700 year cycles in the last ~2500 cal. yr. B.P. and between ~5500 and ~8500 cal. yr. B.P. whereas between ~2500 cal. yr. B.P. and ~5500 cal. yr. B.P., the ~200 year and ~500-700 year cycles are very weak (Figure 4.12A). An ~1300 year cyclicity occurs throughout the entire section of the Mer Bleue core but is most prominent in the interval between ~4500 cal. yr. B.P. and ~7300 cal. yr. B.P. (Figure 4.12A).

4.7.2.6 Solar activity proxies

Wavelet analysis of reconstructed solar activity proxy records, such as the reconstructed sunspot number (Solanki et al., 2004), solar irradiance (Bard et al., 2003) and ^{14}C production rate (Reimer et al., 2009) revealed a wide spectrum of persistent and intermittent cycles (Figure 4.13).

The wavelet analysis of the reconstructed solar activity records shows cycles of ~90 years, ~150 years, and 220 years over the last ~9200 cal. yr. B.P. The ~90 year cycles are strong and persistent in the ~9200 cal. yr. B.P. time interval. The ~150 year and ~220 year cycles are strong and dominate in the last ~3000 years in the intervals between ~4500-6000 cal. yr. B.P. and ~7500-9200 cal. yr. B.P. (Figure 4.13A-D). The wavelet analysis of the reconstructed ^{14}C production rate record shows additional cycles of ~350 years and 550 years duration (Figure 4.13C). Longer ~650 year and ~1300 year cycles occur in the entire ~9200 year record but are weakly developed except the interval between ~4000 cal. yr. B.P. and ~9200 cal. yr. B.P. (Figure 4.13A, B). A strong and persistent cycle of ~2100-2500 year length occurs throughout the ~9200 cal. yr. B.P.

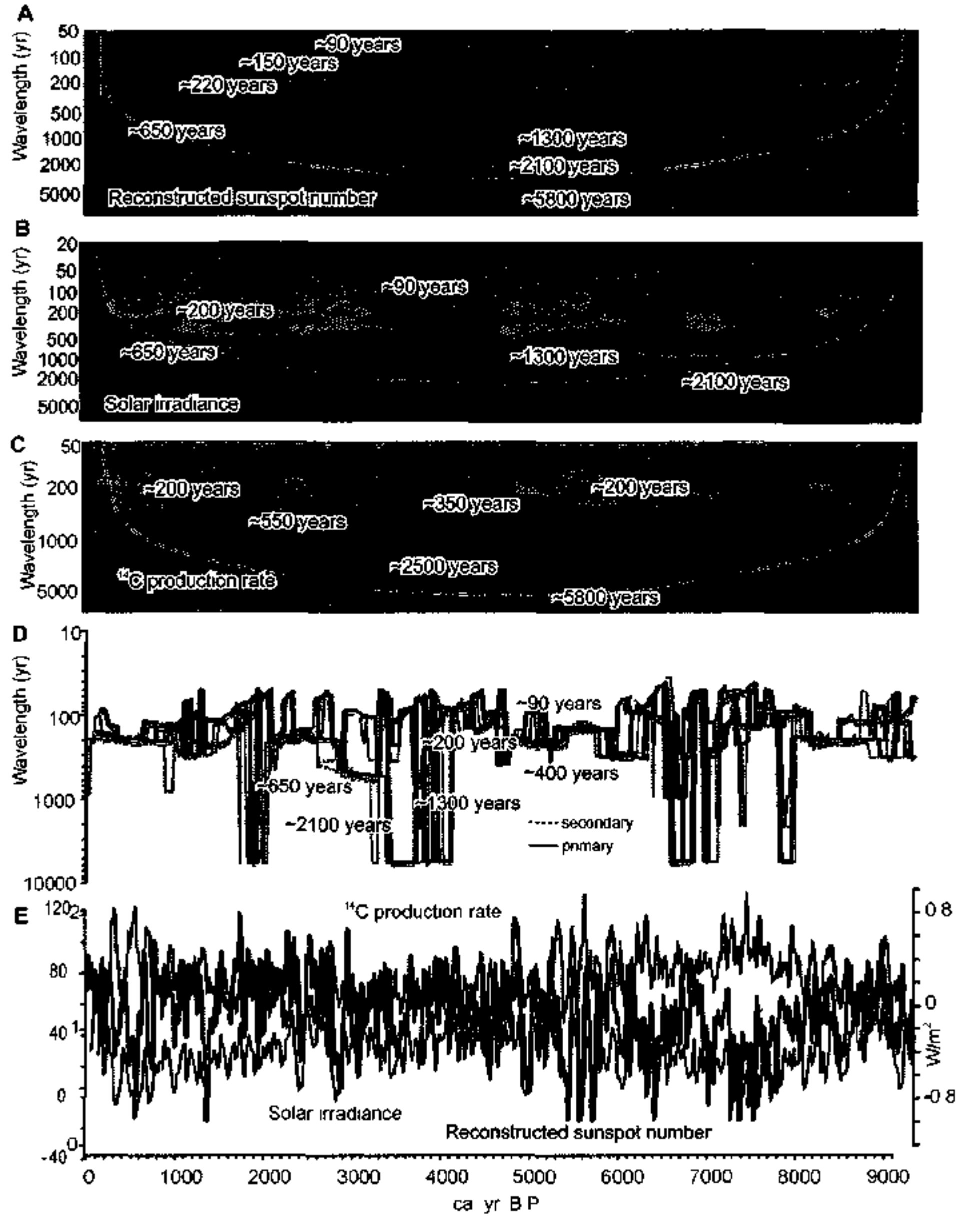

Figure 4.13: Wavelet analysis of reconstructed solar activity proxies:
Wavelet scalogram of A) reconstructed sunspot number B) solar irradiance and C) ^{14}C production rate records with cone of influence (stripped line) and marked important wavelengths; for color scale Yellow-red indicates high magnitude of signal and blue low or no signal in specific wavelength as specific time. D) Temporal changes of wavelength with strongest (primary=solid lines) and second strongest (secondary=stripped lines) signals in line-scan of X-ray image. Line color represent different solar activity proxies as shown in E; E) reconstructed solar activity proxies with time scale.

time interval in all records (Figure 4.13A-C), whereas a ~5800 year cycle is restricted to the ^{14}C and reconstructed sunspot number record.

4.7.2.7 Spectral analysis

Spectral analysis was conducted on the digital photo and X-ray line-scans, $\delta^{18}O_{cel}$, %O, ^{14}C production rate, solar irradiance, and reconstructed sunspot number records to identify stationary climate cycles archived in the peat sediment of Mer Bleue core and to evaluate their confidence level. Spectral analysis indicates robust and strong cycles and confirms most of the cycles detected by wavelet analysis. Spectral analysis yields periodicities at the decadal, centennial, and millennial range from 80-2600 years (Figure 4.14).

A 150 year cycle with >90% confidence is well documented in paleorecords of ^{14}C production rate, solar irradiance, reconstructed sunspot number, digital photos line scans, and %O records (Figure 4.14A, B, C, E, G). This cycle is also found with >90% confidence in X-ray line-scan data (Figure 4.14D) but at <90% confidence in $\delta^{18}O_{cel}$ record (Figure 4.14F). A 200-210 year cycle with >95% confidence occurs in ^{14}C production rate, solar irradiance, reconstructed sunspot number, and $\delta^{18}O_{cel}$ records (Figure 4.14A, B, E, F). The 200-220 year cycle is recognized with >90% confidence in the digital photo and X-ray line-scan data (Figure 4.14C, D) but with <90% confidence in %O record (Figure 4.14G).

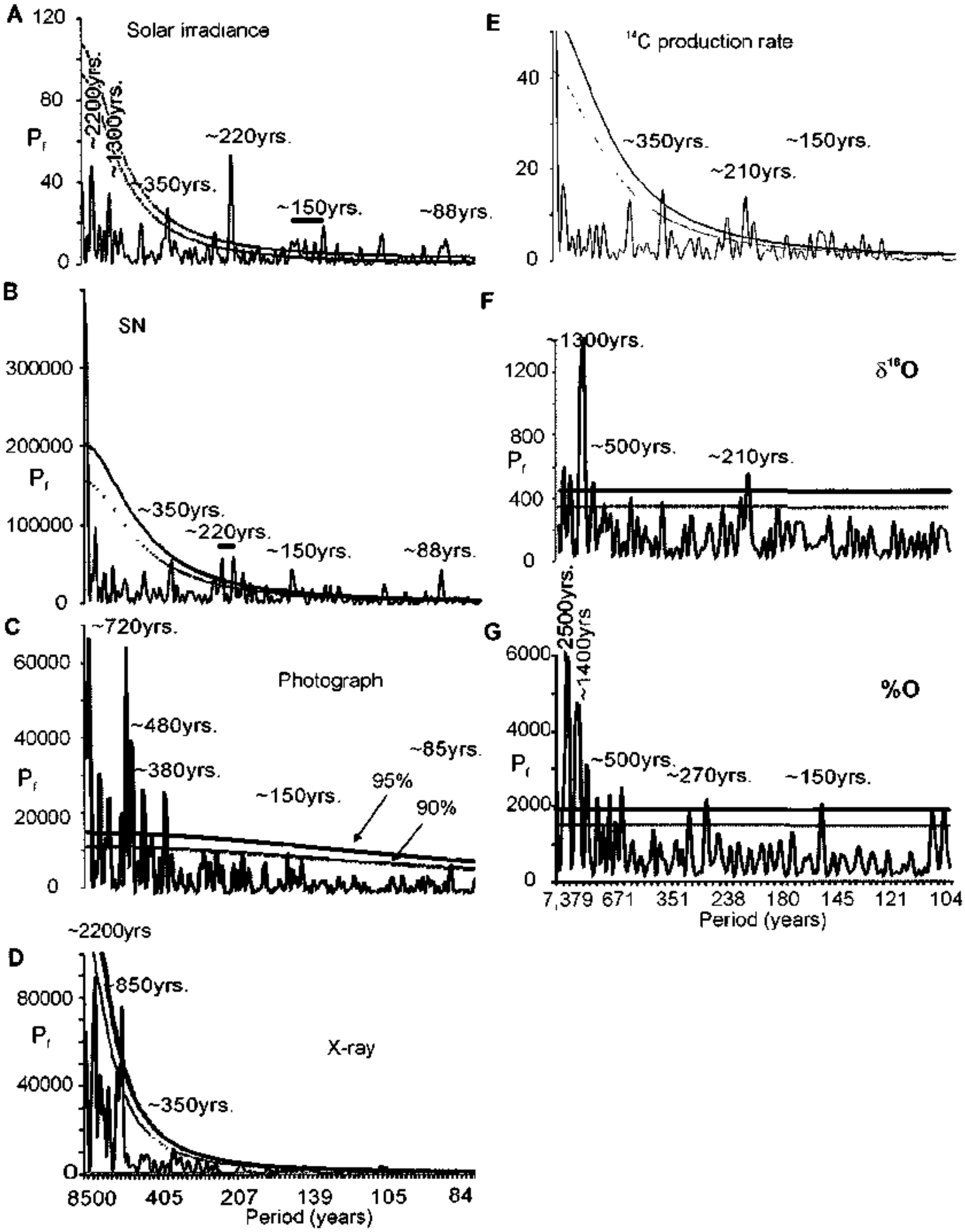

Figure 4.14: Periodograms of spectral analysis of photo (C) and X-ray (D) line-scans, cellulose oxygen isotope composition (F) and oxygen concentration (G), and reconstructed solar activity proxies (A, D, E). Gray areas highlight correlative solar and peat sediment cycles.

The 350-380 year waveband is significant in all records, except for %O (Figure 4.14A, B, C, E, F). Periodicities of 480, 720, and 820 years occur in the >90% confidence interval and are particularly significant in the digital photo, X-ray line-scan, and $\delta^{18}O_{cel}$ data (Figure 4.14C, D, F). However, these cycles are not recorded in the solar activity proxy records.

The 1300 year cyclicity is particularly significant in the $\delta^{18}O_{cel}$, %O, and digital photo line-scan records (Figure 4.14C, F, G). A 1300 year cycle is also present in the other proxy records but below 90% confidence level (Figure 4.14A, B, D, E).

A 2200-2500 year cycle occurs at >95% confidence in the $\delta^{18}O_{cel}$, %O, ^{14}C production rate, reconstructed sunspot number, and digital photo and X-ray line-scan records (Figure 4.14B, C, E, F, G). 2200-2500 year cycles are also present in the other proxy records but are below 90% confidence level (Figure 4.14A, D).

4.8 Discussion

4.8.1 Image analysis

In this study time-series analysis of line-scans from X-ray images and digital photographs of the peat core surface revealed significant periodic signals, gradual changes in the periodicity of the signals as well as abrupt transitions in dominant cycle length (see Figures 4.9-4.12). These image-derived signals have a resolution of <1 mm or <1 year and cannot be detected at such a resolution in peat using geochemical, paleontological, or other sedimentary analytical methods. The ranges of ~70 gray-values for digital photos and ~50 gray-values for X-rays are similar to that found in other non-laminated sediment records without visually obvious color changes (e.g., Prokoph and Thurow, 2001; Patterson et al., 2004; Nederbragt and Thurow, 2005).

The peat density increases due to increasing compaction near the top of the core and in the peat/clay transition near the bottom of the core are well captured in the X-ray record (Figure 4.9), demonstrating that this method is suitable for peat core analysis. Moreover, both X-ray and photo gray-values show changes in the cycle length at ~320 cm depth coincident with the transition from a fen to an ombrotrophic environment, indicating that a change in sedimentation rate rather than changes in average peat density or color occurred at that depth.

In Mer Bleue core, low photo gray-values ("dark peat") from 80-190 cm depth are associated with a strong 25 cm-cyclicity occurring during a rhizome-dominant peat-facies (see Figure 4.2). This interval is equivalent to a strong ~200 year cyclicity from ~700 – 2000 cal. yr. B.P. (Figure 4.12). The mostly low-density (i.e. low X-ray gray-values) interval from 240-480 cm is characterized by a dominant ~65 cm cycle (Figure 4.10), which is equivalent with a ~900 year cycle through this interval (Figure 4.11). Moreover most of the photo and X-ray gray-value cycles of 80 - 380 years wavelength and >1200 year wavelength can be related to solar cycles (Figure 4.14), hence solar forcing of peat density and color.

We argue that the reason for the absence of an annual to ~80 year cyclicity in both image records is due to the relatively high plant heterogeneity and coarseness of the incompletely decomposed plant material in the bogs of eastern Canada. The preservation of shorter cycles in the core surface photograph compared to the X-ray is probably due to the fact that the X-ray scan measures not only the value of individual pixels on the core surface but averages this pixel value from the diameter of the core. Thus, depending on heterogeneity of the sediment, X-ray images may average longer time-intervals than the pixel resolution on the surface indicates.

4.8.2 $\delta^{18}O$ variation in Sphagnum cellulose

The $\delta^{18}O_{cel}$ of *Sphagnum* changes gradually from ~15‰ at ~7300 cal. yr. B.P. to ~19‰ currently, with greater multicentennial variability before ~400 cal. yr. B.P. than afterwards (Figures 4.6, 4.7). Records for the last ~40 years in Ottawa (eastern Canada) show that an ~2‰ increase in $\delta^{18}O_{cel}$ corresponds to an average 1°C temperature increase (e.g. Global Network of Isotopes in Precipitation (GNIP) 2001; El Bilali and Patterson, 2009; and chapter III). Thus, the 15‰ to ~19‰ increase would provide an average mean air temperature increase of 2°C over the last ~7300 years. This corroborates previous studies that have demonstrated the sensitivity of *Sphagnum* growth in ombrotrophic bogs to temperature in eastern North America (Daley, 2007; Taylor, 2008; Daley et. al., 2009). Furthermore, the correlation between air temperature and $\delta^{18}O$ of precipitation, from which sphagnum cellulose receives its oxygen, is much larger in eastern Canada than observed in northwest Europe (Global Network of Isotopes in Precipitation (GNIP) 2001; and chapter V).

Cycles and other patterns with wavelength <100 year cannot be distinguished in the $\delta^{18}O_{cel}$ and %O records, because of the average sampling resolution of ~2 cm = ~43 years resulting in a minimum Nyquist frequency of ~86 years. The sample resolution in the fen part of the bog (older than 5300 years) is even lower with 5 cm sampling interval, so only cycles >200 years can be documented.

4.8.3. Solar, volcanic and atmospheric-oceanic forcing of Holocene paleoclimate in eastern Canada

A series of stationary and non-stationary cycles identified at >90% confidence and >80 years wavelength have been detected in image and geochemical records in the Mer Bleue section through the last ~8500 years. Most of the image and geochemical cycles can be linked to solar cycles, both in magnitude and temporal variability as evident from the wavelet analyses (Figures 4.7-4.13) indicating a link between solar forcing, temperature variability and peat lithology in eastern Canada. The following solar activity cycles are evident in the peat record:

1. A weak 85-90 year cycle in photo gray-values (Figure 4.14) occurs sporadically in several intervals through the last 4000 years (Figure 4.12) and correlates to the "Gleissberg" sunspot cycle (Gleissberg, 1958) that is evident in the reconstructed sunspot number and solar irradiance record (Figure 4.13).

2. A weak 110-150 year cycle in both image and geochemical records is also evident in the solar activity records (Figure 4.14), particularly throughout the last 2500 years

(Figure 4.8, 4.13A) confirming suggestions (e.g., Brown et al., 2005) that this cyclicity is also solar forced. Periodicities of ~150 years were also found in the $d^{18}O$ records from the Greenland Ice Sheet Project 2 (GISP2) and other Greenland ice cores (Yiou et al., 1997; Davis et al., 2001), suggesting that this cyclicity occurs in the entire northern Hemisphere.

3. A strong ~180-250 year cycle is evident in both $\delta^{18}O_{cel}$ as well as %O records from ~700-2500 cal. yr. B.P. and ~4000-6500 cal. yr. B.P. (Figures 4.7, 4.8). The same cyclicity occurs at weaker magnitude in the image data (Figures 4.11, 4.12). We correlate this cyclicity to the "Suess" solar cycle (Suess, 1980).

4. A 330-380 year cycle (Figuree 4.14) that is evident from ~4000-5000 cal. yr. B.P. is particularly strong in the image records and maybe related to a similar solar activity cyclicity (Figure 4.13). Cycles of similar duration were also recognized in Effingham Inlet (Patterson et al., 2004a) and on the Great Plains of North America, where they have been associated with intervals of drought (Yu and Ito, 1999; Dean et al., 2002).

5. In the ~500-900 year waveband, there appears to be a cyclicity, particularly in the image gray-values (Figures 4.11, 4.12) and in the solar irradiance record for the last ~3500 years (Figure 4.13). In their wavelet analysis of ^{10}Be and ^{14}C record Debret et al. (2007) also found a ~700 year cyclicity for the last ~3500 years, which also suggests a solar and/or cosmic forcing of the ~700 year cyclicity in eastern Canada.

6. A strong ~1200-1500 year cyclicty occurs in $\delta^{18}O_{cel}$ and %O records (Figures 4.7, 4.8), which is also evident in the solar proxy records before ~3500 cal. yr. B.P. (Figure 4.13A,B) and has been previously related to solar forcing of northern Hemisphere climate (e.g., Bond et al., 2001). Debret et al. (2007) also found this cyclicity in the ^{10}Be and ^{14}C records before 3500 cal. yr. B.P., but attributed the ~1500 year cyclicity to regular oscillations in atmospheric-oceanic circulation patterns in the North Atlantic and not to solar variability. The North Atlantic Oscillation (NAO) is one of the most important atmospheric-oceanic fluctuations in the North Atlantic Region (Shindell et al., 2001). For example, when the difference in the pressure is large (positive NAO index), strong westerlies and, consequently, hot summers and cold winters dominate in eastern Canada (e.g., Appenzeller et. al, 1998; Charman et. al., 2009; Magny, 2004; De Jong et al., 2006). Thus, the results suggest that a relative weak ~1300 year solar cycle is amplified by the NAO resulting in relative strong northern Hemisphere temperature variability in this waveband.

7. An ~2500 year cyclicity in %O and X-ray records (Figures 4.8, 4.11) has been related to the Hallstatt solar cycle (Vasiliev and Dergachev, 2002).

Thus, changes in peat sedimentation, and the $\delta^{18}O_{cel}$ as paleotempeature proxy in particular at time intervals >80 years can be predominantly linked to solar activity variations. Moreover, the shift at ~3500 cal. yr. B.P. in the $\delta^{18}O_{cel}$ record from a ~1300 year to a ~650 year cyclicity is associated with a paleotemperature drop of >1°C (ie. $\delta^{18}O_{cel}$ drop of 2‰) (Figure 4.7). Such a regime shift at this time with a similar cooling effect has also been recognized along the NE Pacific (e.g., Patterson et al., 2004a). Similarly, at ~3400 cal. yr. B.P. there was also a regime shift from a low to high hurricane activity with more than tripled landfalls along the U.S. Atlantic coast that lasted until ~1000 cal. yr. B.P (Liu and Fearn, 2000). Such an increase in hurricane activity may lead to wetter and cooler climate in eastern Canada since ~3500 cal. yr. B.P.

4.9 Conclusions

Digital peat core surface photography and X-ray imaging have been shown to be very useful methodologies to detect changes in peat sedimentation. Cycles and trends found by core imaging correlate well with independently determined geochemical variability and solar activity records. Wavelet and spectral analysis detected significant cyclic signals in peat that can be related to coeval changes in solar activity.

Solar activity fluctuations with ~80-year to ~2500-year periods appear to have a major influence on regional and global climate in eastern Canada as recorded in peat color and X-ray density, and isotope data from Mer Bleue core, Ottawa. In particular the results suggest that 180-250 year "Suess" and ~1300 year "Bond" solar cycles controlled long-term variability in temperature and peat sedimentation in eastern Canada. A shift to >1°C cooler temperatures at ~ at ~3500 cal. yr. B.P. correlates well with a shift in the long-term solar activity and North American temperature pattern.

4.10 References

Anderson, T.W., 1988. Late Quaternary pollen stratigraphy of the Ottawa valley – Lake Ontario region and its application in dating the Champlain Sea. In: Gadd, N.R., (Ed.), The Late Quaternary Development of the Champlain Sea Basin. *Geological Association of Canada Special Paper*, 35: 207–224.

Appenzeller C., Stocker T.F., and Anklin, M., 1998. North Atlantic oscillation dynamics recorded in Greenland ice cores. *Science*, 282: 446-449.

Aucour, A.-M., Hillaire-Marcel, C., and Bonnefille, R., 1996. Oxygen isotopes in cellulose from modern and Quaternary intertropical peatbogs: implications for palaeohydrology. *Chemical Geology*, 129: 341-359.

Auer, V., 1930. Peat bogs in southeastern Canada. Canada Department of Mines, Ottawa. *Memoir*, 162: 32 pp.

Barber, K.E., and Langdon, P.G., 2007. What drives the peat-based palaeoclimate record? A critical test using multi-proxy climate records from northern Britain. *Quaternary Science Reviews*, 26: 3318-3327.

Bard, E., Raisbeck, G., Yiou, F., and Jouzel, J., 2003. Reconstructed Solar Irradiance Data. IGBP PAGES/World Data Center for Paleoclimatology Data Contribution Series #2003-006. NOAA/NGDC Paleoclimatology Program, Boulder CO, USA.

Blaauw, M., van Geel, B., and van der Plicht, J., 2004. Solar forcing of climatic change during the mid-Holocene: indications from raised bogs in The Netherlands. *The Holocene*, 14: 1-35.

Bolton, E.W., Maasch, K.A., and Lilly, J.M., 1995. A wavelet analysis of Plio-Pleistocene climate indicators: A new view of periodicity evolution. *Geophys. Res. Letters*, 22: 2753-2756.

Bond, G., Kromer, B., Beer, J., Muscheler, R., Evans, M.N., Showers, W., Hoffmann, S., Lotti-Bond, R., Hajdas, I., and Bonani, G., 2001. Persistent Solar Influence on North Atlantic Climate During the Holocene. *Science*, 294: 2130-2136.

Bond, G., Showers, W., Cheseby, M., Lotti, R., Almasi, P., deMenocal, P., Priore, P., Cullen, H., Hajdas, I., and Bonani, G., 1997. A Pervasive Millennial-Scale Cycle in North Atlantic Holocene and Glacial Climates. *Science*, 278: 1257–1266.

Booth, R.K., and Jackson, S.T., 2003. A high-resolution record of late-Holocene moisture variability from a Michigan raised bog. *The Holocene*, 13: 865–78.

Booth, R.K., Notaro, M., Jackson, S.T., and Kutzbach, J.E., 2006. Widespread drought episodes in the western Great Lakes during the past 2000 years: geographic extent and potential mechanisms. *Earth and Planetary Science Letters*, 242: 415-427.

Brown, K.J., Clark, J.S., Grimm, E.C., Donovan, J.J., Mueller, P.G., Hansen, C.S., and Stefanova, I., 2001. Fire cycles in North American interior grasslands and their relation to prairie drought. *PNAS*, 102: 8865–8870.

Brenninkmeijer, C.A.M., van Geel, B., and Mook, W.G., 1982. Variations in the D/H and 18O/16O ratios in cellulose extracted from a peat bog core. *Earth and Planetary Science Letters*, 61: 283-290.

Burk, R.L., and Stuiver, M., 1976. Oxygen isotope ratios in trees reflect mean annual temperature and humidity. *Science*, 211: 1417-1419.

Carslaw, K.S., Harrison, R.G., and Kirkby, J., 2002. Cosmic rays, clouds, and climate. *Science*, 298: 1732-1737.

Chao, B.F., and Naito, I., 1995. Wavelet analysis provides a new tool for studying Earth's rotation. *EOS*, 76: 161, 164-165.

Charman, D.J., 2010. Centennial climate variability in the British Isles during the mid–late Holocene. Quaternary Science Review.

Charman, D.J., Barber, K.E., Blaauw, M., Langdon, P.G., Mauquoy, D., Daley, T.J., Hughes, P.D.M., and Karofeld, E., 2009. Climate drivers for peatland palaeoclimate records. *Quaternary Science Reviews*, 28: 1811–1819.

Charman, D.J., Brown, A.D., Hendon, D., and Karofeld, E., 2004. Testing the relationship between Holocene peatland palaeoclimate reconstructions and instrumental data at two European sites. *Quaternary Science Reviews*, 23: 137–143.

Charman, D.J., Hendon, D., and Packman, S., 1999. Multiproxy surface wetness records from replicate cores on an ombrotrophic mire: implications for Holocene palaeoclimate records. *Journal of Quaternary Science*, 14: 451–463.

Chiverrell, R.C., 2001. A proxy record of late Holocene climate change from May Moss, northeast England. *Journal of Quaternary Science*, 16: 9-29.

Cumming, B.F., Laird, K.R., Bennett, J.R., Smol, J.P., and Salomon, A.K., 2002. Persistent millennial-scale shifts in moisture regimes in western Canada during the past six millennia. *PNAS*, 99: 16117-16121

Daley, T.J., 2007. Tracking Holocene climate change using peat bog stable isotopes. Ph.D. thesis, University of Southampton, UK, 358 p.

Daley, T.J., Barber K.E., Street-Perrott, F.A., Loader, N.J., Marshall, J.D., Crowley, S.F., and Fisher, E.H., 2010. Holocene climate variability revealed by oxygen isotope analysis of *Sphagnum* cellulose from Walton Moss, northern England. *Quaternary Science Reviews*, 29: 1590-1601.

Daley, T.J., Street-Perrott, F.A., Loader, N.J., Barber, K.E., Hughes, P.D.M., Fisher, E.H., and Marshall, J.D., 2009. Terrestrial climate signal of the '8200 yr B.P. cold event' in the Labrador Sea region. *Geology*, 37: 831–834.

Davis, J.C., 1986. Statistics and data analysis in Geology. Wiley: New York; 646 p.

Davis, J.C., and Bohling, G.C., 2001. The search for patterns in ice-core temperature curves. In: Gerhard, L.C., Harrison, W.E., and Hanson, B.M. (Eds.) Geological Perspectives of Global Climate Change, Kansas Geol. Survey and Am. Assoc. Petrol. Geol. Div. Environ. Geosci., Tulsa,OK: pp. 213–229.

De Jong, R., Bjorck, S., Bjorkman, L., and Clemmensen, L.B., 2006. Storminess variation during the last 6500 years as reconstructed from an ombrotrophic peat bog in Halland, southwest Sweden. *Journal of Quaternary Science*, 21: 905–919.

Dean, W., Anderson, R., Bradbury, J.P., and Anderson, D., 2002. A 1500-year record of climatic and environmental change in Elk Lake, Minnesota I: Varve thickness and grey-scale density. *Journal of Paleolimnology*, 27: 287-299.

Debret, M., Bout-Roumazeilles, V., Grousset, F., Desmet, M., McManus, J.F., Massei, N., Sebag, D., Petit, J-R., Copard, Y., and Trentesaux, A., 2007. The origin of the 1500-year climate cycles in Holocene North-Atlantic records. *Climate Past*, 3: 569–575.

DeNiro, M.J., and Epstein, S., 1981. Isotopic composition of cellulose from aquatic organisms. *Geochimica et Cosmochimica Acta*, 45: 1885–1894.

Edwards, T.W.D., Aravena, R.O., Fritz, P., and Morgan, A.V., 1985. Interpreting paleoclimate from 18O and 2H in plant cellulose: comparison with evidence from fossil insects and relict permafrost in southwestern Ontario. *Canadian Journal of Earth Sciences*, 22: 1720–1726.

El Bilali, H., and Patterson R.T., 2009. Holocene Paleoclimate Reconstruction in eastern Canada: Evidence from $\delta^{18}O$ of plant cellulose from the Mer Bleue Bog, Ottawa, Ontario. American Geophysical Union, Fall Meeting 2009, abstract # PP21D-07I.

Elson, J.A., and Elson, J.B., 1969. Phases of the Champlain sea indicated by littoral mollusks. *Geological Society of America Bulletin*, 70: 1596.

Environment Canada, 1990. The climates of Canada. 176 p.

Environment Canada, 2010. National Climate Data and Information Archive. www.climate.weatheroffice.gc.ca.

Epstein, S., Thompson, P., and Yapp, C.J., 1977. Oxygen and Hydrogen Isotopic Ratios in Plant Cellulose. *Science*, 198: 1209 – 1215.

Epstein, S., Yapp, C.J., and Hall, J.H., 1976. Determination of the D/H Ratios of Nonexchangeable Hydrogen in Cellulose Extracted from Aquatic and Land Plants. *Earth Planet Sci. Lett.*, 30: 241–251.

Esper, J., Cook, E.R., and Schweingruber, F.H., 2002. Low-frequency signals in long tree-ring chronologies for reconstructing past temperature variability. *Science*, 295: 2250-2253.

Francey, R.J., and Farquhar, G.D., 1982. An explanation for the 13C/12C variations in tree rings. *Nature*, 297: 28–31.

Frankignoul, C., Muller, P., and Zorita, E. 1997. A simple model of the decadal respone of the ocean to stochastic wind forcing. *J. Phys. Oceanogr.*, 27: 1533–1546.

Friis-Christensen, E., and Lassen K., 1991. Length of the solar cycle: An indicator of solar activity closely associated with climate, *Science*, 254: 698-700.

Frolking, S., Roulet, N.T., Moore, T.R., Lafleur, P.M., Bubier, J.L., and Crill, P.M., 2001. Modeling the seasonal to annual carbon balance of Mer Bleue Bog, Ontario, Canada. *Global Biogeochemical Cycles*, 16: doi 10.1029/2001GB0011457.

Garcia, A., and Mouradian, Z., 1998. The Gleissberg Cycle of minima. *Sol. Phys.*, 180: 495-498.

Frolking, S., Roulet, N.T., Tuittila, E., Bubier, J.L., Quillet, A., Talbot, J., Richard, P.J. H., 2010. A new model of Holocene peatland net primary production, decomposition, water balance, and peat accumulation. *Earth Syst. Dynam. Discuss.*, 1: 115–167.

Gleissberg,W., 1958. The eighty-year sunspot cycle. *Journal of the British Astronomical Association*, 68: 1148-1152.

Global Network of Isotopes in Precipitation (GNIP/ISOHIS), 2001. http://isohis.iaea.org/. International Atomic Energy Agency.

Grosse-Brauckmann, G., 1972. Über pflanzliche Makrofossilien mitteleuropäischer Torfe. I. Gewebereste krautiger Pflanzen und ihre Merkmale. *Telma*, 2: 19-55.

Grosse-Brauckmann, G., 1974. Über pflanzliche Makrofossilien mitteleuropäischer Torfe. II. Weitere Reste (Früchte und Samen, Moose u. a.) und ihre Bestimmungsmöglichkeiten. *Telma*, 4: 51-117.

Hu, F.S., Kauffman, D., Yoneji, S., Nelson, D., Shemesh, A., Huang, Y.,Tian, J., Bond, G., Clegg, B., and Brown, T., 2003. Cyclic variation and solar forcing of Holocene climate in the Alaskan subarctic. *Science*, 301: 1890-1893.

Jansen, E., Overpeck, J., Briffa, K.R., Duplessy, J.-C., Joos, F., Masson-Delmotte, V., Olago, D., Otto-Bliesner, B., Peltier, W.R., Rahmstorf, S., Ramesh, R., Raynaud, D., Rind, D., Solomina, O., Villalba, R., and Zhang, D. 2007. Palaeoclimate. In: Climate

Change 2007: The Physical Science Basis. In: Contribution of Working Group I to the Fourth Assessment Report of the Intergovernmental Panel on Climate Change, In: Solomon, S., Qin, D, Manning, M, Chen, Z, Marquis, M, Averyt, K.B, Tignor M. Miller, H.L. (Eds.). Cambridge University Press, Cambridge, United Kingdom and New York, NY, USA.

Jones, P.D., Osborn, T.J., and Briffa, K.R., 2001. The evolution of climate over the last millennium. *Science*, 292: 662-666.

Jowsey P.C., 1966. An improved peat sampler. *The New Phytologist*, 65: 245–248.

Joyal, R., 1970. Description de la tourbière à Sphaignes Mer Bleue près d'Ottawa. 1. Végétation. *Canadian Journal of Botany*, 48: 1405–1418.

Kilian, M.R., van der Plicht, J., van Geel, B., 1995. Dating raised bogs: new aspects of AMS 14C wiggle matching, a reservoir effect and climatic change. *Quaternary Science Reviews*, 14: 959–966.

Lévesque, P.E.M., Dinel, H., and Larouche, A., 1988. Guide to The identification of Plant Macrofossils in Canadian Peatlands. *Research Branch, Agriculture Canada, Publication 1817*, 65 pp.

Libby, L.M., Pandolfi, L.J., Payton, P.H., Marshall, J., III, Becker, B., and Giertz-Sienbenlist, V., 1976. Isotopic tree thermometers. *Nature*, 261: 284–288.

Liu, K.B., and Fearn, M.L., 2000. Reconstruction of prehistoric landfall frequencies of catastrophic hurricanes in northwestern Florida from lake sediment records. *Quaternary Research*, 54: 238-245.

Magny, M., 2004. Holocene climate variability as reflected by mid-European lake level fluctuations and its probable impact on prehistoric human settlements. *Quaternary International*, 113: 65–79.

Mann, M.E., Park, J., and Bradley, R.S., 1995. Global Interdecadal and Century-Scale Climate Oscillations During the Past Five Centuries. *Nature*, 378: 266-270.

Mann, M.S., and Lees, J.M., 1996., 'Robust estimation of background noise and signal detection in climatic time series'. *Climatic Change*, 33: 409-445.

Mauquoy, D., and van Geel, B., 2007. Plant Macrofossil Methods and Studies/Mire and Peat Macros. Elsevier, pp. 2315-2336.

McCracken, K.G., Dreschhoff, G.A.M., Smart,D.F., and Shea, M.A., 2001. The Gleissberg periodicity in large fluence solar proton events. Proceedings of 27th International Cosmic Ray Conference Hamburg, Germany, pp. 3205-3208.

Ménot-Combes, G., Burns, S.J.,and Leuenberger, M., 2002. Variations of 18O/16O in plants from temperate peat bogs (Switzerland): implications for paleoclimatic studies. *Earth and Planetary Science Letters*, 202: 419–434.

Moberg, A., Sonechkin, D.M., Holmgren, K., Datsenko, N.M., and Karle´n, W., 2005. Highly variable temperatures reconstructed from low- and high-resolution proxy data. *Nature*, 433: 613– 617.

Morlet, J., Arehs, G., Fourgeau, I., and Giard, D., 1982. Wave propagation and sampling theory - part I: complex signal and scattering in multilayered media. *Geophysics*, 47: 203-221.

Mott, R.J., and Camfield, M., 1969. Palynological Studies in the Ottawa Area. Geological Survey of Canada, Ottawa, pp. 1–16.

Munsell Color Company, 1975. Munsell Soil Color Charts. Munsell Color Company, MD, USA.

Nederbragt, A., and Thurow, J., 2005. Digital Sediment Colour Analysis as a Method to Obtain High Resolution Climate Proxy Records. *Developments in Paleoenvironmental Research 7, Part II Springer, Dordrecht*: pp. 105-124.

O'Leary, M.H., Treichel, I., and Rooney, M., 1986. Short-term measurement of carbon isotope fractionation in plants. *Plant Physiology*, 80: 578–582.

Patterson, R.T., Prokoph, A., and Chang, A.S., 2004a. Late Holocene sedimentary response to solar and cosmic ray activity influenced climate variability in the NE Pacific. *Sedimentary Geology*, 172: 67-84.

Patterson, R.T., Prokoph, A., Wright, C., Chang, A., Thomson, R.E., and Ware, D.M., 2004b. Holocene solar variability and pelagic fish productivity in the NE Pacific. *Palaeontologia Electronica, 7.*

Plunkett, G., and Swindles, G.T., 2008. Determining the Sun's influence on Late Glacial and Holocene climates: a focus on climate response to centennial-scale solar forcing at 2800 cal. BP. *Quaternary Science Reviews*, 27: 175–84.

Prokoph, A., and Barthelmes, F., 1996. Detection of nonstationarities in geological time series: Wavelet transform of chaotic and cyclic sequences. *Computers & Geoscience*, 22: 1097-1108.

Prokoph, A., and Thurow, 2001. Orbital forcing on sedimentation in a Boreal epeiric sea: Evidence from well-logs and digital sediment color data of Albian strata. *Palaeogeography, Palaeoclimatology, Palaeoecology*, 174: 67-96.

Prokoph, A., and Patterson, R.T., 2004a. From depth-scale to time-scale: transforming of sediment image color data into high-resolution time-series. In: Francus, P. (ed.) Image Analysis, Sediments and Paleoenvironments. *Developments in Paleoenvironmental Research Series 7, Springer, Dordrecht*: pp. 143-164.

Prokoph, A., and Patterson, R.T., 2004b. Application of wavelet and regression analysis in assessing temporal and geographic climate variability; Eastern Ontario, Canada as a case study. *Atmosphere-Ocean,* 42: 201-212.

Reimer, P.J., Baillie, M.G.L., Bard, E., Bayliss, A., Beck, J.W., Blackwell, P.G., Bronk Ramsey, C., Buck, C.E., Burr, G.S., Edwards, R.L., Friedrich, M., Grootes, P.M., Guilderson, T.P., Hajdas, I., Heaton, T.J., Hogg, A.G., Hughen, K.A., Kaiser, K.F., Kromer, B., McCormac, F.G., Manning, S.W., Reimer, R.W., Richards, D.A., Southon, J.R., Talamo, S., Turney, C.S.M, van der Plicht, J., and Weyhenmeyer, C.E., 2009. IntCal09 and Marine09 radiocarbon age calibration curves, 0–50,000 years cal BP. *Radiocarbon*, 51: 1111–50.

Reimer, P.J., Baillie, M.G.L., Bard, E., Bayliss, A., Beck, J.W., Bertrand, C.J.H., Blackwell, P.G., Buck, C.E., Burr, G.S., Cutler, K.B., Damon, P.E., Edwards, R.L., Fairbanks, R.G., Friedrich, M., Guilderson, T.P., Hogg, A.G., Hughen, K.A., Kromer, B., McCormac, G., Manning, S., Bronk Ramsey, C., Reimer, R.W., Remmele, S., Southon, J.R., Stuiver, M., Talamo, S., Taylor, F.W., van der Plicht, J., and Weyhenmeyer, C.E., 2004. IntCal04 terrestrial radiocarbon age calibration, 0–26 cal kyr BP. *Radiocarbon*, 46: 1029–1058.

Rioul, O., and Vetterli, M., 1991. Wavelets and Signal Processing. *IEEE Special Magazine,* 14-38.

Roulet, N.T., Lafleur, P.M., Richard, P.J.H., Moore, T.R., Humphreys, E., and Bubier, J.L., 2007. Contemporary carbon balance and late Holocene carbon accumulation in a northern peatland *Global Change Biology*, 13: 397–411.

Schaaf, M., and Thurow, J., 1995. Late Pleistocene-Holocene climatic cycles recorded in Santa Barbara Basin Sediments: Interpretation of color density logs from Site 893. In: Kennett, J.P., Baldauf, J.G., and Lyle, M. (Eds.), *Proceedings of the Ocean Drilling Program, Scientific Results146*:31-44.

Schubert, S.D., Suarez, M.J., Pegion, P.J., Koster, R.D., and Bacmeister, J.T., 2004. On the Cause of the 1930s Dust Bowl. *Science*, 303: 1855-1859.

Schulz, M., and Mudelsee, M., 2002. REDFIT: estimating red-noise spectra directly from unevenly spaced paleoclimatic time series. *Computers & Geosciences*, 28: 421–426.

Shindell, D.T., Schmidt, G.A., Mann, M.E., Rind, D., and Waple, A., 2001. Solar Forcing of Regional climate Change during the Maunder Minimum. *Science*, 294: 2149-2152.

Smith, A.J.E., 2004. The moss flora of Britain and Ireland, Second edition. Cambridge University Press, Cambridge.

Solanki, S.K., Usoskin, I.G., Kromer, B., Schüssler , M., and Beer. J., 2004. An unusually active Sun during recent decades compared to the previous 11,000 years. *Nature*, 431: 1084-1087.

Sonett, C.P., and Finney, S.A., 1990. The Spectrum of Radiocarbon. *Philos. Trans. R. Soc. London, Ser., A330*: 413–425.

Speranza, A., van Geel, B., and van der Plicht, J., 2002. Evidence for solar forcing of climate change at ca. 850 cal. BC from a Czech peat sequence. *Global and Planetary Change*, 35: 51-65.

Sternberg, L., Da, S.L., DeNiro, M.J., and Savidge, R.A., 1986. Oxygen isotope exchange between metabolites and water during biochemical reactions leading to cellulose synthesis. *Plant Physiology*, 82: 423–427.

Suess, H.E., 1980. The radiocarbon record in tree rings of the last 8000 years. *Radiocarbon*, 22: 200–209.

Sukumar, R., Ramesh, R., Pant, R.K., and Rajagopalan, G., 1993. A $\delta^{13}C$ record of late Quaternary climate change from tropical peat in southern India. *Nature*, 364: 703-706.

Svensmark, H., and Friis-Christensen, E., 1997. Variation of cosmic ray flux and global cloud coverage - a missing link in solar-climate relationships. *Journal of Atmospheric and Solar-Terrestrial Physics*, 59: 1225-1232.

Talbot, J., Richard, P.J.H., Roulet, N.T., Booth, R.K., 2010. Assessing long-term hydrological and ecological responses to drainage in a raised bog using paleoecology and a hydrosequence. *Journal of Vegetation Science*, 21: 143-156.

Taylor, M.A., 2008. Continental-scale validation of the temperature signal in oxygen isotopes of *Sphagnum* cellulose and its application as paleoclimate proxy. M.Sc. thesis, University of Wyoming, USA, 86 p.

Torrence, C., and Compo, G.P., 1998. A Practical Guide to Wavelet Analysis. *Bull. Amer. Meteor. Soc.,* 79: 61-78.

Usoskin, I.G., and Kovaltsov, G.A., 2004. Long-Term Solar Activity: Direct and Indirect Study. *Solar Phys.,* 224:37– 47.

Van Geel, B., Buurman, J., and Waterbolk, H.T., 1996. Archeological and paleoecological indications for an abrupt climate change in The Netherlands and evidence for climatological teleconnections around 2650 BP. *Journal of Quaternary Science*, 11: 451- 460.

Van Geel, B., van der Plicht, J., Kilian, M.R., Klaver, E.R., Kouwenberg, J.H.M., Renssen, H., Reynaud-Farrera, I., and Waterbolk, H.T., 1998. The sharp rise of d14C c. 800 cal BC: possible causes, related climatic teleconnections and the impact on human environments. *Radiocarbon*, 40: 535-550.

Vasiliev, S.S., and Dergachev, V.A., 2002. The ~2400-year cycle in atmospheric radiocarbon concentration: bispectrum of 14C data over the last 8000 years. *Ann. Geophys.*, 20: 115–120.

Veizer, J., 2005. Celestial Climate Driver: A Perspective From Four Billion Years Of The Carbon Cycle. *Geoscience Canada*, 32:13-30.

Ware, D.M., and Thomson, R.E., 2000. Interannual to multidecadal timescale climate variations in the Northeast Pacific. *J. Climate*, 13: 3209-3220.

White, J.W.C., Ciais, P., Figge, R.A., Kenny, R., and Margraft, V., 1994a. A high-resolution record of atmospheric CO2 content from carbon isotopes in peat. *Nature*, 367: 153-56.

White, J.W.C., Figge, R.A., Markraft, V., Ciais, P., and Kenny, R., 1994b. Climate in the Pleistocene. *Nature*, 371: 111-12.

Yiou, P., Fuhrer, K., Meeker, L. D., Jouzel, J., Johnsen, S.,and Mayewski, P.A., 1997. Paleoclimate variability inferred from spectral analysis of Greenland and Antarctic ice core data. *J. Geophys. Res.*, 102 : 26441–26454.

Yu, Z.C., and Eicher, U., 1998. Abrupt climate oscillations during the last deglaciation in central North America. *Science*, 282: 2235-2238.

Yu, Z., and Ito, E., 1999. Possible solar forcing of century-scale drought frequency in the northern Great Plains. *Geology*, 27: 263-266.

Yu, Z., and Wright, H.E., 2001. Response of interior North America to abrupt climate oscillations in the North Atlantic region during the last deglaciation. *Earth-Sci. Rev.*, 52: 333-369.

Zhentao, X., 1990. Solar Observations in Ancient China and Solar Variability. *Philos. Trans. R. Soc. London, Ser.*, A330 : 513–516.

CHAPTER FIVE

5. MID-HOLOCENE CLIMATE RESPONSE TO SOLAR FORCING: EVIDENCE FROM THE GLEN WEST BOG, NORTHERN IRELAND, UK.

5.1 Abstract

A novel combination of sediment imaging and geochemical proxies was applied to a portion of a peat core from Glen West Bog, Northern Ireland, UK to improve an understanding of paleoclimate changes through the late Holocene in Northern Ireland. Time-series analysis such as trend, spectral and wavelet analysis of data derived from digital core surface photographs and X-ray scans, and cellulose oxygen isotope data were used to determine the driving forces for paleoclimate fluctuations through a 30 cm core monolith spanning 2880 to 2500 cal. yr. B.P. Sedimentary and geochemical trends, cycles, and abrupt shifts were compared with global ^{14}C production rates and the local water table record. The results suggest that ~11-year (equivalent to Schwabe cycle) and ~250-year (equivalent to Suess/de vries cycle) solar cycles exerted a major influence on regional Northern Ireland climate as recorded in the peat coloration, X-ray density, and isotope data.

An ~11-year cycle is restricted to a low ^{14}C production period from 2650-2500 cal. yr. B.P. indicating that it may only impact the climate record during intervals of high solar activity. A period of high ^{14}C production rate (i.e. low solar activity) from ~2760-2650 cal. yr. B.P. with ~20-45 year cyclicity correlates with a shift from a relatively dry to a wet climate in Northern Ireland as also evident from image data. Some other more intermittent cycles (e.g., 80-100 years) correlate with ^{14}C production rate variability, while a 30-50 year cycle correlates with the fluctuations in modern climate regimes in the North Atlantic such as the North Atlantic Oscillation (NAO).

Keywords: Raised bog, oxygen isotopes, plant cellulose, cyclicity, climate variability.

5.2 Introduction

Peatlands contain important archives of Holocene paleoclimate change over decadal to millennial timescales (e.g., Brenninkmeijer et al., 1982; Francey and Farquhar, 1982; O'Leary et al., 1986; Charman et al., 1999; Chiverrell, 2001). In several studies peat sections have been used to determine the relationships between solar activity and climate change (e.g., Kilian et al., 1995; van Geel et al., 1996, 1998; Speranza et al., 2002; Blaauw et al., 2004) through a large range of paleoclimate proxies (Swindles et al., 2007a, 2007b; Plunkett and Swindles, 2008; Charman, 2010).

In Northern Ireland, several projects utilized peatlands for paleoclimate studies (Holmes, 1998; Plunkett, 1999, 2006; Barber et al., 2000; Swindles et al., 2007a, 2007b; Plunkett and Swindles, 2008; Swindles and Plunkett, 2010; Charman, 2010). Some of these studies compared the ^{14}C production rate (Reimer et al., 2004) to multiproxy paleoclimate records from Northern Ireland peatlands in order to investigate the potential influence of solar activity on paleoclimate (Swindles et al., 2007a, 2007b; Plunkett and Swindles, 2008; Swindles and Plunkett, 2010; Charman, 2010).

Previous studies in continental Europe reported an abrupt climate cooling concurrent with a $\Delta^{14}C$ maximum between 2800 and 2710 cal. yr. B.P. (Kilian et al., 1995; van Geel et al., 1996, 1998; Speranza et al., 2002; Blaauw et al., 2004). The 2800 cal. yr. B.P. cooling event is considered to be the result of a deep water perturbation in the North Atlantic at 2700 cal. yr. B.P. (Hall et al., 2004) that correlates with Ice Rafted Debris (IRD) event 2 (Bond et al., 2001). For the same time interval, previous analysis of the entire Glen West Bog peat profile shows a distinct visible change in sedimentology at ~101 cm depth where *Monocotyledon*-dominated peat changes to *Sphagnum*-dominated peat (Swindles et al., 2007a, 2007b; Plunkett and Swindles, 2008). Moreover, multiproxy records indicate relatively dry bog surface conditions at ca 2800 cal. yr. B.P., followed by a shift to wetter bog surface conditions at around ca 2700 cal. yr. B.P. (Swindles et al., 2007a, 2007b; Plunkett and Swindles 2008; Swindles and Plunkett, 2010). Increased bog surface wetness in Europe, including the Glen West core, has been associated with periods of transition to increasing ^{14}C production, suggesting solar forcing of the climate (e.g., Swindles et al., 2007b, Plunkett and Swindles, 2008; Swindles and Plunkett, 2010; Charman et al., 2009).

This study introduces geochemical, sediment imaging, and time-series analysis methods to a portion of the Glen West Bog section from 90-120 cm depth with the aim to elucidate paleoclimate variations and to better understand the role of solar forcing on climate between ~2880 and 2500 cal. yr. B.P. in the North Atlantic Region. The methods used in this study primarily involve oxygen isotope analysis of plant cellulose (*Sphagnum*), image analysis and statistical analysis techniques. Wavelet analysis (WA) and spectral analysis (SA) are used to detect long-term trends and cycles in the digital peat images (X-ray and photographs) and oxygen isotope composition of plant cellulose records. These records are compared to ^{14}C productivity (Reimer et al., 2009) and water table fluctuations (e.g., Swindles et al., 2007a, 2007b; Plunkett and Swindles, 2008) between 2880 and 2500 cal. yr. B.P. In addition, this study attempts to evaluate the importance of both external (orbital, solar and volcanic) and internal (ocean and atmosphere) forcing factors on late Holocene climate fluctuations by reconciling several paleoclimate and solar activity proxies.

5.3 Background

5.3.1 Climate forcing and dynamics

5.3.1.1. Ocean and atmospheric circulation

The oceans are the principal source of atmospheric moisture. Because of the ocean's capacity to retain heat, maritime climates are more moderate and have less extreme seasonal variations than continental climates. The North Atlantic Oscillation (NAO) is one of the most important atmospheric-oceanic cyclic phenomena in the North Atlantic Region. Permanent low-pressure systems over Iceland (the Icelandic Low) and high-pressure systems over the Azores (the Azores High) control the direction and strength of westerly winds into Europe. The difference between the strengths and positions of these systems is measured as the NAO index. A large difference in atmospheric pressure (positive NAO index) results in strong westerlies with consequent cool summers and mild and wet winters in northwest Europe. In contrast, if the difference in the pressure is low (negative NAO index), westerlies are suppressed, and the winters are cold with increased storm activity in southern Europe and North Africa (e.g., Appenzeller et. al, 1998; Magny, 2004; De Jong et al., 2006; Charman et. al., 2009). The periodic fluctuation between strong and weak NAO modes over 20-60 year intervals is accompanied by 1-2°C temperature variations (e.g., Shindell et al., 2001).

5.3.1.2 Celestial forcing

The magnitude of variations in the output of solar energy are thought to be too small to explain observed climate variability. However, it is now understood that modulation of Cosmic Ray Flux (CRF) by solar irradiance controls global low-altitude cloud cover and, consequently enhances the climate impact of solar irradiance fluctuations (Svensmark and Friis-Christensen, 1997; Carslaw et al., 2002; Svensmark et al., 2006). In addition, solar ultraviolet radiation (UV) is the main agent for producing ozone in the stratosphere and varies by ~4% during an 11-year solar cycle (e.g., Gray, 2010), impacting significantly the ozone production (Haigh, 1994). These systematic changes in the distribution of ozone through a solar cycle in the atmosphere correlate with significant changes in atmospheric pressure distribution and temperature in the stratosphere (van Loon and Labitzke, 2000; Hameed and Lee, 2005), troposphere (Crooks and Gray, 2005; Gleisner et al., 2005) and ocean (Bond et al., 2001; Weng, 2005).

The influence of solar irradiance on global climate is well documented at the frequency of the ~9-12 year "Schwabe" sunspot cycle (Friis-Christensen and Lassen, 1991), and quasi-periodic ~80-90 year "Gleissberg" cycles (Gleissberg, 1958; Garcia and Mouradian, 1998). Global sea-surface temperature (SST) fluctuations of up to 0.4°C have been attributed to solar irradiance variability during "Schwabe" sunspot cycles (Jones et al, 2001). Longer solar activity cycles cannot be studied using direct observations, but several such cycles have been found in cosmogenic isotope data. High ^{14}C production rates are commonly associated with relatively low solar activity, because ^{14}C is naturally produced in the upper atmosphere by cosmic-ray bombardment, which is diminished at periods of increased solar activity (e.g., Svensmark, 1998).

A solar activity cycle with a period of 205–210 years, often called the de Vries or Suess cycle has been observed in several cosmogenic isotope records (e.g., Suess, 1980; Sonett and Finney, 1990; Zhentao, 1990; Usoskin et al., 2004). The "Suess-cycle" is also associated with several worldwide cool periods through the last millennium, for example the Maunder Minimum of the Little Ice Age (McCracken et al., 2001).

Millennial scale (1000-1500 years) cycles in paleoclimate records throughout the northern Hemisphere (e.g., Esper et al., 2002; Hu et al., 2003) are recognized in coeval fluctuations in proxies for solar irradiance such as cosmogenic nuclides ^{14}C and ^{10}Be, and ice-rafted debris distribution (e.g., Bond et al., 2001).

5.3.2 Sphagnum cellulose, ombrotrophic bogs and paleoclimate

Ombrotrophic bogs are *Sphagnum*-dominated (Brenninkmeijer et al., 1982; Booth and Jackson, 2003; Booth et al., 2006) and their surface moisture is solely derived from atmospheric moisture. Moreover, *Sphagnum* mosses are ectohydric bryophytes and thus the water is conducted to the plants by external capillaries (Taylor, 2008). Consequently, *Sphagnum* is restricted to short growth forms occurring in areas of high relative humidity (Taylor, 2008). Due to the absence of stomata and vascular tissues, *Sphagnum* mosses possess limited ability to control water loss and thus follow a simple physiological water-use strategy. Given its lack of roots and stomata cells, all isotopic fractionation of the plant water, and its oxygen, is environmentally controlled prior to its assimilation and cellulose synthesis (Ménot-Combes et al., 2002).

The stable isotope composition of plant macrofossils and other organic matter from peat profiles has been found to be an important source of paleoclimate information (e.g., O'Leary et al., 1986; Francey and Farquhar, 1982; Aucour et al., 1996). Several studies have demonstrated a direct correlation between the isotopic ratios of carbon, oxygen, and hydrogen of cellulose and mean annual temperature (e.g., Libby et al., 1976; Epstein et al., 1976, 1977; DeNiro and Epstein, 1981; Edwards et al., 1985; Sternberg et al., 1986; Sukumar et al., 1993; White et al., 1994; Daley, 2007; Taylor, 2008; Daley et al., 2009, 2010).

Other studies have shown that the stable isotope composition of meteoric water at mid to high latitudes is strongly correlated with temperature and relative humidity, and meteoric water is often the source water for cellulose (Dansgaard, 1964; Fricke and O'Neil, 1999; Rozanski et al., 1993). Consequently, the isotopic composition of *Sphagnum* cellulose is widely used to reconstruct the isotopic composition of meteoric water (Aucour et al., 1996; Pendall et al., 2001; Menot-Combes et al., 2002; Zanazzi and Mora, 2005).

The relationship between cellulose oxygen isotope composition and that of the source water (Yapp and Epstein, 1982; Roden et al., 2000; Pendall et al., 2001; Anderson et al., 2002; Zanazzi and Mora, 2005) can be summarised as:

$$\delta_{cell} = \delta_{sw} + \varepsilon_b + (\varepsilon_e + \varepsilon_k)(1 - h) \qquad (1)$$

where

δ_{cell} : isotopic composition of cellulose,

δ_{sw} : isotopic composition of the source water,

ε_b : biochemical enrichment factor,

ε_e : liquid-vapour equilibrium enrichment factor,

ε_k : liquid-vapour kinetic enrichment factor due to evaporation,

h : relative humidity (value from 0 to 1).

Sphagnum inhabits moist environments where *h* is close to 1 (Vitt et al., 1975; Clymo and Hayward, 1982; Zanazzi and Mora, 2005). Consequently equation (1) can be simplified to:

$$\delta_{cell} = \delta_{sw} + \varepsilon_b \qquad (2)$$

Experimental measurements suggest that the biochemical enrichment factor (ε_b) value is 27 ± 3‰ for oxygen isotopes relative to source water (Epstein et al., 1977; DeNiro and Epstein, 1981; Wolfe et al., 2001; Sternberg, 1989, Farquhar et al., 1998; Daley, 2007; Daley et al., 2009, 2010). Several studies reported the preservation of this evaporative-enrichment signal in the cellulose of *Sphagnum* relative to peat pore waters (Brenninkmeijer et al., 1982; Aravena and Warner, 1992), whereas others reported that such evaporative effects are negligible (Daley, 2007; Taylor, 2008; Daley et al., 2009).

5.4 Study Area and Material Collection

5.4.1 Study area

Glen West is a raised bog located in the vicinity of the River Roogagh in County Fermanagh, Northern Ireland (Figure 5.1). It is located at approximately 90 m above sea level (a.s.l.) and forms part of an extensive stretch of peatland in northwest Ireland (Plunkett, 2006; Swindles et al., 2007a). Rainfall generally exceeds 1200 mm per annum. Mean January temperatures are ~4.3°C, and mean July temperatures are ~14.3°C (Swindles et al., 2007a, 2007b).

The northern part of the bog has a well-developed hummock, lawn and pool topography with abundant typical peatland vegetation, including *Sphagnum cuspidatum* in pools and *Sphagnum imbricatum on small isolated hummocks* (Swindles et al., 2007a, 2007b). Other plants include *Narthecium ossifragum*, *Molinia caerulea*, *Calluna vulgaris*, *Erica tetralix*, *Trichophorum cespitosum*, *Eriophorum vaginatum* and *Eriophorum angustifolium* (Swindles et al., 2007a, 2007b; Plunkett and Swindles, 2008).

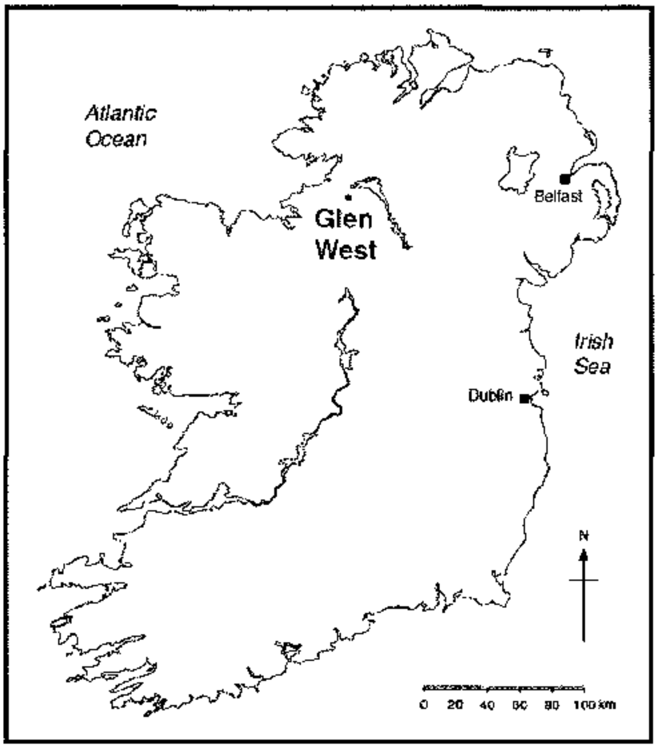

Figure 5.1: Map of Ireland, showing the location of Glen West Bog, County Fermanagh, after Swindles et al.(2007a).

5.4.2 Material collection

A 30 cm monolith (90-120 cm depth) was subsampled from core taken from Glen West Bog. The monolith was carefully covered in plastic foil, placed in labelled plastic half-shells (half-tubes), and stored at 4°C in a core storage facility at Carleton University. The investigated core material is mostly composed of *Sphagnum* peat with herbaceous remains and amorphous organic material (Swindles et al., 2007a, 2007b).

A vertical cut section (~ 8 cm x 30 cm x 3 cm) of the Glen West monolith was used for digital sediment surface photography and X-ray scanning. Another ~ 4 cm x 30 cm x 3 cm part of the remaining section was used for oxygen isotope analyses of *Sphagnum* cellulose. The core was sampled at 0.5 cm intervals in the laboratory using a stainless steel knife and a stainless steel spatula. Samples were labelled, placed in zip-lock bags, and stored at +4°C prior to subsequent microscopic and geochemical analyses.

5.5 Methodology

Oxygen isotope analysis of plant cellulose (*Sphagnum*), image analyses of digital sediment surface photographs and X-ray images, and statistical data analysis techniques were applied to a 30 cm peat section "monolith" in the Glen West area. The data were transformed from depth to time scale using a previously published age-depth model from this section (Swindles et al., 2007a, 2007b).

5.5.1 Glen West age-depth model

Time–depth curve for Glen West profile showing calibrated date ranges (at 2σ) obtained by tephrochronology (correlation AD860 and Hekla 4 tephras that were dated by Pilcher et al. (1995)), five high-precision ^{14}C wiggle-matched determinations on bulk peat samples (Plunkett et al., 2004) and two conventional ^{14}C determinations on bulk peat samples (Swindles et al., 2007a, 2007b). UB-4374 corresponds to the level of the BMR-190 tephra, UB 4375 corresponds to the level of the Microlite tephra, while the GB4-150 tephra is located 1 cm above UB-4376 (Table 5.1, Figure 5.2).

5.5.2 Plant macrofossil separation and identification

Peat samples were gently heated in a 5% KOH solution for about 30 min to dissolve humic and fulvic acids. Plant macrofossil samples were then disaggregated on a 125 μm sieve using deionized water. Isolated plant remains on the sieve were kept immersed to avoid too much damage and disintegration and subsequently transferred to a plastic container. Distilled water was added to suspend the plant macrofossil remains prior to examination using an Olympus SZH-1 stereo microscope. Macrofossils were identified using several illustrated moss identification guides (Smith, 2004; Mauquoy and van Geel, 2007). Once the optical macrofossil analysis was completed, each sample was stored in a sealed plastic container with deionized water and returned to the cool room.

5.5.3 Cellulose oxygen isotope analytical technique

Sixty samples were taken every 0.5 cm through the entire 30 cm length of the monolith. For $\delta^{18}O_{Cel}$ analyses, a 43-sample set was selected as follows: 26 samples from the

Table 5.1: Results of geochronological samples and correlation from Glen West

Laboratory reference	Depth cm	composition	14Cage BP	Calibrated age at 2σ range	Wiggle-match calibrated dates (+-range)	reference
AD860 Tephra	25-27*	humine/ humic acid	1191±21	AD 776-887		Pilcher et al., 1995
Beta-20092	49-51	Bulk peat	1950±60	91 cal BC-cal AD221		Swindles et al., 2006
UB-4374	97-98	*Sphagnum and Enophorum*	2493±25	790-520 cal BC	645(+-60) cal BC	Plunkett et al., 2004
UB-4375	103-104	*Sphagnum*	2399±25	760-390 cal BC	718(+-38) cal BC	Plunkett et al., 2004
UB-4376	110-111	*Sphagnum and Enophorum*	2572±26	820-600 cal BC	790(+-19) cal BC	Plunkett et al., 2004
UB-4377	116-117	*Sphagnum and Enophorum*	2691±26	905-810 cal BC	868(+-38) cal BC	Plunkett et al., 2004
UB-4378	122-123	*Sphagnum and Enophorum*	2794±26	1020-890 cal BC	940(+-55) cal BC	Plunkett et al., 2004
Beta-20092	148-150	Bulk peat	3220±60	1637-1387 cal BC		Swindles et al. 2006
Hekla 4 Tephra	340-341*	Tephra	3884±24	2395-2279 cal BC		Pilcher et al., 1995

*from Sluggan Bog, Ireland

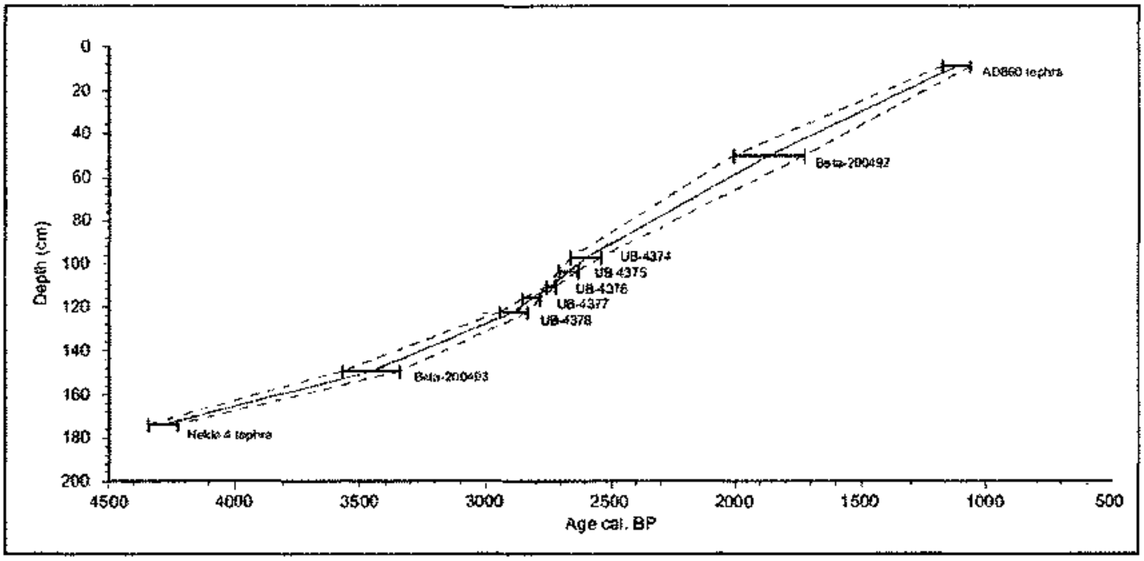

Figure 5.2: Age model of entire Glen West core (after Swindles et al., 2007a, 2007b). Note that the core segment studied (90-120 cm) has five wiggle-matched radiocarbon ages, and that the suggested age model is linear through this interval.

uppermost 13 cm (i.e., one sample every 0.5 cm) and 17 samples from the lowermost 17 cm (i.e., 1 sample every 1 cm). Higher resolution sampling of the upper 13 cm of the monolith was conducted to verify the high-frequency cyclicity detected in this depth interval by image analysis. Stem sections from *Sphagnum* remains were handpicked from petri-dishes, placed in porcelain crucibles and oven-dried at 50°C for 24 hours. Afterwards samples were powdered, weighed, labelled, and placed in small plastic vials.

Cellulose isotopic analyses were performed at the University of Saskatchewan isotope laboratories. Cellulose samples were baked at 60°C in a vacuum oven for 2 hours to drive off moisture, then immediately transferred and flushed in the zero blank autosampler. Samples were analyzed using a Thermo Finnigan TC/EA coupled to a Conflo III and a Delta Plus XL mass spectrometer. Samples were dropped under helium into a glassy carbon furnace and pyrolyzed at 1450°C to form hydrogen and/or carbon monoxide gases. The gases were carried in a helium stream to a GC column held at 100°C to separate the gases before being diluted in the Conflo III and passed to the mass spectrometer for analysis. Isotope ratios were blank-corrected and reported in per mil notation relative to the VSMOW-VSLAP scale.

In-house oxygen standards were calibrated against international standards USGS-34 ($\delta^{18}O$ = -27.9‰ VSMOW) and USGS-35 ($\delta^{18}O$ = 57.5‰ VSMOW). An intermediate international standard, IAEA-NO3, gave the result $\delta^{18}O = 25.53 \pm 0.27$‰ VSMOW (n = 23) during calibration of in-house standards compared to the accepted value of $\delta^{18}O$ = 25.6 ± 0.4‰ VSMOW. Two in-house standards were used to set up a calibration line, and a third was used to monitor accuracy of data. Accuracy of the $\delta^{18}O$ data is ±0.11‰ (n = 25). Measurements of %O have an accuracy of ±0.5%. Actual sample errors may be greater due to heterogeneity, and more accurate data may be obtained through repetition.

5.5.4 Image analyses

Image analysis of sediment surface photographs and X-ray scans has proven to be useful to detect high-resolution paleoclimate and paleodepositional fluctuations (e.g., Nederbragt and Thurow, 2001). The gray scale-value line extraction and calibration used in this study follows mostly the methodology outlined by Schaaf and Thurow (1995).

5.5.4.1 Digital core photography

In this study, digital core photography was carried out using a 6 Megapixel digital Sony camera equipped with a high-quality Zeiss lens. To provide equal lighting to the entire photographed core section, a total of four lamps, one at each corner, were placed on the four corners. The four lamps were fixed at about 15 cm high (vertically) and 10 cm away (horizontally) from each corner of the 30 cm monolith. This ensured a continuous illumination of the core. For scale a mm-resolution ruler that spanned the entire photographed segment was used.

Core photographs were saved as jpeg files. Each photograph was rotated so that the top (lowest depth) was always to the left. Furthermore, a gamma-balance of 1.79 was applied to all photographs to reduce the effect of reflections and to allow for easier detection of cracks and holes in the photographs. Gray scale-value line-scans were extracted from the gamma-balanced photographs using the publicly available software ImageJ (www.nih.gov). Twenty-pixel wide line-scan parallel to the depth scale was obtained from three undisturbed core segments separated by cracks in the monolith section. Afterwards, a complete line-scan for the entire core was compiled by connecting the line-scan data of all segments. The original gray scale-value line-scan contains ~2,330 pixels over the 30 cm depth providing an average data interval of 0.1 mm.

5.5.4.2 Digital X-ray scanning

Digital X-ray images were obtained with a medical image scanner that provided a 4 Megapixel resolution over an area of 30 x 30 cm. A scale was included on the side of the digital image. A single X-ray image was produced in jpeg-format, which encompassed the entire 30 cm Glen West monolith.

X-ray gray scale-value line-scan was also extracted from the balanced photograph using ImageJ. Twenty-pixel wide line-scan parallel to the depth scale was extracted from three undisturbed core segments and pieced together. The original gray scale-value line-scan contains ~2,000 pixels over 30 cm depth providing an average data interval of 0.167 mm. The gray scale-values can range from 0 (black) to 255 (white). The gray scale-value extraction of both photograph and X-ray line-scans are shown in Figure 5.3. Both image records potentially allow for detection of sub-annual signals (~2000 pixel/~400 year =~5 pixel/year).

5.5.5 Time series analyses

Time-series analysis can be used to evaluate trends, cycles, and relationships in and between geological records (e.g., Davis, 1986). Here wavelet analysis (WA) and spectral analysis (SA) were applied in particular to determine persistence, wavelengths (periodicities), and confidence intervals of cellulose oxygen isotopes, digital photographs and X-ray line-scans. Linear correlation was used to determine potential relationships between these data and previously published water table data from this section (Swindles et al., 2007a, 2007b), and with ^{14}C productivity variations (Reimer et al., 2009) from ~2880 and 2500 cal. yr. B.P. (90-120 cm depth). Spectral and wavelet analysis (Appenzeller, 1998; Bolton et. al., 1995; Morlet et al., 1982) were applied to line-scans and isotope data in both time-scale and depth-scale to reconstruct the paleotemperature record of the 2500-2880 cal. yr. B.P. time interval in the Glen West peat profile.

5.5.5.1 Spectral analysis

Spectral analysis (SA) was applied to geochemical and line-scan data after the data was transformed into the time-scale. Davis (1986) defined spectral analysis (Fourier transform) using the following equation:

$$P^2{}_f = \int x(t)e^{-i2\pi ft}dt \,, \qquad (3)$$

where $x(t)$ the discrete time series, f the frequency, and P^2 the spectral power. There are different ways to calculate the spectral power. In this study, the software REDFIT (Schulz and Mudelsee, 2002) was used. The software calculates the periodogram to

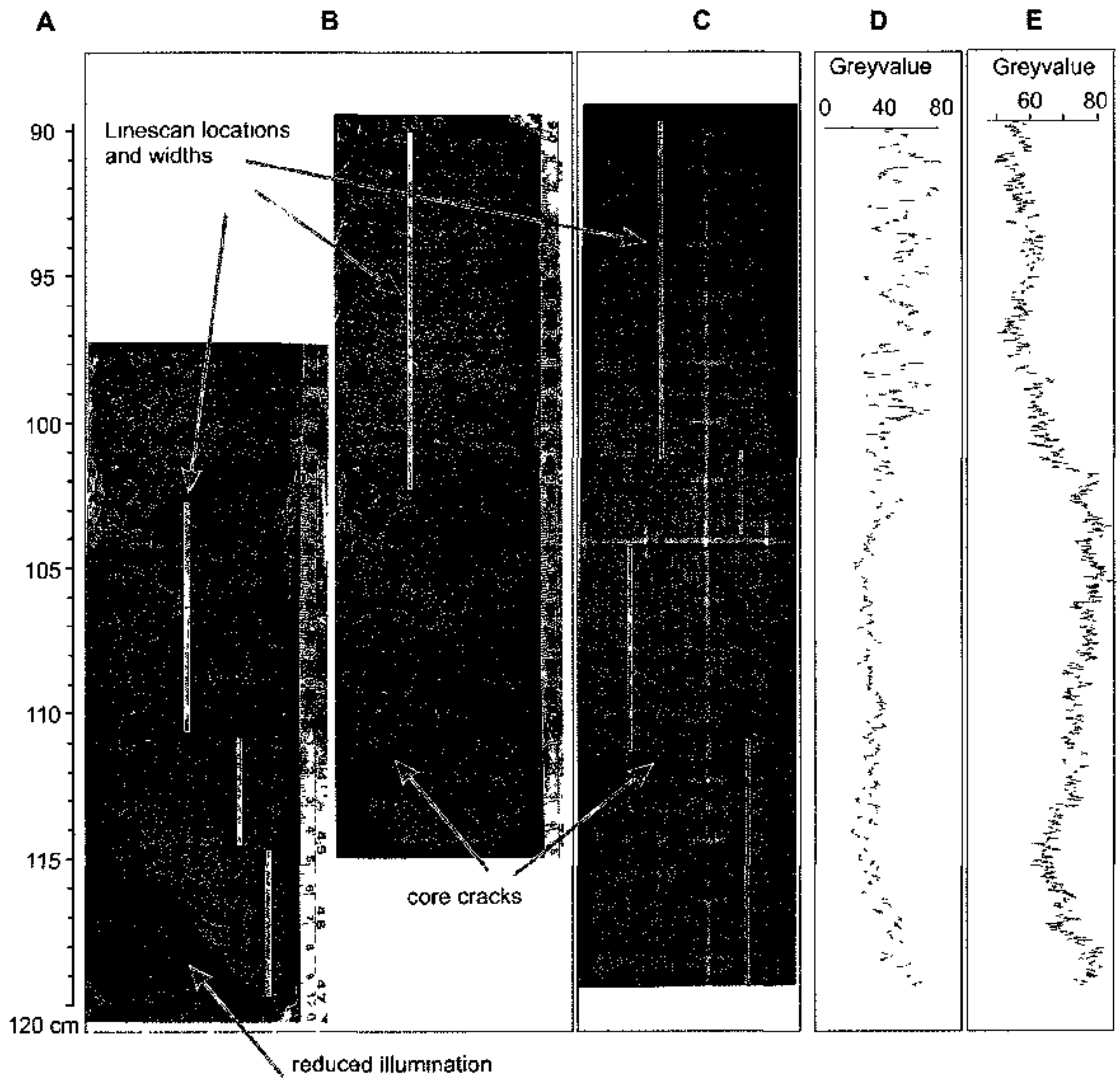

Figure 5.3: Digital image line-scan extraction.

A) Depth scale of the monolith;

B) overlapping digital color photographs of the monolith segment with location of cracks, illumination problems and line-scan segments perpendicular to bedding that have been stacked to compile a complete line-scan dataset;

C) digital X-ray image of ~ 3cm thick monolith segment;

D) compiled gray scale-value line-scan from color photograph;

E) compiled gray scale-value line-scan from X-ray scan.

express the spectral power, that is, the raw, squared Fourier coefficients, and confidence intervals for the spectral peaks. Confidence intervals were calculated using the combined white noise (average variance) and red noise (autocorrelation at lag 1) assumptions outlines by Mann and Lees (1996).

5.5.5.2. Wavelet analysis:

Wavelet analysis (WA) was used to detect trends, cycles and abrupt changes in the peat sedimentation pattern in time-domain. WA emerged as a filtering and data compression method in the 1980s (e.g., Morlet et al., 1982) and has since been widely used. Wavelet analysis transforms a time-series simultaneously from a 'depth' or 'time' domain into a scale (or frequency) domain by using various shapes and sizes of short filtering functions called 'wavelets'.

Continuous wavelet transform (WT) allows for the automatic localization of periodic-signals, gradual shifts, abrupt interruptions, and trends in time series (Rioul and Vetterli, 1991). In contrast to the so called Sliding-Window Fourier transform that uses shifting analysis windows of constant width (Rioul and Vetterli, 1991), WT uses narrow band analysis windows at high frequencies, and wide analysis windows at low frequencies. The wavelet coefficients W of a time series x(s) are calculated by a simple convolution

$$W_{\psi}(a,b)=\left(\frac{1}{\sqrt{a}}\right)\int x(s)\psi\left(\frac{s-b}{a}\right)ds \qquad (4)$$

where ψ is the mother wavelet; the variable a is the scale factor that determines the characteristic frequency or wavelength; and b represents the shift of the wavelet over $x(s)$ (Chao and Naito, 1995). The bandwidth resolution for a wavelet transform varies with $\Delta a = \Delta f = \frac{\sqrt{2}}{4\pi a l}$, and a location resolution $\Delta b = \frac{al}{\sqrt{2}}$. Note that due to Heisenberg's uncertainty principle $\Delta f \Delta b \geq 1/4\pi$, the resolution of Δb and Δf cannot be both small. Parameter l is used to modify wavelet transform bandwidth resolution either in favor of time (or depth) or in favor of frequency.

In this study, the WT was used with the Morlet wavelet as the mother function (Morlet et al., 1982). The Morlet wavelet is simply a sinusoid with wavelength/period a modulated by a Gaussian function, and has previously provided robust results in analyses of climate-related records (Torrence and Compo, 1998; Prokoph and Patterson, 2004b; Patterson et al., 2004; 2005; 2007). The influence of the edge effects is well defined for the Morlet wavelet, and increases with increasing wavelength (scale) and parameter l. Thus, the boundary of edge effects on the wavelet coefficients forms a wavelength dependent curve, called the 'cone of influence' (Torrence and Compo, 1998), which separates the location-frequency space with reliable wavelet coefficients from one with limited reliability. The wavelet coefficients W are normalized to represent the amplitude of Fourier frequencies by replacing $\sqrt{a}$ with a, which allows for a simplified reconstruction of frequency dependent signals. The parameter $l = N^*\Delta t = 6$ was chosen for all analyses, which gives sufficiently precise results in resolution of depth and frequency (Ware and Thomson, 2000). The shifted and scaled Morlet mother wavelet is defined as

$$\psi^{l}_{a,b}(s) = \pi^{-\frac{1}{4}}(al)^{-\frac{1}{2}} e^{-i2\pi\frac{1}{a}(s-b)} e^{-\frac{1}{2}(\frac{s-b}{al})^2} \tag{5}$$

The relative bandwidth error is constant in all scales and for $l = 6$ is ~1/6 = 0.16 = 16%. The wavelet analysis technique used in this article is explained in detail in Prokoph and Barthelmes (1996). In this study the edge effects were eliminated by dividing the wavelet coefficient of wavelength a extracted from equation (4) by a standing sine wave of amplitude 1 and wavelength a. The matrix of the wavelet coefficients $W_l(a,b)$, the so called "scalogram", was color-coded (Orange: high W, blue low W) for superior graphical interpretation. Details of the extraction methodology and its accuracy are explained in Prokoph and Patterson (2004a).

5.6 Results

5.6.1 Cycles and trends in depth and time scales

5.6.1.1 $\delta^{18}O_{cel}$ signature and oxygen content in plant cellulose

Oxygen concentrations and isotope compositions of plant cellulose from samples of the Glen West monolith cover the time interval ~2500 and 2880 cal. yr. B.P. (90 to 120 cm depth; Table 5.2). Figure 5.4 shows that $\delta^{18}O_{cel}$ values of *Sphagnum* vary from 15.2‰ at 95.25 cm depth (~2665 cal. yr. B.P.) to 31.33‰ at 90.75 cm depth (~2510 cal. yr. B.P.). These values fluctuate strongly in the 90-96 cm interval (~2500-2575 cal. yr. B.P.) at 20.41±4.41‰ (standard deviation) followed by relatively steady values around 20.4 ± 0.96‰ in the remaining section of the monolith (96-120 cm, 2575-2880 cal. yr. B.P.) (Figure 5.4A,C). Oxygen concentrations (O%) range from 26.88% at 90.75 cm (~2510 cal. yr. B.P.) to 45.05% at 111.75 cm depth (~2765 cal. yr. B.P.). The O% fluctuates strongly in the 90-96 cm at 37.05±4.38% and 105-120 cm depth intervals (~2500-2575 cal. yr. B.P. and 2690-2880 cal. yr. B.P.) at 37.05±4.38% and 42.67±1.84% respectively. The O% shows steady values around 41.83±0.83% in 96-105 cm interval (2575-2690 cal. yr. B.P.) (Figure 5.4A,B).

5.6.1.2 Wavelet analysis

i) Wavelet analysis of $\delta^{18}O_{cel}$ and O%

Important wavelengths in the O% and $\delta^{18}O_{cel}$ records were observed in the wavelet scalograms in Figures 5.4D and 5.4E, respectively. Both the $\delta^{18}O_{cel}$ and O% records between ~2500-2575 cal. B.P. record strong ~30-35 year and 80 year cycles (Figure 5.4B,C,D, and E). Progressing deeper, weaker 30 and 45 years cycles are observed in both $\delta^{18}O_{cel}$ and O% while a strong 150-200 year cycle is observed for O% (Figure 5.4D and E). The 150-200 year cycle is weak in the $\delta^{18}O_{cel}$ record compared to the O% record (Figure 5.4D and E).

ii) Gray-scale values of digital photographs

Wavelet time series analysis of the monolith peat sediment color (gray-scale values) data revealed a wide spectrum of stationary and non-stationary cycles in the 1 to 380 years band (Figure 5.5). A weak 200-300 year cycle occurs through the entire monolith, whereas a weak 100 year cycle is evident in the lower section of the core segment at 101-120 cm (~2640-2880 cal. B.P.). Furthermore, the peat sedimentary record between ~

~2500 and 2650 cal. B.P. shows a strong high-frequency ~11 year cycle with a less intense 30-40 year cycle (Figure 5). The ~11 year and 30-40 years cyclic patterns become very weak and disappear below 2650 cal. B.P. where they are replaced by ~200-300 year and 100 year cycles (Figure 5.5).

~30-40 year cycle (Figure 5). The ~11 year and 30-40 years cyclic patterns become very weak and disappear below 2650 cal. B.P. where they are replaced by ~200-300 year and 100 year cycles (Figure 5.5).

iii) Gray-scale values of X-ray images

Wavelet analysis of the X-ray image line-scan revealed a wide spectrum of persistent and intermittent cycles (Figure 5.5). A very strong low-frequency ~200-300 year cycle occurs throughout the monolith in the X-ray line-scan. The 200-300 year cycle overprints a weaker 100 year cycle. Furthermore, the X-ray gray-values between ~ 2500 and 2650 cal. B.P. show a strong ~11 year cyclicity with less intense cycles at ~30-40 years. These cycles are much weaker in the X-ray than in the photograph line-scans (see Figure 5.5).

The ~20 year and 50 year cyclic patterns are dominant between ~2500 cal. yr. B.P. and ~2700 cal. yr. B.P. and become very weak and disappear below 2710 cal. yr. B.P. The ~11 and ~20 year bands reappear at ~2820 cal. yr. B.P. and continue towards the bottom of the monolith.

Table 5.2: Oxygen isotopes and concentration of *sphagnum* cellulose

Depth (cm)	Age (cal. yr. BP)	%O	d18O (‰, VSMOW)
90.25	2503.15	34.08	16.74
90.75	2509.45	26.88	31.33
91.25	2515.75	35.07	18.07
91.75	2522.05	38.57	23.45
92.25	2528.35	34.15	16.37
92.75	2534.65	39.59	20.22
93.25	2540.95	34.90	16.56
93.75	2547.25	42.21	22.12
94.25	2553.55	42.19	20.54
94.75	2559.85	41.56	22.17
95.25	2566.15	32.99	15.20
95.75	2572.45	42.43	22.07
96.25	2578.75	39.81	20.68
96.75	2585.05	40.98	20.58
97.25	2591.35	41.20	21.73
97.75	2597.65	41.16	21.47
98.25	2603.95	41.27	21.86
98.75	2610.25	41.81	20.99
99.25	2616.55	42.34	21.26
99.75	2622.85	41.86	21.07
100.25	2629.15	42.06	19.35
100.75	2635.45	42.49	20.36
101.25	2641.75	42.49	20.54
101.75	2648.05	41.69	21.87
102.25	2654.35	42.36	20.41
102.75	2660.65	41.67	20.86
103.75	2673.25	42.76	20.00
104.75	2685.85	43.27	21.37
105.75	2698.45	38.51	19.02
106.75	2711.05	42.04	20.16
107.75	2723.65	44.95	20.52
108.75	2736.25	42.24	20.35
109.75	2748.85	45.03	18.49
110.75	2761.45	43.14	20.53
111.75	2774.05	45.05	19.87
112.75	2786.65	41.17	17.75
113.75	2799.25	42.09	20.46
114.75	2811.85	43.45	20.78
115.75	2824.45	43.50	19.57
116.75	2837.05	40.36	20.78
117.75	2849.65	41.25	18.81
118.75	2862.25	43.65	20.29
119.75	2874.85	43.57	20.62
92.25	2528.35	39.45*	22.46*

* repeat of non-*sphagnum* peat material

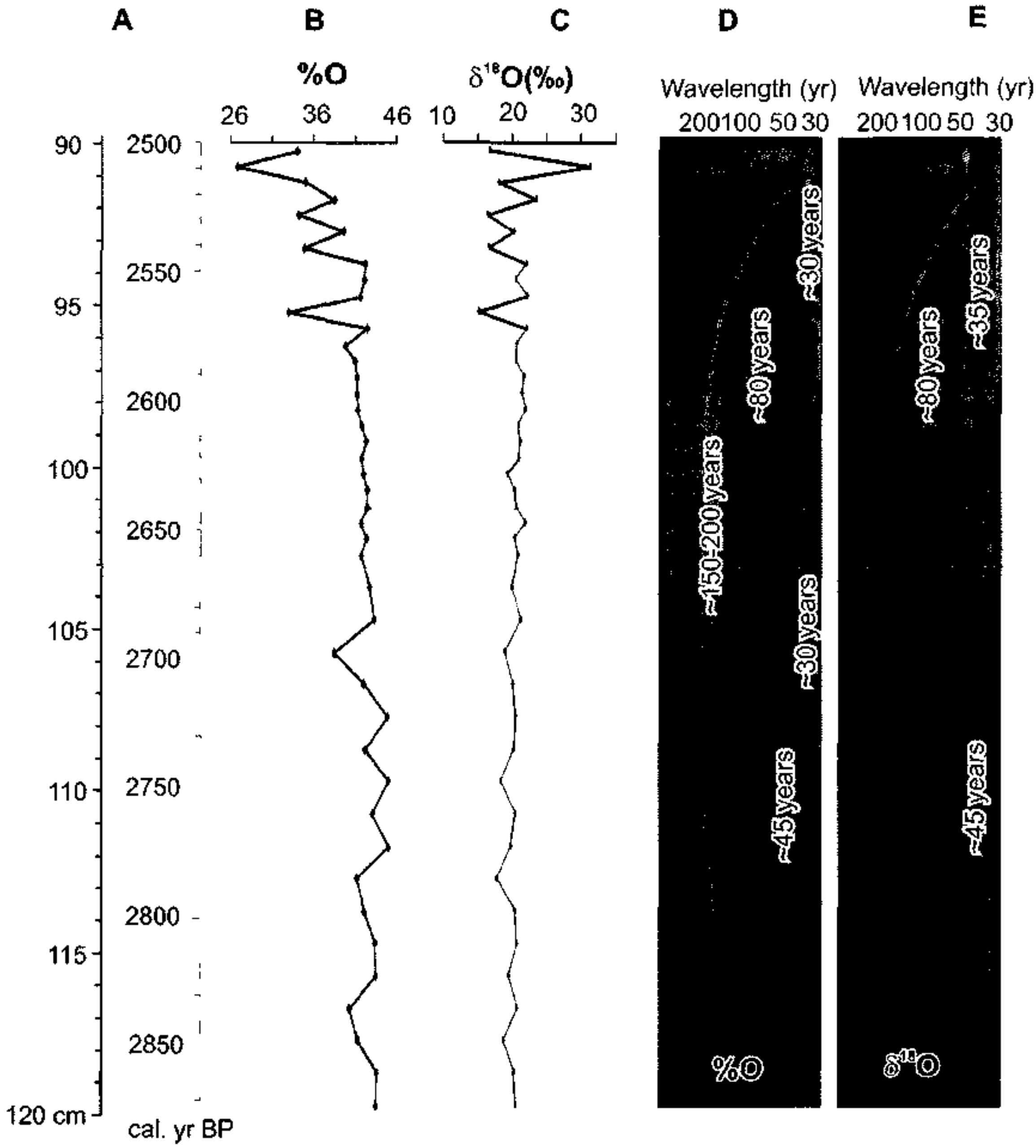

Figure 5.4: Oxygen isotope and concentration of *Sphagnum* cellulose in depth and time-scale, A) time and depth scale, B) oxygen concentration (in %), C) $\delta^{18}O_{cel}$ in ‰ SMOW, D) wavelet scalogram of oxygen concentration with cone of influence (stripped line) and marked important wavelengths. E) wavelet scalogram of $\delta^{18}O_{cel}$ with cone of influence (stripped line) and marked important wavelengths. For D and E) Yellow-red indicates high magnitude of signal and blue low or no signal in specific wavelength and specific time.

In summary, wavelet analysis carried out on digital X-ray and photos line-scans (gray-values), oxygen concentration and oxygen isotope composition of plant cellulose, revealed the presence of several strong and often persistent cycles: an ~11 year cycle, which is dominant in the digital photos; an ~30-35 year cycle dominant in the $\delta^{18}O_{cel}$ and O% data; an ~80 year cycle in the $\delta^{18}O_{cel}$ data; ~100 year and ~200-300 year cycles dominant in the X-ray images and to lesser extend in the O% and digital photos and not recorded in $\delta^{18}O_{cel}$ record (Figures 5.5 and 5.6).

5.6.1.3 Spectral analysis

Spectral analysis was carried out on the digital photo, X-ray line-scans, ^{14}C production rate (Reimer et al., 2009), $\delta^{18}O_{cel}$ and O% data to identify climate cycles archived in the peat sediment of the Glen West monolith. Spectral analysis confirms the occurrence of statistically significant cycles in the decadal and centennial range (Figure 5.7). The 200-300 year cycle occurs at the >90% confidence interval in the digital photographs and X-ray line-scans, and O% data (Figure 5.7A,C, and D). The 100 year cycle occurs with >90% confidence in the O% data and <90% confidence in the digital photographs and X-ray line-scans. A 30-35 years cycle occurs with >90% confidence in $\delta^{18}O_{cel}$. A 20-28 years cycle occurs with >90% confidence in $\delta^{18}O_{cel}$ and O% (Figure 5.7B,C). Periodicities in the 11 year waveband with >95% confidence are found in the digital photograph line-scan record (Figure 5.7C).

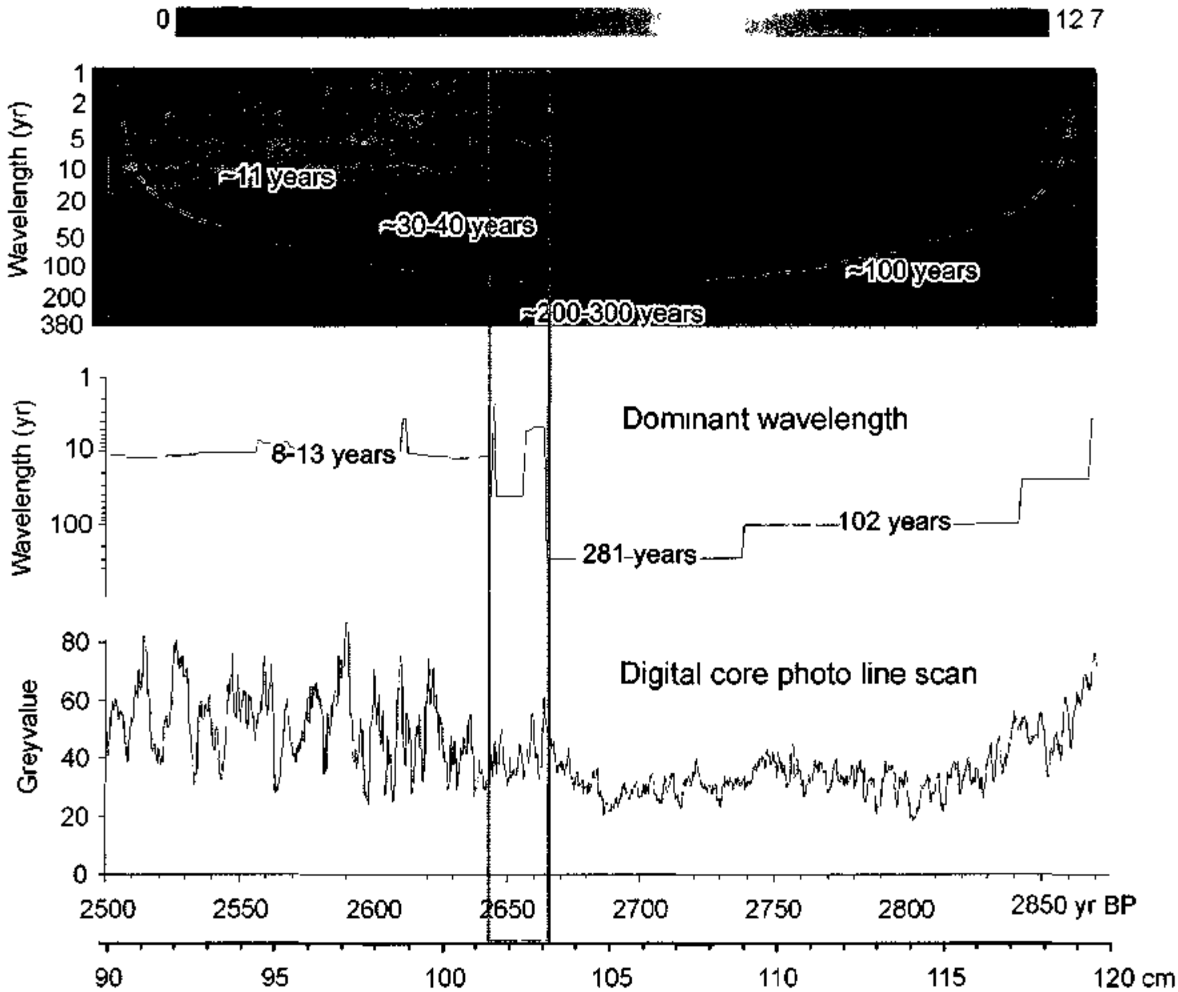

Figure 5.5: Wavelet analysis of image line-scan from digital core surface photography from the monolith segment:

Top: wavelet scalogram of line-scan of photograph with cone of influence (stripped line), and marked important wavelengths; for color scale interpretation see figure 5.4

Middle: temporal changes of wavelength with strongest signals in line-scan of photograph,

Bottom: line-scan of photograph with time and depth scale.

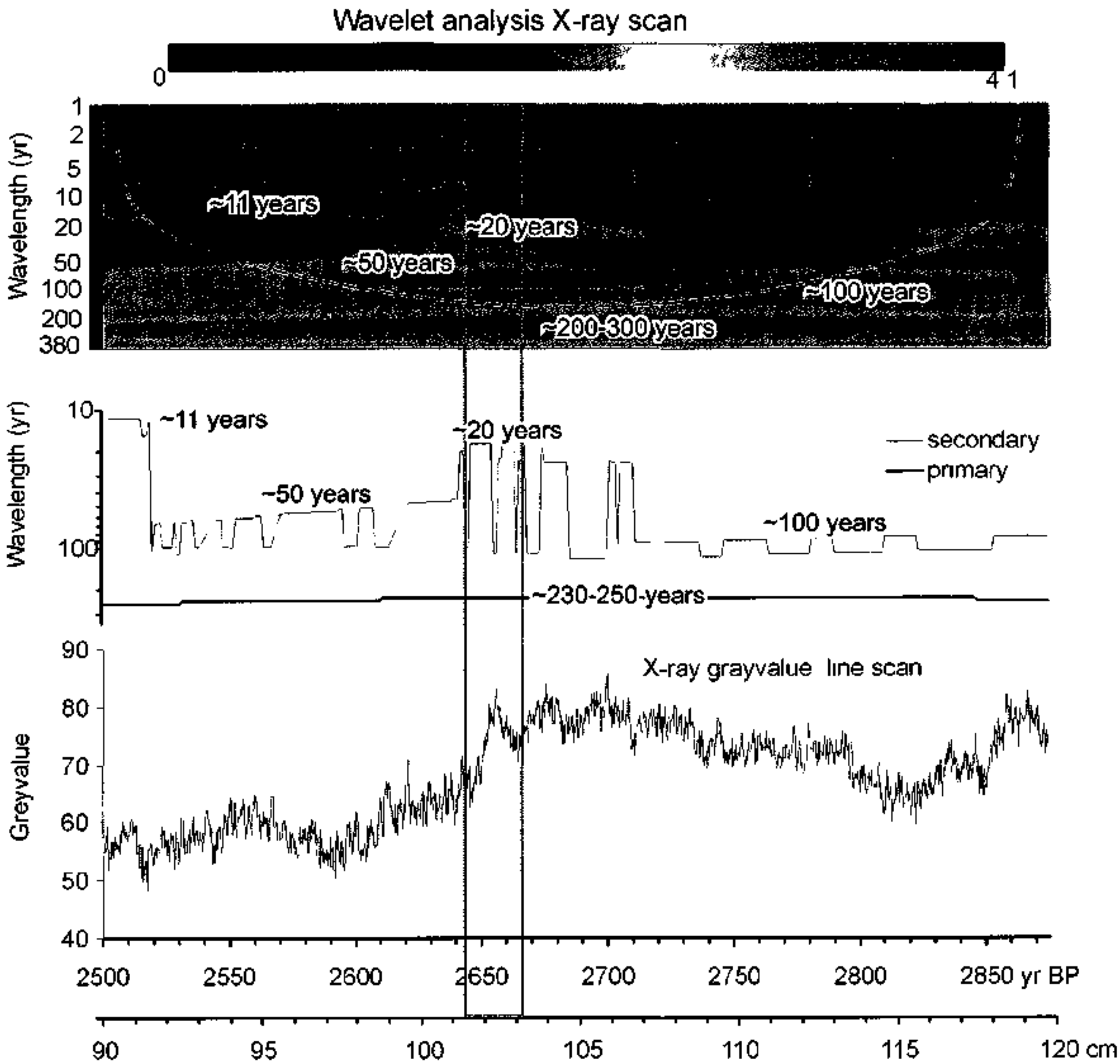

Figure 5.6: Wavelet analysis of X-ray image line-scan from the monolith segment:
Top: Wavelet scalogram of line-scan of X-ray image with cone of influence (stripped line) and marked important wavelengths; for color scale interpretation see figure 5.4,
Middle: Temporal changes of wavelength with strongest (primary) and second strongest (secondary) signals in line-scan of X-ray image,
Bottom: Line-scan of X-ray image with time and depth scale.

5.7 Discussion

This study demonstrates the applicability of geochemical, image analysis, and time-series analysis in Northern Ireland peat sections as proxies for Mid-Holocene paleoclimate changes in maritime climates

5.7.1 Image analysis

Time-series analysis of line-scans from X-ray images and digital photographs of the peat core surface revealed significant periodic signals as well as abrupt transitions (see Figures 5.5-5.7). These signals have been recognized at a resolution of <1 mm or <1 year and cannot be detected at such a resolution using geochemical, paleontological, or sedimentary analytical methods due to sample size requirements. The signal to noise ratio of the major signals (cycle amplitude compared to background variability- see Figure 5.7A,C), determined herein, is similar to that found in laminated marine sediments (e.g., Schaaf and Thurow, 1995; Prokoph and Patterson, 2004a). The highest-frequency cycle detected with both imaging methods is a ~10-12 year cycle that can be related to the ~11-year "Schwabe" sunspot cycle (Friis-Christiansen and Lassen, 1991). Digital core photography records a stronger signal than X-ray imaging for the Schwabe cycle. In contrast, a longer ~200-300 year cycle that may represent a "Suess" sunspot cycle is more pronounced in the X-ray image than in the digital core photography (Figures 5.5, 5.6).

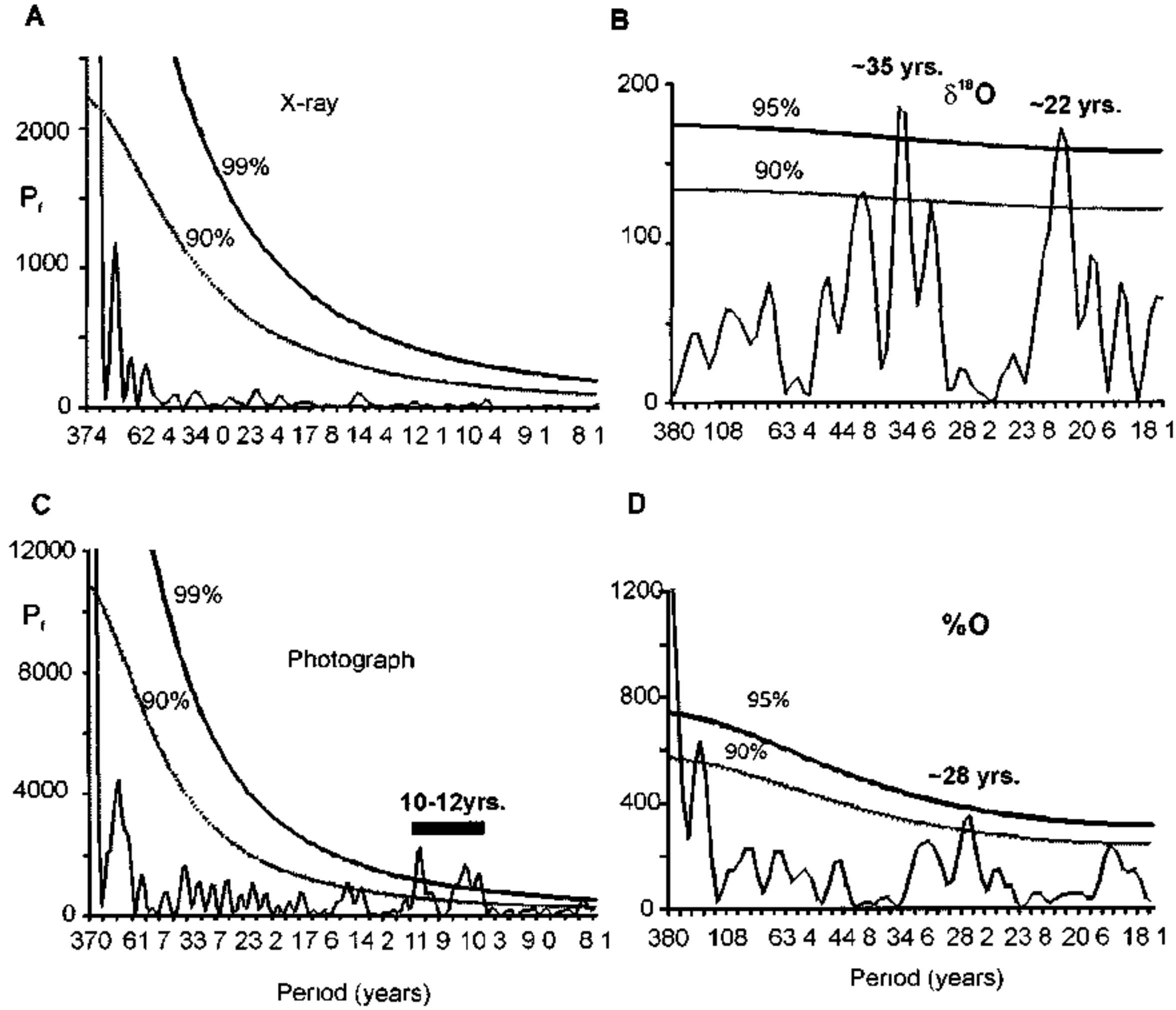

Figure 5.7: Periodograms of spectral analysis of line-scans and oxygen data from the monolith segment with confidence intervals. A: X-ray image line-scan, B: $\delta^{18}O_{cel}$ record, C: Digital photo line-scan, D: %O record.

The absence of an annual, varve-like cyclicity in both digital photographs and X-ray images is due to the relatively high heterogeneity and coarseness of the partially decomposed plant material compared to marine varves and relatively weak winter-summer seasonality in Northern Ireland. The mean annual temperature difference between winter and summer is only 10 degrees in Northern Ireland (Swindles et al., 2007a), which is about 1/3 of that in more continental mid-latitude settings such as central Canada (Environment Canada, 2010). The high-frequency Schwabe cycle is better preserved in the core surface photographs compared to the X-ray. This is probably due to the fact that the X-ray machine measures not only the value of individual pixels on the core surface but averages this pixel value across the diameter of the core. Thus, depending on heterogeneity of the sediment, X-ray images may average longer time-intervals than the pixel resolution indicates. Moreover X-ray analysis predominantly measures the density of the sediment whereas the core-surface photograph can reflect surface humidity, redox coloration, sediment texture and potentially mineralogy (e.g., Schaaf and Thurow, 1995).

5.7.2 $\delta^{18}O$ variation in Sphagnum cellulose

The variability of $\delta^{18}O_{cel}$ values changes from <1‰/cm at the bottom of the core (~2850 cal B.P.) to >10‰/cm on the top (~2500 cal B.P.), but such a change in $\delta^{18}O_{cel}$ variability is not reflected in the other proxy records (Figure 5.8). In the continental climate of eastern Canada an ~2‰ increase in $\delta^{18}O$ cellulose corresponds to an average 1°C temperature increase (e.g., El Bilali and Patterson, 2009; and chapter III of this study). For the Glen West section, a 2‰/1°C ratio would provide unrealistic mean air temperature variations of up to 5°C over less than 10 years. This confirms previous studies showing that in more continental climate areas with a much larger annual temperature gradient, such as eastern Canada, the sensitivity of *Sphagnum* growth in ombrotrophic bogs to temperature is much larger than observed in northwest Europe (Taylor, 2008; Daley et. al., 2009, 2010).

Qualitatively, the Mid-Holocene long-term variability of $\delta^{18}O_{cel}$ of *Sphagnum* in Northern Ireland correlates partially with ^{14}C production rate and paleoclimate proxies (Figure 5.8). For example, the correspondence of the low $\delta^{18}O$ values with high ^{14}C production rate before 2650 cal. B.P. in the Glen West monolith can be interpreted as the result of a relatively cool period due to diminished solar activity. While low $\delta^{18}O_{cel}$ record shows some correlation with high ^{14}C production rate after 2650 cal. B.P. (Figure 5.8), it is difficult to decipher the 11-year solar cycle. The absence of the 11-year cycle in the $\delta^{18}O_{cel}$ record could be related to the fact that the sampling resolution of 0.5 cm = ~6 years was not sufficient to capture this cycle and/or that $\delta^{18}O_{cel}$ is more controlled by other climate forcing such as the North Atlantic Oscillation as indicated in Figure 5.4.

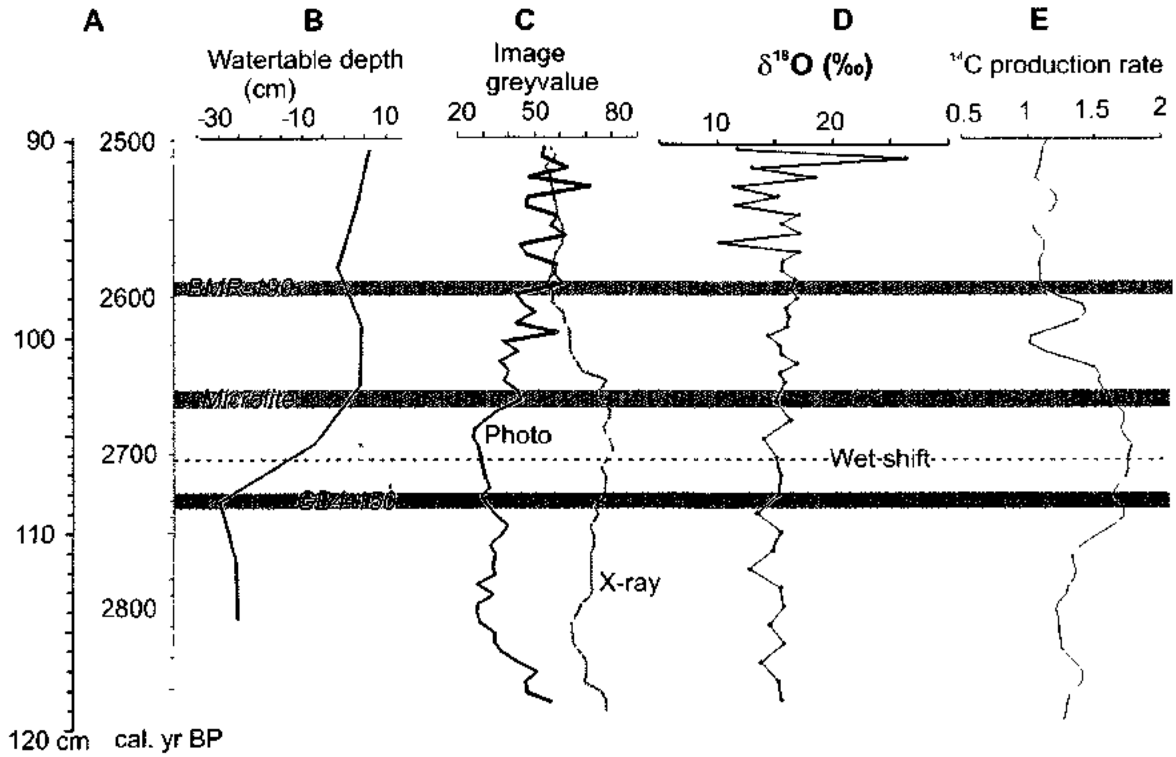

Figure 5.8: Comparison in time and depth scale (A) of B: water table depth and volcanic eruptions (Swindles at al., 2007a); C: 5-yr average image gray scale-value line-scans, D: oxygen isotope data, and E: ^{14}C production rate (atoms/cm^2/sec) record (Reimer et al., 2009). Gray interval marks high ^{14}C production for comparison. BMR-190, Microlite, and GB4-150 are tephras (Swindles et al., 2007a and b).

5.7.3 Solar, volcanic and atmospheric-oceanic forcing on Mid-Holocene paleoclimate in Northern Ireland

Wavelet analysis reveals a major change in the pattern of cyclicity in the records at ~2650 cal. yr. B.P. This is most clearly represented by the first appearance of the 11-year cycle (see Figure 5.5). The time at ~2650 cal. yr. B.P. has been recognized in fossil records and water table depth in this monolith (Swindles et al., 2007a, 2007b; Plunkett and Swindles, 2008) as a regime shift to wet climate in Northern Ireland (Swindles et al., 2007a, 2007b; Plunkett and Swindles, 2008) and throughout the British Isles (Charman, 2010). Furthermore, comparison of the image (digital photos and X-ray) gray-values and geochemical analysis shows good correlation with the water table and ^{14}C production rate records (see Figure 5.8 and Swindles et al., 2007a, 2007b; Plunkett and Swindles, 2008).

Relatively weak 20-100 year cycles are evident from wavelet and spectral analysis during the "cool" period from ~2800-2650 cal. yr. B.P., which may be driven by atmospheric-oceanic oscillation patterns and not solar activity, such as the ~30-40 year cyclicity in the North Atlantic Oscillation modes (Appenzeller et al., 1998).

The image records, in particular the X-ray image line-scan record, correlate well with ^{14}C production rate from ~2850 to 2650 cal. yr. B.P. (Figure 5.8). This correlation is also evident by the occurrence in the ~200-300 year cycle in both digital photograph and X-ray image records (Figures 5.5-5.7). In addition, generally high X-ray image gray-values, due to denser plant material and less peat porosity, correlated very well with the cold period, and lower values with the following warm period after 2650 cal. yr. B.P.

identified by Bond et al. (2001) based on ice rafted debris (Figure 5.8). In summary there are several independent indications that solar variability as reflected in atmospheric ^{14}C (Figure 5.6) exhibited an important influence on Mid-Holocene climate variability in Northern Ireland, and likely in the North Atlantic Region.

In contrast, the image and isotope analyses don't show any indication that the three volcanic eruptions (BMR-190, Microlite, GB4-150) identified in the section (Swindles et al., 2007a) had any significant impact on climate or peat sedimentation pattern (see Figure 5.8). The wet-shift (i.e. transition from dry to wet climate) that has been detected in the water table reconstruction at ~2705 cal. yr. B.P. (Swindles et al., 2007a, 2007b) is not pronounced in image and isotope records. This is likely due to the fact that water table fluctuations are more sensitive to precipitation-evaporation balance while $\delta^{18}O_{cel}$ are more sensitive to temperature variation.

5.8 Conclusions

Digital peat core surface photography and X-ray imaging have been shown to be very useful in detecting high-frequency fluctuations in peat sedimentation. Solar activity fluctuations at the ~11-year and ~250-year cycle-band appear to have a major influence on regional and global climate as is recorded in the peat coloration, X-ray density and isotope data from Glen West core, Northern Ireland. In particular the results suggest:

1. An ~11-year cycle corresponding to the Schwabe solar cycle occurs only during low ^{14}C production from 2650-2500 cal. yr. B.P. indicating that this cycle has the most impact on the peat records during periods of overall high solar activity. To our knowledge, this represents the best record of the Schwabe cycle in materials older than 500 years.

2. A period of high ^{14}C production rate from ~2760-2650 cal. yr. B.P. correlates well with high X-ray gray-scale values indicating denser peat sedimentation, as well as darker peat surface coloration. This suggests a shift from dry to wet climate in Northern Ireland.

3. While some cycles such as of 80 and 200-300 year wavelength are likely solar driven, others are likely related to atmospheric-oceanic regimes in the North Atlantic such as North Atlantic Oscillation (NAO). Some of these cycles (i.e. 20-40 years) correlate particularly well with the variability in X-ray gray-values and sediment color from ~2650-2500 cal. yr. B.P.

5.9 References

Anderson, W.T., Bernasconi, S.M., McKenzie, J.A., Saurer, M., and Schweingruber, F., 2002. Model evaluation for reconstructing the oxygen isotopic composition in precipitation from tree ring cellulose over the last century. *Chemical Geology*, 182: 121–137.

Appenzeller C., Stocker, T.F., and Anklin, M., 1998. North Atlantic oscillation dynamics recorded in Greenland ice cores. *Science*, 282: 446-449.

Aravena, R., and Warner, B.G., 1992. Oxygen-18 composition of Sphagnum, and microenvironmental water relations: *The Bryologist*, 95: 445–448.

Aucour, A.-M., Hillaire-Marcel, C., and Bonnefille, R., 1996. Oxygen isotopes in cellulose from modern and Quaternary intertropical peatbogs: implications for palaeohydrology. *Chemical Geology*, 129: 341-359.

Blaauw, M., van Geel, B., and van der Plicht, J., 2004. Solar forcing of climatic change during the mid-Holocene: indications from raised bogs in The Netherlands. *The Holocene*, 14: 1-35.

Bolton, E.W., Maasch, K.A., and Lilly, J.M., 1995. A wavelet analysis of Plio-Pleistocene climate indicators: A new view of periodicity evolution. *Geophys. Res. Let.*, 22: 2753-2756.

Bond, G., Showers, W., Cheseby, M., Lotti, R., Almasi, P., deMenocal, P., Priore, P., Cullen, H., Hajdas, I., and Bonani, G., 1997. A Pervasive Millennial-Scale Cycle in North Atlantic Holocene and Glacial Climates. *Science*, 278: 1257–1266.

Bond, G., Kromer, B., Beer, J., Muscheler, R., Evans, M.N., Showers, W., Hoffmann, S., Lotti-Bond, R., Hajdas, I., and Bonani, G., 2001. Persistent Solar Influence on North Atlantic Climate During the Holocene. *Science*, 294: 2130-2136.

Booth, R.K., and Jackson, S.T., 2003. A high-resolution record of late-Holocene moisture variability from a Michigan raised bog. *The Holocene*, 13: 865–78.

Booth, R.K., Notaro, M., Jackson, S.T., and Kutzbach, J.E., 2006. Widespread drought episodes in the western Great Lakes during the past 2000 years: geographic extent and potential mechanisms. *Earth and Planetary Science Letters*, 242: 415-427.

Brenninkmeijer, C.A.M., van Geel, B., and Mook, W.G., 1982. Variations in the D/H and $^{18}O/^{16}O$ ratios in cellulose extracted from a peat bog core. *Earth and Planetary Science Letters*, 61: 283-290.

Carslaw, K.S., Harrison, R.G., and Kirkby, J., 2002. Cosmic rays, clouds, and climate. *Science*, 298: 1732-1737.

Chao, B.F., and Naito, I., 1995. Wavelet analysis provides a new tool for studying Earth's rotation. *EOS*, 76: 161, 164-165.

Charman, D.J., Hendon, D., and Packman, S., 1999. Multiproxy surface wetness records from replicate cores on an ombrotrophic mire: implications for Holocene palaeoclimate records. *Journal of Quaternary Science*, 14: 451–463.

Charman, D.J., Barber, K.E., Blaauw, M., Langdon, P.G., Mauquoy, D., Daley, T.J., Hughes, P.D.M., and Karofeld, E., 2009. Climate drivers for peatland palaeoclimate records. *Quaternary Science Reviews*, 28: 1811–1819.

Charman, D.J., 2010. Centennial climate variability in the British Isles during the mid–late Holocene. *Quaternary Science Review*, 29: 1539-1554.

Chiverrell, R.C., 2001: A proxy record of late Holocene climate change from May Moss, northeast England. *Journal of Quaternary Science*, 16: 9-29.

Clymo, R.S., and Hayward, P.M., 1982. The ecology of *Sphagnum*. In: Smith, A.J.E. (Ed.), Bryophyte Ecology. Chapman Hall, London, pp. 229–291.

Crooks, S.A., and Gray, L.J. 2005. Characterisation of the 11-year solar signal using a multiple regression analysis of the ERA-40 dataset, *Journal of Climate*, 18: 996-1015.

Daley, T.J., 2007. Tracking Holocene climate change using peat bog stable isotopes. Ph.D. thesis, University of Southampton, UK, 358 p.

Daley, T.J., Street-Perrott, F.A., Loader, N.J., Barber, K.E., Hughes, P.D.M., Fisher, E.H., and Marshall, J.D., 2009. Terrestrial climate signal of the '8200 yr B.P. cold event' in the Labrador Sea region. *Geology*, 37: 831–834.

Daley, T.J., Barber K.E., Street-Perrott, F.A., Loader, N.J., Marshall, J.D., Crowley, S.F., and Fisher, E.H., 2010. Holocene climate variability revealed by oxygen isotope analysis of *Sphagnum* cellulose from Walton Moss, northern England. *Quaternary Science Reviews*, 29: 1590-1601.

Dansgaard, W., 1964. Stable isotopes in precipitation. *Tellus*, 16: 436–468.

Davis, J.C., 1986. Statistics and data analysis in Geology. Wiley: New York; 646 p.

De Jong, R., Bjorck, S., Bjorkman, L., and Clemmensen, L.B., 2006. Storminess variation during the last 6500 years as reconstructed from an ombrotrophic peat bog in Halland, southwest Sweden. *Journal of Quaternary Science*, 21: 905–919.

DeNiro, M.J., and Epstein, S., 1981. Isotopic composition of cellulose from aquatic organisms. *Geochimica et Cosmochimica Acta*, 45: 1885–1894.

Edwards, T.W.D., Aravena, R.O., Fritz, P., and Morgan, A.V., 1985. Interpreting paleoclimate from 18O and 2H in plant cellulose: comparison with evidence from fossil insects and relict permafrost in southwestern Ontario. *Canadian Journal of Earth Sciences*, 22: 1720–1726.

El Bilali, H., and Patterson R.T., 2009. Holocene Paleoclimate Reconstruction in Eastern Canada: Evidence from $\delta^{18}O$ of plant cellulose from the Mer Bleue Bog, Ottawa, Ontario. American Geophysical Union, Fall Meeting 2009, abstract # PP21D-07I.

Environment Canada, 2010. National Climate Data and Information Archive. www.climate.weatheroffice.gc.ca

Epstein, S., Yapp, C.J., and Hall, J.H., 1976. Determination of the D/H Ratios of Nonexchangeable Hydrogen in Cellulose Extracted from Aquatic and Land Plants. *Earth Planet Sci. Lett.,* 30: 241–251.

Epstein, S., Thompson, P., and Yapp, C.J., 1977. Oxygen and Hydrogen Isotopic Ratios in Plant Cellulose. *Science*, 198: 1209 – 1215.

Esper, J., Cook, E.R., and Schweingruber, F.H., 2002. Low-frequency signals in long tree-ring chronologies for reconstructing past temperature variability. *Science*, 295: 2250-2253.

Farquhar, G.D., Barbour, M.M., and Henry, B.K., 1998. Interpretation of oxygen isotope composition of leaf material. In: Griffiths, H. (Ed.), Stable Isotopes: integration of biological, ecological, and geochemical processes. Environmental Plant Biology. BIOS Scientific Publishers Ltd, Oxford, UK, pp. 27-60.

Francey, R.J., and Farquhar, G.D., 1982. An explanation for the 13C/12C variations in tree rings. *Nature*, 297: 28–31.

Fricke, H.C., and O'Neil, J.R., 1999. The correlation between 18O/16O ratios of meteoric water and surface temperature: its use in investigating terrestrial climate change over geologic time. *Earth and Planetary Science Letters*, 170: 181–196.

Friis-Christensen, E., and Lassen, K., 1991. Length of the solar cycle: An indicator of solar activity closely associated with climate. *Science*, 254: 698-700.

Garcia, A., and Mouradian, Z., 1998. The Gleissberg Cycle of minima. *Sol. Physics*, 180: 495-498.

Gleissberg, W., 1958. The eighty-year sunspot cycle. *Journal of the British Astronomical Association*, 68: 1148-1152.

Gleisner, H. , Thejll, P., Stendel, M., Kaas, E., and Machenhauer, B., 2005. Solar signals in tropospheric re-analysis data: Comparing NCEP/NCAR and ERA40. *Journal of Atmospheric and Solar-Terrestrial Physics*, 67: 785-791.

Gray, L.J., Beer, J., Geller, M., Haigh, J.D., Lockwood, M., Matthes, K., Cubasch, U., Fleitmann, D., Harrison, G., Hood, L., Luerbacher, J., Meehl., G.A., Shindell, D., van geel, B., and White, W., 2010. Solar Influence on Climate. Review in Geophysics. 110 p.

Haigh, J.D., 1994. The role of stratospheric ozone in modulating the solar radiative forcing of climate. *Nature*, 370: 544-546.

Hameed, S., and Lee, J.N., 2005. A mechanism for sun-climate connection. *Geophysical Research Letters*, 32: L23817, 3 pp.

Hall, I.R., Bianchi, G.G., and Evans, J.R., 2004. Centennial to millennial scale Holocene climate deep water linkage in the North Atlantic. *Quaternary Science Reviews*, 23: 1529-36.

Holmes, J.A., 1998. A tephra-dated study of vegetation and climate change in the mid-Holocene of north-west Europe. Ph.D. thesis, Queen's University, Belfast.

Hu, F.S., Kauffman, D., Yoneji, S., Nelson, D., Shemesh, A., Huang, Y.,Tian, J., Bond, G., Clegg, B., and Brown, T., 2003. Cyclic variation and solar forcing of Holocene climate in the Alaskan subarctic. *Science*, 301: 1890-1893.

Jones, P.D., Osborn, T.J., and Briffa, K.R., 2001. The evolution of climate over the last millennium. *Science*, 292: 662-666.

Kilian, M.R., van der Plicht, J., and van Geel, B., 1995. Dating raised bogs: new aspects of AMS 14C wiggle matching, a reservoir effect and climatic change. *Quaternary Science Reviews*, 14: 959-66.

Libby, L.M., Pandolfi, L.J., Payton, P.H., Marshall, J., Becker, B., and Giertz-Sienbenlist, V., 1976. Isotopic tree thermometers. *Nature*, 261: 284–288.

Magny, M., 2004. Holocene climate variability as reflected by mid-European lakelevel fluctuations and its probable impact on prehistoric human settlements. *Quaternary International*, 113: 65–79.

Mann, M.S., and Lees, J.M., 1996. Robust estimation of background noise and signal detection in climatic time series. *Climatic Change*, 33: 409-445.

Mauquoy, D., and van Geel, B., 2007. Plant Macrofossil Methods and Studies/Mire and Peat Macros. Elsevier, 2315-2336.

McCracken, K.G., Dreschhoff, G.A.M., Smart, D.F., and Shea, M.A., 2001. The Gleissberg periodicity in large fluence solar proton events. *Proceedings of 27th International Cosmic Ray Conference Hamburg, Germany*, 3205-3208.

Ménot-Combes, G., Burns, S.J., and Leuenberger, M., 2002. Variations of 18O/16O in plants from temperate peat bogs (Switzerland): implications for paleoclimatic studies. *Earth and Planetary Science Letters*, 202: 419–434.

Morlet, J., Arehs, G., Fourgeau, I., and Giard, D., 1982. Wave propagation and sampling theory. *Geophysics*, 47: 203-212.

Nederbragt, A.J., and Thurow, J., 2001. A 6,000 years varve record of Holocene sediments in Saanich Inlet, British Columbia, from digital sediments colour analysis of ODP Leg 169S cores. *Marine Geology*, 174: 95-110.

O'Leary, M.H., Treichel, I., and Rooney, M., 1986. Short-term measurement of carbon isotope fractionation in plants. *Plant Physiology*, 80: 578–582.

Patterson, R.T., Prokoph, A., and Chang, A., 2004. Late Holocene sedimentary response to solar and cosmic ray activity influenced climate variability in the NE Pacific. *Sedimentary Geology*, 172: 67-84.

Patterson, R.T., Prokoph, A., Kumar, A., Chang, A.S., and Roe, H.M., 2005. Holocene variability in pelagic fish and phytoplankton productivity along the west coast of Vancouver Island, NE Pacific Ocean. *Marine Micropaleontology*, 55: 183-204

Patterson, R.T., Prokoph, A., Reinhardt, A., and Roe, H.M., 2007, Climate cyclicity in late Holocene anoxic marine sediments from the Seymour-Belize Inlet Complex, British Columbia: *Marine Geology*, 242: 123-140.

Pendall, E., Markgraf, V., Huber, U., White, J.W.C., Dreier, M., and Kenny, R., 2001. A multiproxy record of Pleistocene-Holocene climate and vegetation. changes from a peat bog in Tierra del Fuego. *Quaternary Research*, 55: 168-78.

Pilcher, J.R., Hall, V.A., and McCormac, F.G., 1995. Dates of Holocene Icelandic volcanic eruptions from tephra layers in Irish peats. *The Holocene*, 5: 103-110.

Plunkett, G.M., 1999. Environmental change in the Late Bronze Age in Ireland (1200–600 cal. BC). Unpublished Ph.D. Thesis, Queen's University Belfast.

Plunkett, G.M., 2006. Tephra-linked peat humification records from Irish ombrotrophic bogs questions nature of solar forcing at 850 cal. yr BC. *Journal of Quaternary Science*, 21: 9–16.

Plunkett, G.M., and Swindles, G.T., 2008. Determining the Sun's influence on Late Glacial and Holocene climates: a focus on climate response to centennial-scale solar forcing at 2800 cal. BP. *Quaternary Science Reviews*, 27: 175–84.

Plunkett, G.M., Pilcher, J.R., McCormac, F.G., and Hall, V.A., 2004. New dates for first millennium BC tephra isochrones in Ireland. *The Holocene*, 14: 780–786.

Prokoph, A., and Barthelmes, F., 1996. Detection of nonstationarities in geological time series: Wavelet transform of chaotic and cyclic sequences. *Computers & Geoscience*, 22: 1097-1108.

Prokoph, A., and Patterson, R.T. 2004a. From depth-scale to time-scale: transforming of sediment image color data into high-resolution time-series. In: Francus, P. (Ed.) Image Analysis, Sediments and Paleoenvironments. *Developments in Paleoenvironmental Research Series* 7, chapter 8, Springer, Dordrecht, pp. 143-164.

Prokoph, A., and Patterson, R.T., 2004b. Application of wavelet and regression analysis in assessing temporal and geographic climate variability; Eastern Ontario, Canada as a case study. *Atmosphere-Ocean*, 42: 201-212.

Reimer, P.J., Baillie, M.G.L., Bard, E., Bayliss, A., Beck, J.W., Blackwell, P.G., Bronk Ramsey, C., Buck, C.E., Burr, G.S., Edwards, R.L., Friedrich, M., Grootes, P.M., Guilderson, T.P., Hajdas, I., Heaton, T.J., Hogg, A.G., Hughen, K.A., Kaiser, K.F., Kromer, B., McCormac, F.G., Mannin,g S.W., Reimer, R.W., Richards, D.A., Southon, J.R., Talamo, S., Turney, C.S.M, van der Plicht, J., and Weyhenmeyer, C.E., 2009.

IntCal09 and Marine09 radiocarbon age calibration curves, 0–50,000 years cal BP. *Radiocarbon*, 51(4): 1111–50.

Reimer, P.J., Baillie, M.G.L., Bard, E., Bayliss, A., Beck, J.W., Bertrand, C.J.H., Blackwell, P.G., Buck, C.E., Burr, G.S., Cutler, K.B., Damon, P.E., Edwards, R.L., Fairbanks, R.G., Friedrich, M., Guilderson, T.P., Hogg, A.G., Hughen, K.A., Kromer, B., McCormac, G., Manning, S., Bronk Ramsey, C., Reimer, R.W., Remmele, S., Southon, J.R., Stuiver, M., Talamo, S., Taylor, F.W., van der Plicht, J., and Weyhenmeyer, C.E., 2004. IntCal04 terrestrial radiocarbon age calibration, 0–26 cal kyr BP. *Radiocarbon*, 46: 1029–1058.

Rioul, O., and Vetterli, M., 1991. Wavelets and Signal Processing. *IEEE Special Magazine*, 14-38.

Roden, J.S., Lin, G.G., and Ehleringer, J.R., 2000. A mechanistic model for interpretation of hydrogen and oxygen isotope ratios in tree-ring cellulose. *Geochimica and Cosmochimica Acta*, 64: 21–35.

Rozanski, K., Araguas-Araguas, L., and Gonfiantini, R., 1993. Isotopic patterns in modern global precipitation. *Climate Change in Continental Isotopic Records*, 78: 1–36.

Schaaf, M., and Thurow, J., 1995. Late Pleistocene-Holocene climatic cycles recorded in Santa Barbara Basin Sediments: Interpretation of color density logs from Site 893. in: Kennett, J.P., Baldauf, J.G., and Lyle, M. (Eds.), Proceedings of the Ocean Drilling Program, Scientific Results, 146 (2): 31-44.

Schulz, M., and Mudelsee, M., 2002. REDFIT: estimating red-noise spectra directly from unevenly spaced paleoclimatic time series. *Computers & Geosciences*, 28: 421–426.

Shindell, D.T., Schmidt, G.A., Mann, M.E., Rind, D., and Waple, A., 2001. Solar Forcing of Regional climate Change during the Maunder Minimum. *Science*, 294: 2149-2152.

Smith, A.J.E., 2004. The moss flora of Britain and Ireland, Second edition. Cambridge University Press, Cambridge.

Sonett, C.P., and Finney, S.A., 1990. The Spectrum of Radiocarbon. *Philos. Trans. R. Soc. London, Ser.,* A330: 413–425.

Speranza, A., van Geel, B., and van der Plicht, J., 2002. Evidence for solar forcing of climate change at ca. 850 cal. BC from a Czech peat sequence. *Global and Planetary Change*, 35: 51-65.

Sternberg, L., Da, S.L., DeNiro, M.J., and Savidge, R.A., 1986. Oxygen isotope exchange between metabolites and water during biochemical reactions leading to cellulose synthesis. *Plant Physiology*, 82: 423–427.

Suess, H.E., 1980. The radiocarbon record in tree rings of the last 8000 years. *Radiocarbon*, 22; 200–209.

Sukumar, R., Ramesh, R., Pant, R.K., and Rajagopalan, G., 1993. A $\delta^{13}C$ record of late Quaternary climate change from tropical peat in southern India. *Nature*, 364: 703-706.

Svensmark, H., and Friis-Christensen, E., 1997. Variation of cosmic ray flux and global cloud coverage - a missing link in solar-climate relationships. *Journal of Atmospheric and Solar-Terrestrial Physics*, 59: 1225-1232.

Svensmark, H., 1998. Influence of cosmic rays on Earth's climate. *Phys. Rev. Lett.,* 81: 5027-5030.

Svensmark, H., Pedersen, J.O.P., Marsh, N.D., Enghoff, M.B., and Uggerhøj, U.I., 2006. Experimental evidence for the role of ions in particle nucleation under atmospheric conditions: Proceedings of the Royal Society A, doi:10.1098/rspa.2006.1773

Swindles, G.T., and Plunkett, G., 2010. Testing the palaeoclimatic significance of the Northern Irish bog oak record. *The Holocene*, 20: 155–159.

Swindles, G.T., Plunkett, G., and Roe, H.M., 2007a. A multi-proxy climate record from a raised bog in County Fermanagh, Northern Ireland: a critical examination of the link between bog surface wetness and solar variability. *Journal of Quaternary Science*, 22: 667–79.

Swindles, G.T., Plunkett, G., and Roe, H.M., 2007b. A delayed climatic response to solar forcing at 2800 cal. BP: multi-proxy evidence from three Irish peatlands. *The Holocene*, 17: 177–82.

Taylor, M.A., 2008. Continental-scale validation of the temperature signal in oxygen isotopes of *Sphagnum* cellulose and its application as paleoclimate proxy. M.Sc. thesis, University of Wyoming, USA, 86 p.

Torrence, C, and Compo, G.P., 1998. A Practical Guide to Wavelet Analysis. *Bull. Amer. Meteor. Soc.*, 79: 61-78.

Usoskin, I.G., and Kovaltsov, G.A., 2004. Long-Term Solar Activity: Direct and Indirect Study. *Solar Phys.*, 224: 37–47.

van Geel, B., Buurman, J., and Waterbolk, H.T., 1996. Archeological and paleoecological indications for an abrupt climate change in The Netherlands and evidence for climatological teleconnections around 2650 BP. *Journal of Quaternary Science*, 11: 45-60.

Van Geel, B., van der Plicht, J., Kilian, M.R., Klaver, E.R., Kouwenberg, J.H.M., Renssen, H., Reynaud-Farrera, I., and Waterbolk, H.T., 1998: The sharp rise of $\Delta^{14}C$ c. 800 cal BC: possible causes, related climatic teleconnections and the impact on human environments. *Radiocarbon*, 40: 535 50.

Vitt, D.H., Crum, H., and Snider, A.J., 1975. The vertical zonation of *Sphagnum* species in hummock-hollow complexes in northern Michigan. *Michigan Botany*, 14: 190–200.

Van Loon, I., and Labitzke, K., 2000. The Influence of the 11-year Solar Cycle on the Stratosphere Below 30□km: a Review. *Space Science Reviews*, 94: 259-278

Ware, D.M., and Thomson, R.E., 2000. Interannual to multidecadal timescale climate variations in the Northeast Pacific. *J. Climate*, 13: 3209-3220.

Weng, H., 2005. The influence of the 11 yr solar cycle on the interannual–centennial climate variability. *Journal of Atmospheric and Solar-Terrestrial Physics*, 67: 793-805.

White, J.W.C., Ciais, P., Figge, R.A., Kenny, R., and Markgraf, V., 1994. A high resolution record of atmospheric CO_2 content from carbon isotopes in peat. *Nature*, 367: 153–156.

Wolfe, B.B., Edwards, T.W.D., Beuning, K.R.M., and Elgood, R.J., 2001. Carbon and oxygen isotope analysis of lake sediment cellulose: methods and applications. In: Last, W.M., and Smol, J.P. (Eds.), Tracking Environmental Change Using Lake Sediments. Physical and Geochemical Methods, 2. Kluwer Academic Publishers, Dordrecht, The Netherlands, pp. 373–400.

Yapp, C.J., and Epstein, S., 1982. A reexamination of cellulose carbon bound hydrogen dD measurements and some factors affecting plant-water D/H relationships. *Geochimica et Cosmochimica Acta*, 46: 955–965.

Zanazzi, A., and Mora, G., 2005. Paleoclimatic Implications of the Relationship Between Oxygen Isotope Ratios of Moss Cellulose and Source Water in Wetlands of Lake Superior. *Chem. Geol.,* 26: 281–291.

Zhentao, X., 1990. Solar Observations in Ancient China and Solar Variability. Philos. *Trans. R. Soc. London, Ser.* A330: 513–516.

CHAPTER SIX

6. GENERAL CONCLUSION

Data from core drilled to 6m depth in Mer Bleue Bog, Ottawa, has provided a paleoclimate record of the last ~9200 years of the Holocene in the region and revealed the major drivers of its fluctuations. Although, there might be some limitations due to the analytical and sampling methods used, this study represents a good foundation for future research and future climate projections. The research contributions are summarized below.

6.1 Bulk peat versus separated peat plant components

This study demonstrates that paleoclimate reconstructions based on $\delta^{18}O_{cel}$ derived from bulk peat material without consideration of the observed differences between the isotopic composition of *Sphagnum* and the other plant macrofossils could lead to erroneous conclusions. As such, $\delta^{18}O_{cel}$ based paleoclimate studies must take into account that significant stable oxygen isotopic offsets occur between cellulose from *Sphagnum* and rhizomes. In addition, the lack of statistically significant differences between $\delta^{18}O_{cel}$ of the different *Sphagnum* species analyzed implies that segregation of different *Sphagnum* species prior to isotope analyses is not necessary. As a result, the practice of selecting only *Sphagnum* for $\delta^{18}O_{cel}$ based temperature reconstructions is recommended.

6.2 *Sphagnum* cellulose-based paleotemperature and drivers for paleoclimate fluctuations

We demonstrate that the $\delta^{18}O$ of *Sphagnum* cellulose can provide a reliable paleotemperature proxy in continental settings (Mer Bleue Bog, Ottawa). In contrast in maritime settings (Glen West Bog, Northern Ireland) $\delta^{18}O$ of *Sphagnum* cellulose does not reflect ambient air temperature well. We conclude that this different response is due to the fact that $\delta^{18}O$ of precipitation water in continental setting responds to ambient air temperature, whereas in maritime settings such as Northern Ireland, the $\delta^{18}O$ of precipitation water is also impacted by the complex pathways of cloud formation and transport over the open ocean (Figure 6.1). The $\delta^{18}O_{cel}$ record obtained from the Mer Bleue Bog core correlates well with the northern Hemisphere paleotemperature reconstructions (e.g., Moberg, 2005; Frank et al., 2007) as well as reconstructed solar activity records (e.g., Bard et al., 2000; 2003; Solanki et al., 2004).

There is however no indication for a significant warming trend in Eastern Canada since 1850 A.D. as indicated in paleoclimate reconstructions (e.g., Jansen et al., 2007). A good correlation between the Mer Bleue Bog $\delta^{18}O_{cel}$ data, the records based on ice-rafted sediment from the Atlantic Ocean (Bond et al., 2001) and European records (e.g., Bond et al., 1997) indicate that Eastern Canada experienced a similar ~1300 year climate cycle as recognized in those areas. Moreover, the $\delta^{18}O_{cel}$ record at Mer Bleue Bog shows an excursion that correlates well with pronounced cooling during the ~1810-1820 A.D. interval that is likely triggered by the Dalton solar minima and amplified by the Mount

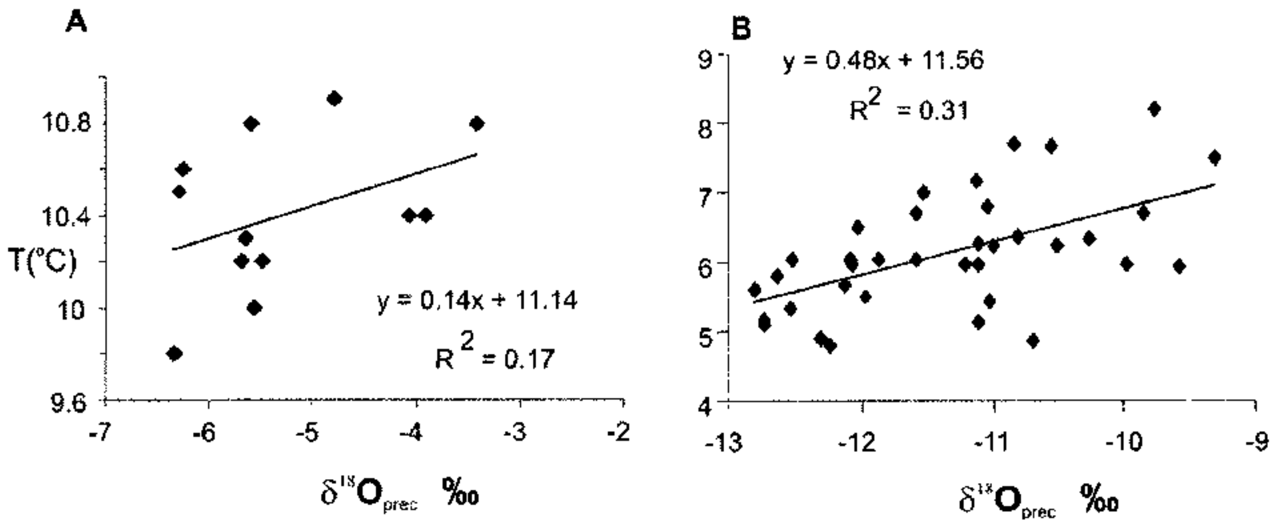

Figure 6.1: Cross-plots of $\delta^{18}O$ of precipitation with annual averages of air temperature from 1970-2007 A.D. at (A) Valentia Weather Station in Ireland and (B) at the Ottawa Airport Weather Station in Ottawa (GNIP: Global Network of Isotopes in Precipitation, 2001; Environment Canada, 2010).

Tambora, Indonesia eruption of 1815 (e.g., Rampino et al., 1988; Usoskin and Kovaltsov, 2004).

6.3 Image and time series analyses

Digital surface photography and X-ray imaging of peat core have been shown, for the first time, to be very useful methodologies for detecting cyclic changes in peat sedimentation. Cycles and trends found by core imaging correlate well with published records of geochemical variability and solar activity. Solar cycles with ~80 year to ~2500 year periodicities detected by wavelet and spectral analysis appear to have a major influence on regional and global climate as recorded in peat color and X-ray density, and isotope data from Mer Bleue core, Ottawa. In particular the results suggest that 180-250 years "Suess" and ~1300 years "Bond" cycles controlled long-term variability in temperature and peat sedimentation in Eastern Canada.

Digital peat core surface photography and X-ray imaging of the Glen West monolith in Northern Ireland, have also proven to be very useful tools to detect cyclic changes in a less decomposed type of peat sedimentation. Solar activity fluctuations at the ~11 year and ~250 year cycle-band appear to have a major influence on regional and global climate as recorded in the peat coloration and X-ray density, and isotope data from Glen West core. Additional ~20 year, ~30-40 year, and ~80-100 year cycles form significant portions of the peat color and X-ray as well as $\delta^{18}O_{cel}$ data variability.

6.4 References

Bard, E., Raisbeck, G., Yiou, F., and Jouzel, J., 2000. Solar Irradiance during the last 1200 years based on cosmogenic nuclides. *Tellus*, 52B: 985-992.

Bard, E., Raisbeck, G., Yiou, F., and Jouzel, J., 2003. Reconstructed Solar Irradiance Data. IGBP PAGES/World Data Center for Paleoclimatology Data Contribution Series #2003-006. NOAA/NGDC Paleoclimatology Program, Boulder CO, USA.

Bond, G., Kromer, B., Beer, J., Muscheler, R., Evans, M.N., Showers, W., Hoffmann, S., Lotti-Bond, R., Hajdas, I., and Bonani, G., 2001. Persistent Solar Influence on North Atlantic Climate During the Holocene. *Science*, 294: 2130-2136.

Bond, G., Showers, W., Cheseby, M., Lotti, R., Almasi, P., deMenocal, P., Priore, P., Cullen, H., Hajdas, I., and Bonani, G., 1997. A Pervasive Millennial-Scale Cycle in North Atlantic Holocene and Glacial Climates. *Science*, 278: 1257–1266.

Environment Canada, 2010. National Climate Data and Information Archive. www.climate.weatheroffice.gc.ca

Frank, D., Esper, J.D., and Cook, E.R., 2007. Adjustment for proxy number and coherence in a large-scale temperature reconstruction. *Geophysical Research Letters*, 34: L16709, doi:10.1029/2007GL030571.

GNIP/ISOHIS, 2001. http://isohis.iaea.org/. International Atomic Energy Agency.

Jansen, E., Overpeck, J., Briffa, K.R., Duplessy, J.-C., Joos, F., Masson-Delmotte, V., Olago, D., Otto-Bliesner, B., Peltier, W.R., Rahmstorf, S., Ramesh, R., Raynaud, D., Rind, D., Solomina, O., Villalba, R., and Zhang, D. 2007. Palaeoclimate. In: Climate Change 2007: The Physical Science Basis. In: Contribution of Working Group I to the Fourth Assessment Report of the Intergovernmental Panel on Climate Change, In:

Solomon, S., Qin, D, Manning, M, Chen, Z, Marquis, M, Averyt, K.B, Tignor M., and Miller, H.L. (Eds.). Cambridge University Press, Cambridge, United Kingdom and New York, NY, USA.

Moberg, A., Sonechkin, D.M., Holmgren, K., Datsenko, N.M., and Karle´n, W., 2005. Highly variable Northern Hemisphere temperatures reconstructed from low- and high-resolution proxy data. *Nature*, 433: 613– 617.

Rampino, M.R., Self, S., and Stothers, R.B., 1988. Volcanic Winters. *Annual Review of Earth and Planetary Sciences*, 16: 73-99.

Solanki, S.K., Usoskin, I.G., Kromer, B. Schüssler , M., and Beer. J., 2004. An unusually active Sun during recent decades compared to the previous 11,000 years. *Nature*, 431: 1084-1087.

Usoskin, I.G., and Kovaltsov, G.A., 2004. Long-Term Solar Activity: Direct and Indirect Study. *Solar Phys*., 224: 37–47.

Appendices

Appendix A: X-Ray images - Mer Bleue Core -Image 1

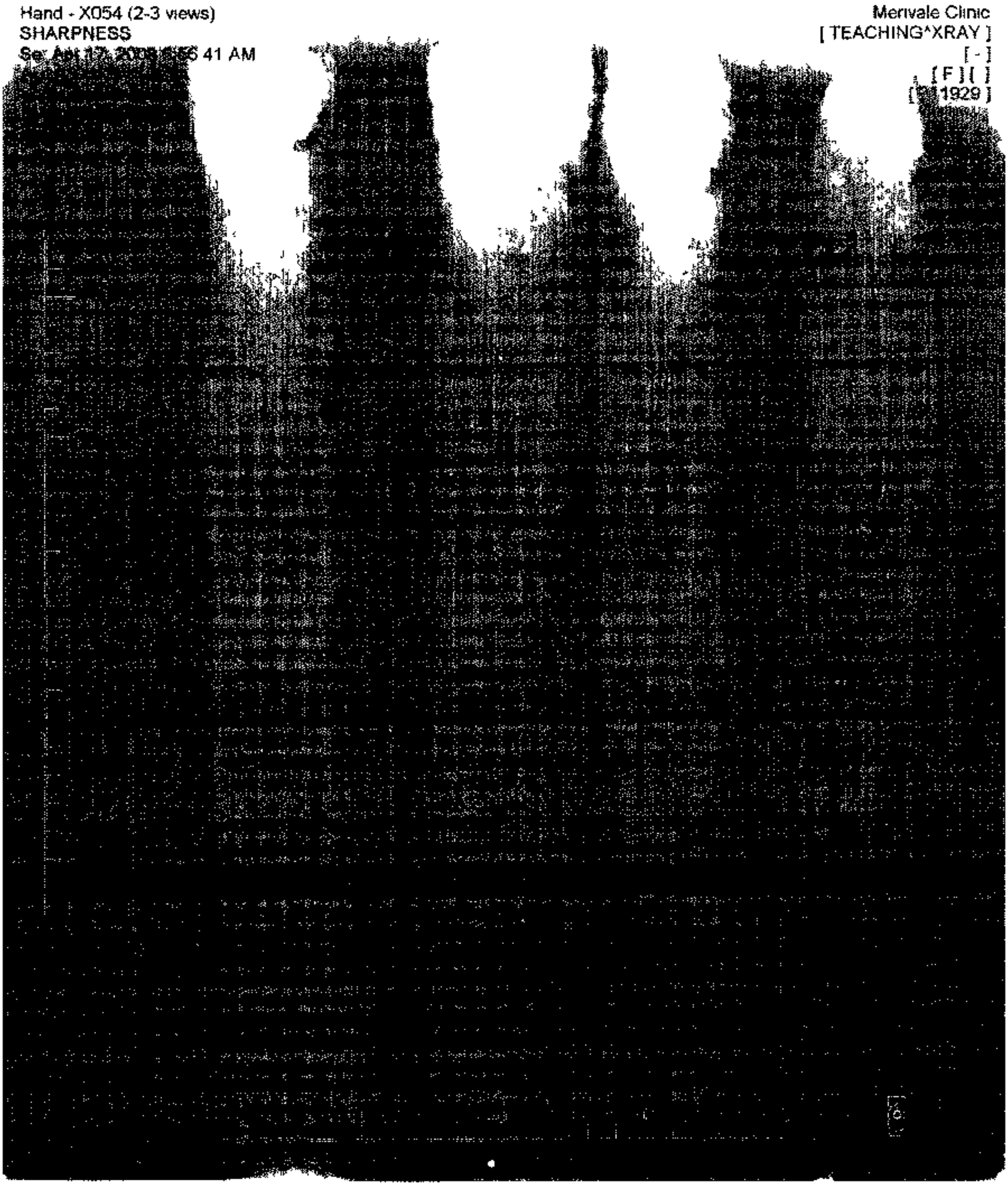

Appendix A: X-Ray images - Mer Bleue Core -Image 2

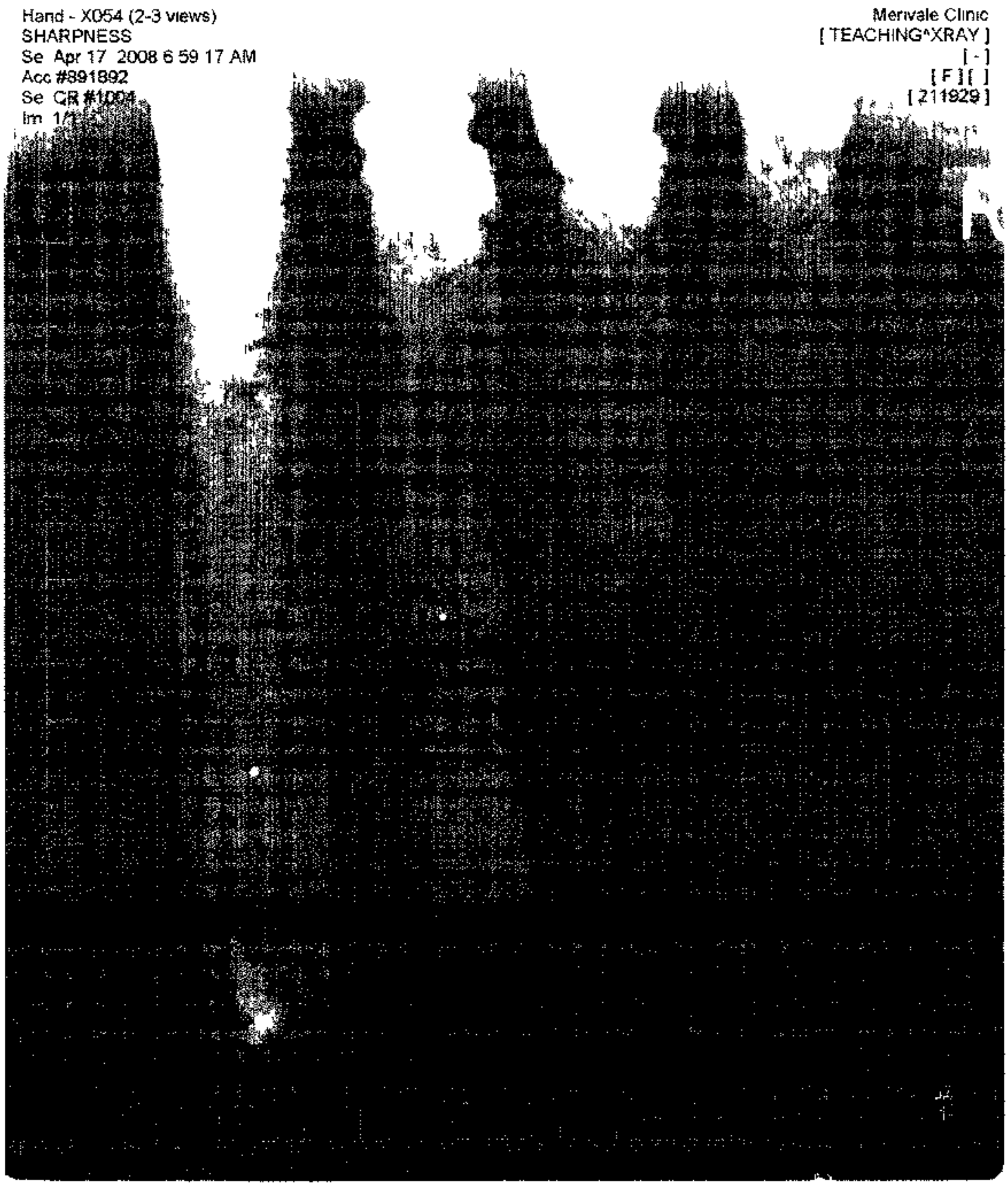

Appendix A: X-Ray images - Mer Bleue Core -Image 3

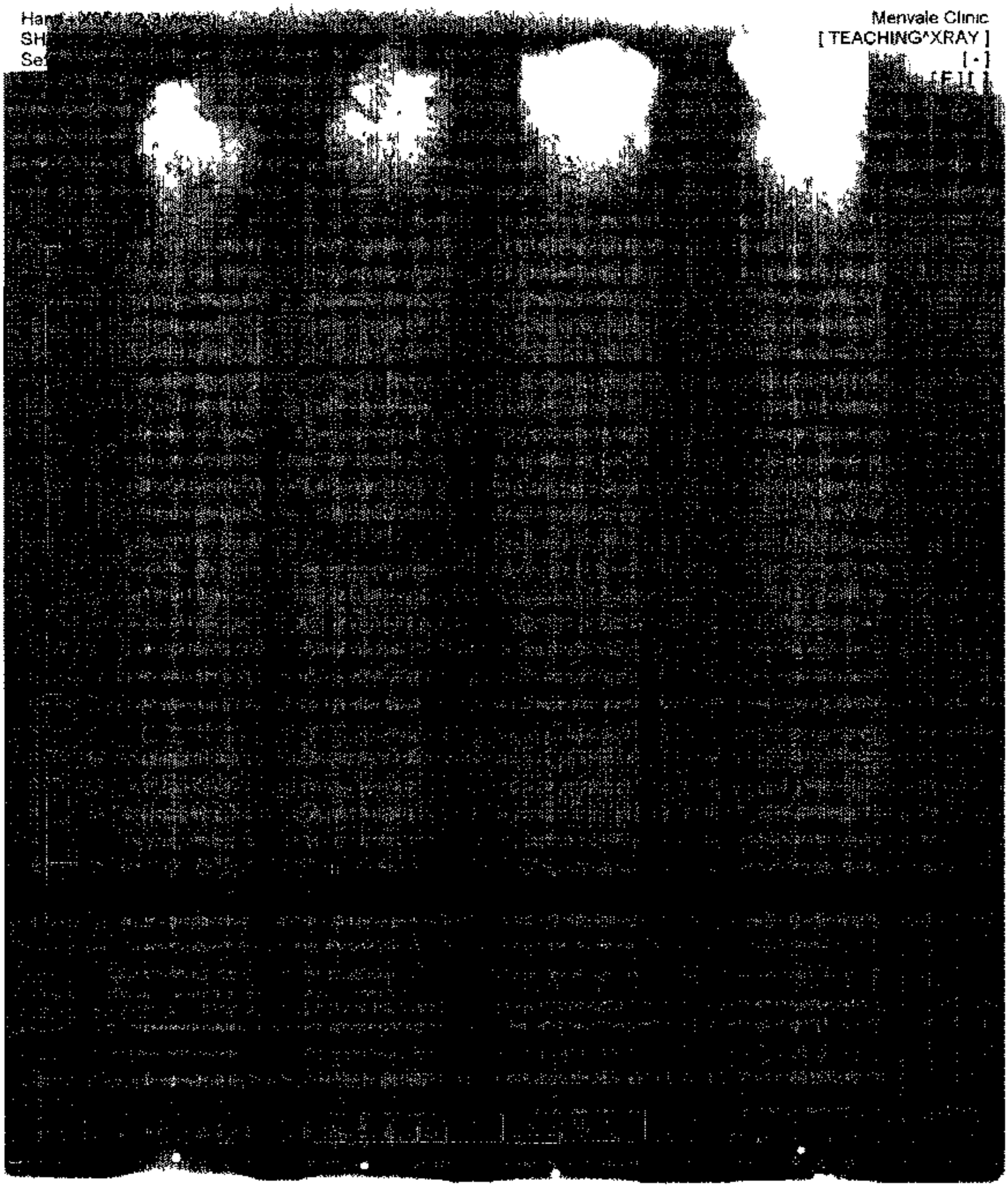

Appendix A: **X-Ray images - Mer Bleue Core -Image 4**

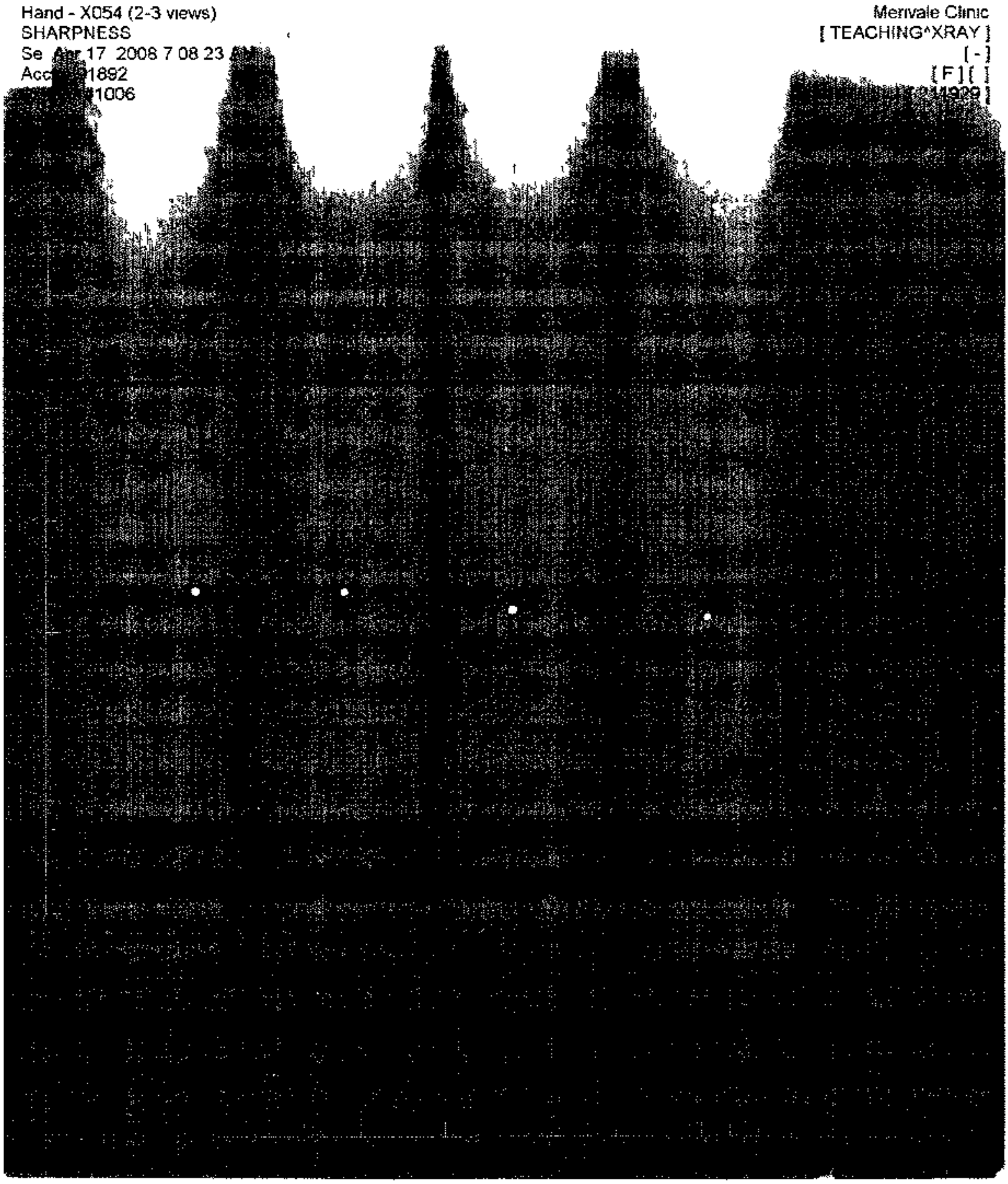

Appendix A: X-Ray images - Mer Bleue Core -Image 5

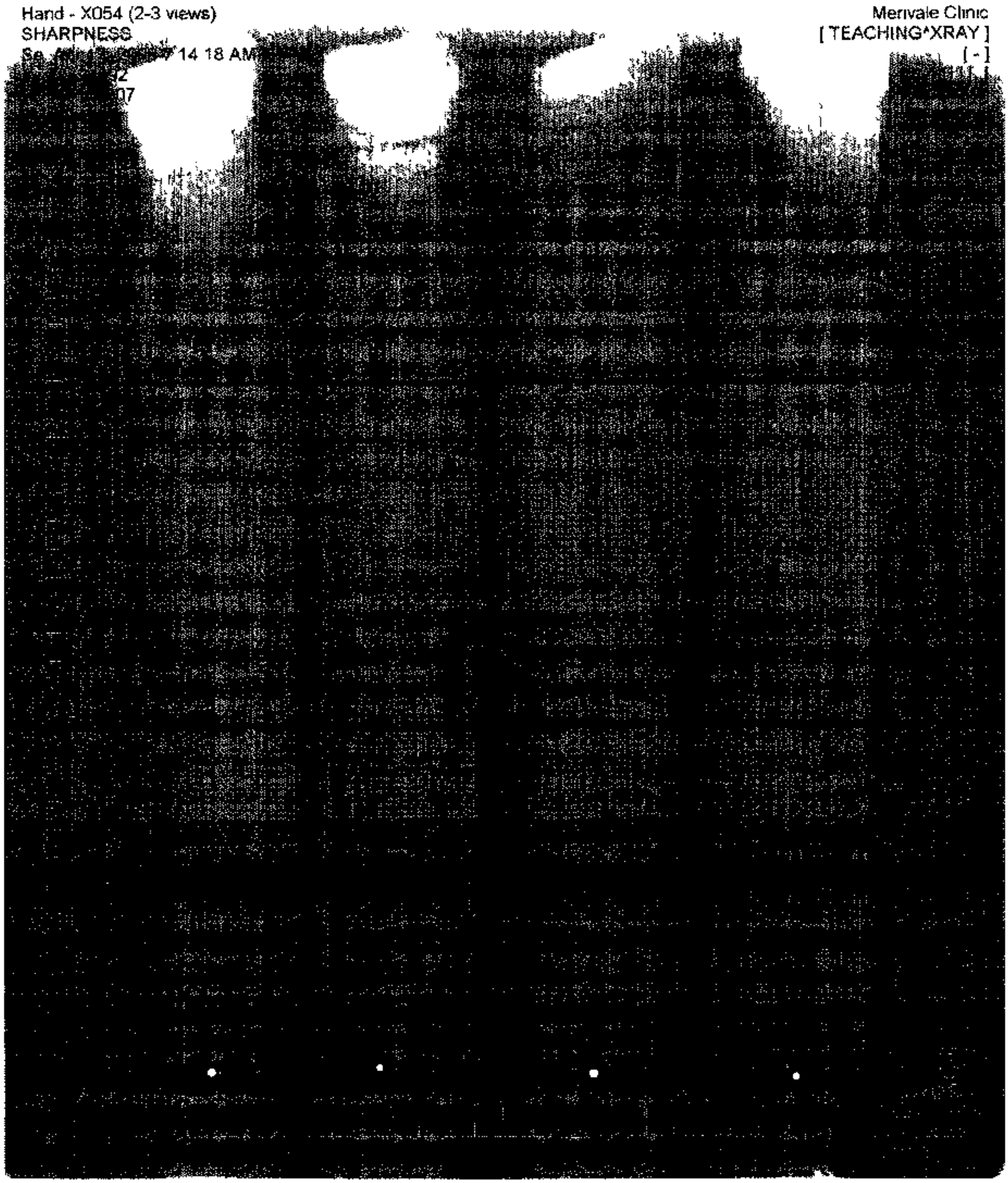

Appendix A: X-Ray images - Mer Bleue Core -Image 6

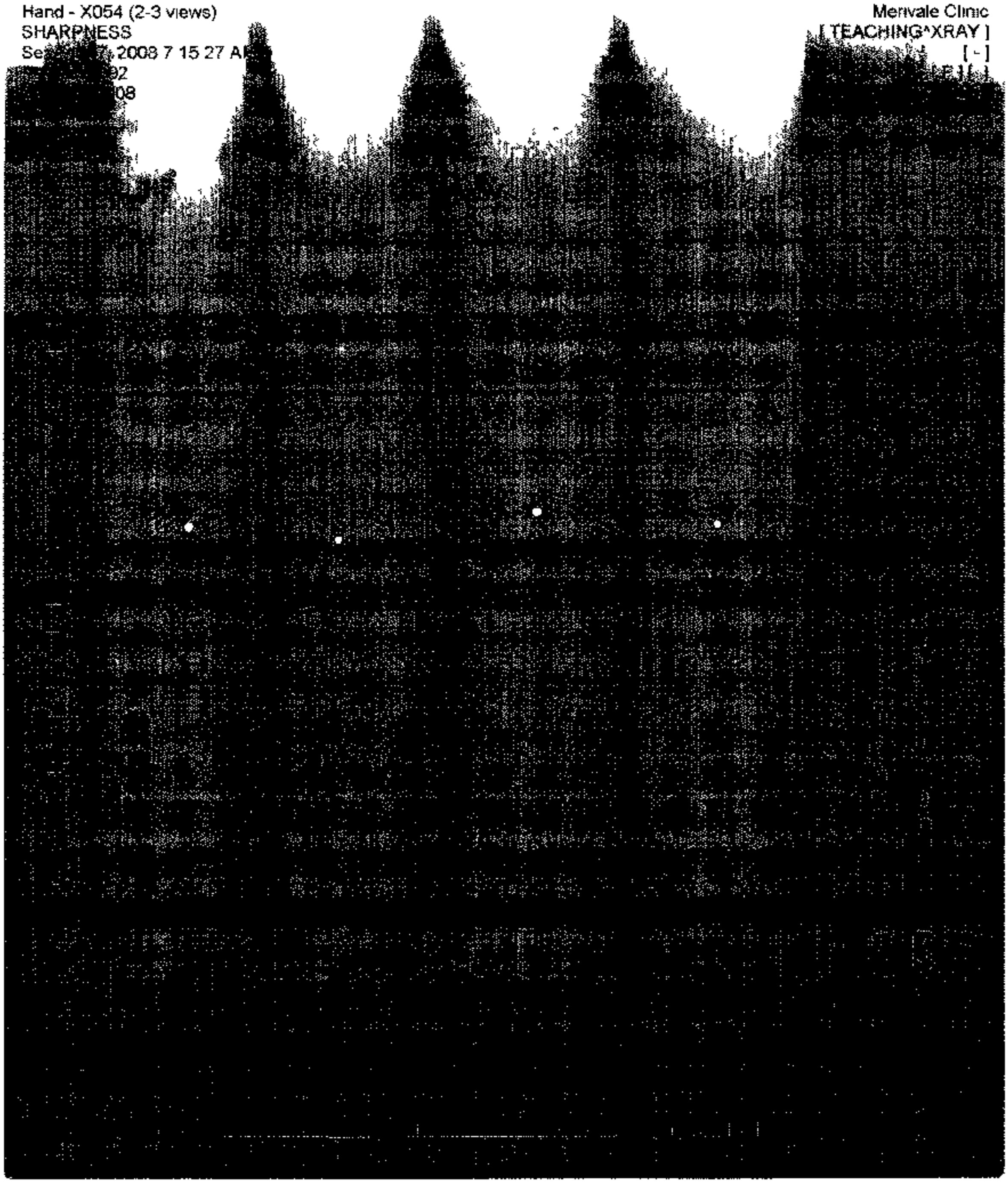

Appendix A: X-Ray images - Mer Bleue Core -Image 7

Appendix A: X-Ray images - Mer Bleue Core -Image 8

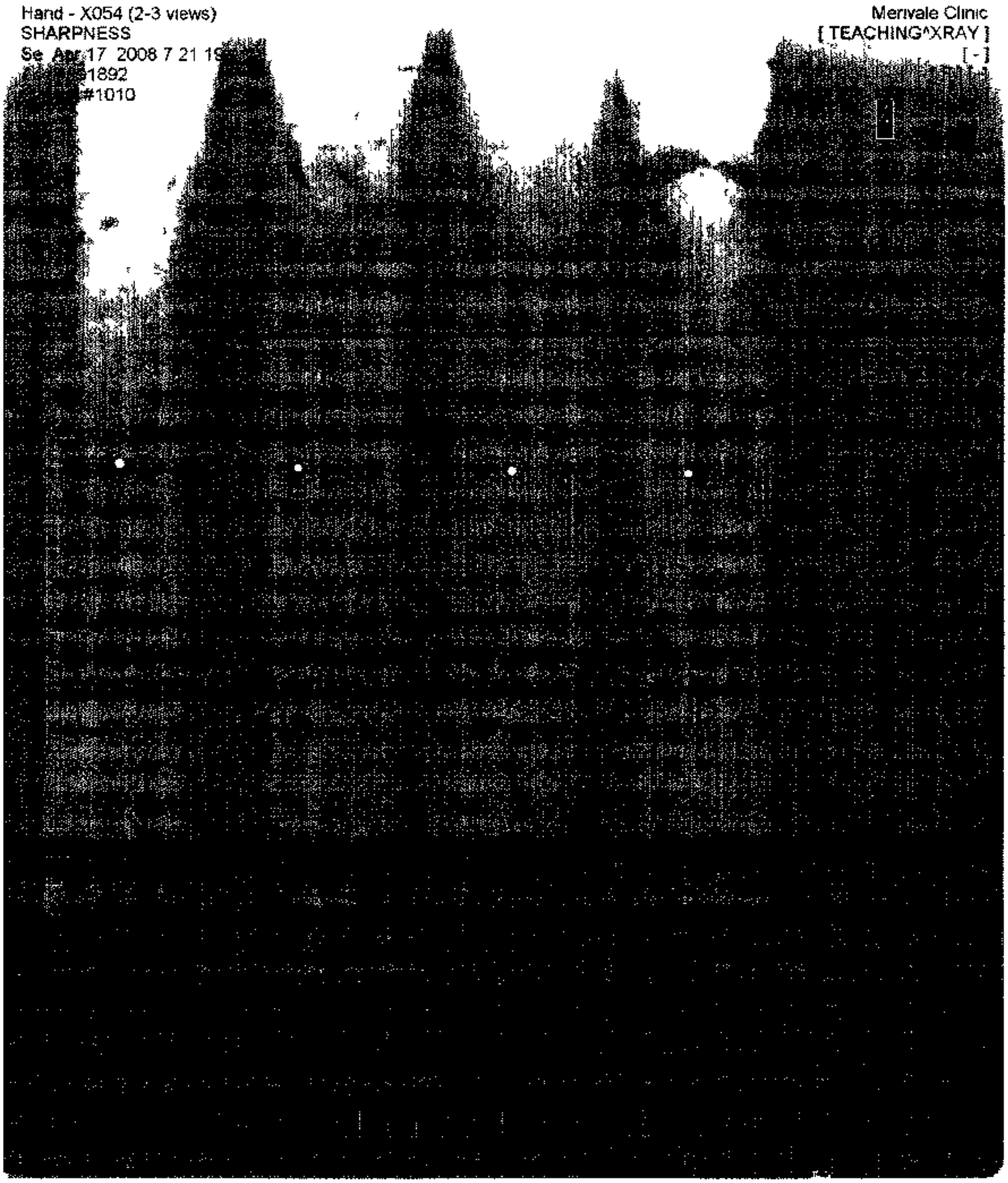

Appendix A: X-Ray images - Mer Bleue Core -Image 9

Appendix A: **X-Ray images - Mer Bleue Core -Image 10**

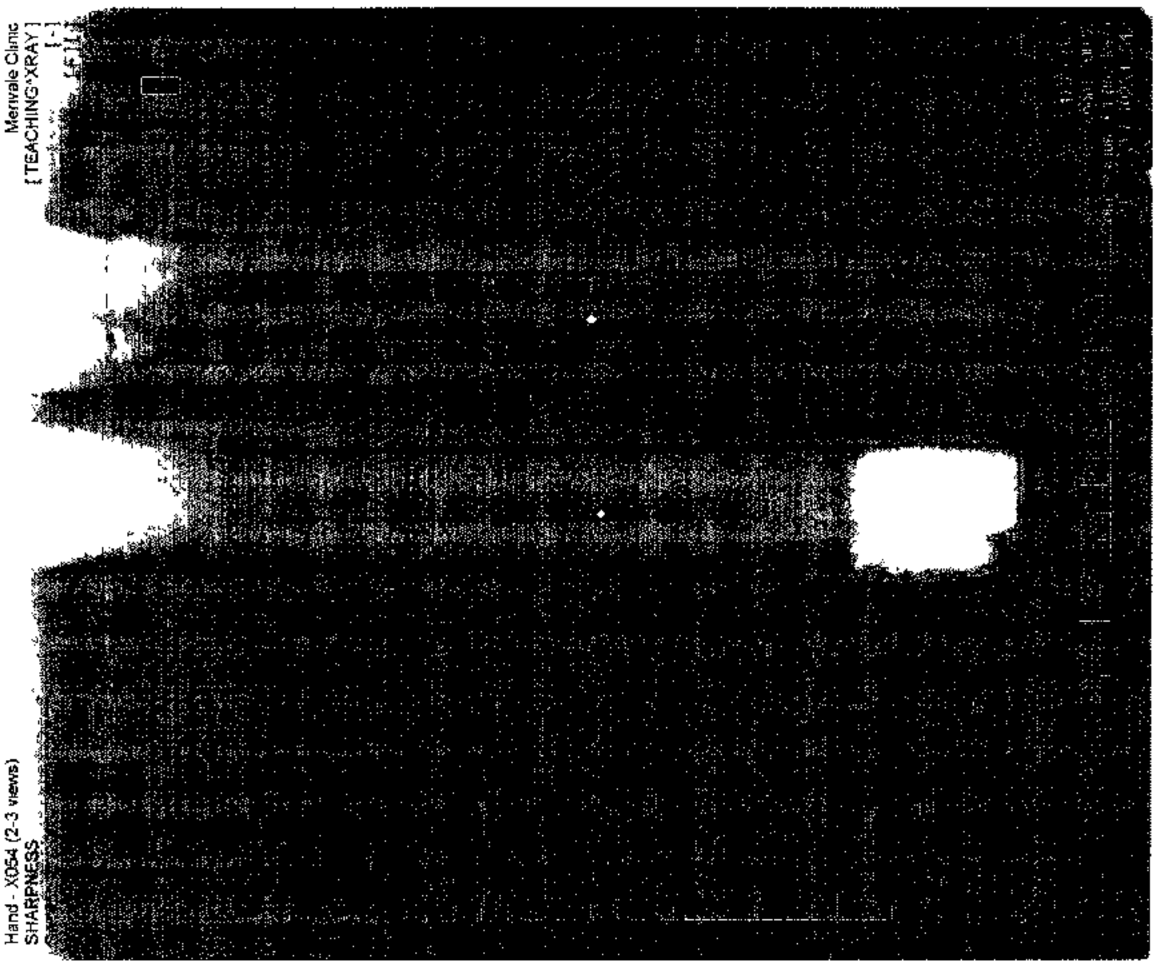

Appendix B: Digital core surface photographs - Mer Bleue Core -Image 1

Image : Core 1A-All.JPG

Appendix B: Digital core surface photographs - Mer Bleue Core -Image 2

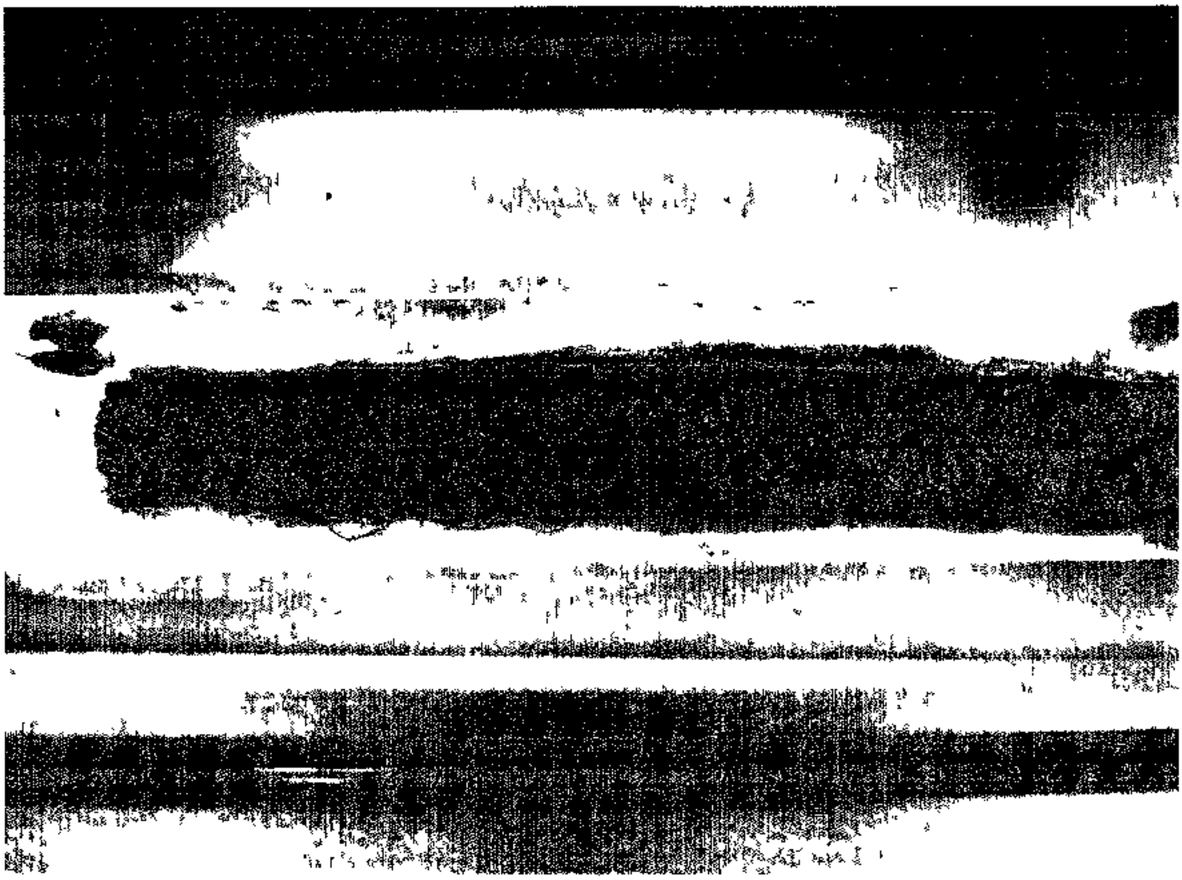

Image : Core 1B-Top JPG

Appendix B: Digital core surface photographs - Mer Bleue Core -Image 3

Image. Core 1B-Bottom JPG

Appendix B: Digital core surface photographs - Mer Bleue Core -Image 4

Image: Core 2A-Top.JPG

Appendix B: Digital core surface photographs - Mer Bleue Core -Image 5

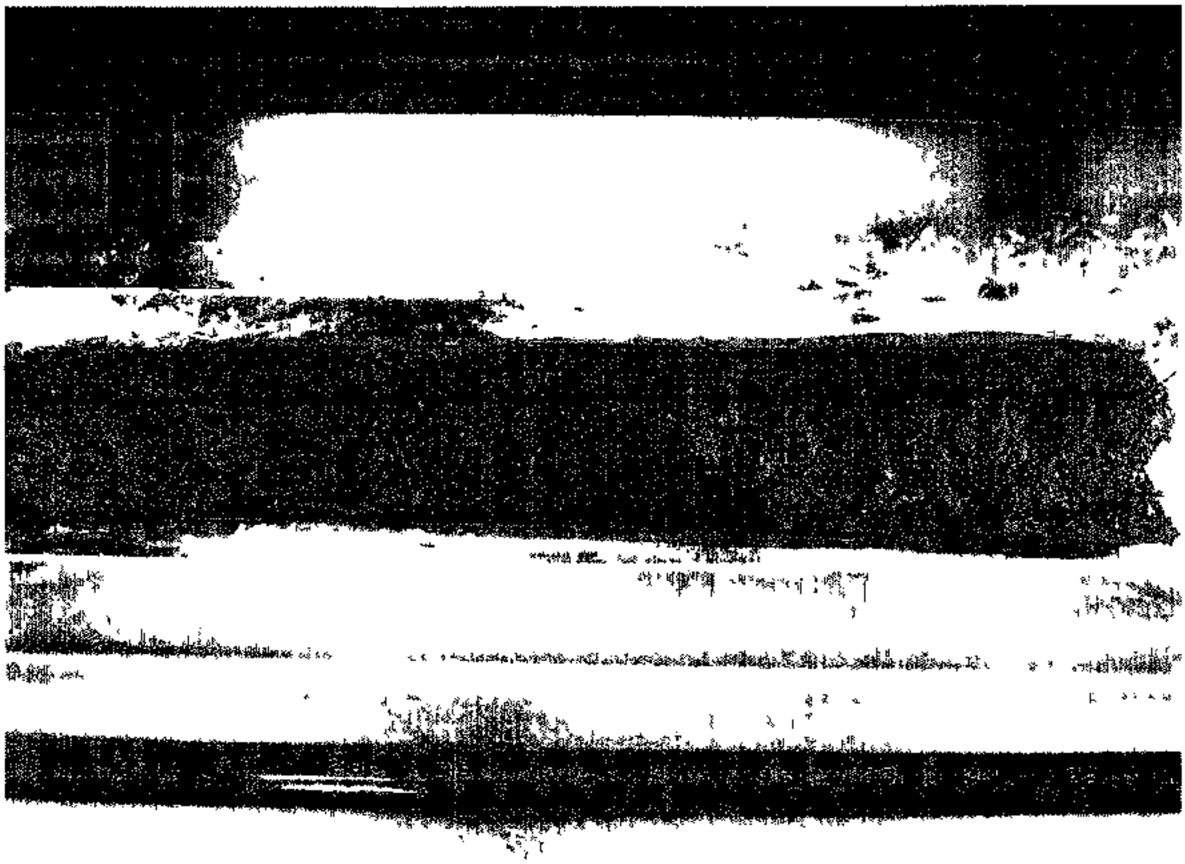

Image: Core 2A-Bottom.JPG

Appendix B: Digital core surface photographs - Mer Bleue Core -Image 6

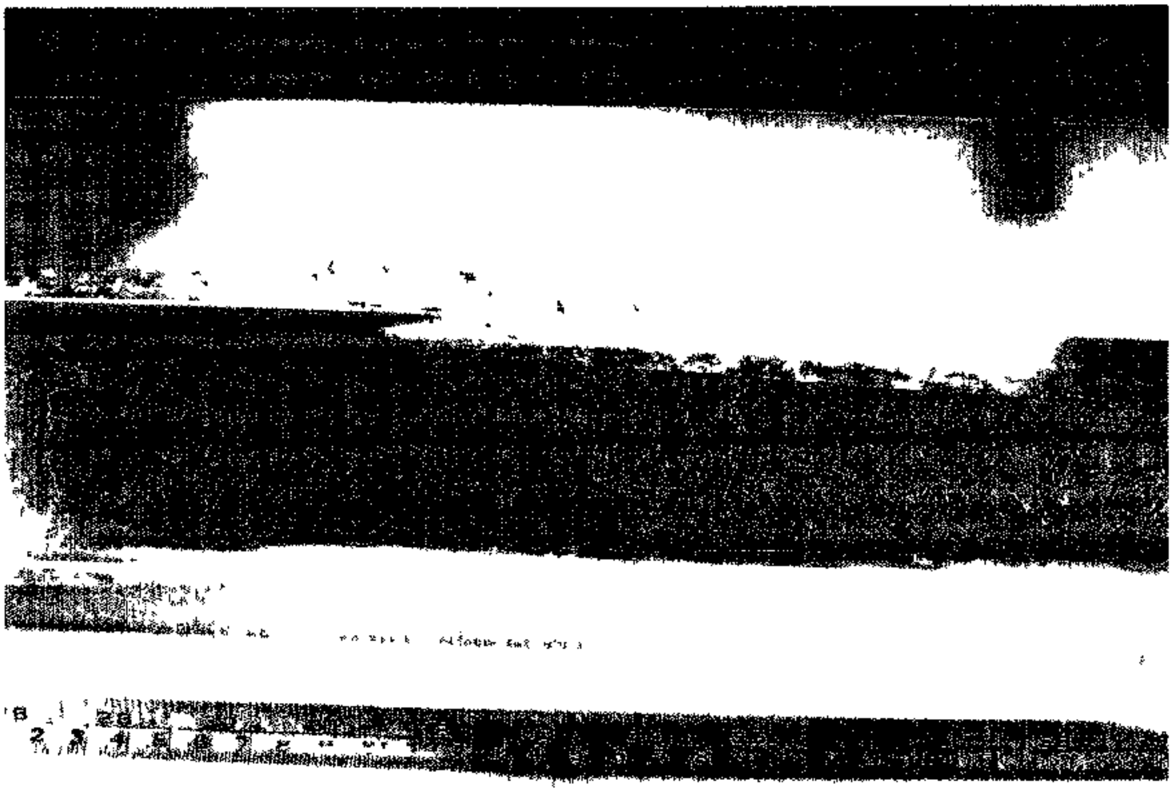

Image: Core 2B-Top.JPG

Appendix B: Digital core surface photographs - Mer Bleue Core -Image 7

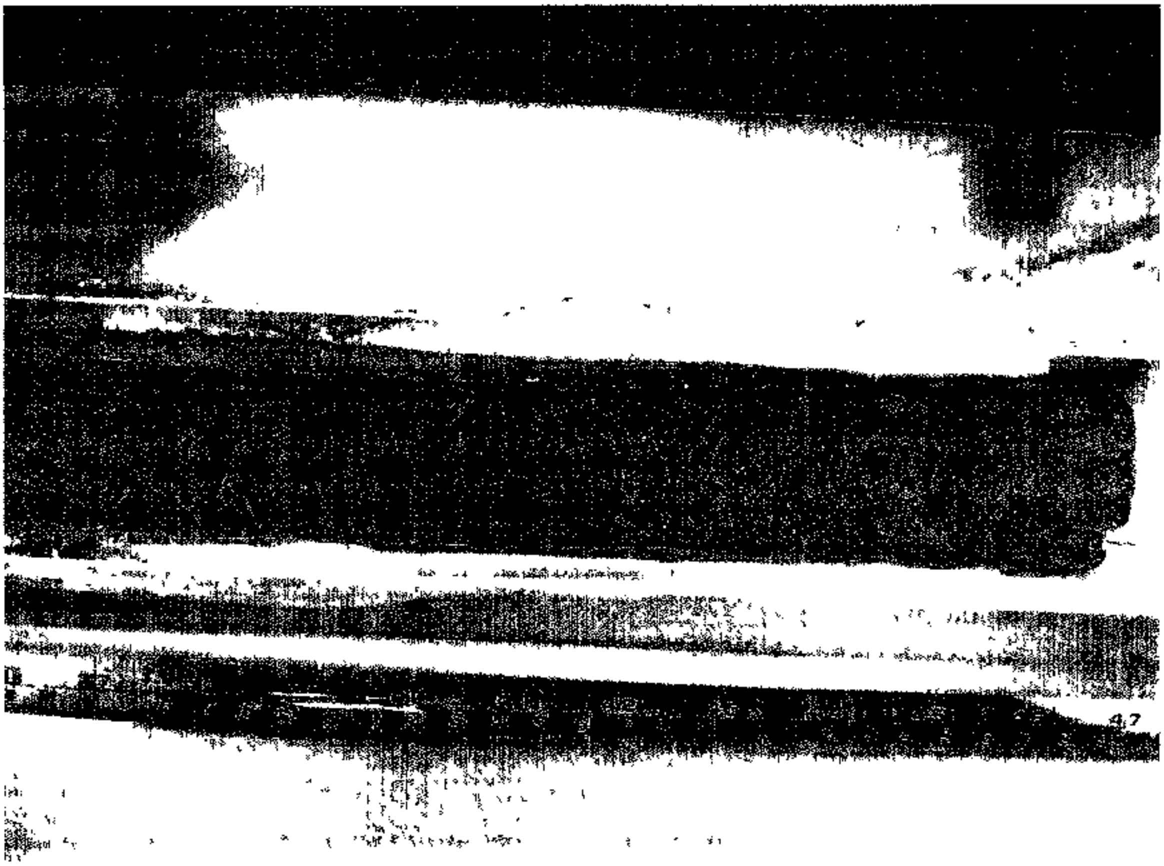

Image: Core 2B-Bottom.JPG

Appendix B: Digital core surface photographs - Mer Bleue Core -Image 8

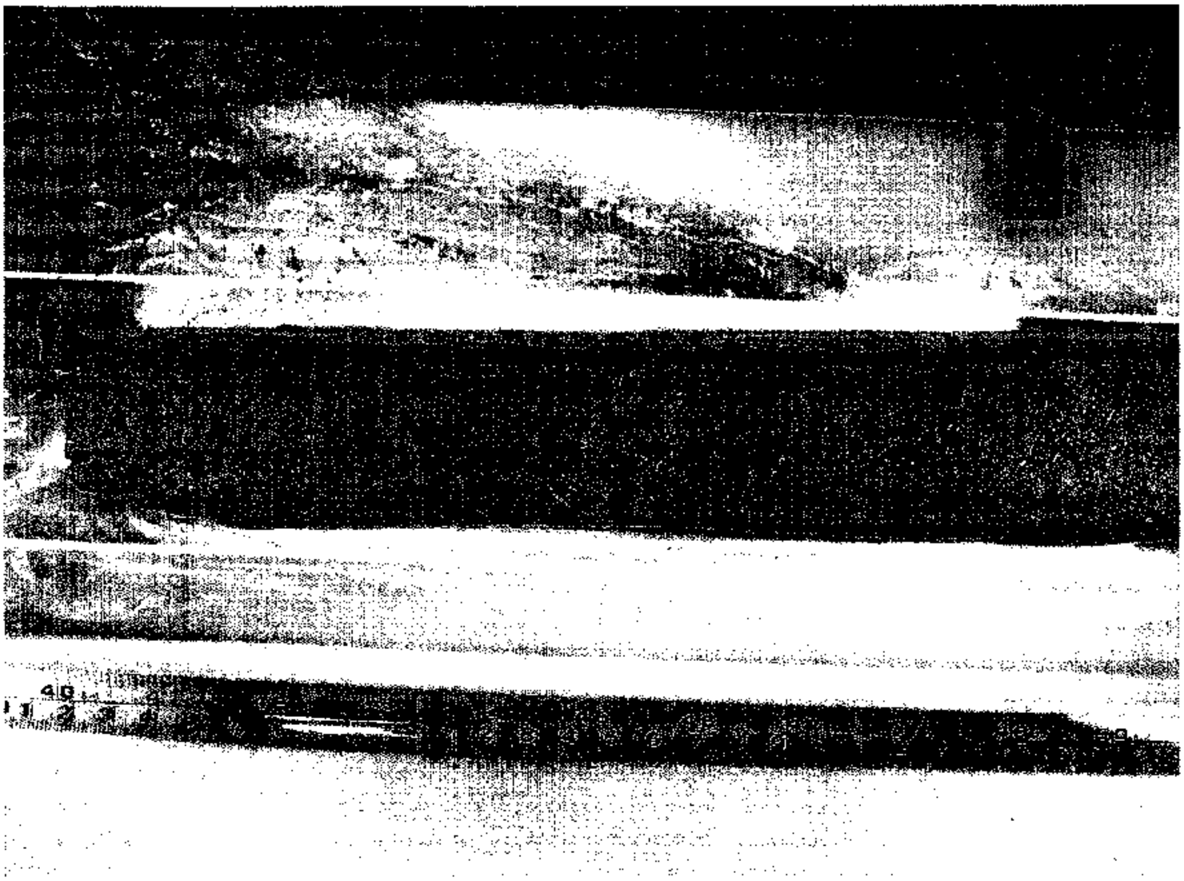

Image: Core 3A-Top.JPG

Appendix B: Digital core surface photographs - Mer Bleue Core -Image 9

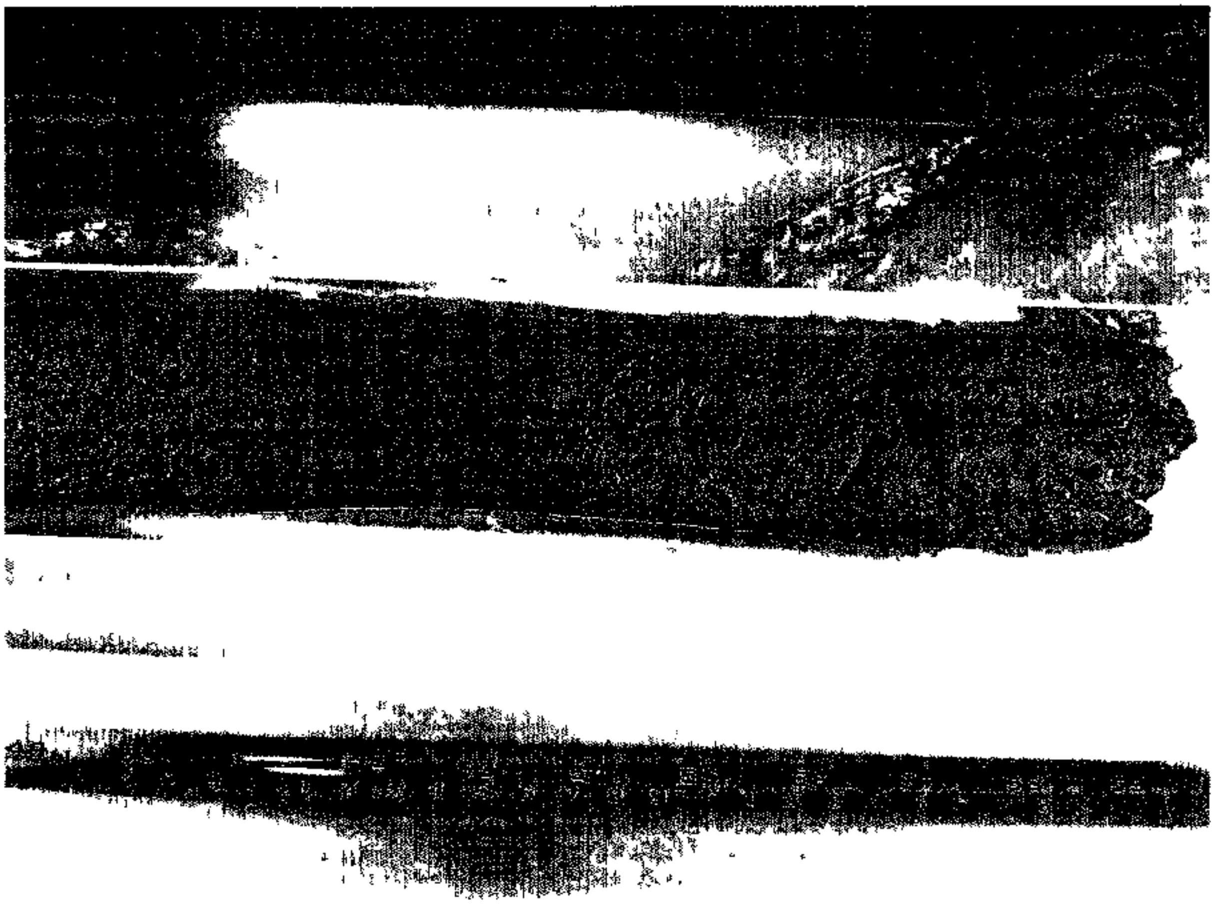

Image: Core 3A-Bottom.JPG

Appendix B: Digital core surface photographs - Mer Bleue Core -Image 10

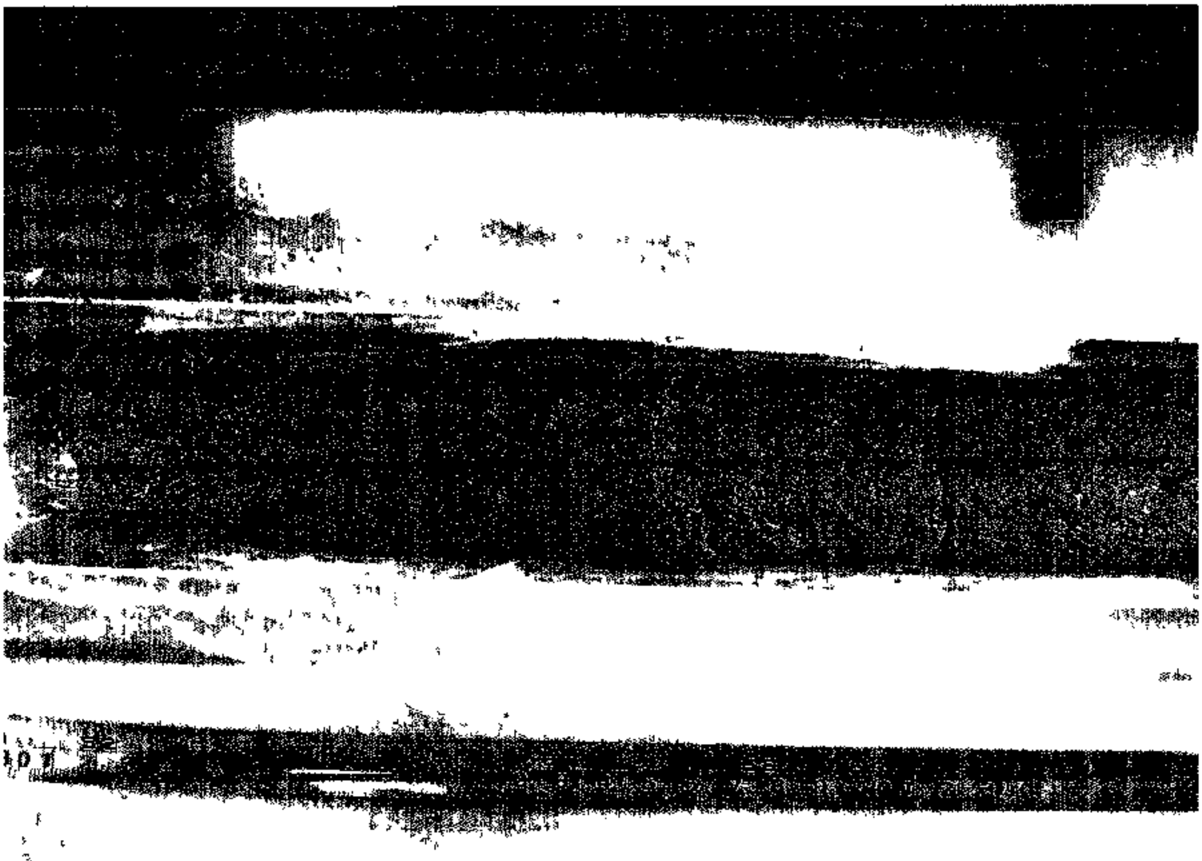

Image: Core 3B-Top.JPG

Appendix B: Digital core surface photographs - Mer Bleue Core -Image 11

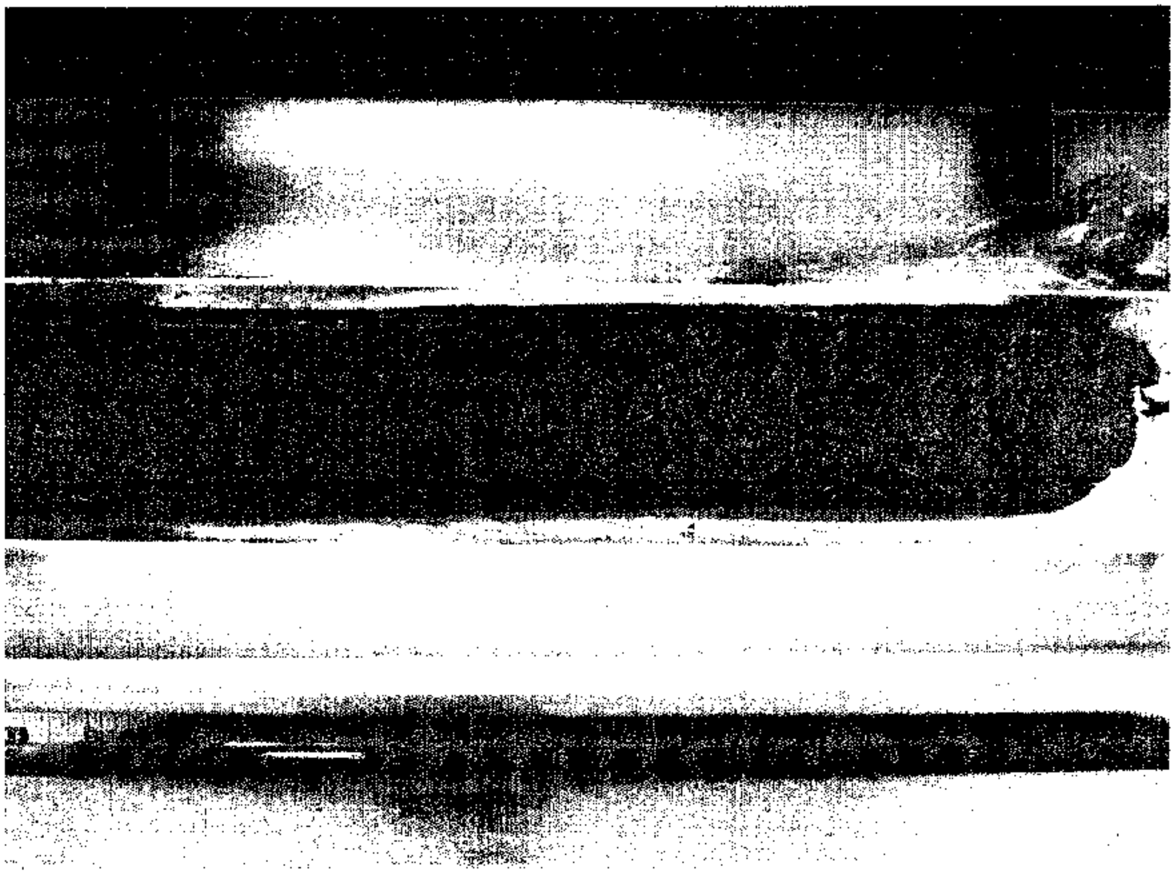

Image: Core 3B-Bottom.JPG

Appendix B: Digital core surface photographs - Mer Bleue Core -Image 12

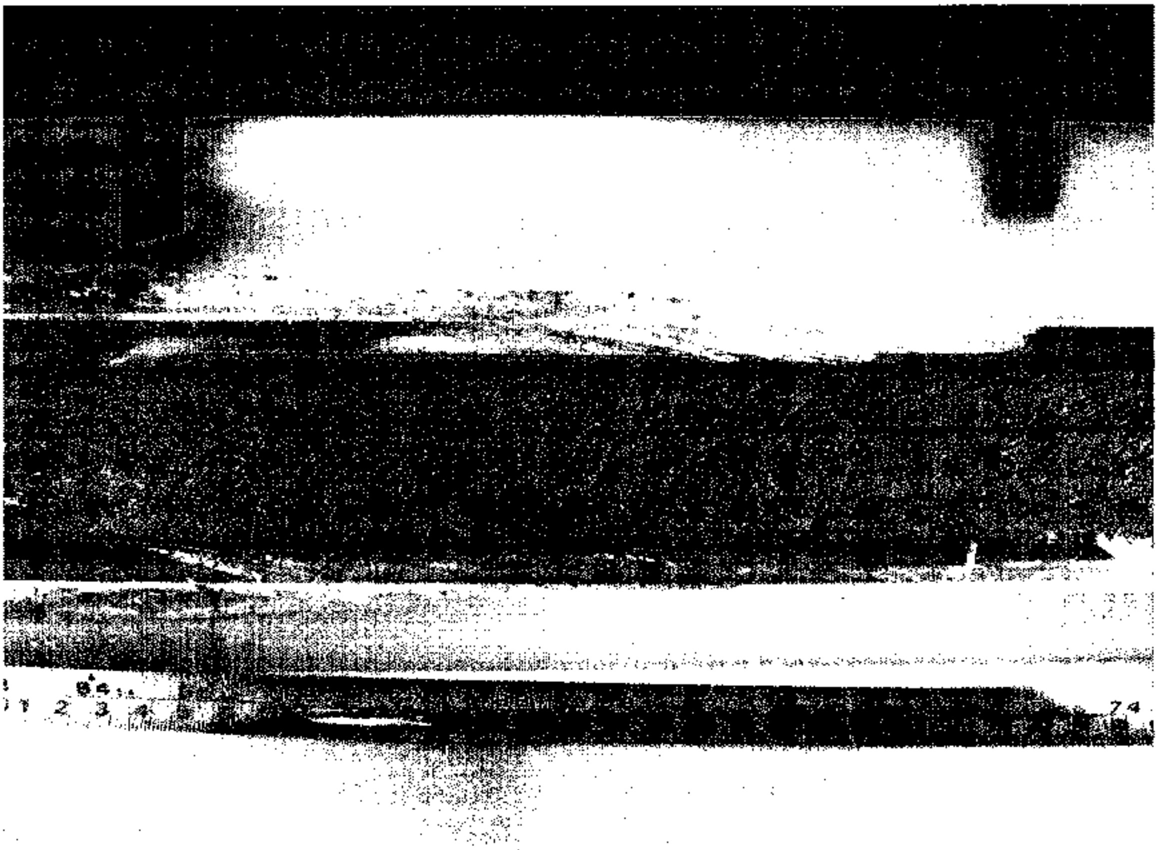

Image: Core 4A-Top.JPG

Appendix B: Digital core surface photographs - Mer Bleue Core -Image 13

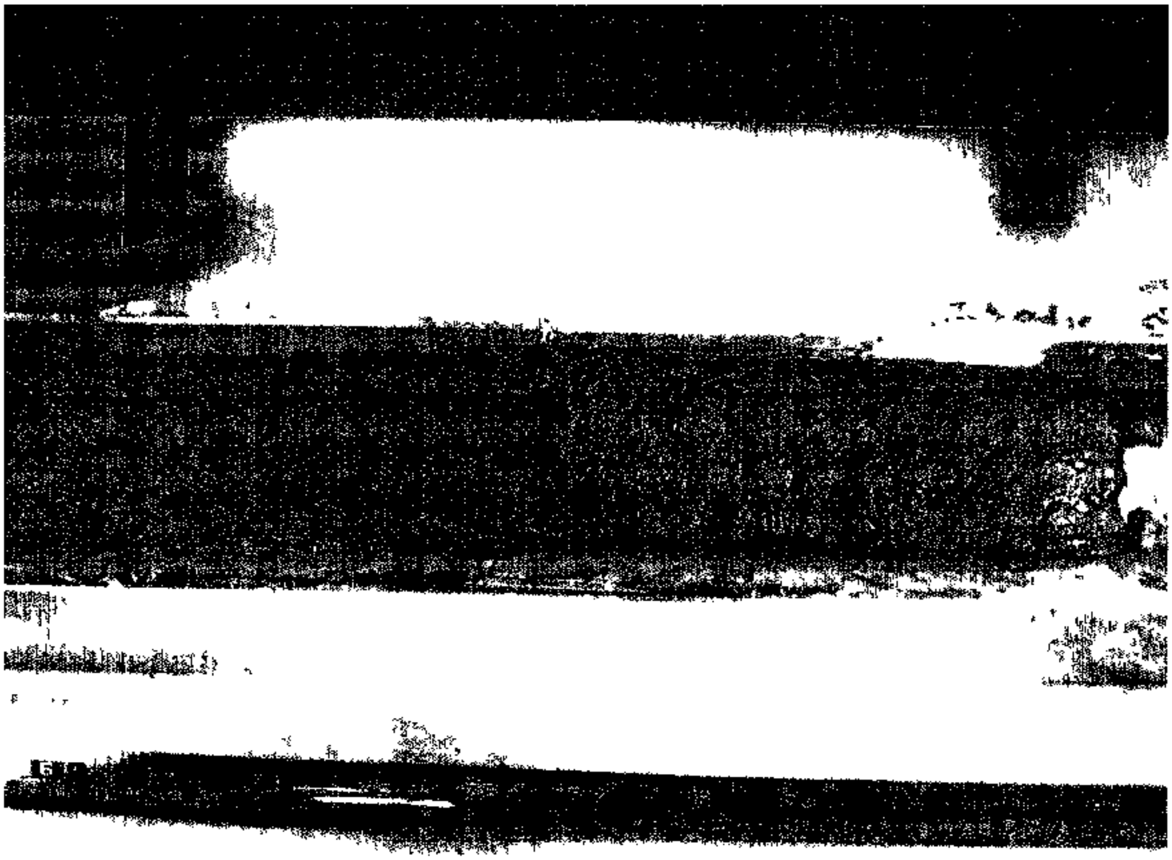

Image: Core 4A-Bottom.JPG

Appendix B: Digital core surface photographs - Mer Bleue Core -Image 14

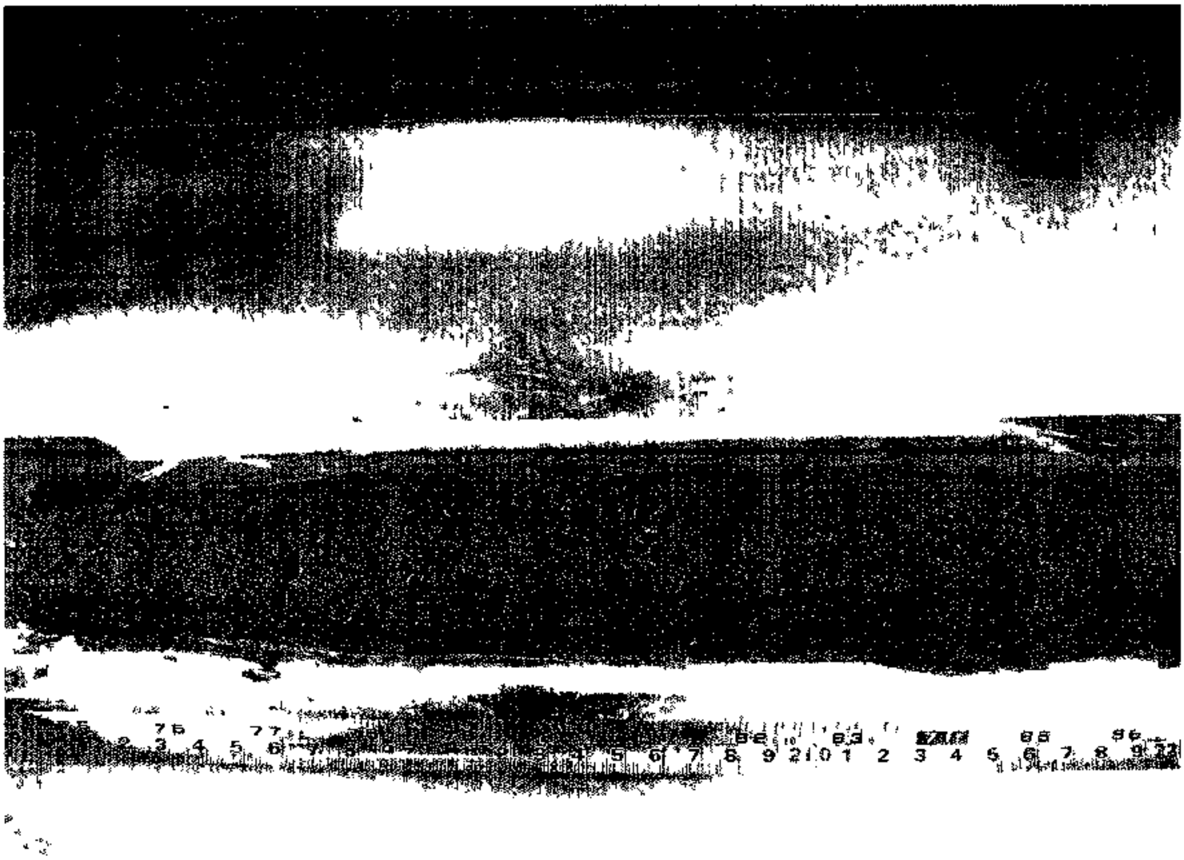

Image. Core 4B-Top JPG

Appendix B: Digital core surface photographs - Mer Bleue Core -Image 15

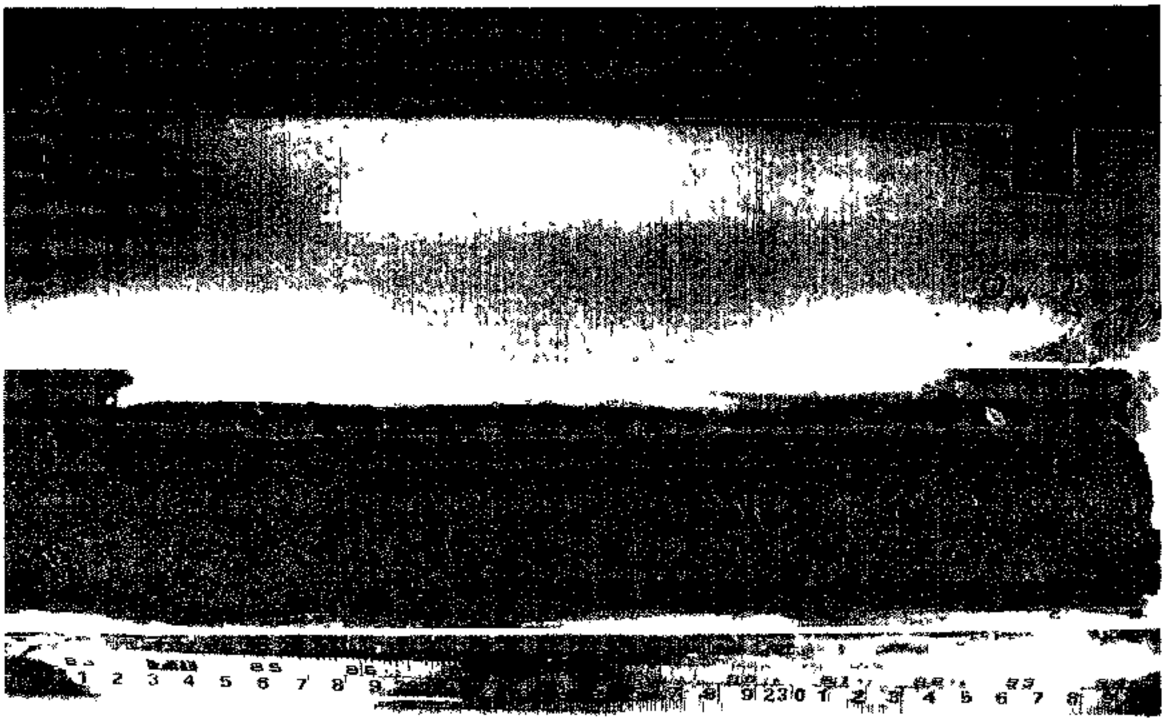

Image: Core 4B-Bottom.JPG

Appendix B: Digital core surface photographs - Mer Bleue Core -Image 16

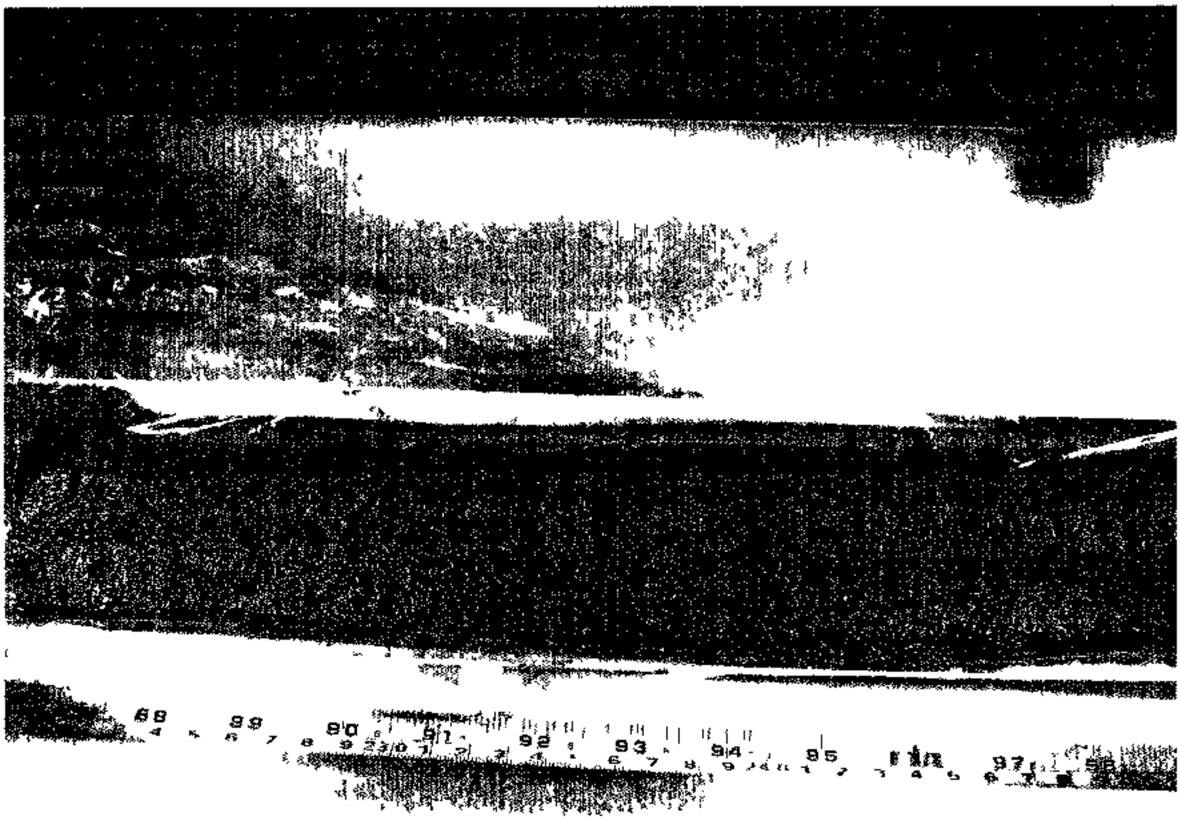

Image: Core 5A-Top.JPG

Appendix B: Digital core surface photographs - Mer Bleue Core -Image 17

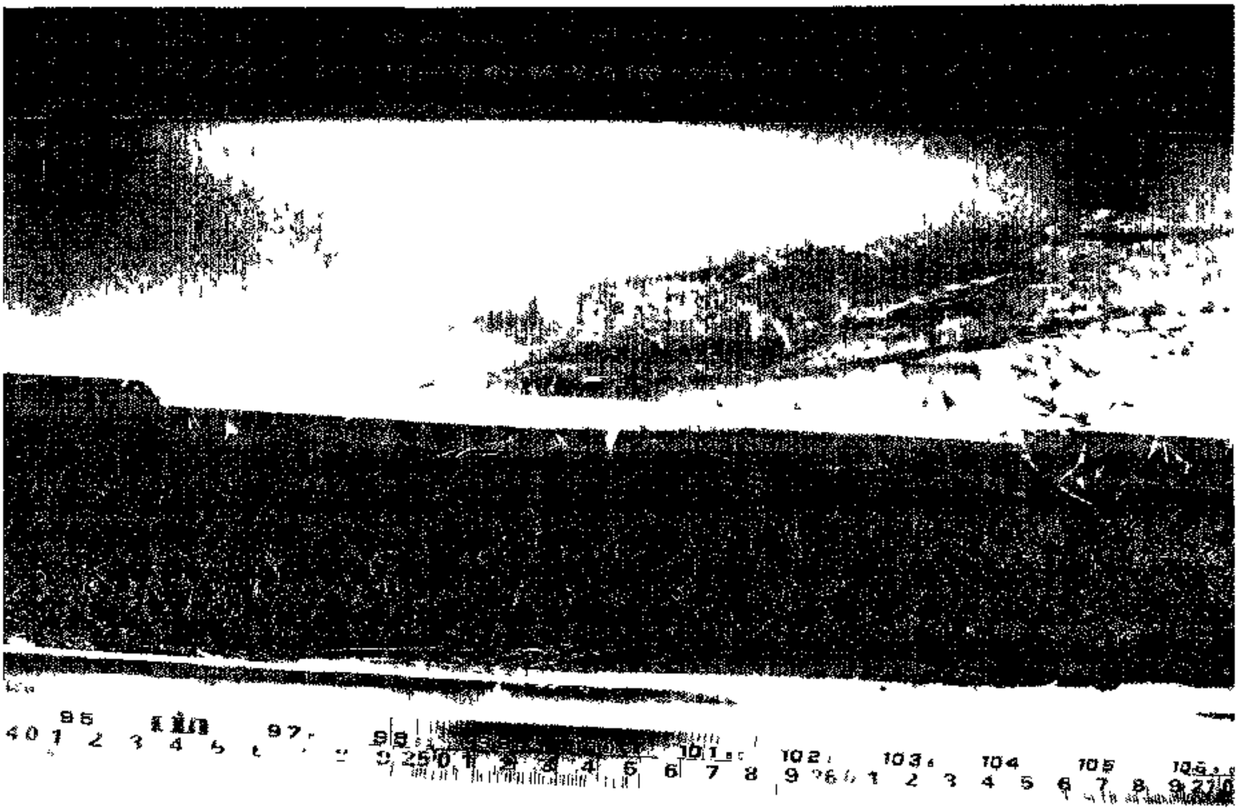

Image: Core 5A-Bottom JPG

Appendix B: Digital core surface photographs - Mer Bleue Core -Image 18

Image: Core 5B-Top.JPG

Appendix B: Digital core surface photographs - Mer Bleue Core -Image 19

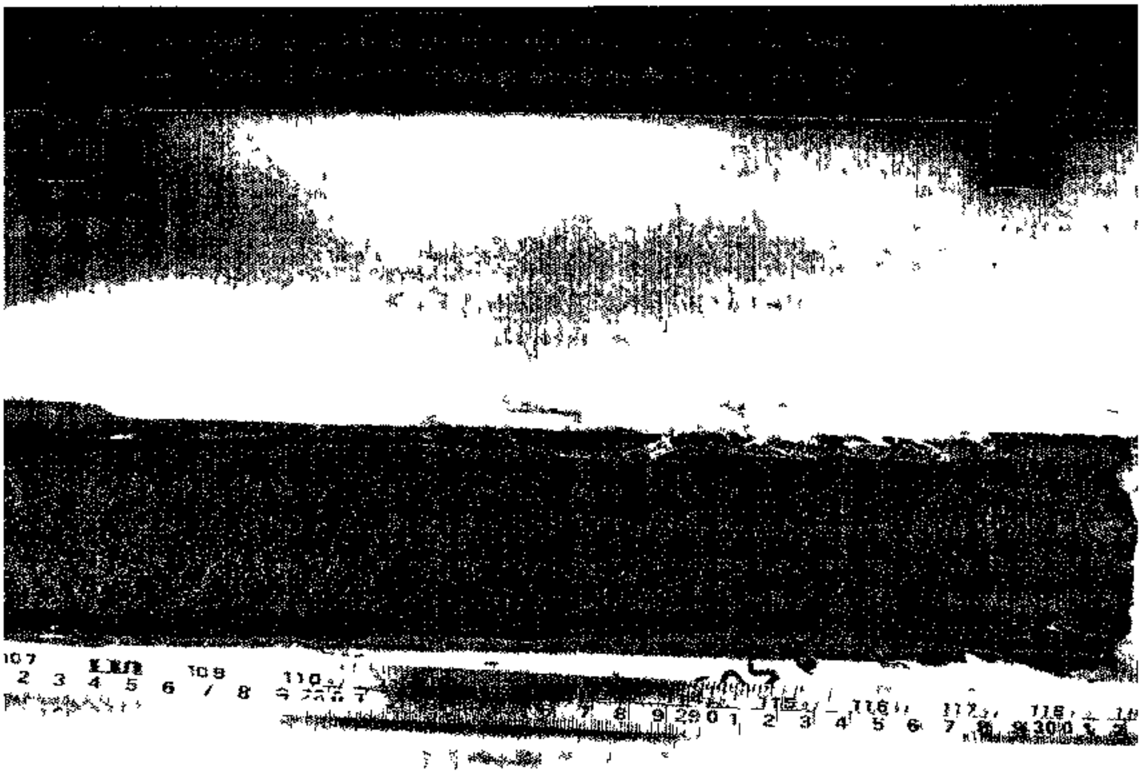

Image: Core 5B-Bottom.JPG

Appendix B: Digital core surface photographs - Mer Bleue Core -Image 20

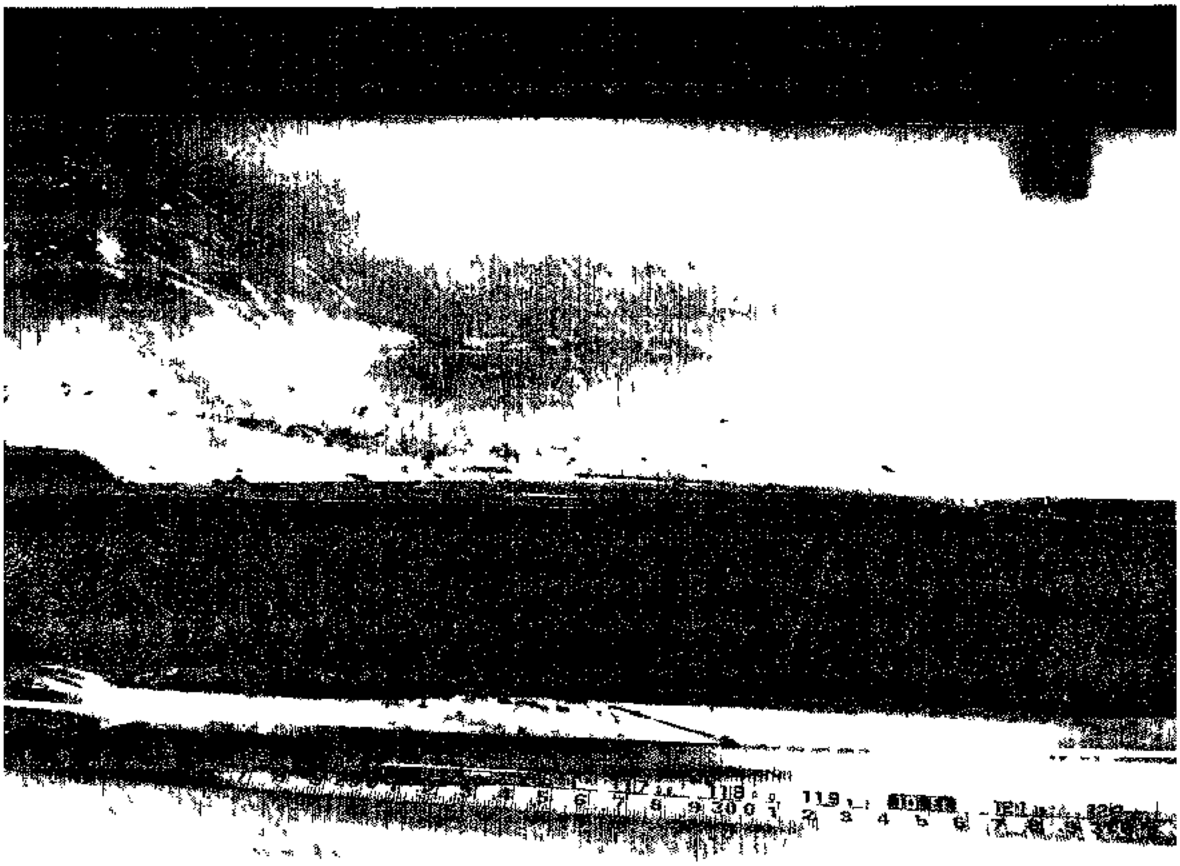

Image Core 6A-Top JPG

Appendix B: Digital core surface photographs - Mer Bleue Core -Image 21

Image: Core 6A-Bottom.JPG

Appendix B: Digital core surface photographs - Mer Bleue Core -Image 22

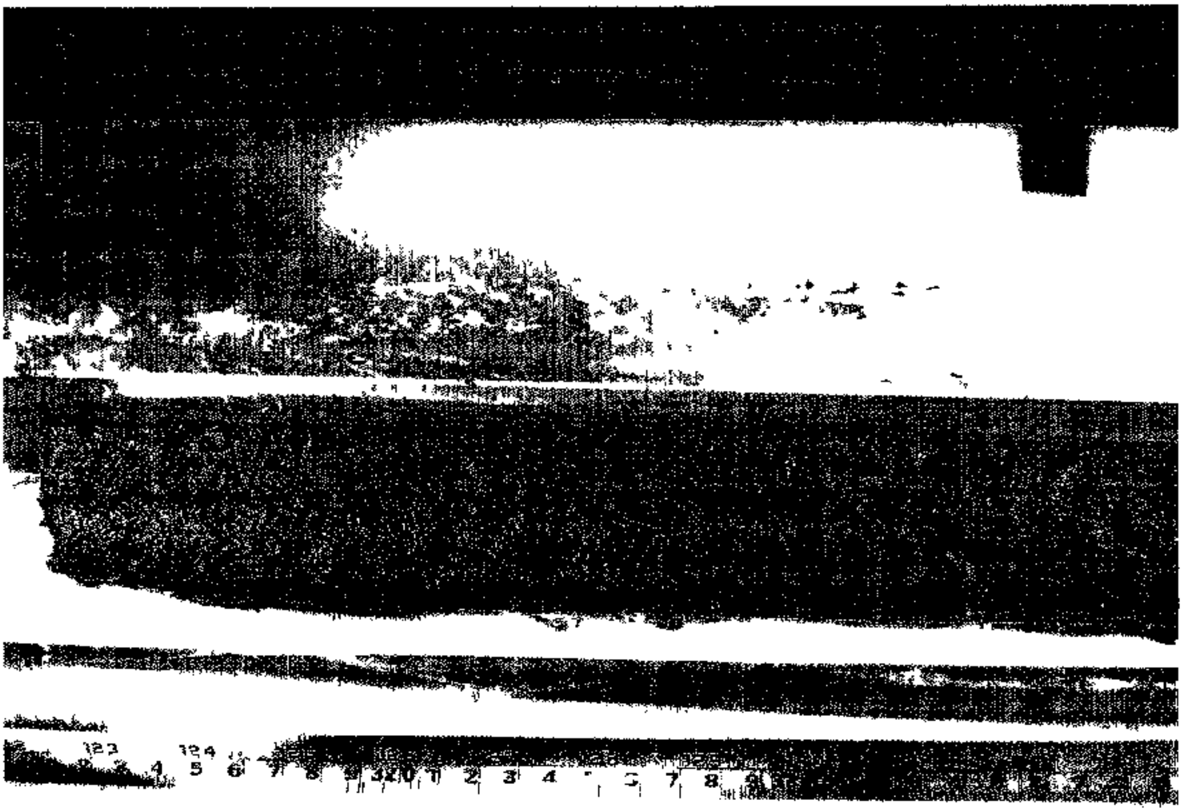

Image. Core 6B-TOP JPG

Appendix B: Digital core surface photographs - Mer Bleue Core -Image 23

Image: Core 6B-Bottom JPG

Appendix B: Digital core surface photographs - Mer Bleue Core -Image 24

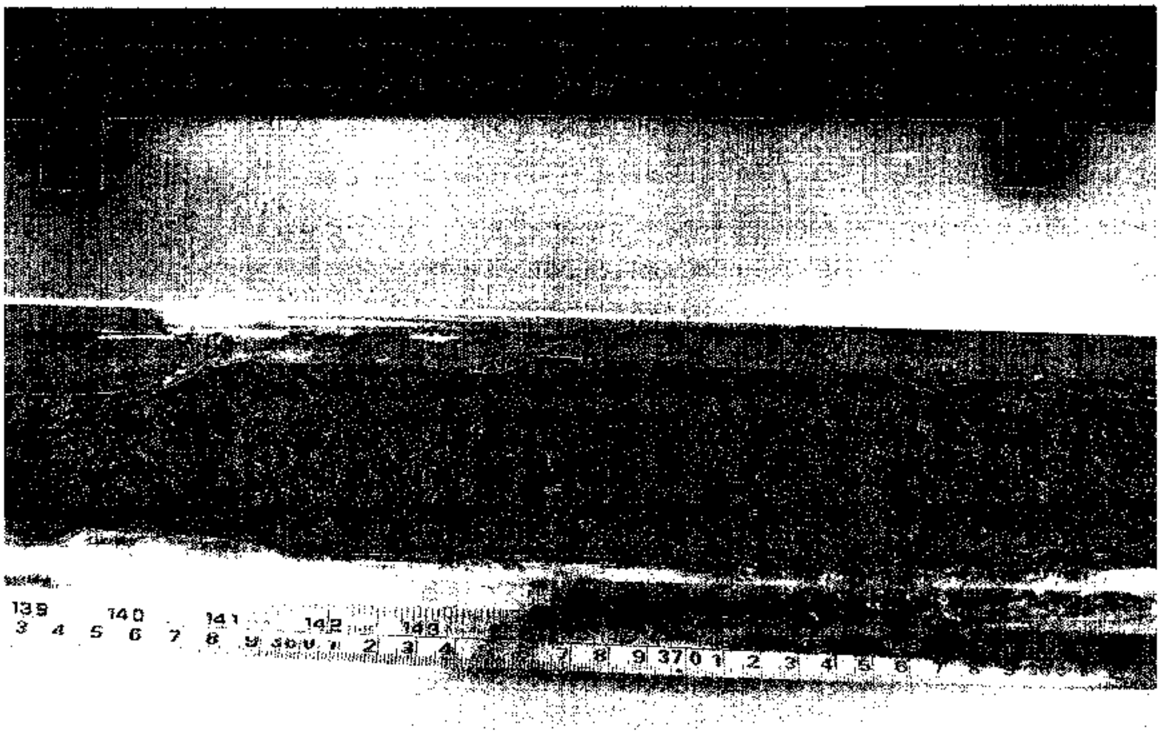

Image: Core 7A-Top.JPG

Appendix B: Digital core surface photographs - Mer Bleue Core -Image 25

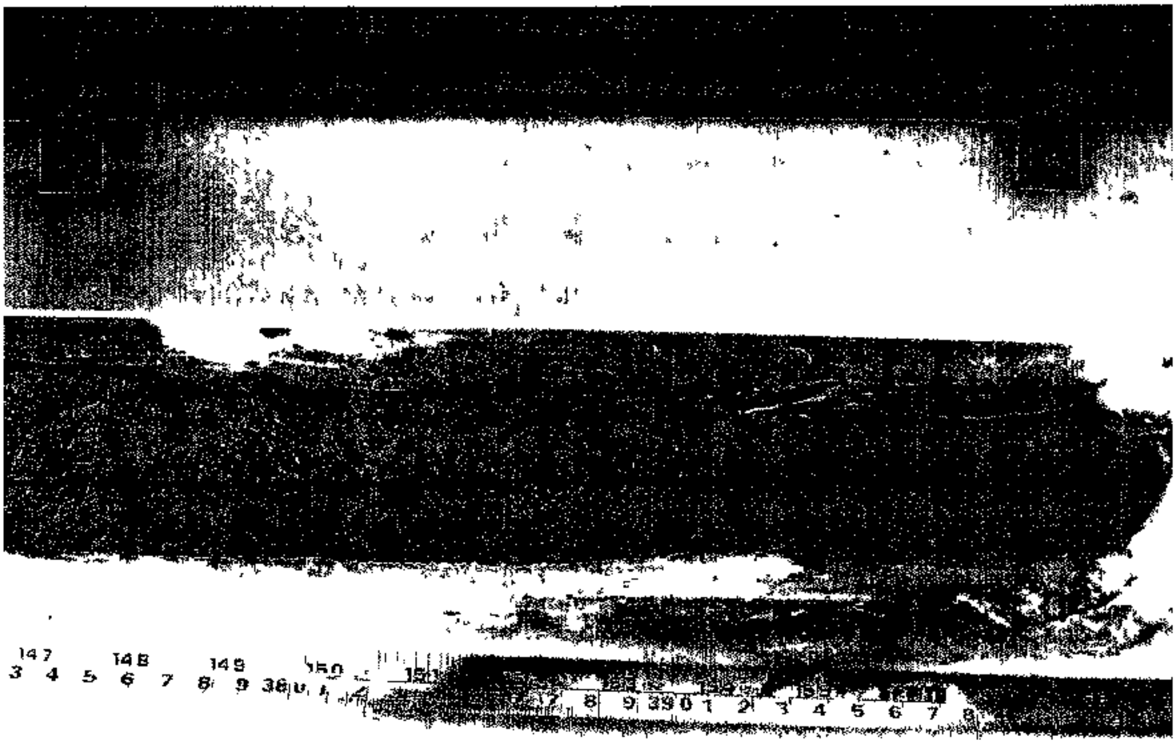

Image: Core 7A-Bottom.JPG

Appendix B: Digital core surface photographs - Mer Bleue Core -Image 26

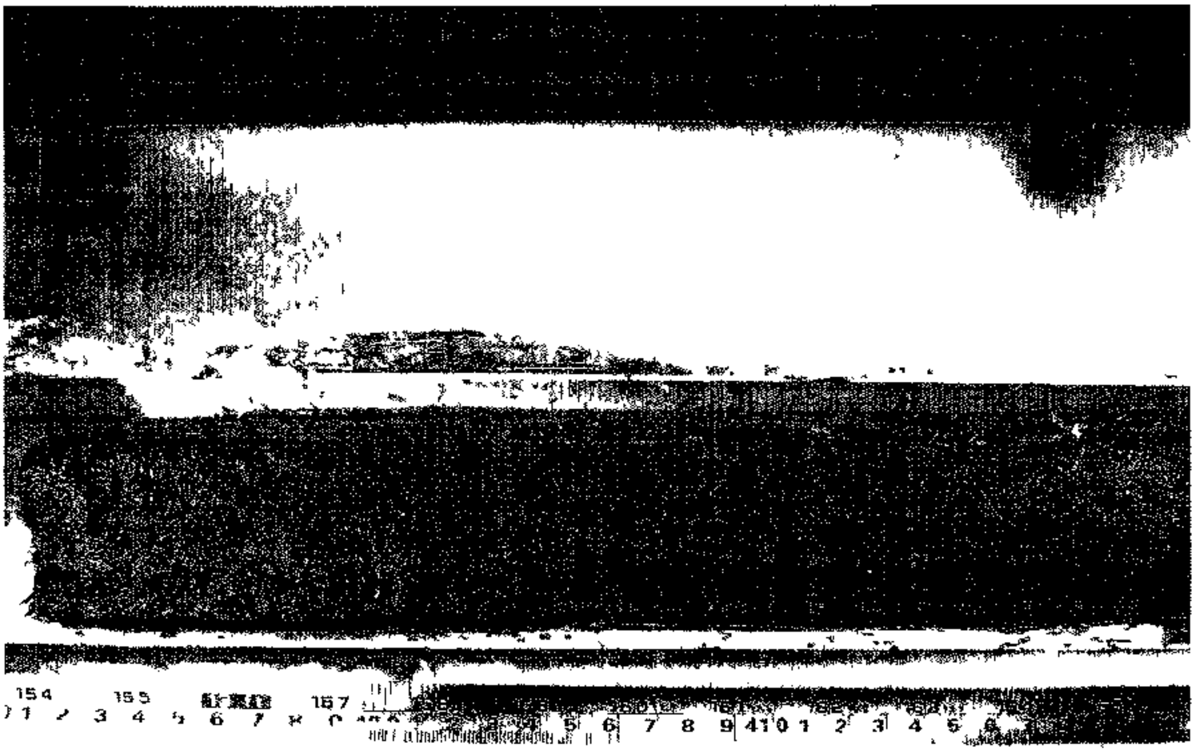

Image: Core 7B-Top.JPG

Appendix B: Digital core surface photographs - Mer Bleue Core -Image 27

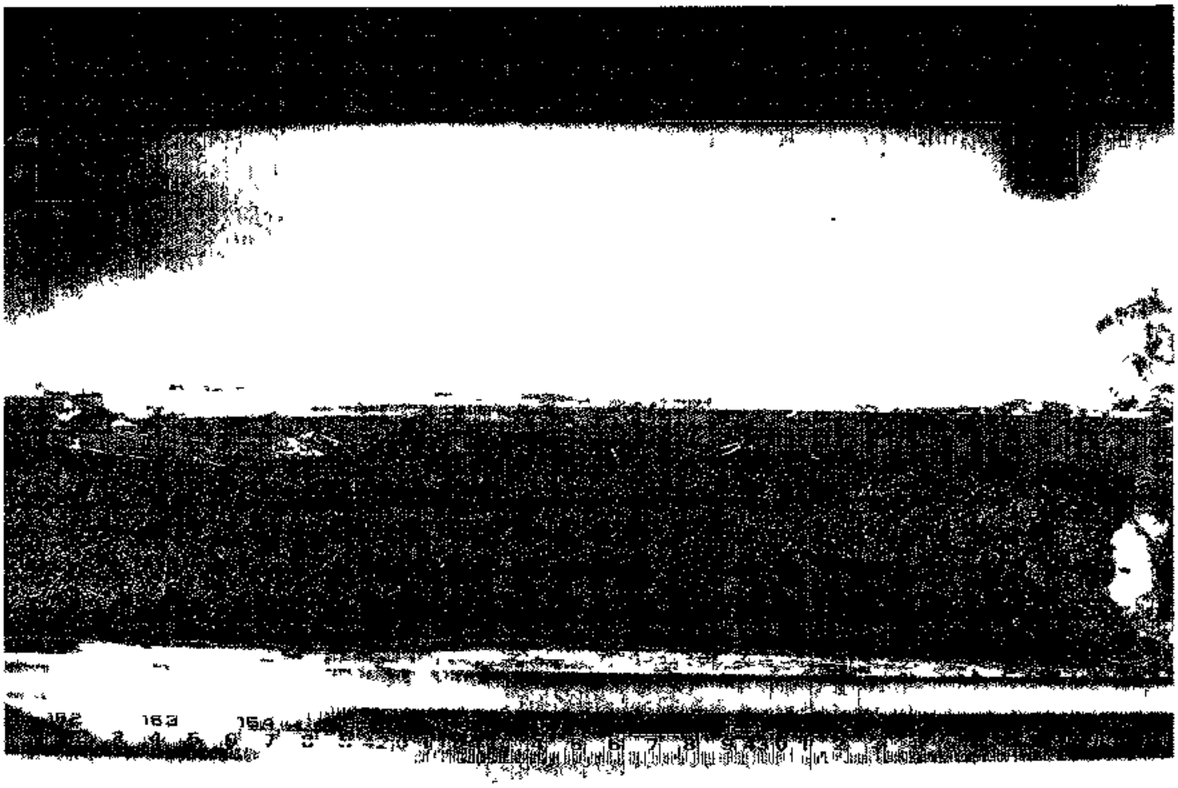

Image: Core 7B-Bottom.JPG

Appendix B: Digital core surface photographs - Mer Bleue Core -Image 28

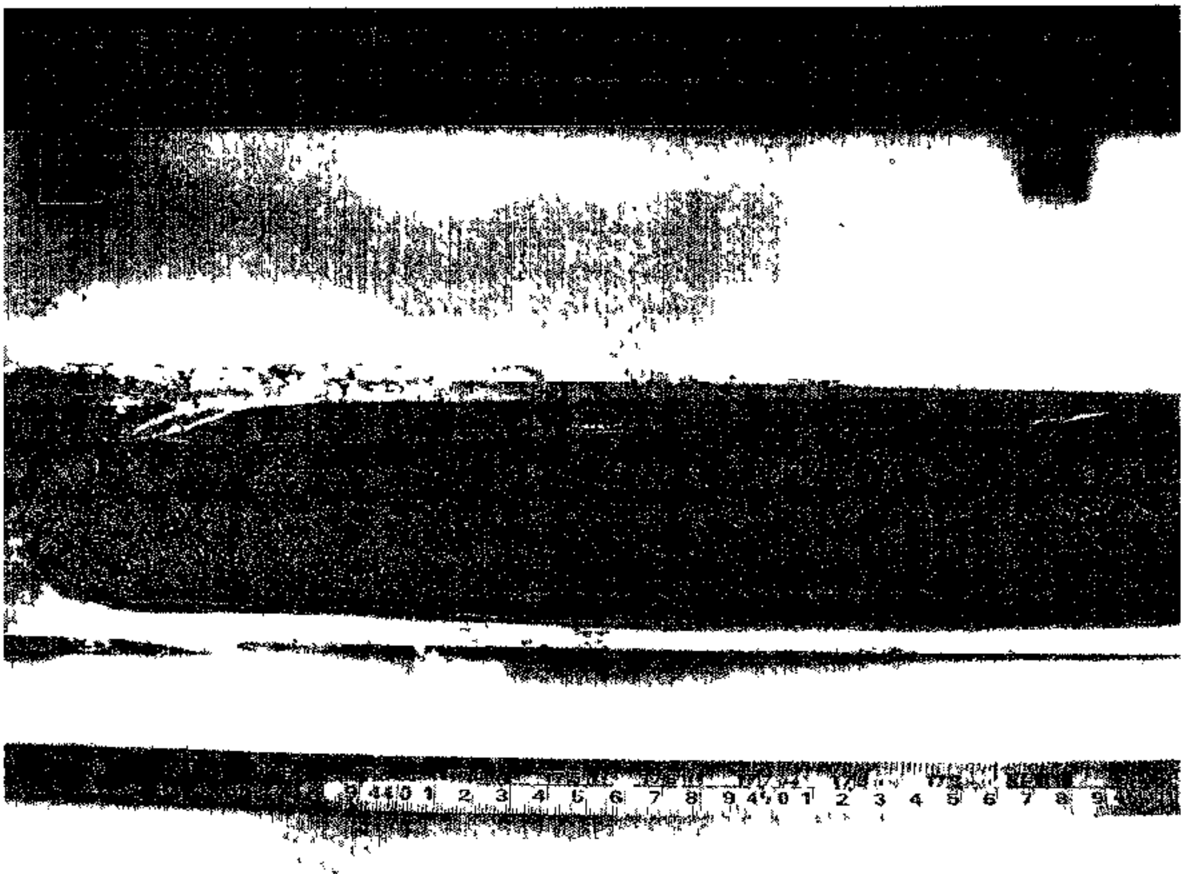

Image: Core 8A-Top.JPG

Appendix B: Digital core surface photographs - Mer Bleue Core -Image 29

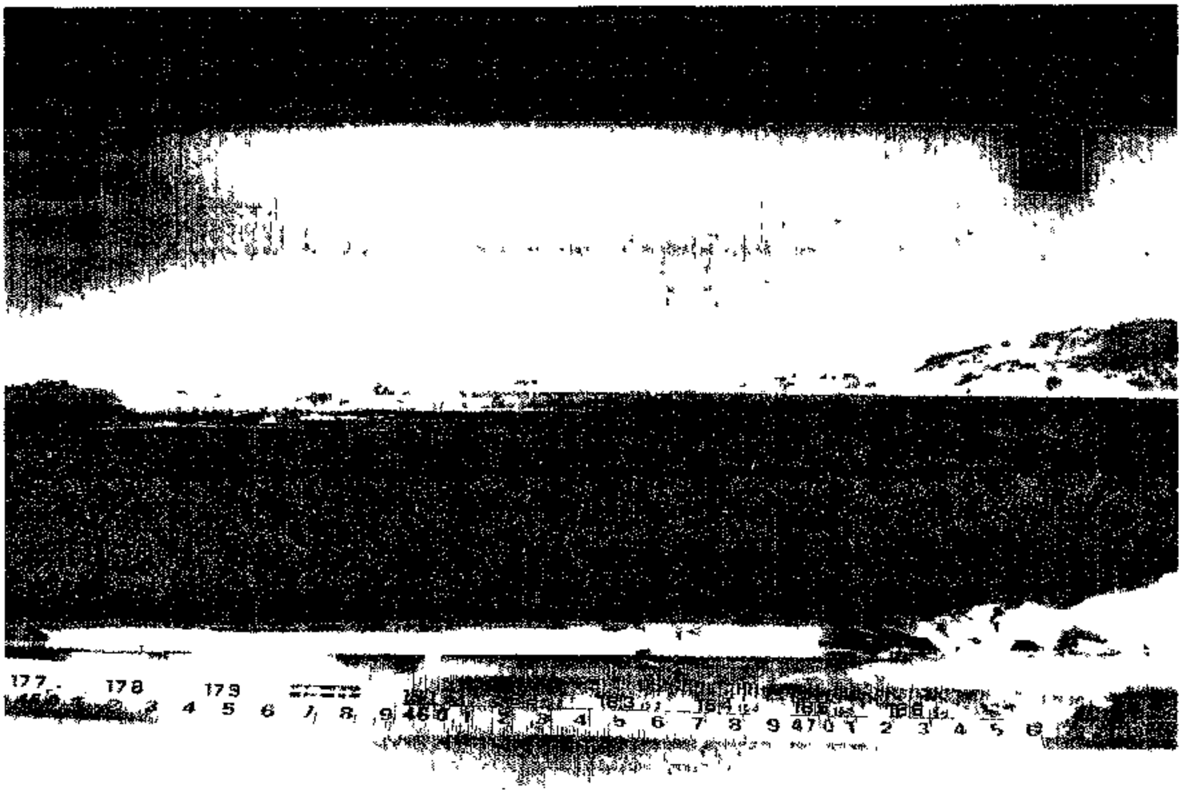

Image: Core 8A-Bottom.JPG

Appendix B: Digital core surface photographs - Mer Bleue Core -Image 30

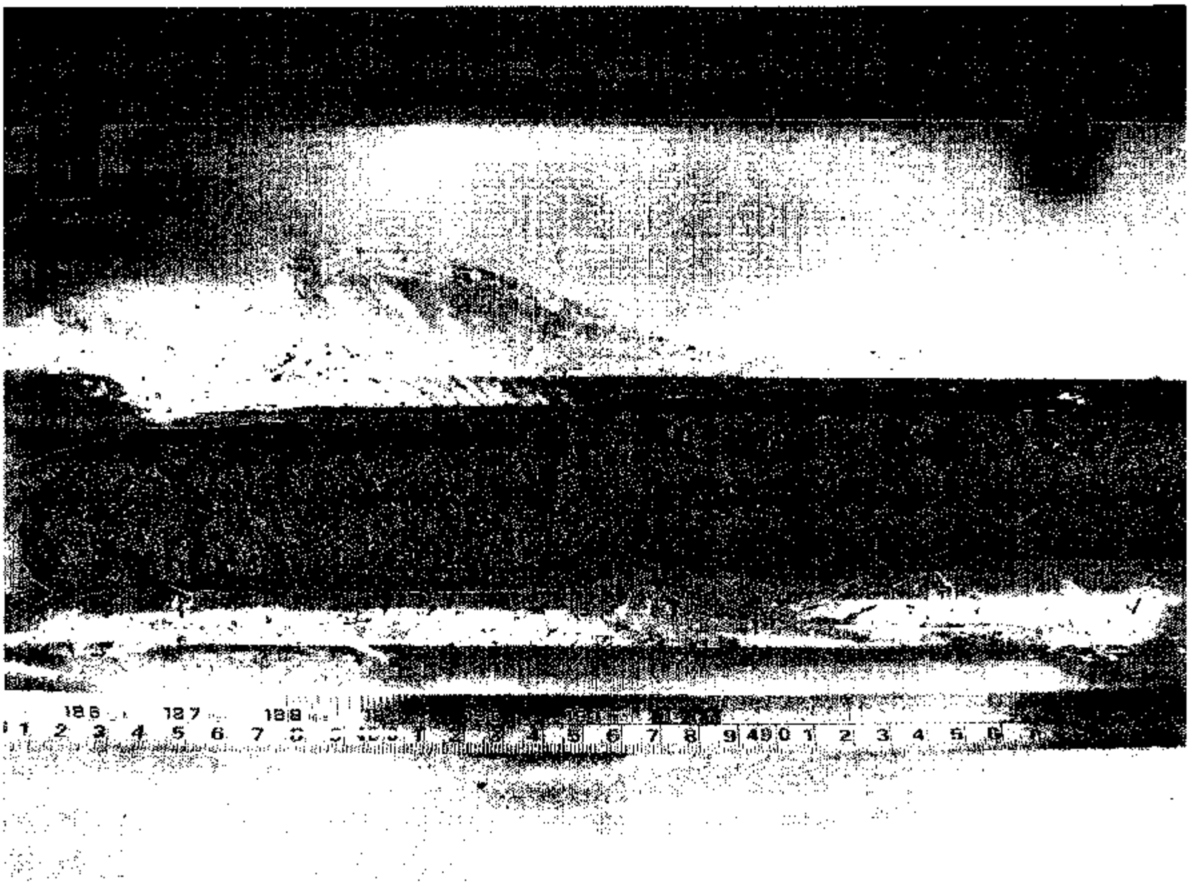

Image: Core 8B-Top.JPG

Appendix B: Digital core surface photographs - Mer Bleue Core -Image 31

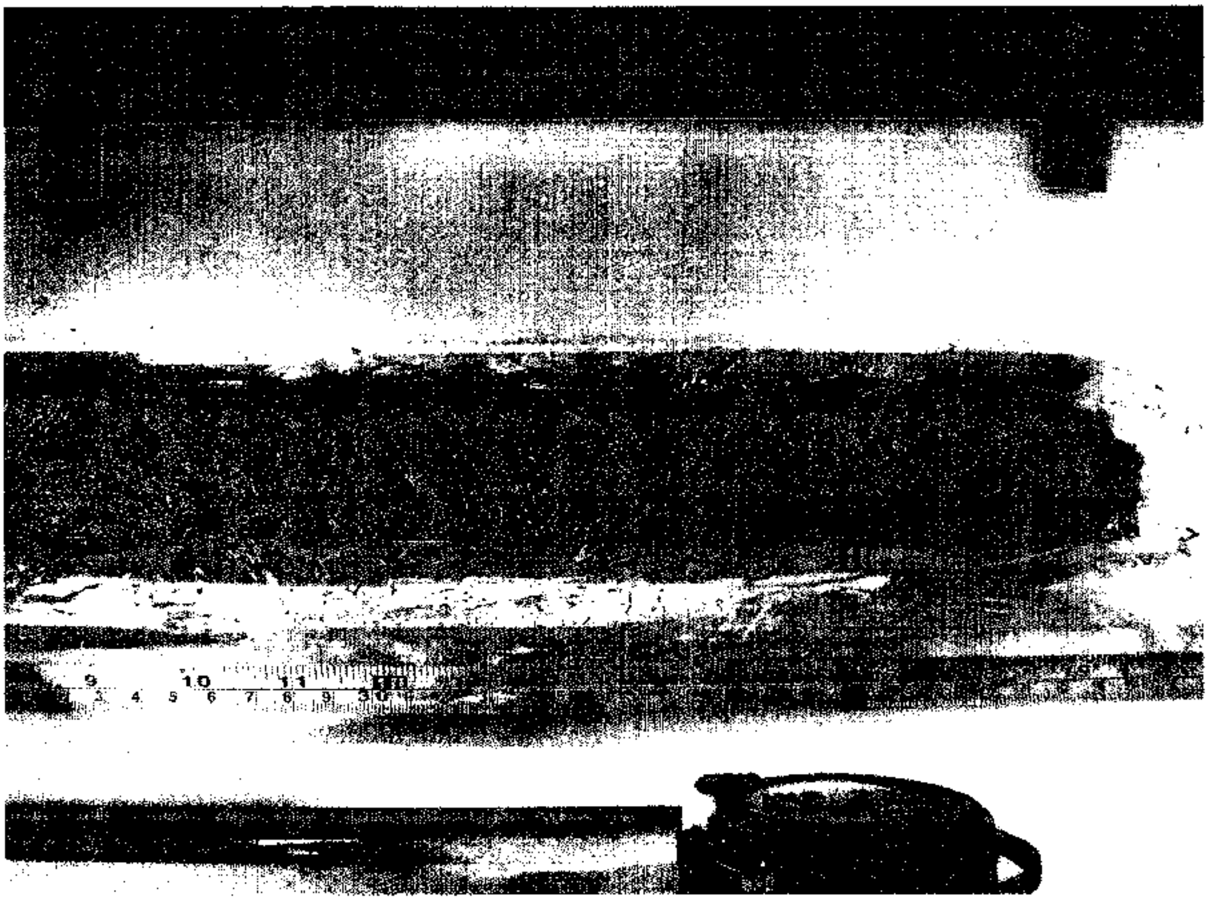

Image: Core 8B-Bottom.JPG

Appendix B: Digital core surface photographs - Mer Bleue Core -Image 32

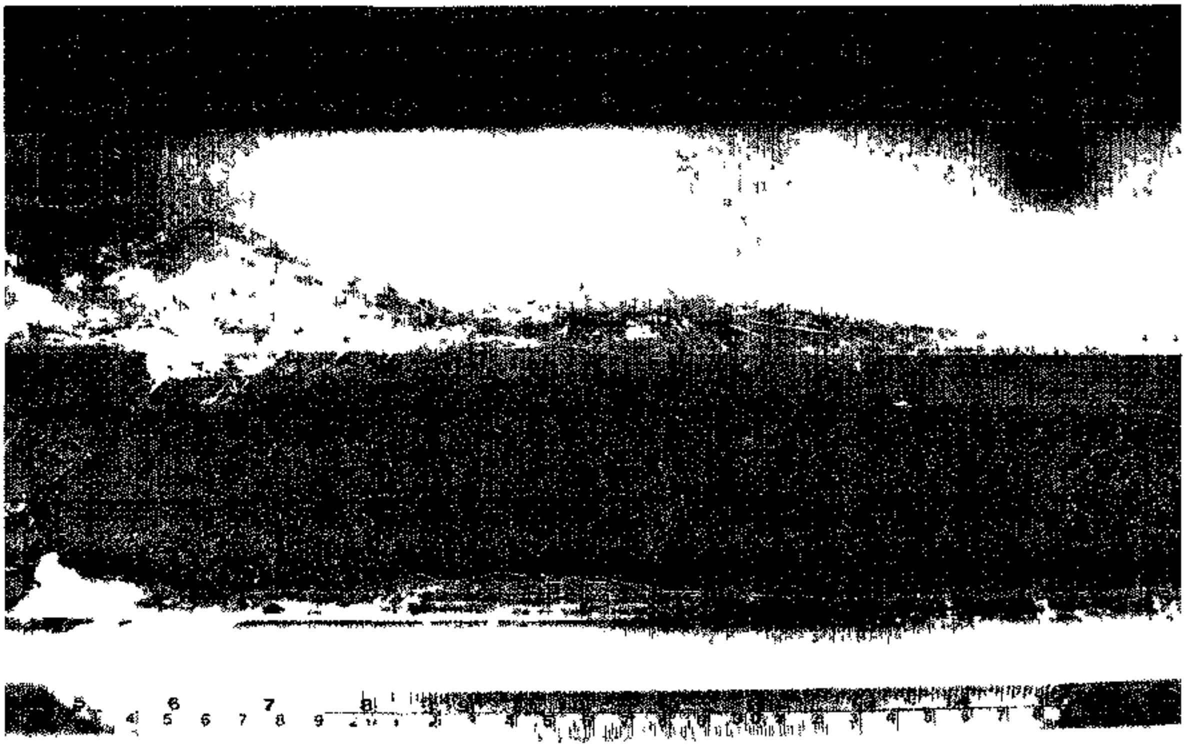

Image: Core 9A-Top.JPG

Appendix B: Digital core surface photographs - Mer Bleue Core -Image 33

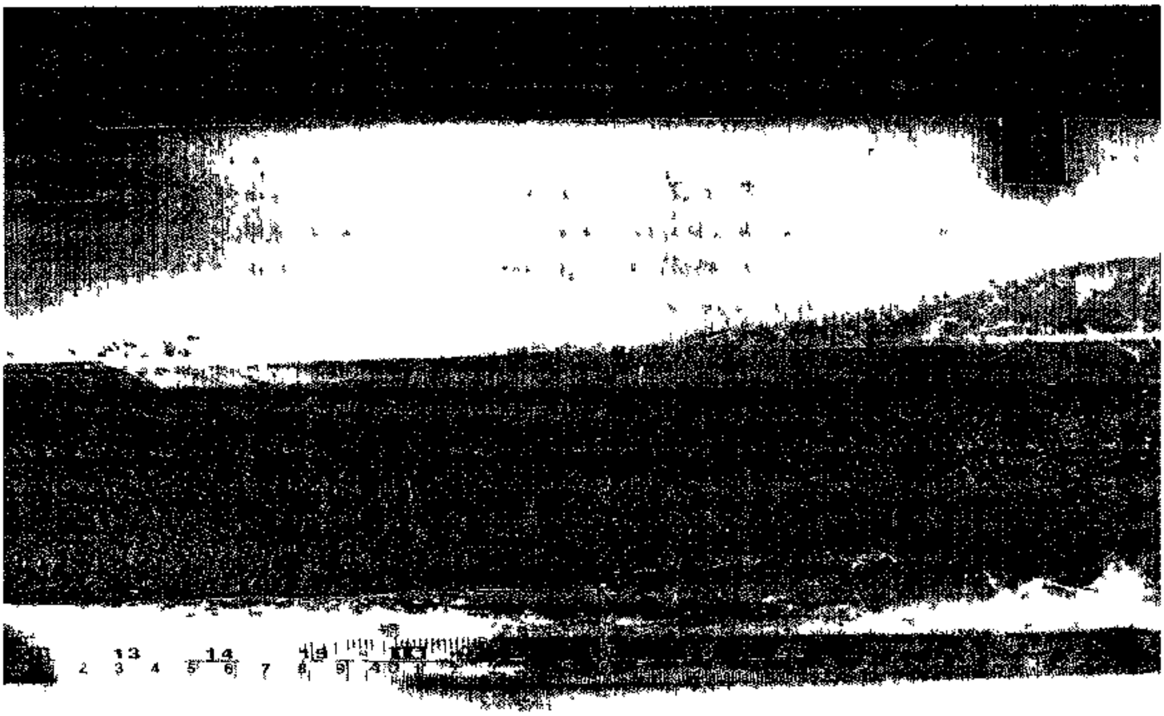

Image: Core 9A-Bottom.JPG

Appendix B: Digital core surface photographs - Mer Bleue Core -Image 34

Image: Core 9B-Top.JPG

Appendix B: Digital core surface photographs - Mer Bleue Core -Image 35

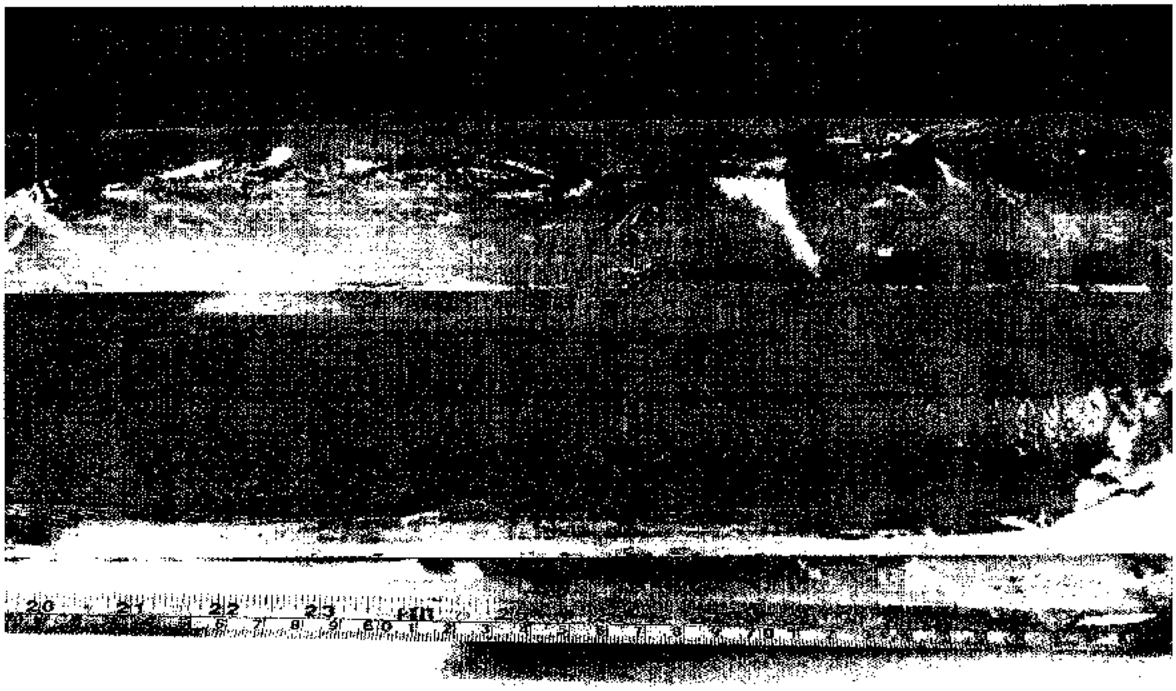

Image: Core 9B-Bottom.JPG

Appendix C: Radiocarbon Ages for Mer Bleue Core -Chronos Lab, Belfast

Suzanne Elliott
Queen's University
University Road
Belfast BT7 1NN
Northern Ireland

14CHRONO

^{14}CHRONO Centre
Queens University Belfast
42 Fitzwilliam Street
Belfast BT9 6AX
Northern Ireland

Radiocarbon Date Certificate

UBANo	Sample ID	^{14}C Age	±	AMS δ^{13}C	F14C	±
UBA-11976	MB16			-29.6	1.2544	0.0029
UBA-11977	MB22			-28.2	1.0840	0.0024
UBA-11978	MB31	204	28	-28.3	0.9749	0.0034
UBA-11979	MB61	1566	26	-29.2	0.8229	0.0027
UBA-11980	MB93	2860	22	-24.4	0.7005	0.0019
UBA-11981	MB99	2959	22	-26.0	0.6918	0.0019

UBANo	Sample ID	^{14}C Age	±	AMS δ^{13}C	F14C	±
UBA-11982	MB137	4449	32	-29.4	0.5747	0.0023
UBA-11983	MB163	4659	31	-28.4	0.5599	0.0022
UBA-11984	MB185	5934	33	-26.1	0.4777	0.0020

Appendix D: Radiocarbon Ages for Mer Bleue Core -Univ. of Georgia

RADIOCARBON ANALYSIS REPORT

University of Georgia
Center for Applied Isotope Studies

October 1, 2009

UGAMS #	Sample ID	Material	$\delta^{13}C$ in ‰	^{14}C age, years BP	±	pMC	±
5026	MB 23	peat	-27.4	post-bomb		144.39	0.41
5027	MB 210	peat	-27.1	6070	30	47.00	0.17
5028	MB 240	peat	-28.0	6130	30	46.62	0.18
5029	MB 280	peat	-22.4	7640	30	38.63	0.14

The peat samples were sieved through nylon screen to remove any roots and plant fragments. The peat was treated with 1N HCl to remove any carbonates, after that the samples was filtered on fiberglass filter, washed with deionized water and dried at 105°C. For accelerator mass spectrometry analysis the cleaned sample was combusted at 900°C in evacuated / sealed ampoules in the presence of CuO. The resulting carbon dioxide was cryogenically purified from the other reaction products and catalytically converted to graphite using the method of Vogel *et al.* (1984) Nuclear Instruments and Methods in Physics Research B5, 289-293. Graphite $^{14}C/^{13}C$ ratios were measured using the CAIS 0.5 MeV accelerator mass spectrometer. The sample ratios were compared to the ratio measured from the Oxalic Acid I (NBS SRM 4990). The sample $^{13}C/^{12}C$ ratios were measured separately using a stable isotope ratio mass spectrometer and expressed as $\delta^{13}C$ with respect to PDB, with an error of less than 0.1‰.
The quoted uncalibrated dates have been given in radiocarbon years before 1950 (years BP), using the ^{14}C half-life of 5568 years. The error is quoted as one standard deviation and reflects both statistical and experimental errors. The date has been corrected for isotope fractionation.

Appendix E: Calibrated radiocarbon ages for Mer Bleue Core using CALIB5.0.2 - part 1

```
CALIB RADIOCARBON CALIBRATION PROGRAM*
Copyright 1986-2006 M Stuiver and PJ Reimer

*To be used in conjunction with:
 Stuiver, M., and Reimer, P.J., 1993, Radiocarbon, 35, 215-230.

Labcode MB16
Description
Radiocarbon Age BP -1820 +/- 18
Calibration data set: intcal04.14c # Reimer et al. 2004
*Invalid age* for this calibration curve

Labcode MB22
Description
Radiocarbon Age BP -648 +/- 18
Calibration data set: intcal04.14c # Reimer et al. 2004
*Invalid age* for this calibration curve


Labcode MB31
Description
Radiocarbon Age 204±28
Calibration data set: intcal04.14c # Reimer et al. 2004
10 Year moving average
One Sigma Ranges: [start:end] relative area
                  [cal AD 1657: cal AD 1678] 0.310193
                  [cal AD 1766: cal AD 1801] 0.523314
                  [cal AD 1940: cal AD 1951*] 0.166493
Two Sigma Ranges: [start:end] relative area
                  [cal AD 1648: cal AD 1684] 0.290673
                  [cal AD 1734: cal AD 1806] 0.554229
                  [cal AD 1930: cal AD 1951*] 0.155098

Labcode MB61
Description
Radiocarbon Age 1566±26
Calibration data set: intcal04.14c # Reimer et al. 2004
10 Year moving average
One Sigma Ranges: [start:end] relative area
                  [cal AD 436: cal AD 492] 0.708437
                  [cal AD 507: cal AD 520] 0.152246
                  [cal AD 528: cal AD 539] 0.139316
Two Sigma Ranges: [start:end] relative area
                  [cal AD 424: cal AD 552] 1.
```

Appendix E: Calibrated radiocarbon ages for Mer Bleue Core using CALIB5.0.2 - part 2

```
Labcode MB93
Description
Radiocarbon Age 2860±22
Calibration data set: intcal04.14c # Reimer et al. 2004
10 Year moving average
One Sigma Ranges: [start:end] relative area
                  [cal BC 1071: cal BC 1068] 0.017393
                  [cal BC 1057: cal BC 978] 0.982607
Two Sigma Ranges: [start:end] relative area
                  [cal BC 1118: cal BC 973] 0.93944
                  [cal BC 958: cal BC 938] 0.06056

Labcode MB99
Description
Radiocarbon Age 2959±22
Calibration data set: intcal04.14c # Reimer et al. 2004
10 Year moving average
One Sigma Ranges: [start:end] relative area
                  [cal BC 1254: cal BC 1239] 0.151497
                  [cal BC 1214: cal BC 1154] 0.633489
                  [cal BC 1148: cal BC 1129] 0.215014
Two Sigma Ranges: [start:end] relative area
                  [cal BC 1269: cal BC 1112] 0.982415
                  [cal BC 1100: cal BC 1085] 0.012924
                  [cal BC 1064: cal BC 1058] 0.004661

Labcode MB137
Description
Radiocarbon Age 4449±32
Calibration data set: intcal04.14c # Reimer et al. 2004
10 Year moving average
One Sigma Ranges: [start:end] relative area
                  [cal BC 3318: cal BC 3271] 0.237109
                  [cal BC 3268: cal BC 3236] 0.209889
                  [cal BC 3169: cal BC 3163] 0.026216
                  [cal BC 3111: cal BC 3079] 0.206002
                  [cal BC 3071: cal BC 3024] 0.320784
Two Sigma Ranges: [start:end] relative area
                  [cal BC 3335: cal BC 3210] 0.417678
                  [cal BC 3192: cal BC 3151] 0.081551
                  [cal BC 3138: cal BC 3010] 0.470411
                  [cal BC 2981: cal BC 2958] 0.019591
                  [cal BC 2952: cal BC 2939] 0.01077
```

Appendix E: Calibrated radiocarbon ages for Mer Bleue Core using CALIB5.0.2 - part 3

```
Labcode MB163
Description
Radiocarbon Age 4659±31
Calibration data set: intcal04.14c # Reimer et al. 2004
10 Year moving average
One Sigma Ranges: [start:end] relative area
                  [cal BC 3505: cal BC 3481] 0.261169
                  [cal BC 3478: cal BC 3427] 0.613972
                  [cal BC 3381: cal BC 3370] 0.124859
Two Sigma Ranges: [start:end] relative area
                  [cal BC 3518: cal BC 3365] 1.

Labcode MB185
Description
Radiocarbon Age 5934±33
Calibration data set: intcal04.14c # Reimer et al. 2004
10 Year moving average
One Sigma Ranges: [start:end] relative area
                  [cal BC 4845: cal BC 4768] 0.929027
                  [cal BC 4754: cal BC 4744] 0.070973
Two Sigma Ranges: [start:end] relative area
                  [cal BC 4903: cal BC 4864] 0.106669
                  [cal BC 4856: cal BC 4721] 0.893331

Labcode MB 210
Description
Radiocarbon Age 6070±30
Calibration data set: intcal04.14c # Reimer et al. 2004
10 Year moving average
One Sigma Ranges: [start:end] relative area
                  [cal BC 5020: cal BC 4940] 1.
Two Sigma Ranges: [start:end] relative area
                  [cal BC 5190: cal BC 5185] 0.004456
                  [cal BC 5057: cal BC 4896] 0.969955
                  [cal BC 4867: cal BC 4851] 0.025589

Labcode MB 240
Description
Radiocarbon Age 6130±30
Calibration data set: intcal04.14c # Reimer et al. 2004
10 Year moving average
One Sigma Ranges: [start:end] relative area
                  [cal BC 5205: cal BC 5167] 0.312964
                  [cal BC 5076: cal BC 4999] 0.687036
Two Sigma Ranges: [start:end] relative area
                  [cal BC 5208: cal BC 4992] 1.
```

Appendix E: Calibrated radiocarbon ages for Mer Bleue Core using CALIB5.0.2 - part 4

```
Labcode MB 280
Description
Radiocarbon Age 7640±30
Calibration data set: intcal04.14c # Reimer et al. 2004
10 Year moving average
One Sigma Ranges: [start:end] relative area
                  [cal BC 6496: cal BC 6450] 1.
Two Sigma Ranges: [start:end] relative area
                  [cal BC 6568: cal BC 6544] 0.06484
                  [cal BC 6531: cal BC 6435] 0.93516

Ranges marked with a * are suspect due to impingment on the end of
the calibration data set
```

References for calibration datasets:
PJ Reimer, MGL Baillie, E Bard, A Bayliss, JW Beck, C Bertrand, PG Blackwell,
CE Buck, G Burr, KB Cutler, PE Damon, RL Edwards, RG Fairbanks, M Friedrich,
TP Guilderson, KA Hughen, B Kromer, FG McCormac, S Manning, C Bronk Ramsey,
RW Reimer, S Remmele, JR Southon, M Stuiver, S Talamo, FW Taylor,
J van der Plicht, and CE Weyhenmeyer (2004), Radiocarbon 46:1029-1058.

```
Comments:
* This standard deviation (error) includes a lab error multiplier.
** 1 sigma = square root of (sample std. dev.^2 + curve std. dev.^2)
** 2 sigma = 2 x square root of (sample std. dev.^2 + curve std. dev.^2)
where ^2 = quantity squared.
[ ] = calibrated range impinges on end of calibration data set
0* represents a "negative" age BP
1955* or 1960* denote influence of nuclear testing C-14
NOTE: Cal ages and ranges are rounded to the nearest year which
may be too precise in many instances. Users are advised to
round results to the nearest 10 yr for samples with standard
deviation in the radiocarbon age greater than 50 yr.
```

Appendix F: Coring strategy - Mer Bleue Core -Part 1

Field sampling date: 13th March 2008.
Sampling site coordinates: N45° 24'.653"
W75°31'.064"

Coring:

- **1A1:** 0-17 cm
  1A2: 0-21 cm
  1A3: 0-29 cm

- **1B1:** 17-43 cm
  1B2: 17-53 cm
  1B3: 17- 55 cm

- **2A1:** 40-91 cm
  2A2: 40-91 cm
  2A3: 40-91 cm

- **2B1:** 71-121 cm
  2B2: 71-121 cm
  2B3: 71-121 cm

- **3A1:** 1-1.50 m
  3A2: 1-1.50 m
  3A3: 1-1.50 m

- **3B1**: 1.30-1.80 m
  3B2: 1.30-1.80 m
  3B3: 1.30-1.80 m

- **4A1:** 1.60-2.10 m
  4A2: 1.60-2.10 m
  4A3: 1.60-2.10 m

- **4B1:** 1.90-2.40 m
  4B2: 1.90-2.40 m
  4B3: 1.90-2.40 m

- **5A1:** 2.20-2.70 m
  5A2: 2.20-2.70 m
  5A3: 2.20-2.70 m

- **5B1:** 2.50-3 m
  5B2: 2.50-3 m
  5B3: 2.50-3 m

Appendix F: Coring strategy - Mer Bleue Core -Part 2

- **6A1:** 2.80-3.30 m
  6A2: 2.80-3.30 m
  6A3: 2.80-3.30 m

- **6B1:** 3.10-3.60 m
  6B2: 3.10-3.60 m
  6B3: 3.10-3.60 m

- **7A1:** 3.50-4 m
  7A2: 3.50-4 m
  7A3: 3.50-4 m

- **7B1:** 3.90-4.40 m
  7B2: 3.90-4.40 m
  7B3: 3.90-4.40 m

- **8A1:** 4.30-4.80 m
  8A2: 4.30-4.80 m
  8A3: 4.30-4.80 m

- **8B1:** 4.70-5.20 m
  8B2: 4.70-5.20 m
  8B3: 4.70-5.20 m

- **9A1:** 5.10-5.60 m
  9A2: 5.10-5.60 m
  9A3: 5.10-5.60 m

- **9B1:** 5.50-6 m
  9B2: 5.50-6 m
  9B3: 5.50-6 m

Appendix F: Coring strategy - Mer Bleue Core -Part 3

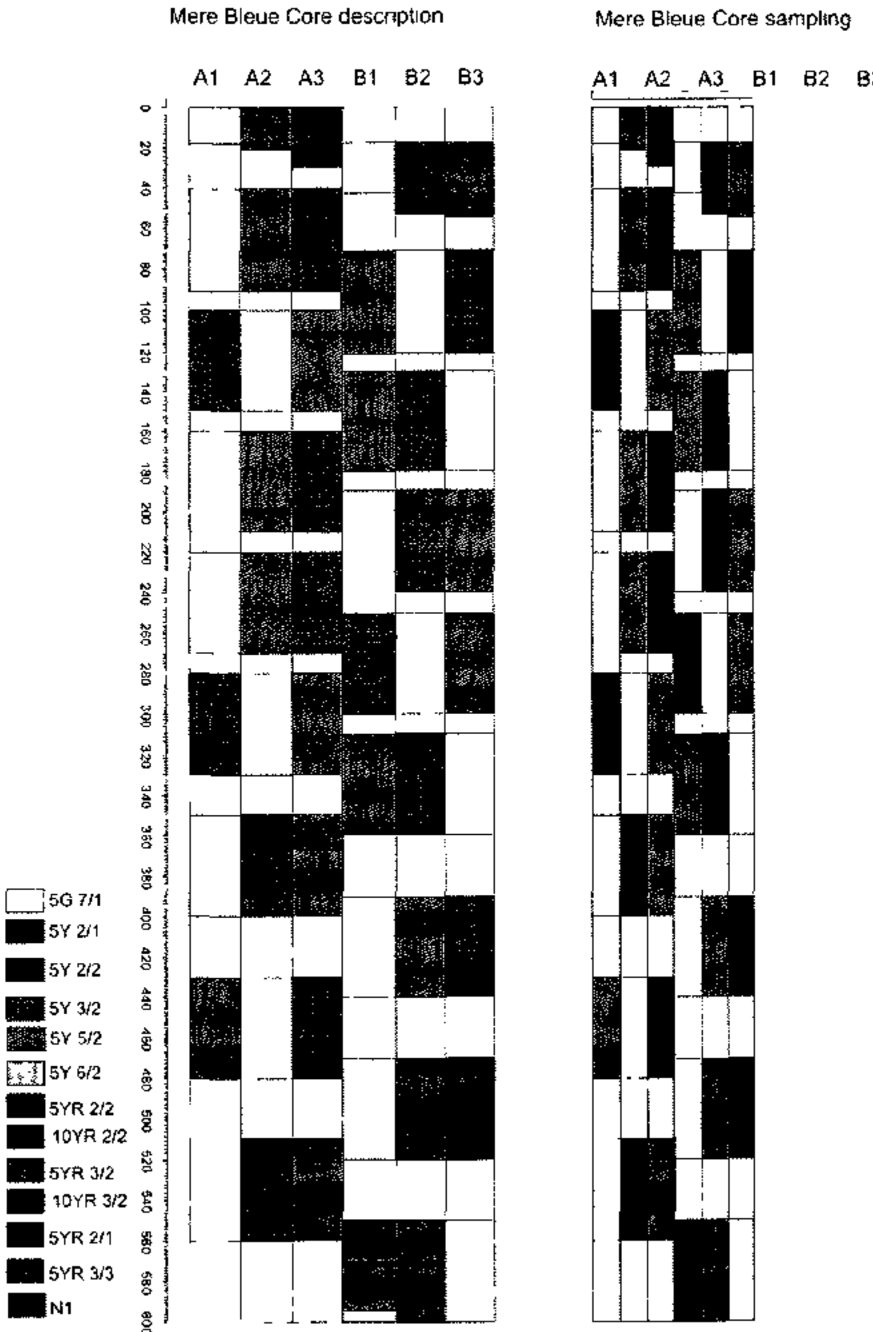

Munsell-color Munsell-color/red – Master core -archived
green - Sampling core # 1 (Carleton University)
grey - Sampling core #2 (Queen's University Belfast)

Appendix G: Sampling - Mer Bleue Core part 1

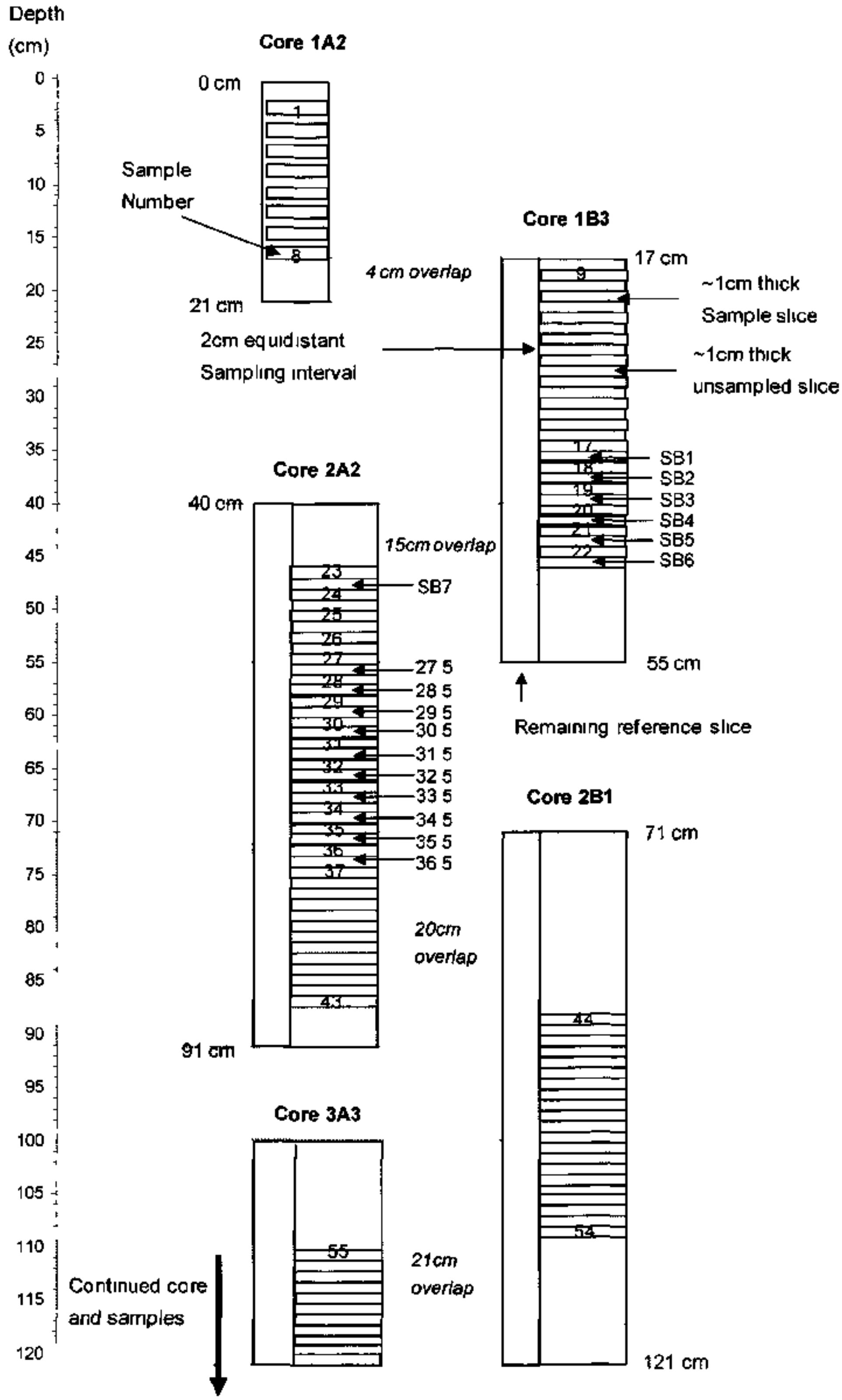

Appendix G: Sampling - Mer Bleue Core part 2

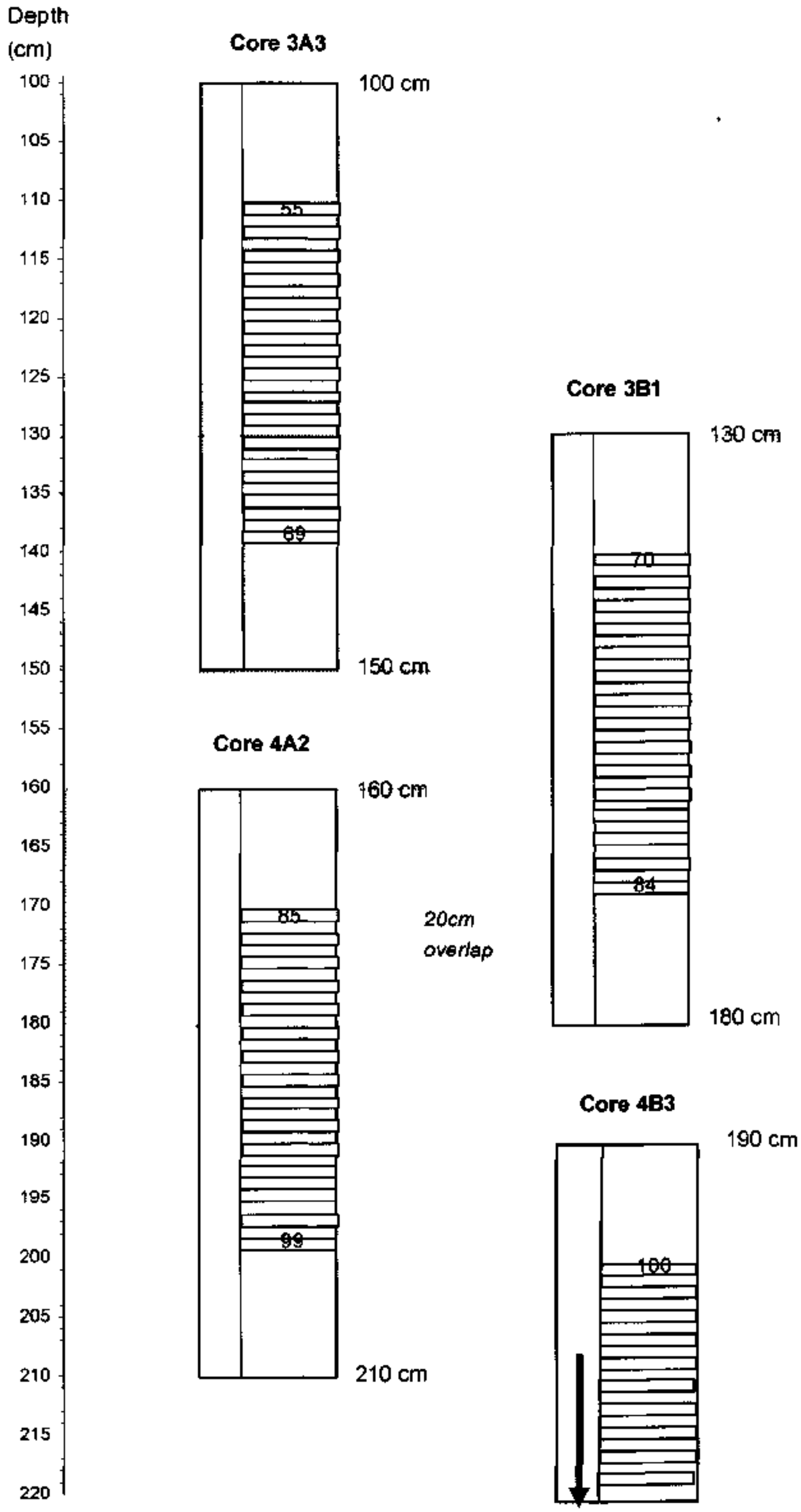

Appendix G: Sampling - Mer Bleue Core part 3

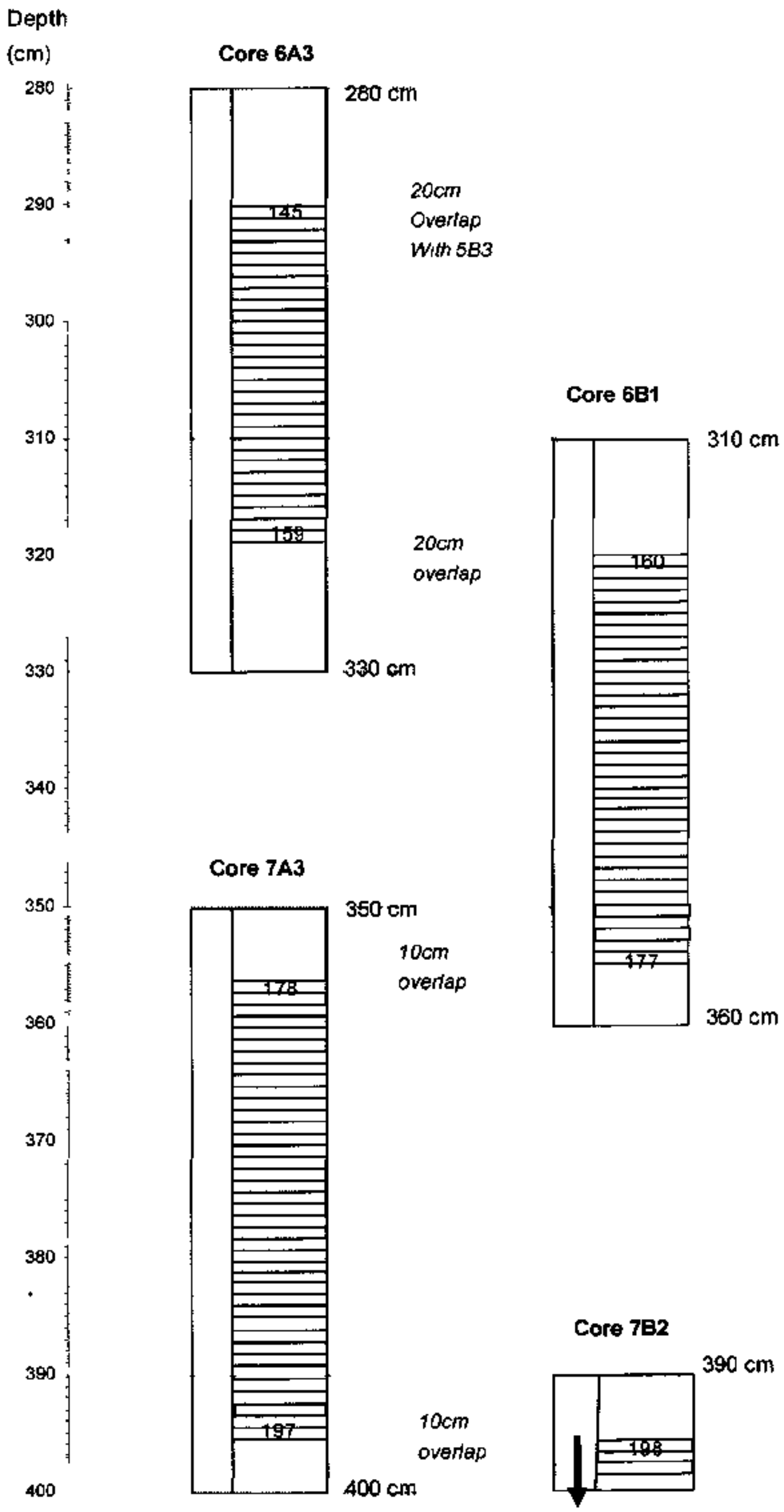

Appendix G: Sampling - Mer Bleue Core part 4

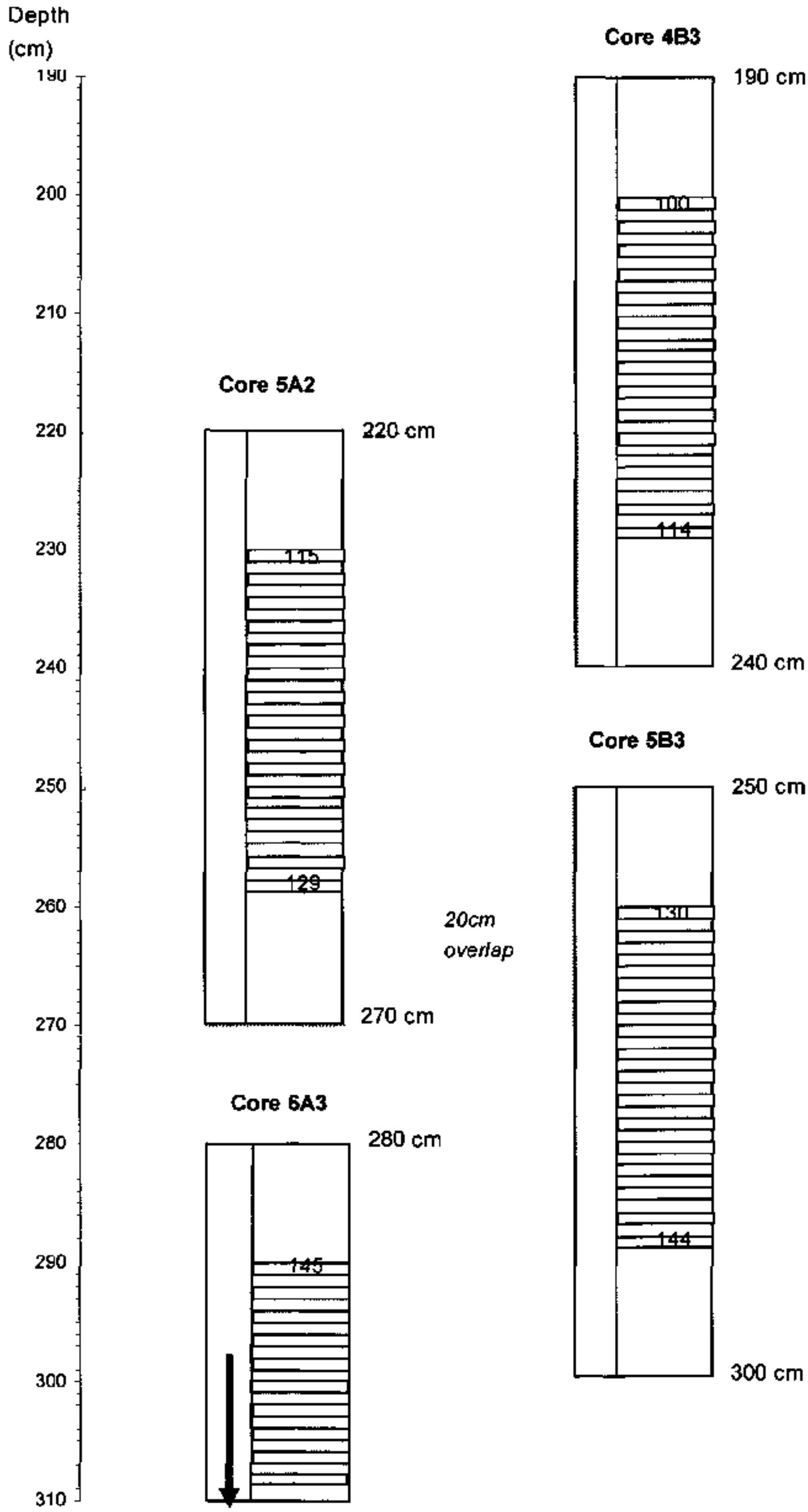

Appendix G: Sampling - Mer Bleue Core part 5

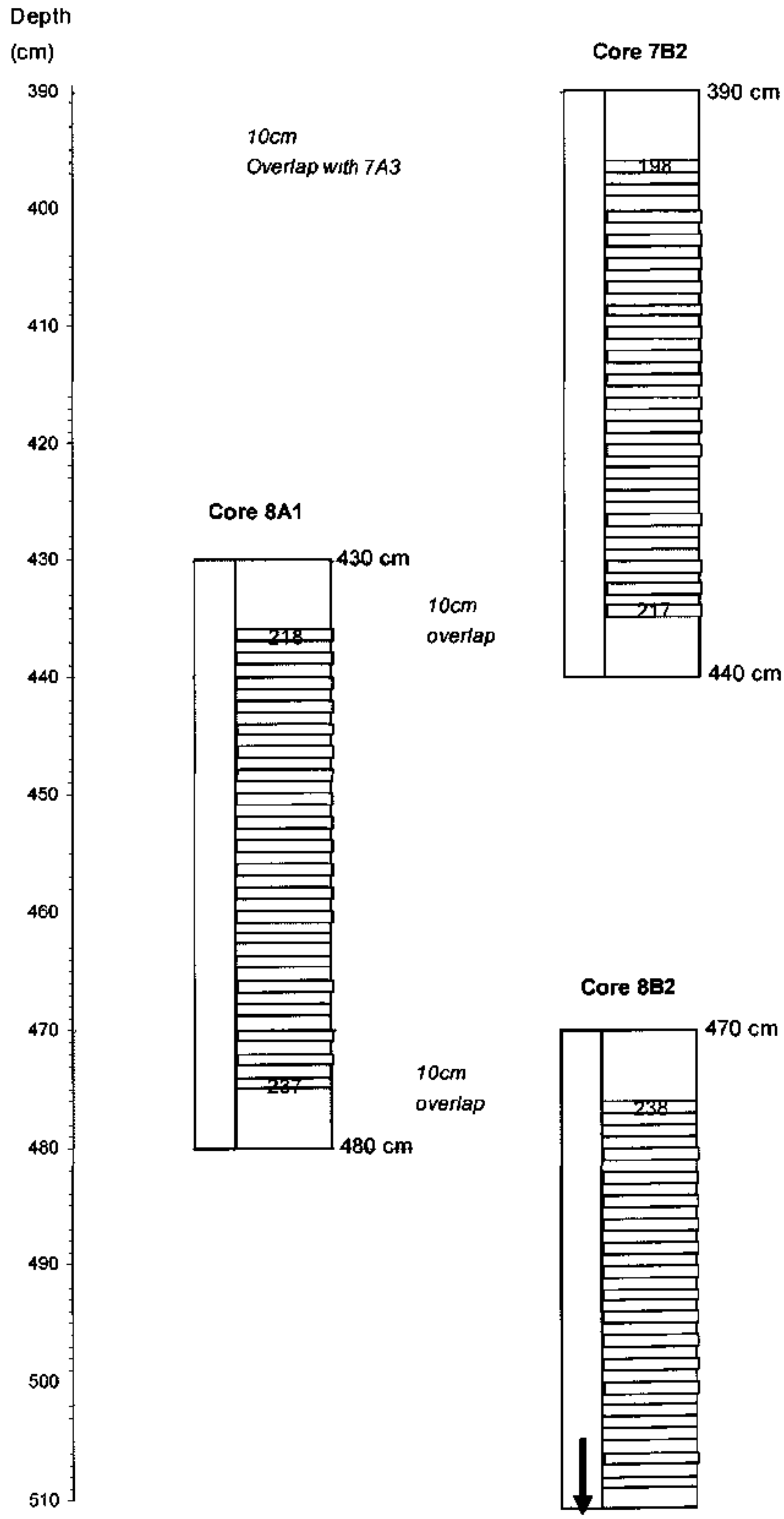

Appendix G: Sampling - Mer Bleue Core part 6

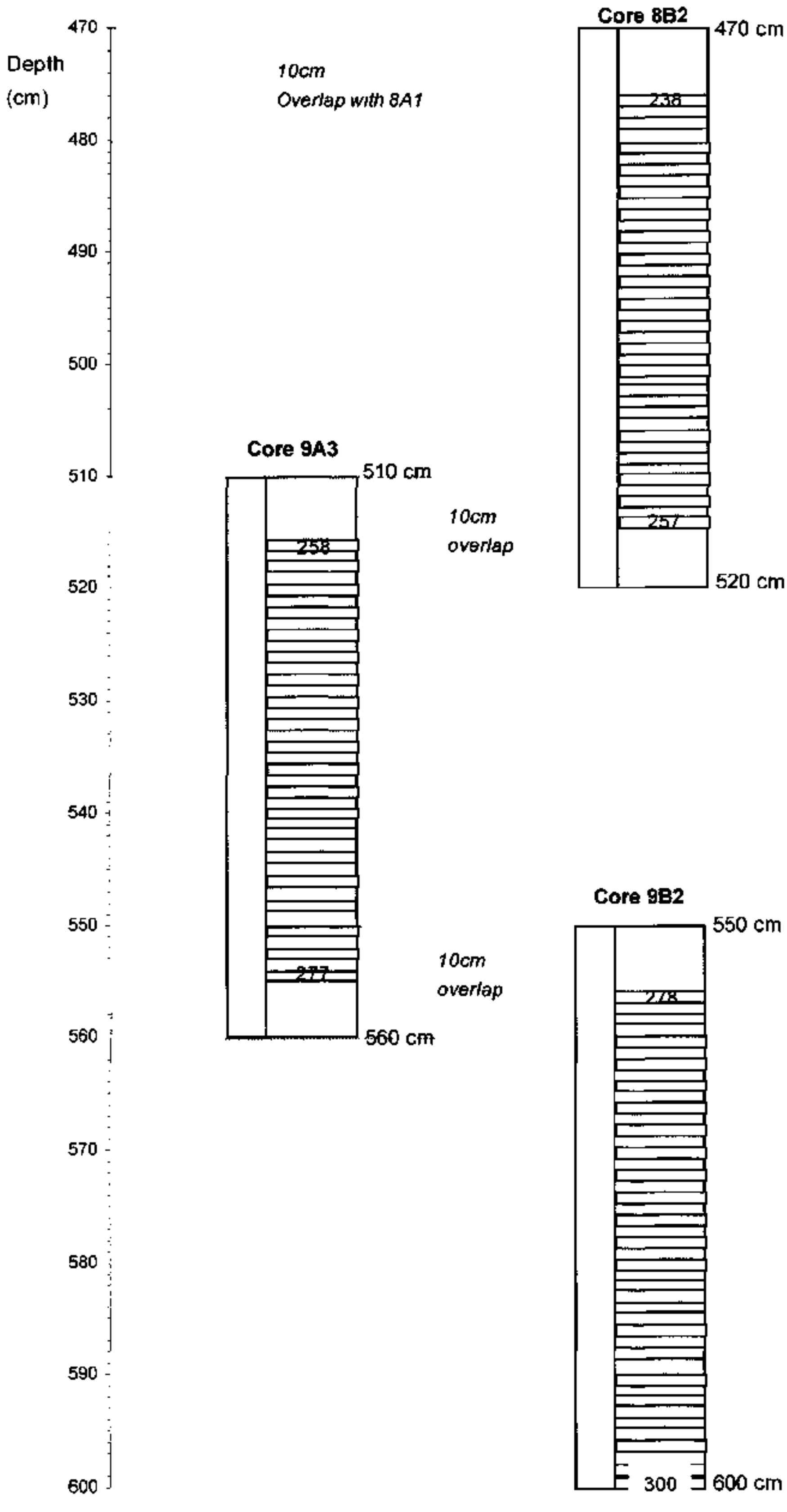

Appendix H: $\delta^{18}O_{cellulose}$ and Oxygen concentration - Mer Bleue Core part 1

Sample ID	Depth (cm)	%O	δ18O (‰, VSMOW)	Macrofossils Taxa
1yss	2	41.4	18.61	*S. capillifolium*
2yss	4	42.0	18.32	*S. capillifolium*
3r	6	37.3	19.14	Rhizome
4yss	8	43.3	20.22	*S. capillifolium*
5yss	10	43.4	20.64	*S. capillifolium*
6yss	12	42.7	18.88	*S. capillifolium*
7yss	14	42.4	19.28	*S. capillifolium*
8yss	16	43.4	20.05	*S. capillifolium*
9yss	18	41.7	16.91	*S. capillifolium*
10yss	20	41.7	17.13	*S. capillifolium*
10bss	20	42.9	18.58	*S. fuscum*
11yss	22	41.9	18.48	*S. capillifolium*
12yss	24	42.8	18.64	*S. capillifolium*
13yss	26	43.2	19.34	*S. capillifolium*
14yss	28	36.8	17.17	*S. capillifolium*
15yss	30	43.8	19.38	*S. capillifolium*
16yss	32	43.7	18.95	*S. capillifolium*
17yss	34	45.1	19.08	*S. capillifolium*
Sb1yss	35	43.6	18.99	*S. capillifolium*
18yss	36	43.4	20.43	*S. capillifolium*
Sb2yss	37	44.0	17.82	*S. capillifolium*
Sb2bss	37	41.0	18.94	*S. fuscum*
19yss	38	44.5	19.32	*S. capillifolium*
Sb3bss	39	42.3	19.49	*S. fuscum*
20bss	40	42.6	17.88	*S. fuscum*
Sb4yss	41	43.1	21.32	*S. capillifolium*
21yss	42	40.8	18.13	*S. capillifolium*
Sb5yss	43	43.6	18.15	*S. capillifolium*
22yss	44	46.0	17.41	*S. capillifolium*
Sb6yss	45	45.4	16.89	*S. capillifolium*
23yss	46	46.6	18.13	*S. capillifolium*
Sb7yss	47	43.0	20.28	*S. capillifolium*
24yss	48	48.2	18.38	*S. capillifolium*
25yss	50	45.1	19.18	*S. capillifolium*
26yss	52	44.0	18.92	*S. capillifolium*
27yss	54	45.4	19.97	*S. capillifolium*
27.5yss	55	44.9	19.40	*S. capillifolium*
28yss	56	43.0	19.15	*S. capillifolium*
28.5yss	57	46.6	17.21	*S. capillifolium*
29yssRE	58	48.2	17.71	*S. capillifolium*
29yss	58	44.7	17.09	*S. capillifolium*
29.5yss	59	46.3	18.68	*S. capillifolium*
30yss	60	38.3	19.47	*S. capillifolium*
30.5yss	61	47.3	19.43	*S. capillifolium*
31yss	62	42.8	20.15	*S. capillifolium*
31.5yss	63	45.4	19.06	*S. capillifolium*
32bss	64	44.1	19.23	*S. fuscum*
32.5yss	65	44.8	17.17	*S. capillifolium*
33bss	66	44.5	18.57	*S. fuscum*
33.5yss	67	45.9	20.75	*S. capillifolium*
34bss	68	44.3	18.78	*S. fuscum*
34ayss	69	45.5	18.24	*S. capillifolium*
35bss	70	42.0	18.34	*S. fuscum*
35ayss	71	45.0	20.17	*S. capillifolium*
36bss	72	45.3	18.74	*S. fuscum*
36dbss	72	44.3	18.86	*S. magellanicum*
36ayss	73	45.9	19.52	*S. capillifolium*
37dbss	74	44.7	18.61	*S. magellanicum*
37bss	74	34.0	17.11	*S. fuscum*
38dbss	76	42.7	19.57	*S. magellanicum*
38bss	76	43.5	18.16	*S. fuscum*
39bss	78	43.1	19.38	*S. fuscum*

Sample ID	Depth (cm)	%O	δ18O (‰, VSMOW)	Macrofossils Taxa
98yss	196	41.0	17.74	*S. capillifolium*
99bss	198	41.2	17.80	*S. fuscum*
99yss	198	39.7	16.94	*S. capillifolium*
100	200	40.0	19.11	*S. fuscum*
101dbss	202	41.8	19.36	*S. magellanicum*
101 dbss repeat	202	40.5	19.72	*S. magellanicum*
102bss	204	42.1	19.18	*S. fuscum*
103dbss	206	40.9	19.68	*S. magellanicum*
104bss	208	40.6	19.26	*S. fuscum*
105bss	210	40.1	18.79	*S. fuscum*
105r	210	32.7	14.05	Rhizome
106bss	212	41.9	17.72	*S. fuscum*
107dbss	214	41.1	19.81	*S. magellanicum*
109bss	218	40.7	19.53	*S. angustifolium*
110bss	220	41.4	19.11	*S. fuscum*
111bss	222	35.0	17.49	*S. fuscum*
112bss	224	36.4	18.58	*S. fuscum*
113Lbss	226	39.1	20.00	*S. angustifolium*
114bss	228	40.3	19.74	*S. fuscum*
115bss	230	23.7	17.55	*S. fuscum*
115r	230	35.4	16.95	Rhizome
116bss	232	37.9	16.43	*S. fuscum*
117bss	234	39.6	18.16	*S. fuscum*
118r	236	38.7	19.14	Rhizome
119r	238	32.0	15.86	Rhizome
119bss	238	37.3	18.70	*S. fuscum*
120r	240	34.7	16.88	Rhizome
121r	242	35.3	16.77	Rhizome
121r repeat	242	39.1	18.18	Rhizome
121dbss	242	32.5	13.89	*S. magellanicum*
122DS	244	27.5	12.92	Root networks of Pteridophytae
122dbss	244	37.3	14.92	*S. magellanicum*
123dbss	246	39.0	19.54	*S. magellanicum*
124dbss	248	37.9	16.46	*S. magellanicum*
125r	250	34.9	15.19	Rhizome
125DS	250	26.3	12.11	Root networks of Pteridophytae
125bss	250	42.5	18.56	*S. fuscum*
126dbss	252	40.0	17.59	*S. magellanicum*
127dbss	254	41.3	18.67	*S. magellanicum*
129dbss	258	39.0	20.83	*S. magellanicum*
130dbss	260	41.6	18.47	*S. magellanicum*
131dbss	262	42.9	18.82	*S. magellanicum*
132dbss	264	40.2	17.98	*S. magellanicum*
133dbss	266	40.5	19.78	*S. magellanicum*
134DS	268	34.5	13.33	Root networks of Pteridophytae
135DS	270	35.6	14.95	Root networks of Pteridophytae
135r	270	37.4	17.63	Rhizome
136DS	272	33.9	13.11	Root networks of Pteridophytae
137dbss	274	42.5	21.92	*S. magellanicum*
139dbss	278	39.6	18.46	*S. magellanicum*
139r	278	lost	lost	Rhizome
140r	280	33.3	14.80	Rhizome
141r	282	30.5	15.08	Rhizome
142r	284	34.1	15.54	Rhizome
143r	286	33.0	14.26	Rhizome
145r	290	34.2	14.08	Rhizome
145bss	290	43.7	17.82	*S. fuscum*
146dbss	292	38.6	15.11	*S. magellanicum*
147r	294	30.9	17.71	Rhizome
148dbss	296	40.8	17.03	*S. magellanicum*
149r	298	28.9	15.67	Rhizome
150r	300	35.6	16.20	Rhizome

Appendix H: δ18O and oxygen concentration - Mer Bleue Core part 2

40bss	80	42 5	18 97	*S fuscum*	151r	302	32 3	16 56	Rhizome
41bss	82	43 8	18 21	*S fuscum*	151dbss	302	35 3	16 34	*S magellanicum*
42bss	84	43 7	19 68	*S fuscum*	152dbss	304	39 5	17 63	*S magellanicum*
43bss	86	43 3	18 09	*S fuscum*	153dbss	306	39 3	19 71	*S magellanicum*
44bss	88	40 4	18 45	*S fuscum*	154dbss	308	40 5	18 16	*S magellanicum*
45r	90	37 7	17 60	Rhizome	155dbss	310	36 6	15 27	*S magellanicum*
45Lbss	90	42 7	19 43	*S angustifolium*	157dbss	314	39 2	19 54	*S magellanicum*
46bss	92	40 1	18 49	*S fuscum*	158r	316	36 2	16 40	Rhizome
46r	92	34 3	15 65	Rhizome	159dbss	318	37 4	18 25	*S magellanicum*
47bss	94	39 9	23 21	*S fuscum*	160bss	320	40 2	17 75	*S fuscum*
48yss	96	43 1	19 56	*S capillifolium*	160dbss	320	41 3	17 21	*S magellanicum*
49bss	98	34 8	19 18	*S fuscum*	161dbss	322	38 1	17 34	*S magellanicum*
49yss	98	41 0	19 23	*S capillifolium*	162dbss	324	40 9	15 97	*S magellanicum*
50r	100	33 3	15 22	Rhizome	162bss	324	39 6	17 38	*S fuscum*
50yss	100	39 3	19 73	*S capillifolium*	163dbss	326	39 4	17 76	*S magellanicum*
51bss	102	40 5	19 80	*S fuscum*	164bss	328	39 0	16 89	*S fuscum*
52bss	104	41 4	20 27	*S fuscum*	165r	330	35 0	14 89	Rhizome
53dbss	106	33 0	19 21	*S magellanicum*	165bss	330	40 8	19 89	*S fuscum*
54dbss	108	39 5	19 22	*S magellanicum*	166bss	332	40 6	15 26	*S fuscum*
55Lbss	110	40 5	17 76	*S angustifolium*	167r	334	42 6	24 96	Rhizome
56yss	112	42 1	19 65	*S capillifolium*	167 r repeat	334	39 8	25 18	Rhizome
57bss	114	42 3	19 12	*S fuscum*	167bss	334	40 4	19 51	*S fuscum*
58yss	116	42 2	19 68	*S capillifolium*	168bss	336	38 9	16 79	*S fuscum*
59bss	118	37 6	19 70	*S fuscum*	169r	338	37 4	19 06	Rhizome
60bss	120	35 9	16 20	*S fuscum*	169bss	338	37 7	24 62	*S fuscum*
61bss	122	39 8	18 44	*S fuscum*	170syss	340	36 3	15 13	*S papillosum*
62bss	124	41 2	19 32	*S fuscum*	171r	342	30 6	13 53	Rhizome
63bss	126	49 3	19 06	*S fuscum*	171syss	342	39 3	15 17	*S papillosum*
64yss	128	37 2	19 23	*S capillifolium*	172syss	344	37 7	16 08	*S papillosum*
65Lbss	130	40 9	19 31	*S angustifolium*	173DS	346	37 5	17 88	Root networks of Pteridophytae
66yss	132	41 7	20 29	*S capillifolium*	174dbss	348	39 9	17 23	*S magellanicum*
67yss	134	41 1	21 42	*S capillifolium*	175bss	350	39 8	17 51	*S fuscum*
68yss	136	45 9	17 47	*S capillifolium*	176dbss	352	40 3	18 71	*S magellanicum*
69yss	138	39 8	18 37	*S capillifolium*	177dbss	354	39 7	18 99	*S magellanicum*
70yss	140	42 3	19 49	*S capillifolium*	178dbss	356	39 8	18 14	*S magellanicum*
71bss	142	43 7	19 50	*S fuscum*	179dbss	358	37 0	16 21	*S magellanicum*
72yss	144	41 5	19 50	*S capillifolium*	180dbss	360	40 0	17 69	*S magellanicum*
73bss	146	40 7	17 95	*S fuscum*	181DS	362	22 1	14 24	Root networks of Pteridophytae
74bss	148	41 4	18 42	*S fuscum*	181dbss	362	29 3	18 16	*S magellanicum*
75bss	150	42 6	18 50	*S fuscum*	185bss	370	39 5	17 06	*S fuscum*
76bss	152	39 5	18 16	*S fuscum*	190DS	380	36 1	14 59	Root networks of Pteridophytae
77bss	154	40 5	20 52	*S fuscum*	195bss	390	39 9	16 33	*S fuscum*
78bss	156	40 6	17 80	*S fuscum*	195dbss	390	37 0	15 63	*S magellanicum*
79bss	158	43 1	19 02	*S fuscum*	200r	400	33 3	16 97	Rhizome
80bss	160	39 4	19 69	*S fuscum*	205dbss	410	40 5	16 39	*S magellanicum*
81yss	162	42 1	19 50	*S capillifolium*	210bss	420	37 4	15 68	*S fuscum*
82bss	164	42 2	19 15	*S fuscum*	215bss	430	37 8	15 91	*S fuscum*
83bss	166	42 5	19 56	*S fuscum*	220 r	440	36 9	22 08	Rhizome
84bss	168	43 0	18 30	*S fuscum*	220rbl	440	34 8	13 38	Unknown Reddish brown leaves
85yss	170	41 5	19 28	*S capillifolium*	220dbss	440	39 7	16 85	*S magellanicum*
85r	170	38 4	19 61	Rhizome	225bss	450	40 6	16 85	*S fuscum*
86r	172	35 3	15 93	Rhizome	230bss	460	39 2	17 65	*S fuscum*
86yss	172	41 6	17 34	*S capillifolium*	230rbl	460	27 4	14 77	Unknown Reddish brown leaves
87yss	174	42 3	17 78	*S capillifolium*	235dbss	470	42 3	16 49	*S magellanicum*
88yss	176	42 0	17 37	*S capillifolium*	235r	470	36 3	16 83	Rhizome
89bss	178	35 3	17 94	*S fuscum*	240bss	480	40 2	16 99	*S fuscum*
90bss	180	41 9	17 61	*S fuscum*	245bss	490	42 5	15 17	*S fuscum*
91bss	182	41 4	17 36	*S fuscum*	250rbl	500	28 4	17 88	Unknown Reddish brown leaves
92bss	184	41 4	16 90	*S fuscum*	250dbss	500	39 0	15 08	*S magellanicum*
92r	184	36 4	13 47	Rhizome	255trh	510	35 5	13 19	Tissue remains of Herbacea
93bss	186	42 0	15 86	*S fuscum*	260bss	520	38 6	16 56	*S fuscum*
94bss	188	41 9	17 18	*S fuscum*	265trh	530	32 2	13 37	Tissue remains of Herbacea
95yss	190	41 3	18 09	*S capillifolium*	270trh	540	33 0	12 15	Tissue remains of Herbacea
95bss	190	35 8	16 74	*S fuscum*	275trh	550	34 7	12 10	Tissue remains of Herbacea
95r	190	40 2	18 66	Rhizome	280trh	560	29 8	11 94	Tissue remains of Herbacea
96bss	192	40 6	17 62	*S fuscum*	290trh	580	34 0	13 55	Tissue remains of Herbacea
97bss	194	41 0	18 29	*S fuscum*	295trh	590	33 5	7 99	Tissue remains of Herbacea
98bss	196	42 2	18 06	*S fuscum*					

Appendix I: X-Ray image – Glen West Monolith

X-ray image: tic interval = 1 inch
taken at Hospital Gatineau: July 14th, 2009

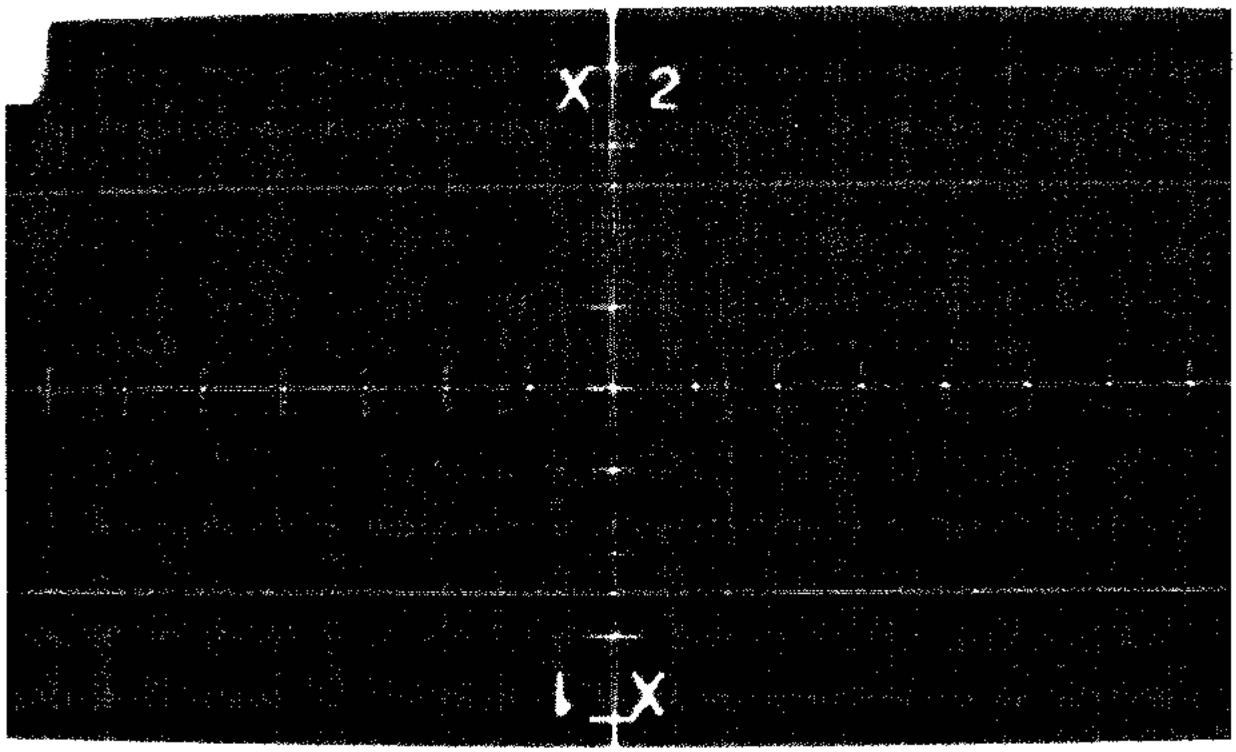

Appendix J: Digital core surface photographs - Glen West Monolith part 1

Monolith – upper part

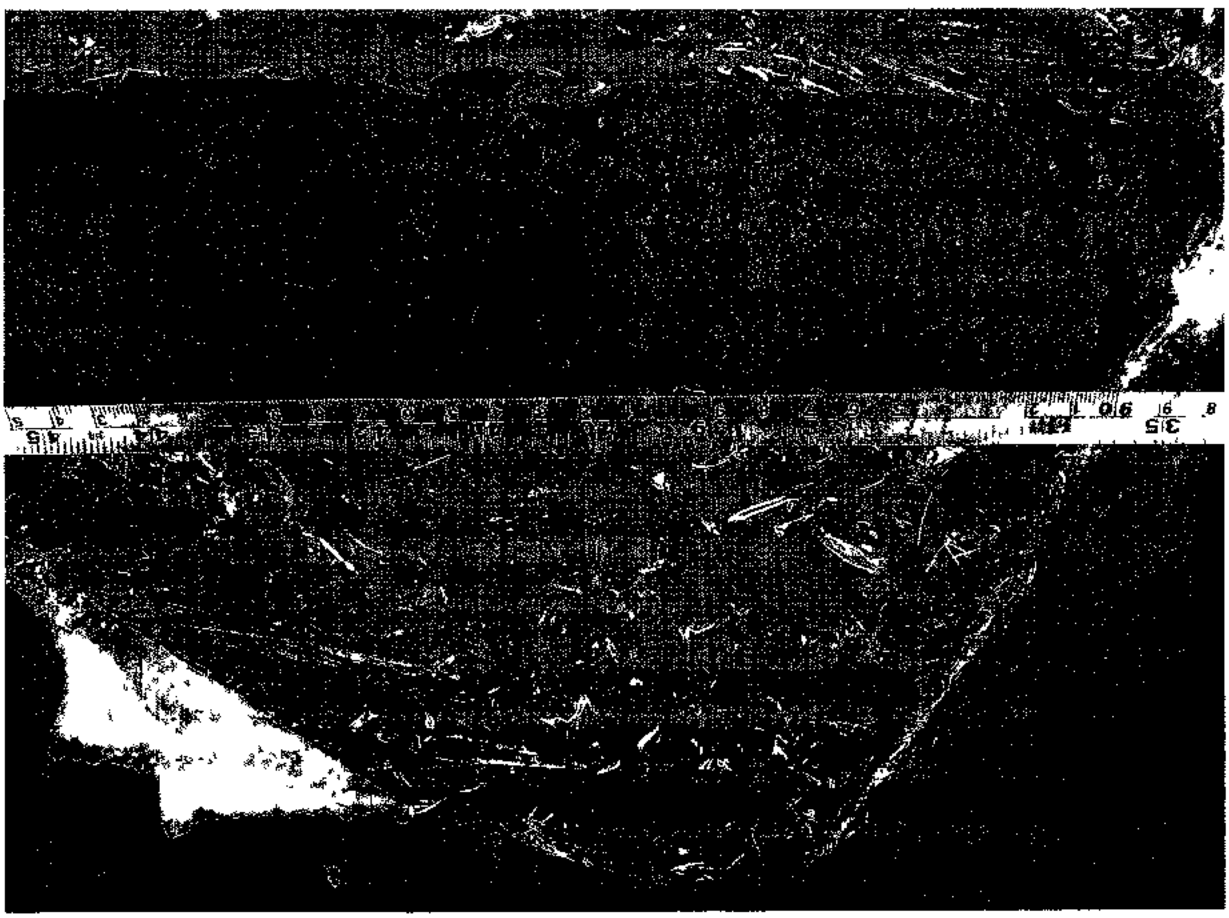

Appendix J: Digital core surface photographs - Glen West Monolith part 2

Monolith – lower part

Appendix K: $\delta^{18}O_{cellulose}$ and oxygen concentration measurements - Glen West Monolith

Operator Name: Tim Prokopiuk
Client Name: Hafida El Bilali
Project Name: Cellulose
Date Received: January 20 2010
Date Analyzed: February 2-5 2010

Billing Address: Hafida El Bilali
Dept of Earth Sciences
Carleton University
(613) 520-2600 ext 1851
ha'da.el@sympatico.ca

Data

41903	MON 1	90 25	34 08	16 73
41904	MON 2	90 75	26 98	31 33
41905	MON 3	91 25	35 07	18 07
41906	MON 4	91 75	38 57	23 45
41907	MON 5	92 25	34 15	16 37
41908	MON 6	92 76	39 59	20 22
41909	MON 7	93 26	34 90	16 56
41910	MON 8	93 75	42 21	22 12
41913	MON 9	94 26	42 19	20 54
41914	MON 10	94 75	41 56	22 17
41915	MON 11	95 26	32 99	15 20
41916	MON 12	95 75	42 43	22 07
41917	MON 13	96 25	39 81	20 68
41918	MON 14	96 75	40 98	20 58
41919	MON 15	97 25	41 20	21 73
41922	MON 16	97 75	41 16	21 47
41923	MON 17	98 25	41 27	21 86
41924	MON 18	98 75	41 81	20 89
41925	MON 19	99 25	42 34	21 26
41926	MON 20	99 76	41 86	21 07
41927	MON 21	100 25	42 06	19 35
41928	MON 22	100 75	42 49	20 36
41929	MON 23 S	101 25	42 49	20 64
41933	MON 24	101 75	41 69	21 87
41934	MON 25	102 25	42 36	20 41
41935	MON 26	102 75	41 67	20 86
41936	MON 28	103 75	42 76	20 00
41937	MON 30	104 75	43 27	21 37
41938	MON 32	105 75	38 51	19 02
41939	MON 34	106 75	42 04	20 16
41870	MON 36	107 75	44 95	20 52
41871	MON 38	108 75	42 24	20 35
41872	MON 40	109 75	45 03	18 49
41873	MON 42	110 75	43 14	20 53
41874	MON 44	111 75	45 06	19 87
41875	MON 46	112 75	41 17	17 75
41876	MON 48	113 75	42 09	20 46
41877	MON 50	114 75	43 45	20 78
41878	MON 52	115 75	43 50	19 57
41881	MON 54	116 75	40 36	20 78
41882	MON 56	117 75	41 25	18 81
41883	MON 58	118 75	43 65	20 29
41884	MON 60	119 75	43 57	20 62
41890	MON 5N	92 25	39 45	22 46

Standards

41930	IAEA-CH-3		50 31	32 84

Standard Accepted Values

AESAR Silver Phosphate	15 3		19 67
Benzoic B Benzoic Acid	26 3		20 76
IAEA-C3 Cellulose	49 3		32 68

Methodology

Cellulose samples are baked at 60°C in a vacuum oven for 2 hours to drive off moisture then immediately tranferred and flushed in the zero blank autosampler Samples are analyzed using a Thermo Finnigan TC/EA coupled to a Conflo III and a Delta Plus XL mass spectrometer Samples are dropped under helium into a glassy carbon furnace and pyrolyzed at 1450°C to form hydrogen and/or carbon monoxide gases These gases are carried in a helium stream to a GC column held at 100°C to separate the gases before being diluted in the Conflo III and passed to the mass spectometer for analysis Isotope ratios are blank corrected and reported in per mil notation relative to the VSMOW-VSLAP scale

Oxygen

In-house oxygen standards are calibrated against the international standards USGS-34 ($\delta^{18}O$ = -27 9‰ VSMOW) and USGS-35 ($\delta^{18}O$ = 57 5‰ VSMOW) An intermediate international standard IAEA-NO3 gave the result $\delta^{18}O$ = 25 63 ± 0 27‰ VSMOW (n = 23) during calibration of in-house standards Compare to the accepted value of $\delta^{18}O$ = 25 6 ± 0 4‰ VSMOW Two in-house standards are used to set up a calibration line and a third is used to monitor accuracy of data Accuracy of $\delta^{18}O$ data is 0 11‰ (n = 25) %O measurements have an accuracy of 0 5%
Actual sample errors may be greater than these due to heterogeneity and more accurate data may be obtained for such through repetition